SYNTHESIS, CHARACTERIZATION AND SURFACE ATTACHMENT OF SQUARE MIXED-VALENCE COMPLEXES AS BUILDING BLOCKS FOR MOLECULAR QUANTUM CELLULAR AUTOMATA

A Dissertation

Submitted to the Graduate School

of the University of Notre Dame

in Partial Fulfillment of the Requirements

for the Degree of

Doctor of Philosophy

by

Jieying Jiao, B.S., M.S.

Thomas P. Fehlner, Director

Graduate Program in Chemistry and Biochemistry

Notre Dame, Indiana

July 2004

SYNTHESIS, CHARACTERIZATION AND SURFACE ATTACHMENT OF SQUARE MIXED-VALENCE COMPLEXES AS BUILDING BLOCKS FOR MOLECULAR QUANTUM CELLULAR AUTOMATA

Abstract

by

Jieying Jiao

Quantum-dot cellular automata (QCA) were proposed as a new architecture for computation, encoding binary information in the charge configuration of a cell with quantum "dots'. Molecular QCA cells could be mixed-valence compounds, in which the metal redox sites play the role of dots and the tunneling paths are provided by bridging ligands. A suitable building block for constructing QCA circuits is a square of four electronically coupled dots containing two mobile electrons.

Based on the general ideas of building the square compounds, a series of square compounds are designed. Synthetic approaches to the square compounds using molybdenum propiolate as a core linker failed possibly due to radicals generated in the process of the reactions. Alternatively, a known square with four ferrocenyl groups, $\{CpFe(\eta^5\text{-}C_5H_4)\}_4(\eta^4\text{-}C)CoCp$ (**18**), was investigated as a possible QCA cell, and its structure and dynamic NMR were measured. In contrast

to the original work, this square compound does display four reversible waves in cyclic voltammetry and square wave voltammetry corresponding to five oxidation states of the compounds.

By chemical methods, compound **18** can be oxidized to the monocationic and dicationic mixed-valence compounds, each of which are fully characterized by X-ray diffraction, FT-IR, EPR, magnetic susceptibility measurement and Mössbauer spectra. Both mixed-valence compounds display intervalence charge transfer (IVCT) bands in near-IR region. Based on the analysis of the IVCT bands, it is concluded that the monocationic mixed-valence compound belongs to Class-II and the dicationic mixed-valence compound is Class II-III. The electron hopping frequency of the dicationic compound in acetone is estimated to be $10^{7.5}$ s^{-1}, which is appropriately fast for QCA application.

Although a strategy for the attachment of mixed-valence compounds via electrostatic interaction is proposed, the experimental results (XPS and CV) prove that only neutral compounds are bound on the surface via Van de Waals forces. Moreover, due to the existence of silver ion on the surface, reversible waves in CVs of films were not obtained. Conclusive answers about the properties of the compounds on a surface substrate could not be drawn.

To my parents and Xiangdong

CONTENTS

FIGURES

SCHEMES

TABLES

ABBREVIATIONS

AFM	Atomic force microscopy
Anal.	analyzed
Bu	butyl
Calcd.	calculated
Cp	Cyclopentadienyl
Cp*	pentamethylcyclopentadienyl
CPS	Counts per second
CV	Cyclic voltammetry
DBU	1,8-diazabicyclo[5.4.0]undec-7-ene
DDQ	Dichlorodicyano-benzoquinone
DMSO	Dimethyl sulphoxide
dppe	Bis(diphenylphosphine)ethane
dppm	Bis(diphenylphosphine)methane
EPR	Electron paramagnetic resonance
Et	ethyl
ether	ethyl ether
FAB	Fast atom bombardment
FcH	ferrocene
FT	Fourier transform

FWHM	Full width of the half maxmuim
Hz	Hertz
IR	infrared
IVCT	Intervalence charge transfer
Me	methyl
MLCT	Metal to ligand charge transfer
3-MPTMS	(3-mercaptopropyl)trimethoxysilane
MS	Mass spectroscopy
NMR	Nuclear magnetic resonance
Ph	phenyl
ppm	Parts per million
QCA	Quantum-dot cellular automata
RSF	Relative sensitivity factor
SAM	Self-assembled monolayer
SWV	Square wave voltammetry
TBA	tetrabutylammonium
THF	tetrahydrofuran
Vis	Visible
VT	Variable temperature
XPS	X-ray photoelectron spectroscopy

ACKNOWLEDGMENTS

Firstly, I would like to express my sincere gratitude and appreciation to my research advisor, Professor Thomas P. Fehlner, for giving me this opportunity to work under his advice. His guidance, encouragement, patience, enthusiasm and knowledge help me growing as a real chemist. I am sure I will continue to benefit from his advice throughout my life.

I would also like to thank the member of my advisory committee, Professor Marya Lieberman, Professor W. Robert Scheidt and Professor Slavi C. Sevov, for all of their helpful suggestions and reading my dissertation. I am grateful to Dr. Alicia Beatty for her hard work on X-ray crystallography and Dr. Bruce Noll for his kind help to analyze structure data, Mr. Don Schifferl, Dr. Jaroslav Zajicek and Dr. Igor Veretennikov for their assistances with NMR, Ms. Nonka Sevova for mass spectroscopy measurement, Dr. Gary J. Long (Department of Chemistry, University of Missouri-Rolla) and Dr. Fernande Grandjean (Department of Physics, University of Liège, Belgium) for Mössbauer spectroscopy measurements, Dr. Jennifer Velasco and Dr. Graeme Wyllie for their assistances with EPR and Professor Robert G. Hayes for his helpful discussion on EPR data, Dr. Franck

Gascoin for his help on magnetic susceptibility measurements, Dr. Xuejun Wang for his training on X-ray photoelectron spectroscopy instrument.

I wish to acknowledge the members of Professor Fehlner's group, present and past, for their helpful discussions as well as helps in daily life. Special thanks to Dr. Zhaohui Li for her enthusiastic help and valuable discussions about syntheses and electrochemistry, Dr. Hong Yan and Ramón Macías for their helps on variable temperature NMR. The support of Chemistry and Biochemistry Department and hard work of its staff are greatly appreciated.

On more personal note, I would like to thank my parents. Without their hard work and continuous encouragements, I would not be where I am today. I also wish to thank my husband, Xiangdong, for his love, patience and confidence in me.

Finally, I would like to thank all of the people who have been helpful to me throughout my time at Notre Dame.

CHAPTER 1

INTRODUCTION

1.1 Quantum-dot cellular automata (QCA)

Molecular electronics is a research area focusing on the potential utilization of molecular scale systems and molecular materials for electronic or optoelectronic application.[1] Since Aviram and Ratner reported a molecular rectifier based on the use of a single organic molecule in 1974,[2] this research area attracted many peoples' attentions due to the demand for the denser and faster integrated circuits.[3] Most approaches to molecular electronics is to mimic conventional electronic elements such as transistors, wires or diodes with the use of carbon nanotubes,[4-7] nanowires,[8,9] small molecules [10,11] and large biomolecules.[12] Recently, there have been a number of breakthroughs in the fabrication of circuits.[8,13-16] However, all of these ideas focused on crossbar architectures, in which the molecules bridge the crossbars to transport current. Diodes architectures would be a step backwards and the problems the current technology has met, such as heat dissipation, current leakage and tunneling, are not addressed by this approach.

Differing from conventional transistor-based designs, a new architecture for computation, quantum-dot cellular automata (QCA), encoding binary information in the charge configuration of a cell containing a small number of quantum "dots", has been proposed.[17,18] Here, a dot is "a region in which the charge is localized".[19] An ideal QCA cell consists of four quantum dots positioned at the corner of a square or two double-dot cells arranged side by side (Figure 1-1). Each cell has two extra mobile electrons occupying antipodal sites due to Coulomb repulsion. For an isolated cell, two degenerate ground states, which depend on the arrangement of the two extra electrons, are produced. These are donated as a cell polarizations P = +1 and P = -1 as shown in Figure 1-2. The cell polarization, P = +1 and P = -1, is used to represent binary **1** and **0,** respectively. Tunneling of the two mobile electrons between the neighboring sites of the cell constitutes switching between the two degenerate states.

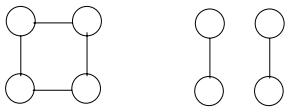

FIGURE 1–1. THE GEOMETRY OF AN IDEAL (a) FOUR-DOT AND (b) A PAIR OF EQUIVALENT TWO-DOT CELLS. THE TUNNELING ENERGY BETWEEN THE ADJACENT SITES IS DESIGNATED BY THE DISTANCE BETWEEN THE DOTS.

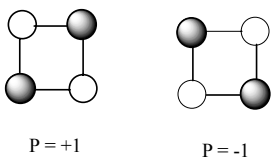

FIGURE 1–2. SCHEMATIC OF TWO BISTABLE STATES WITH CELL POLARIZATION OF P = +1 AND P = -1. THE GRAY DOTS REPRESENT THE LOCATION OF THE EXTRA ELECTRONS.

The electrostatic interaction of the neighboring cells results in two polarization states that are not be energetically equivalent. Figure 1-3[18,20] illustrates how a cell is influenced by the state of the neighbor cell. Considering two nearby cells as shown in the inset of Figure 1-3, the ground state configuration of cell 1 will be +1 polarization when the cell 2 is in the polarization state of +1. Similarly, if the cell 2 has a polarization of -1, cell 1 is also a -1 polarization. Thus, no current flow between the cells is involved in this intercellular interaction and it is this electrostatic interaction which transmits the information. The cell-cell response function has a highly nonlinear nature, which implies that a small polarization in cell 2 results in a very strong polarization in its neighbor (cell 1) and "the polarization of cell 1 saturates quickly to a value of 1 or -1."[18] This bistable saturation is the key to the idea of quantum cellular automata.

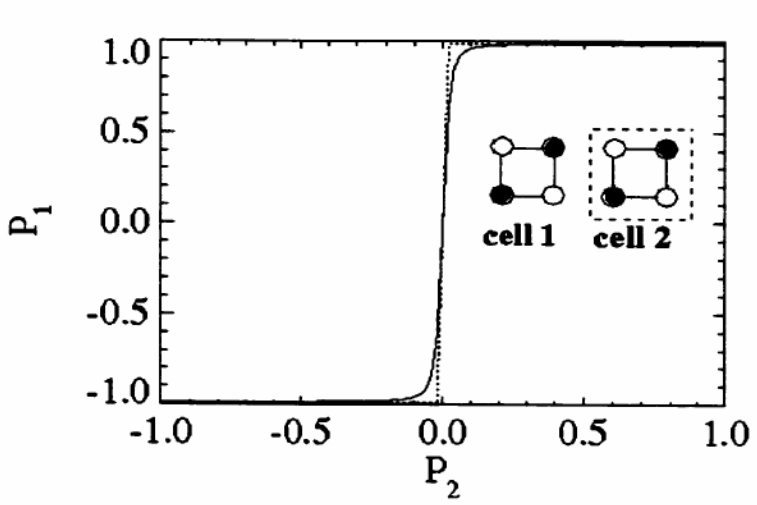

FIGURE 1–3. THE CELL-CELL RESPONSE FUNCTION FOR THE FOUR-DOT CELLS SHOWN IN THE INSET.[18,20] THE NONLINEAR RESPONSE OF THE CELL-CELL INTERACTION SERVES THE SAME ROLE AS VOLTAGE GAIN IN CONVENTIONAL DEVICES. THIS FIGURE IS REPRODUCED FROM *Ann. NY. Acad. Sci.* **2002**, *960*, 225-239.

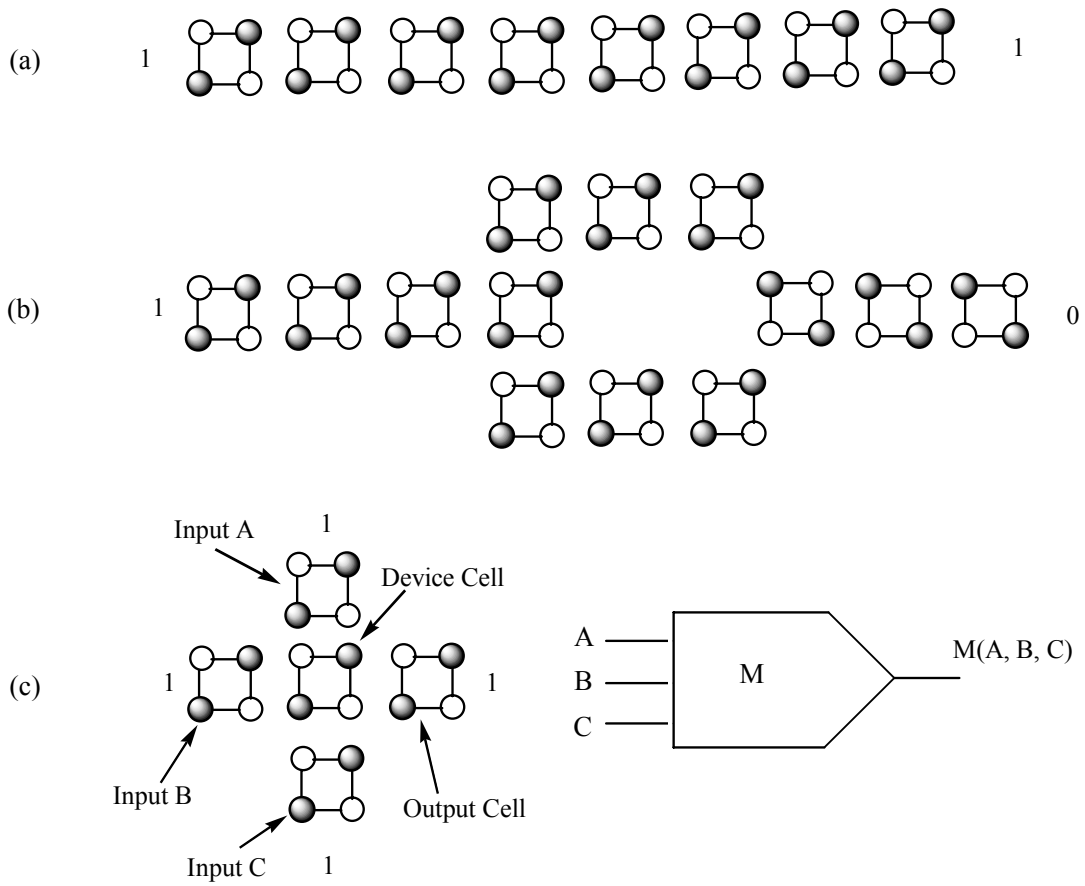

FIGURE 1–4. QCA DEVICES. (a) WIRE: THE OUTPUT REFLECTS THE INPUT; (b) INVERTER: THE INPUT IS CHANGED FROM 1 TO 0; (c) MAJORITY GATE: THE THREE INPUT LINES COVERAGE AT A DEVICE CELL, WHOSE STATE IS DETERMINED BY THE STATE OF THE MAJORITY OF THE INPUTS.[18,20,21]

If a series of cells is placed in a straight line, it creates a QCA wire (Figure 1-4a), which can transmit binary information from one end to the other. Different types of QCA devices can be constructed with using variable physical arrangements of the cells. Figure 1-4 shows the designs of several QCA devices.[18,20,21] Based on these simple QCA devices, more complicated circuits such

as adders[22] and microprocessors[23] within the QCA paradigm have been designed. Since QCA scheme relies on quantum mechanical tunneling and no current flows between the cells, the principal advantage of QCA devices over the other approaches mentioned above is low power dissipation which is estimated to be 10^{-9}–10^{-11} W/device. In addition, power gain is possible via clocking.[24]

QCA devices such as wires and majority gates based on the metallic dots on an oxidized silicon substrate have been reported.[25,26] In these devices, a small metal island plays the role of the dot, which is connected to other islands by small tunnel-junction barriers. The experiments have shown that the rearrangement of charges in one cell can effectively influence the state of the neighboring cells and perform computational tasks. However, these metal dot tunnel junction cells only operate at 80 mK since the energy difference between the ground state and the excited state is very small. The higher temperature operation would erase the bistability and yield random polarities.

Shrinking the size of dots and junctions will increase the energy difference and make the higher temperature operation possible. Room-temperature operation requires QCA cells in the 1–5 nm size range. Although metallic and semiconducting quantum dots are synthetically available, their heterogeneous sizes and the difficulties associated scaling down as well as with assembling them on the surface into QCA cells with appropriate tunnel junctions suggest a molecular approach to QCA cells. Molecular-sized QCA cells are a type of mixed-valence complexes, in which charge is localized on specific sites and can tunnel between

these sites. Thus, the redox sites play the role of "dots" and the tunneling paths are provided by bridging ligand.[27]

1.2 Mixed-valence complexes

Mixed-valence complexes are a class of inorganic compounds which contain ions of elements in two or more different formal states of oxidations.[28] The history of the mixed-valence chemistry can be cast back to 18th century. In 1724, Woodward[29] reported the synthesis of one of the first mixed-valence compounds, Prussian blue, which contains Fe(II) and Fe(III) bridged by cyanide. The deep blue color of the compound is due to the intervalence charge transfer reactions between the ferrous and ferric sites. Developments of the mixed-valence chemistry have gone beyond the original bounds of coordination chemistry. In 1973, Cowen and coworkers[30] described the first mixed-valence organic compound, the tetrathiafulvalence radical cation, which does not include metal ions.

Designed mixed-valence complexes were firstly prepared in 1969 by Creutz and Taube, who also initially characterized the mixed-valence compounds experimentally.[31] The Creutz-Taube ion, $[(NH_3)_5Ru(\mu\text{-pyrazine})Ru(NH_3)_5]^{5+}$, is one of the most studied and well known mixed-valence compound.[31] The 4+ complex displays two reversible one electron oxidations at 0.37 V and 0.76 V *versus* the standard hydrogen electrode. The near-IR spectrum of the mixed-valence 5+ ion shows a weak and broad absorption at 1570 nm assigned to the intervalence charge transfer (IVCT). It is clear that both ruthenium centers communicate through the

bridging ligand. This kind of interaction occurs because the electrons of metals centers in d(π) orbitals are effectively overlapped with the π* orbitals of the ligand (Figure 1-5).[32]

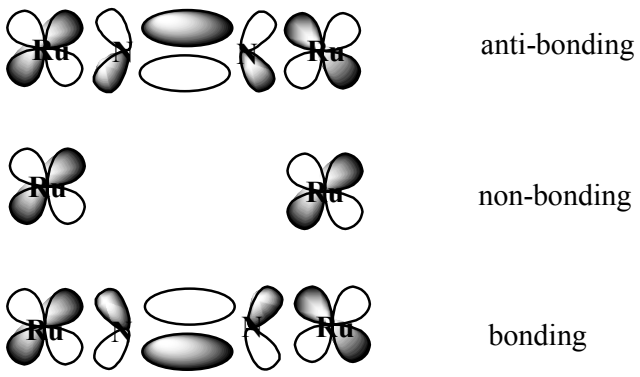

FIGURE 1–5. MOLECULAR π-ORBITALS IN THE CREUTZ-TAUBE ION.[32]

In the decades following the publication of the Creutz-Taube ion, the study of compounds, in which two (or more) metal centers show a pronounced electronic interaction, occupied considerable attention due to their potential application in molecular electronics.[33-36] Although the interaction between the metal centers may occur through space if the metal centers are close enough to place each ion in the electric field of the other,[37] in most of the mixed-valence complexes interaction occurs through the conjugated bridge such as that found in the Creutz-Taube ion.

An obvious manifestation of the interaction between the metal centers is a separation of the two (or more) metal-centered sequential redox potentials for metals. The potential difference ΔE between the waves measured by cyclic voltammetry (CV) represents of the thermodynamic stability of the corresponding

mixed-valence state relative to other redox states and a comproportionation constant K_c can be computed using equation 1-1:

$$[\text{Red, Red}] + [\text{Ox, Ox}] \overset{K_c}{\rightleftharpoons} 2[\text{Red, Ox}]$$
$$K_c = [\text{Red, Ox}]^2/[\text{Red, Red}][\text{Ox, Ox}] \quad \textbf{(1-1)}$$

It is worth noting that the lower limit of K_c is 4 when the metals effectively act independently.[33] A mixed-valence complex may be prepared and studied from either reduced or oxidized complexes. The mixed-valence state can be generated through electrochemical methods (electrolysis exactly at the redox potential of the metals) or, more often, through chemical methods (by addition of stoichiometric amount of an appropriate oxidizing agent to a solution of the compound).

In addition, mixed valence compounds exhibit a weak intervalence charge transfer (IVCT) band characteristic of the optically induced intramolecular electron transfer in the near-IR spectral domain. This band is absent in the spectra of the reduced and oxidized states.[38]

Depending on the delocalization of the unpaired electron over redox sites, mixed-valence materials have been classified into three types: Class I, Class II and Class III by Robin and Day.[28] Usually, the ions in the Class I system are in sites of very different symmetry and ligand field. The interaction between the metal centers is so weak that the valence is totally localized at the sites and the mixed-valence materials exhibit only the properties for isolated mononuclear complexes. In this situation, no through-bridge electron exchange between metal centers occurs and no IVCT band can be observed. On the other hand, the ions in the Class III mixed-

valence compound are in the very similar sites. The interaction between the metals is so great that the valence is totally delocalized over the metal centers and no available spectroscopic technique is able to discriminate between the metal centers. In this case, the potential difference, ΔE, is often larger than 200 mV. In addition, the IVCT band is solvent independent and shows no solvatochromism. The Class II system is the intermediate of these two limiting case. In Class II mixed-valence compound, the valence has some delocalization, but the metals still retain integer oxidation states. In this case, at least one spectroscopic technique is able to distinguish one site from the other.

The criteria have been reviewed by many other chemists.[39,40] Meyer *et al* proposed a type between the Class II and Class III, Class II-III.[39] In Class II, the unpaired electron and solvent are localized. While, Class III mixed-valence compound has electron delocalization and solvent averaging. In the Class II-III system, the complex displays properties of both localization and delocalization. In this case, the electron is localized, but the solvent is averaged, and the complex shows solvent-independent IVCT band or bands.

Obviously, the properties of the mixed-valence complexes are related to the interaction between the metals. When the interaction is strong, K_c is large and the IVCT band occurs at low energy with high intensity. Contrarily, when the interaction is weak, K_c decreases and the lower intensity of IVCT band occurs at higher energy. The magnitude of the interaction can be estimated in terms of coupling parameter H_{AB}, in units of cm^{-1}, which is expressed as equation 1-2:

$$H_{AB} = (2.05\times10^{-2})[\frac{\varepsilon_{max}\Delta\nu_{1/2}}{\nu_{max}}]^{1/2}\frac{\nu_{max}}{d} \quad \textbf{(1-2)}$$

where ε_{max} is the molar extinction coefficient for the maximum of IVCT band in $M^{-1}\cdot cm^{-1}$, $\Delta\nu_{1/2}$ is the width at half-height of the IVCT band in cm^{-1}, ν_{max} is the IVCT band maximum in cm^{-1} and d is the intermatallic separation in Å.[38]

The bridges connecting the metal centers are important in determining the magnitude of the electronic interaction of compounds. In most binuclear complexes, the interaction is transmitted through the delocalized π system of the bridging ligand, such as polyene,[41-44] dipyridyl-polyene[45-47] and polypyridyl.[48-50] Anything affecting the extent of π- delocalization between the ends of the ligand will influence the electronic interaction. For example, mixed-valence compound $[(NH_3)_5\text{-Ru-}(\mu\text{-L})\text{-Ru}(NH_3)_5]^{5+}$, K_c equals to 3×10^6 when L is pyrazine, while K_c is only 20 if L is bipyridine. The reason is that C–C bond rotation affects the extent of π- delocalization. It is established that the length and rigidity of the bridging ligand play key roles in the metal–metal interaction.[51,52]

As described above, the chemical properties of mixed-valence compounds have been well studied. However, most of them are binuclear mixed-valence compounds. A mixed-valence complex with three metal centers was thoroughly analyzed by Lapinte recently.[53] The properties of a tri-nuclear mixed-valence compound are closely related to those of bi-nuclear mixed-valence compounds albeit with additional complexity. Thus, it is reasonable to consider a tetra-nuclear mixed-valence compound utilizing the methods found useful for discussing bi-nuclear mixed-valence complexes.

To be a building block in molecular QCA, the mixed-valence complex must have a stable mixed-valence state, strong interactions between the redox centers and an intervalence charge transfer (IVCT) band indicative of electron exchange in a Class II compound.[20,54] For a four-dot QCA molecule, of first importance is that the compound must possess a square geometry.

1.3 Molecular design for four dots square compound

Reports of molecular designs for the synthesis of square compounds have become numerous recently.[55-57] It is well-known that transition metals have specific, well-defined geometry and variable coordination numbers. The transition metal complexes with two or more accessible *cis*- or *trans*- coordination sites are suitable to form molecular square. Therefore, any transition metal with octahedral, square planar and trigonal bipyramidal geometry can be used to be a corner unit or linear ligand. As a result, the combination of the transition metal complexes and suitable incoming ligands chosen to generate appropriate angles of connection constitutes a popular pathway to molecular squares. Some pertinent studies are discussed below.

In 1983, Verkade and coworkers reported the formation of a self-assembled molecular square from the reaction of *cis*-[$Cr(CO)_4$(norbornadiene)] or *cis*-[$W(CO)_4$(norbornadiene)] with the linear ligand $P(OCH_2)_3P$.[58] Compared to the early transition metal complexes, group 10 transition metals are more likely to have square planar coordination geometries. Fujita and coworkers observed the

quantitative self-assembly of molecular squares in 1990 when treating the ethylenediamine complex of Pd^{II} dinitrate with 4,4′-bipyrine in water.[59] Würthner and Sautter [60] also reported the construction of a nanometer-scale molecular square (the metal-metal diagonal distance is 3.4 nm) from a perylenebisimide derivative and Pt^{II} or Pd^{II} corner. An approach to neutral chiral squares was carried out by Hupp and coworker, who mixed $Re(CO)_5Cl$ with 4,4′-bipyridyl, 1,2-bis-trans-(4′-pyridyl)ethylene, or pyrazine in a mixture of THF and toluene to obtain molecular squares in greater than 95% yields.[61] The reaction of the half-sandwich complex $[Cp^*RhCl_2]_2$ with 4-imidazolecarboxylic acid also gives a molecular square.[62] Cotton and coworkers used dinuclear molybdenum chelate complex linked with oxalate, and ferrocene-1,1'-dicarboxylic anion to get molecular squares.[63] Porphyrin and metal-containing porphyrin are very interesting as the linear or angular binding units in the design of molecular squares. Titration of 5,10-bispyridylporphyrin or its Zn-complex with *cis*-$Pd(NCPh)_2Cl_2$ or *trans*-$Pd(NCPh)_2Cl_2$ provides square complexes.[64]

In principle, there are three ways to construct a molecular square: a) using a metal starting material with a 90° angle between the coordination sites and a rigid linear ligand, b) utilizing a metal complex with opposite coordination sites (180° geometry) and a ligand system with a 90° turn, or c) using the cross-linked ligand and a metal complex with one coordination site. (Scheme 1-1)

Although a large number of square compounds have been synthesized, only a few are suitable for QCA application.[65-67] In order to obtain the designed stable mixed-valence compound, not only the bridging ligands, but also the metal centers

need to be considered. The latter must have reversible redox activity. However, in most existing square compounds, the metal centers are W, Pt, Pd, Re and Rh, which exhibit irreversible electrochemical behaviors or just one reversible wave.[58-62] These properties rule them out for the purposes of QCA application.

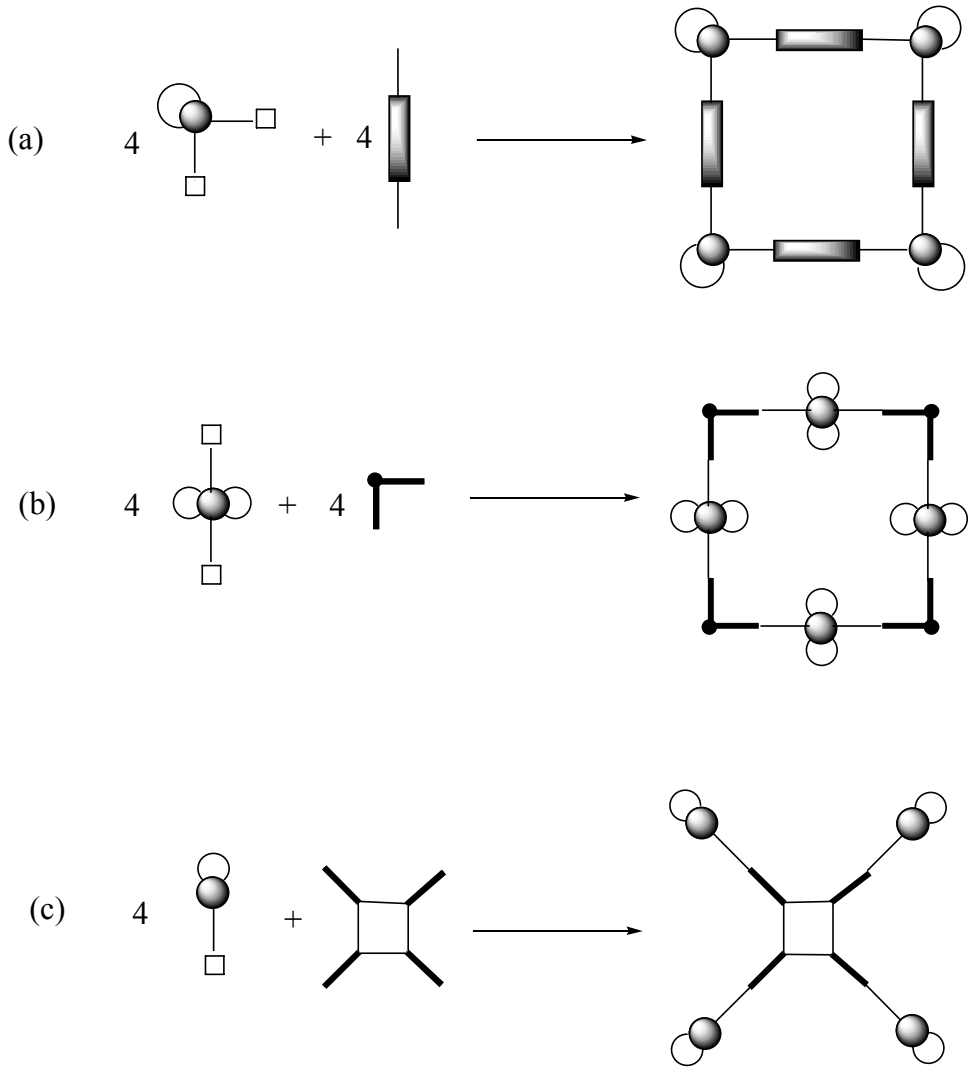

SCHEME 1–1. SYNTHETIC STRATEGIES FOR MOLECULAR SQUARES.

Cotton and coworkers introduced the metal–metal multiple bonds to supramolecular chemistry and synthesized square compounds.[68] Although most of them have no desired redox activity, $[(cis\text{-DAniF})_2Mo_2(CO_3)(H_2O)]_4$ (DAniF = *N, N′*-di-*p*-anisylformamidinate) does show four oxidation processes corresponding to charges of 0 to +4 on the square as shown in Figure 1-6.[65] The molecular square, $[Cp^*Co(2,3\text{-}Et_2C_2B_4H_3\text{-}5\text{-}C{\equiv}C\text{-}7\text{-}C{\equiv}C)]_4$, was synthesized through a multiple step reaction of *closo*-cobaltacarboranes or *nido*-cobaltacarborane with ethynyl derivative. Cyclic voltammetry of square compound revealed two separate one-electron reductions followed by a single two-electron reduction (Figure 1-7).[67] Long *et al* reported a mixed-valence square complex, $[(cyclen)_4Ru_4(pyrazine)_4]^{9+}$ (cyclen = 1, 4, 7, 10-tetraazacyclododecane), which has three Ru^{II} centers and one Ru^{III} center. The compound displays a quasireversible reduction wave and three successive oxidation waves as shown in Figure 1-8 and electron delocalization occurs between four equivalent ruthenium centers.[66]

Although these three molecular squares contain the required redox active metal centers, to date there is no example of an isolated four-metal, mixed-valence complex with two mobile electrons in a square geometry. The independent existence and compatible electronic properties of such species are of fundamental importance to the realization of the QCA paradigm. Thus, the purpose of the thesis is to synthesize mixed-valence compounds with square geometries and two mobile electrons, and measure the properties of the mixed-valence compounds to determine the possibilities for use as a component for QCA circuits.

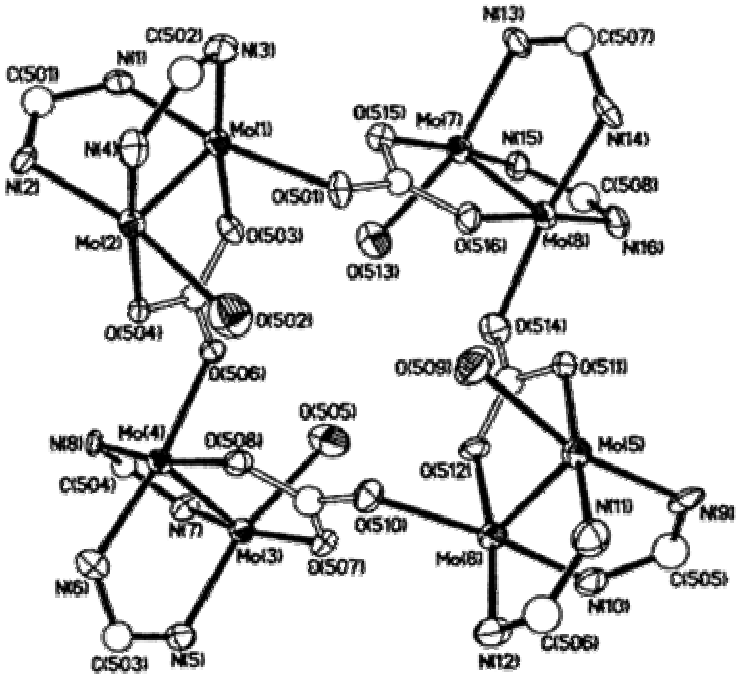

(a)

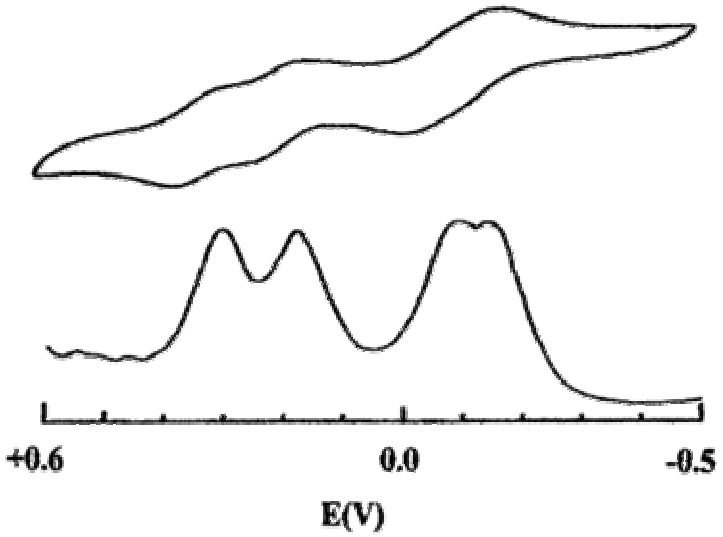

(b)

FIGURE 1–6. [(*cis*-DAniF)$_2$Mo$_2$(CO$_3$)(H$_2$O)]$_4$. (a) MOLECULAR STRUCTURE. (b) CYCLIC AND DIFFERENTIAL PULSE VOLTAMMOGRAMS IN CH_2Cl_2. THE FIGURES ARE REPRODUCED FROM *J. Am. Chem. Soc.* **2001**, *123*, 2670-2671.[65]

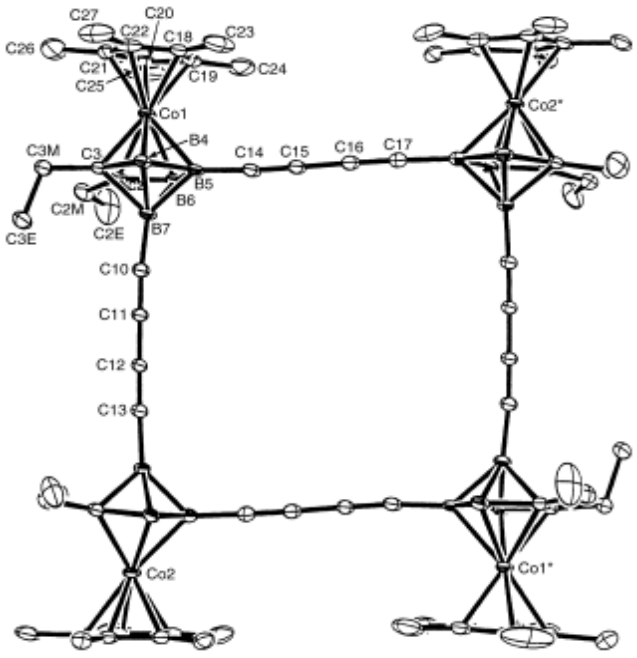

(a)

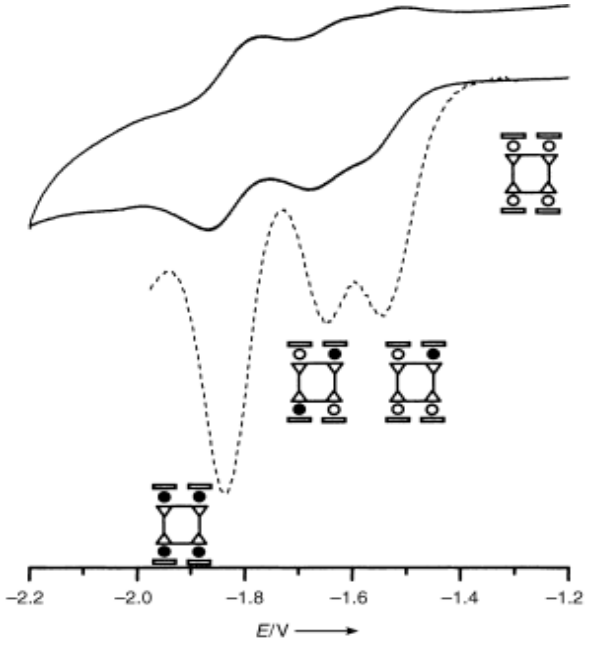

(b)

FIGURE 1–7. [Cp*Co(2,3-$Et_2C_2B_4H_3$-5-C≡C-7-C≡C)]$_4$. (a) MOLECULAR STRUCTURE. (b) CYCLIC AND SQUARE-WAVE VOLTAMMOGRAMS IN THF. THE FIGURES ARE REPRODUCED FROM *Angew. Chem. Int. Ed.* **2003**, *42*, 1002-1005.[67]

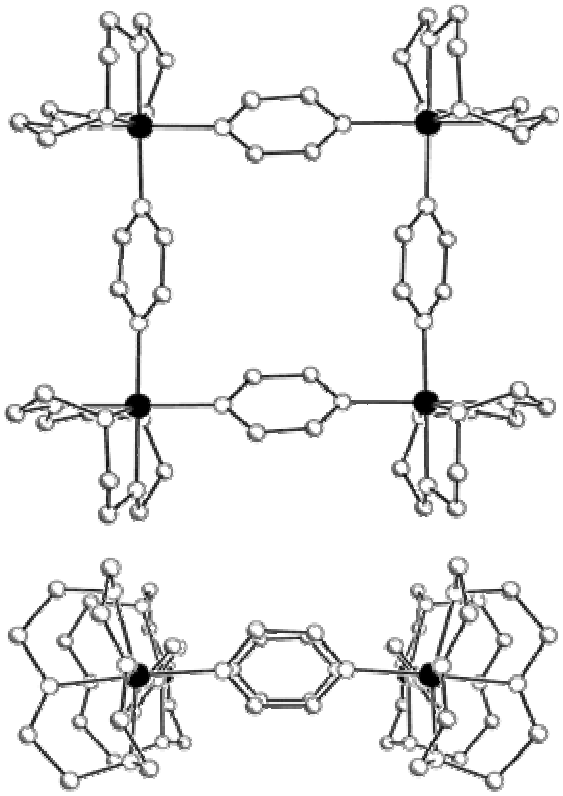

(a)

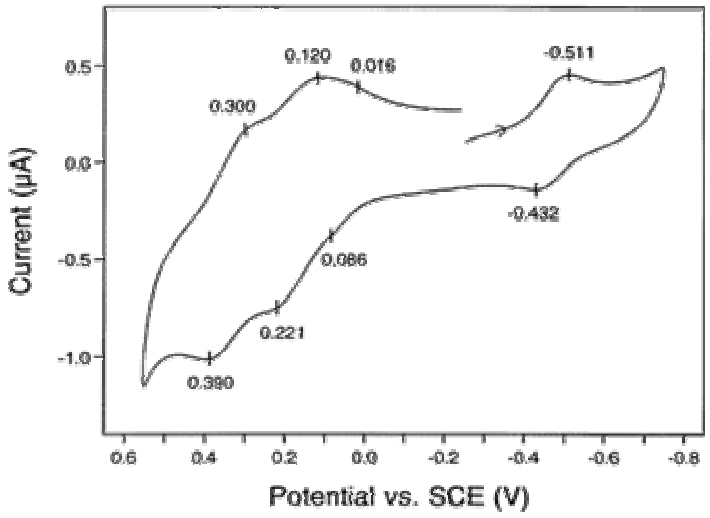

(b)

FIGURE 1–8. $[(cyclen)_4Ru_4(pyrazine)_4]^{9+}$. (a) MOLECULAR STRUCTURE AS TOP VIEW AND SIDE VIEW. (b) CYCLIC VOLTAMMOGRAM IN ACETONITRILE. THE FIGURES ARE REPRODUCED FROM *J. Am. Chem. Soc.* **2002**, *124*, 9042-9043.[66]

Following this introduction, chapter 2 describes the several designed molecular squares using molybdenum propiolate as the core and redox active metal fragments [Cp*Fe(dppe)], [$Ru(dppm)_2Cl$] and [$Co_2(CO)_4(dppm)$] as the dots. Attempted syntheses of these four-dot molecules are addressed and the possible reasons for the failure of syntheses are also discussed.

In chapter 3, the preparation and full characterization of a square complex, $\{(\eta^5\text{-}C_5H_5)Fe(\eta^5\text{-}C_5H_4)\}_4(\eta^4\text{-}C_4)Co(\eta^5\text{-}C_5H_5)$, are present. Electrochemical behavior of the compound implies the possibility to obtain a stable mixed-valence compound with two ferrocenyl units and two ferrocenium moieties (di-oxidized) with chemical methods.

In chapter 4, the successive oxidizations of square compound, $\{(\eta^5\text{-}C_5H_5)Fe(\eta^5\text{-}C_5H_4)\}_4(\eta^4\text{-}C_4)Co(\eta^5\text{-}C_5H_5)$, are given. The characterizations of the mixed-valence compounds are explored by different techniques such as IR, EPR, Mössbauer, near-IR, ^1H VT-NMR spectroscopy and magnetic susceptibility measurement.

The surface attachments of the mixed-valence compounds are investigated in chapter 5 using various techniques including X-ray photoelectron spectrometry (XPS), ellipsometry and cyclic voltammetry.

The final chapter contains the summary of the whole thesis and an outlook for the future work.

1.4 References

(1) Jortner, J.; Ratner, M. A.; International Union of Pure and Applied Chemistry. *Molecular electronics*; Blackwell Science: Osney Mead, Oxford [England] ; Malden, MA, USA, 1997.

(2) Aviram, A.; Ratner, M. A. *Chem. Phys. Lett.* **1974**, *29*, 277-283.

(3) Tseng, G. Y.; Ellenbogen, J. C. *Science* **2001**, *294*, 1293-1294.

(4) Avouris, P. *Acc. Chem. Res.* **2002**, *35*, 1026-1034.

(5) Rueckes, T.; Kim, K.; Joselevich, E.; Tseng, G. Y.; Cheung, C. L.; Lieber, C. M. *Science* **2000**, *289*, 94-97.

(6) Ellenbogen, J. C.; Love, J. C. *Proc. IEEE* **2000**, *88*, 386-426.

(7) GoldhaberGordon, D.; Montemerlo, M. S.; Love, J. C.; Opiteck, G. J.; Ellenbogen, J. C. *Proc. IEEE* **1997**, *85*, 521-540.

(8) Huang, Y.; Duan, X. F.; Cui, Y.; Lauhon, L. J.; Kim, K. H.; Lieber, C. M. *Science* **2001**, *294*, 1313-1317.

(9) Cobden, D. H. *Nature* **2001**, *409*, 32-33.

(10) Chen, J.; Reed, M. A.; Rawlett, A. M.; Tour, J. M. *Science* **1999**, *286*, 1550-1552.

(11) Collier, C. P.; Wong, E. W.; Belohradsky, M.; Raymo, F. M.; Stoddart, J. F.; Kuekes, P. J.; Williams, R. S.; Heath, J. R. *Science* **1999**, *285*, 391-394.

(12) Phadke, R. S. *Appl. Biochem. Biotech.* **2001**, *96*, 269-276.

(13) Tans, S. J.; Verschueren, A. R. M.; Dekker, C. *Nature* **1998**, *393*, 49-52.

(14) Roth, K. M.; Dontha, N.; Dabke, R. B.; Gryko, D. T.; Clausen, C.; Lindsey, J. S.; Bocian, D. F.; Kuhr, W. G. *J. Vac. Sci. Technol. B* **2000**, *18*, 2359-2364.

(15) Bachtold, A.; Hadley, P.; Nakanishi, T.; Dekker, C. *Science* **2001**, *294*, 1317-1320.

(16) Collier, C. P.; Jeppesen, J. O.; Luo, Y.; Perkins, J.; Wong, E. W.; Heath, J. R.; Stoddart, J. F. *J. Am. Chem. Soc.* **2001**, *123*, 12632-12641.

(17) Lent, C. S.; Tougaw, P. D.; Porod, W.; Bernstein, G. H. *Nanotechnology* **1993**, *4*, 49-57.

(18) Tougaw, P. D.; Lent, C. S.; Porod, W. *J. Appl. Phys.* **1993**, *74*, 3558-3566.

(19) Lent, C. S.; Isaksen, B.; Lieberman, M. *J. Am. Chem. Soc.* **2003**, *125*, 1056-1063.

(20) Lieberman, M.; Chellamma, S.; Varughese, B.; Wang, Y. L.; Lent, C.; Bernstein, G. H.; Snider, G.; Peiris, F. C. *Ann. NY. Acad. Sci.* **2002**, *960*, 225-239.

(21) Lent, C. S.; Tougaw, P. D. *J. Appl. Phys.* **1993**, *74*, 6227-6233.

(22) Lent, C. S.; Tougaw, P. D. *Proc. IEEE* **1997**, *85*, 541-557.

(23) Niemier, M. T.; Kogge, P. M. *Int. J. Circuit Theory Appl.* **2001**, *29*, 49-62.

(24) Timler, J.; Lent, C. S. *J. Appl. Phys.* **2002**, *91*, 823-831.

(25) Orlov, A. O.; Amlani, I.; Bernstein, G. H.; Lent, C. S.; Snider, G. L. *Science* **1997**, *277*, 928-930.

(26) Amlani, I.; Orlov, A. O.; Toth, G.; Bernstein, G. H.; Lent, C. S.; Snider, G. L. *Science* **1999**, *284*, 289-291.

(27) Lent, C. S. *Science* **2000**, *288*, 1597-1599.

(28) Robin, M. B.; Day, P. *Adv. Inorg. Chem. Radiochem.* **1967**, *10*, 247-422.

(29) Woodward, J. *Philos. Trans. R. Soc. London* **1724**, *33*, 15.

(30) Cowan, D. O.; Vanda, C. L.; Park, J.; Kaufman, F. J. *Acc. Chem. Res.* **1973**, *6*, 1-7.

(31) Creutz, C.; Taube, H. *J. Am. Chem. Soc.* **1969**, *91*, 3988-3989.

(32) Creutz, C.; Taube, H. *J. Am. Chem. Soc.* **1973**, *95*, 1086-1094.

(33) Ward, M. D. *Chem. Soc. Rev.* **1995**, *24*, 121-134.

(34) Kaim, W.; Klein, A.; Glockle, M. *Acc. Chem. Res.* **2000**, *33*, 755-763.

(35) McCleverty, J. A.; Ward, M. D. *Acc. Chem. Res.* **1998**, *31*, 842-851.

(36) Astruc, D. *Acc. Chem. Res.* **1997**, *30*, 383-391.

(37) Buschel, M.; Helldobler, M.; Daub, J. *Chem. Commun.* **2002**, 1338-1339.

(38) Hush, N. S. *Prog. Inorg. Chem.* **1967**, *8*, 391-444.

(39) Demadis, K. D.; Hartshorn, C. M.; Meyer, T. J. *Chem. Rev.* **2001**, *101*, 2655-2685.

(40) Allen, G. C.; Hush, N. S. *Prog. Inorg. Chem.* **1967**, *8*, 357-389.

(41) Lang, H. *Angew. Chem. Int. Ed.* **1994**, *33*, 547-550.

(42) Zhou, Y. L.; Seyler, J. W.; Weng, W. Q.; Arif, A. M.; Gladysz, J. A. *J. Am. Chem. Soc.* **1993**, *115*, 8509-8510.

(43) Lenarvor, N.; Toupet, L.; Lapinte, C. *J. Am. Chem. Soc.* **1995**, *117*, 7129-7138.

(44) Long, N. J.; Martin, A. J.; White, A. J. P.; Williams, D. J.; Fontani, M.; Laschi, F.; Zanello, P. *J. Chem. Soc., Dalton Trans.* **2000**, 3387-3392.

(45) Ribou, A. C.; Launay, J. P.; Takahashi, K.; Nihira, T.; Tarutani, S.; Spangler, C. W. *Inorg. Chem.* **1994**, *33*, 1325-1329.

(46) Moreira, I. D.; Franco, D. W. *Inorg. Chem.* **1994**, *33*, 1607-1613.

(47) Das, A.; Maher, J. P.; Mccleverty, J. A.; Badiola, J. A. N.; Ward, M. D. *J. Chem. Soc., Dalton Trans.* **1993**, 681-686.

(48) Collin, J. P.; Laine, P.; Launay, J. P.; Sauvage, J. P.; Sour, A. *J. Chem. Soc. Chem. Comm.* **1993**, 434-435.

(49) Beley, M.; Collin, J. P.; Louis, R.; Metz, B.; Sauvage, J. P. *J. Am. Chem. Soc.* **1991**, *113*, 8521-8522.

(50) Sutter, J. P.; Grove, D. M.; Beley, M.; Collin, J. P.; Veldman, N.; Spek, A. L.; Sauvage, J. P.; Vankoten, G. *Angew. Chem. Int. Ed.* **1994**, *33*, 1282-1285.

(51) Meyer, W. E.; Amoroso, A. J.; Horn, C. R.; Jaeger, M.; Gladysz, J. A. *Organometallics* **2001**, *20*, 1115-1127.

(52) Kim, Y.; Lieber, C. M. *Inorg. Chem.* **1989**, *28*, 3990-3992.

(53) Weyland, T.; Costuas, K.; Toupet, L.; Halet, J. F.; Lapinte, C. *Organometallics* **2000**, *19*, 4228-4239.

(54) Li, Z. H.; Beatty, A. M.; Fehlner, T. P. *Inorg. Chem.* **2003**, *42*, 5707-5714.

(55) Lei, X. J.; Wolf, E. E.; Fehlner, T. P. *Eur. J. Inorg. Chem.* **1998**, 1835-1846.

(56) Leininger, S.; Olenyuk, B.; Stang, P. J. *Chem. Rev.* **2000**, *100*, 853-907.

(57) Holliday, B. J.; Mirkin, C. A. *Angew. Chem. Int. Ed.* **2001**, *40*, 2022-2043.

(58) Stricklen, P. M.; Volcko, E. J.; Verkade, J. G. *J. Am. Chem. Soc.* **1983**, *105*, 2494-2495.

(59) Fujita, M.; Yazaki, J.; Ogura, K. *J. Am. Chem. Soc.* **1990**, *112*, 5645-5647.

(60) Wurthner, F.; Sautter, A. *Chem. Commun.* **2000**, 445-446.

(61) Slone, R. V.; Hupp, J. T.; Stern, C. L.; AlbrechtSchmitt, T. E. *Inorg. Chem.* **1996**, *35*, 4096-4097.

(62) Lehaire, M.-L.; Scopelliti, R.; Herdeis, L.; Polborn, K.; Mayer, P.; Severin, K. *Inorg. Chem.* **2004**, *43*, 1609-1617.

(63) Cotton, F. A.; Daniels, L. M.; Lin, C.; Murillo, C. A. *J. Am. Chem. Soc.* **1999**, *121*, 4538-4539.

(64) Drain, C. M.; Lehn, J. M. *J. Chem. Soc. Chem. Comm.* **1994**, 2313-2315.

(65) Cotton, F. A.; Lin, C.; Murillo, C. A. *J. Am. Chem. Soc.* **2001**, *123*, 2670-2671.

(66) Lau, V. C.; Berben, L. A.; Long, J. R. *J. Am. Chem. Soc.* **2002**, *124*, 9042-9043.

(67) Yao, H.; Sabat, M.; Grimes, R. N.; de Biani, F. F.; Zanello, P. *Angew. Chem. Int. Ed.* **2003**, *42*, 1002-1005.

(68) Cotton, F. A.; Lin, C.; Murillo, C. A. *Acc. Chem. Res.* **2001**, *34*, 759-771.

CHAPTER 2

APPROACH TO THE MOLECULAR SQUARES WITH DIMOLYBDENUM PROPIOLATE AS THE CORE LINKER

2.1 Introduction

2.1.1 Molecular dots

The coordination chemistry and redox behavior of the organometallic compound [(η^5-C_5Me_5)Fe(η^2-dppe)Cl] (Cp*Fe(dppe)Cl) is reasonably well understood.[1] The redox activity arises from the large electron density around the Fe(II) center, which is donated from the Cp* and the chelating diphosphine ligands while the coordination chemistry comes from the labile Fe–Cl bond. The Fe–Cl bond is easily dissociated in polar solvents and the chloride can be replaced by a variety of nucleophiles.

Recently, Lapinte and his coworkers have reported series of compounds derived from Cp*Fe(dppe)Cl, where the chlorine is replaced by a terminal or trimethylsilyl substituted terminal alkyne.[2-7] Thus, it is possible to couple two or more Cp*Fe(dppe) fragments together in a complex by using an alkyne linker. In addition to the high yields of the reactions, the complexes exhibit specific

electrochemical properties. For example, the complex [{Cp*Fe(dppe)}$_2$-μ-(C≡CC_6H_4C≡C)] formed by treating Cp*Fe(dppe)Cl with 1,4-bis(acetylene) benzene shows two fully reversible redox waves in the cyclic voltammetry, centered at -55 mV and -315 mV.[3] This illustrates that the oxidation-reduction of one iron center affects the redox properties of the second iron center. Thus, it is possible to oxidize one iron center, leaving another one in the neutral state to form the mixed-valence complex. It is also clear that both iron centers can undergo a redox process. This type of electrochemical behavior is necessary for QCA application.

Compared to the properties of [Cp*Fe(dppe)Cl], the complex [*cis*-Ru(dppm)$_2$ Cl_2] has similar coordination chemistry and electrochemical behavior. It has been reported that one of the Ru–Cl bonds of the compound is easily broken in the presence of sodium hexafluorophosphate ($NaPF_6$) permitting a substitution of a chloride by a terminal alkyne to form the metal-acetylide compound.[8-10] The two or more ruthenium(II) centers connected by the bridging alkynes have redox behaviors similar to that of the complexes based on Cp*Fe(dppe)-alkynes.[11-13] Another advantage of complexes with Ru(dppm)$_2$Cl fragments is the activity of the other Ru–Cl bond in the *trans* position. This chloride also can be replaced by nucleophiles. Thus, another functional group for surface attachment such as NH_2, OCH_3 can be connected to the ruthenium centers.[14,15] This property is very important if the complex is to be used as a building block of a molecular QCA cell.

The formation of complexes with cobalt-alkyne units by treating $Co_2(CO)_8$ with the polyynes is well known.[16,17] The interaction between cobalt carbonyl

cluster systems is possible when the clusters are linked by unsaturated $(C{\equiv}C)_x$ bridges.[18,19] However, the redox activity of alkyne dicobalt units is limited by the fact that facile electrochemical reactions accompany one electron reduction to the radical anion.[20-22] Increase of the electron density in the polynuclear core leads to the conversion of the redox center from a reducible to a readily oxidizable center. This conversion can be reached with a phosphine ligand such as dppm substitution in $Co_2(CO)_6(\mu$-alkyne).[23,24] Due to the "clamping" of the Co–Co bond by dppm, the stability of compound is not affected by the fast ECE (electrochemical-chemical-electrochemical) reactions. The $Co_2(CO)_4$(dppm)(μ-alkyne) series exhibit an electrochemically and chemically reversible 1e oxidation.[25,26] So [$Co_2(CO)_4$ (dppm)(μ-alkyne)] unit is a good fragment for the dot of the QCA molecule.

2.1.2 Linkers

To form a square molecule for QCA application, except for the specific properties of the synthons, a core linker with a perfect square geometry and active groups that can react with the synthons is required. The molybdenum propiolate $Mo_2(O_2C{-}C{\equiv}CH)_4(THF)_2$ (or trimethylsilyl substituted molybdenum propiolate) is composed of two Mo centers bridged by four propiolate groups and two THF molecules attached to the open axial coordination sites of molybdenum. This arrangement of the ligands forces the compound into a square geometry, where each Mo center is found in an octahedral coordination site.[27] More important is the fact that the propiolate group contains terminal alkyne (or trimethylsilyl substituted terminal alkyne) which has the capability to react with the "dot" synthons

mentioned above (Cp*Fe(dppe)Cl, *cis*-$Ru(dppm)_2Cl_2$ and $Co_2(CO)_6(dppm)$). The proposed cluster squares, potential building blocks for molecular QCA, are illustrated in Scheme 2-1. The work in this chapter is concerned with the coupling reaction of molybdenum propiolate with complexes of Cp*Fe(dppe)Cl, *cis*-$Ru(dppm)_2Cl_2$ and $Co_2(CO)_6$ (dppm) to seek a square molecule with the desired properties for QCA application.

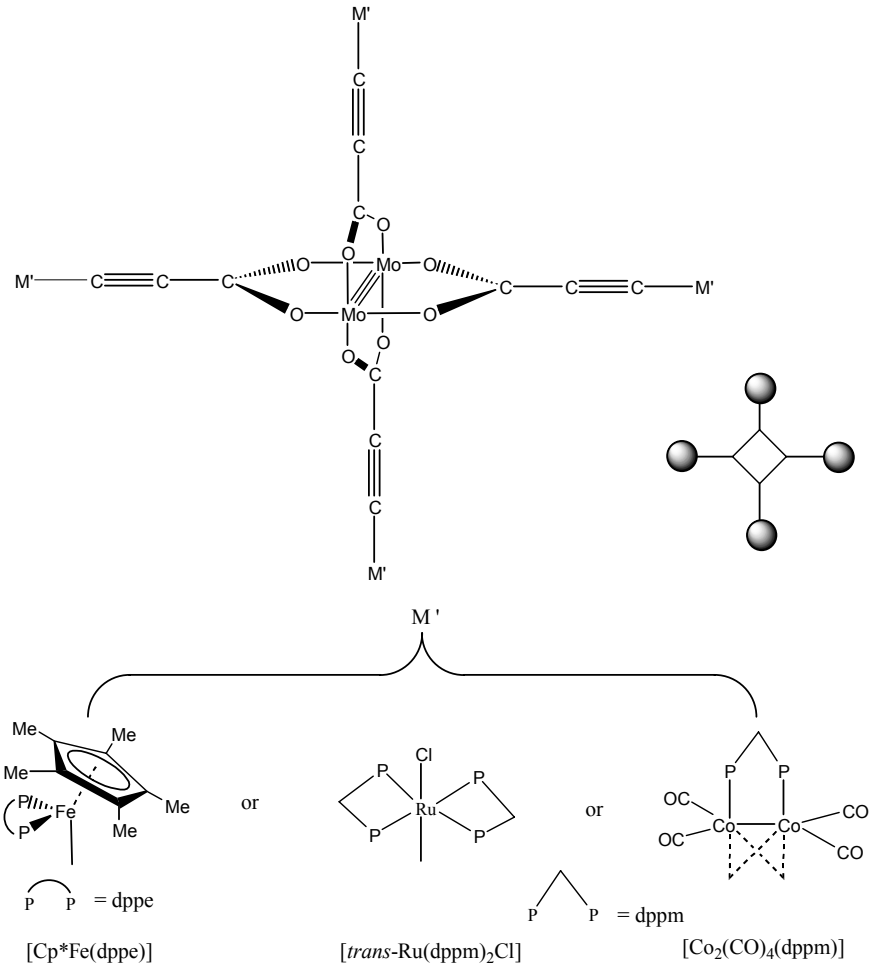

SCHEME 2–1. PROPOSED SQUARE MOLECULES WITH $Mo_2(O_2C{\equiv}C)_4$ AS CORE. THE METAL FRAGMENT M′ IS Cp*Fe(dppe) (Mo–Fe CLUSTER),[28] *trans*-$Ru(dppm)_2Cl$ (Mo–Ru CLUSTER) AND $Co_2(CO)_4(dppm)$ (Mo–Co CLUSTER) RESPECTIVELY.

2.2 Results

2.2.1 Synthesis

$Mo_2(O_2CCH_3)_4$ (1)

The preparation of **1** followed the literature methods.[29] A $\nu_{C\text{-}O}$ (asym.) band at 1514 cm^{-1} and a $\nu_{C\text{-}O}$ (sym.) band at 1443 cm^{-1} are observed in the IR spectrum of the compound, which indicates that the carboxylic groups are bridged on the two metal centers.[30] The complex is a little bit air and moisture sensitive. Exposure to the air for several days results in a color change from yellow to brownish yellow.

$Mo_2(O_2C{-}C{\equiv}CH)_4(THF)_2$ (2) and $Mo_2(O_2C{-}C{\equiv}CSi(CH_3)_3)_4(THF)_2$ (3)

Compounds **2** and **3** were prepared by ligand exchange of $Mo_2(O_2CCH_3)_4$ (**1**) with excess of propiolic acid ($HC{\equiv}C{-}COOH$)[27] and trimethylsilyl propiolic acid ($(CH_3)_3Si{-}C{\equiv}C{-}COOH$) respectively. The purities of the compounds were confirmed by NMR. The NMR data also confirm that the compounds are symmetrical. The ^1H NMR spectrum of **2** shows one signal at 3.91 ppm corresponding to four equivalent acetylene groups. Compound **3** exhibits one CH_3 signal at 0.313 ppm in ^1H NMR spectrum and -0.606 ppm in ^{13}C NMR spectrum. In both compounds, multiple signals at 3.61 and 1.78 ppm in ^1H NMR spectra prove the coordination of two THF molecules to Mo centers. A $\nu_{C{\equiv}C}$ band at 2117 cm^{-1} is observed in IR spectrum of compound **2**, while, this band changes to 2175 cm^{-1}, 58 cm^{-1} shift to higher frequency, for compound **3**, as expected for the higher electron-donating trimethylsilyl group. Thus the substitution of H by $Si(CH_3)_3$ group will increase the electron density on the carbon–carbon triple bond.

Therefore, the vibration of the carbon–carbon triple bond shifts to the higher frequency. The presence of the carbon–carbon triple bonds in compound **3** are also evidenced by the signals at 96.8 and 91.2 ppm in ^{13}C NMR spectrum. The signal of carbon atoms of the carboxylate groups is also observed at 161.4 ppm in ^{13}C NMR spectrum.

Cp*Fe(dppe)Cl (4)

With a modification of the known method,[31] compound **4** is prepared by the treatment of $Fe(dppe)Cl_2$[32] with Cp*Li in THF. The iron(II) chloro complex **4** is easily isolated as the dark green solid after extraction with diethyl ether. The pure compound is obtained by the recrystallization from CH_2Cl_2/pentane with high yield (82%).

***Cis*-$RuCl_2(dppm)_2$ (6)**

Compound **6** is prepared as reported previously.[33] $[RuCl_2(dmso)_4]$ (dmso = dimethyl sulphoxide)[34] is treated with dppm in toluene at 80 ºC, resulting in the formation of [*cis*-$RuCl_2(dppm)_2$] (**6**). The CH_2 groups of dppm ligands show two multiplets at 4.9 and 4.7 ppm in the ^1H NMR spectrum. The ^{31}P NMR spectrum of **6** shows two triplets at 0.253 and -26.01 ppm. All indicate that the compound is the *cis* isomer. The reaction temperature is the key to the preparation of the *cis* isomer. Higher temperature of 90 ºC results in the formation of the *trans* isomer.

$Co_2(CO)_6(dppm)$ (8)

As the literature reports,[35,36] the dppm ligand reacts with $Co_2(CO)_8$ in toluene to give a red solid of formula $Co_2(CO)_6(dppm)$ (**8**). The presence of dppm ligand in the compound is proved by a triplet at 2.94 ppm in the ^1H NMR spectrum and a

singlet at 61.4 ppm in the ^{31}P NMR spectrum. IR spectrum of **8** shows 6 CO bands. The absorptions at 2043, 1997, 1982 and 1972 cm^{-1} are due to the four terminal CO and the bands at 1809 and 1796 cm^{-1} are due to the two bridging CO. The dppm ligand acts as a bridging bidentate ligand replacing one equatorial CO group from each Co atom.

2.2.2 Reaction of $Mo_2(O_2CCCSi(CH_3)_3)_4(THF)_2$ (3) with Cp*Fe(dppe)Cl (4)

It was reported that the iron–chlorine bond in complex **4** is rather weak and a partial dissociation occurs in polar media. [1] The neutral alkynyl-based Cp*Fe(dppe) complexes are obtained in a "three-step one-pot" procedure starting from the alkyne or trimethylsilyl substituted alkyne and the chloro organoiron complex Cp*Fe(dppe)Cl (**4**) in a methanol/THF mixture in the presence of KF and KPF_6 salts.[6,7] A similar reaction procedure (Scheme 2-2) could be used in the synthesis of Mo-Fe cluster proposed in Scheme 2-1.

The reaction solution of **3** and **4** in a mixture of THF/methanol was refluxed for about 36 hours in the presence of KF and KPF_6 salts. The crude product is a mixture with some unreactive starting materials. After extraction with CH_2Cl_2 and washing with THF and pentane, brownish orange solids were isolated. Subsequent recrystallization from CH_2Cl_2/hexane gives analytically pure compound $[\{Cp^*Fe(dppe)\}_2(\mu\text{-}C{=}CHCH_2CH{=}C)][PF_6]_2$ (**5**) as orange crystals, which was characterized by IR, ^{1}H, ^{13}C and ^{31}P NMR.

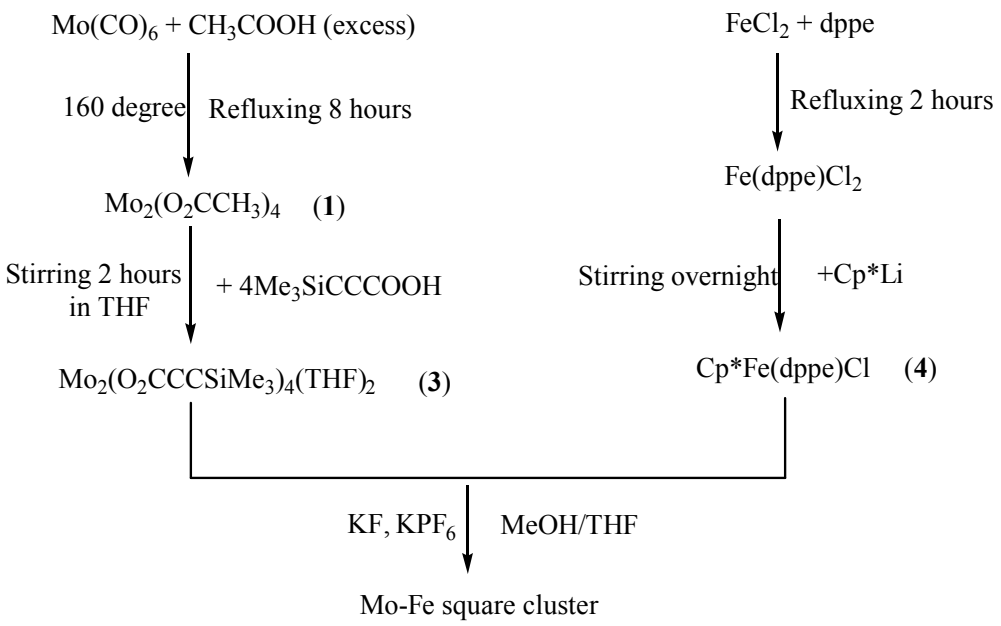

SCHEME 2–2. PROPOSED SYNTHETIC STRATEGY FOR Mo-Fe SQUARE CLUSTER.

The IR spectrum of complex **5** reveals a strong vinylidene C=C stretch at 1613 cm^{-1} and a band at 837 cm^{-1} (ν_{PF6}). However, no absorption due to the vibrations of carboxylate groups is observed in the IR spectrum. Furthermore, the compound displays a vinylic ^{1}H NMR triplet at 4.08 ppm and a vinylic ^{13}C NMR C_{β} signal at 121.2 ppm (the C_{α} signal was not observed due to the limited amount of the compound) typical of metal phosphine-substituted vinylidene complexes.[2,4,37] In the ^{13}C NMR spectrum, no signal at the region from 160 to 200 ppm due to the C atom of the carboxylate group is observed. The ^{31}P NMR spectrum shows a singlet at 87.5 ppm for the P atom at dppe ligands and a septet at -143.1 ppm for the P atom of PF_6^-. All of the spectroscopic data on complex **5** indicate that the there is no molybdenum carboxylate dimer center in the compound and the X-ray diffraction

analysis confirms the conclusion. The structure of compound **5** by X-ray diffraction analysis is shown in Figure 2-1. The formula is [{Cp*Fe(dppe)}$_2$(μ-C=CHCH$_2$CH=C)][PF$_6$]$_2$ as shown in Scheme 2-3.

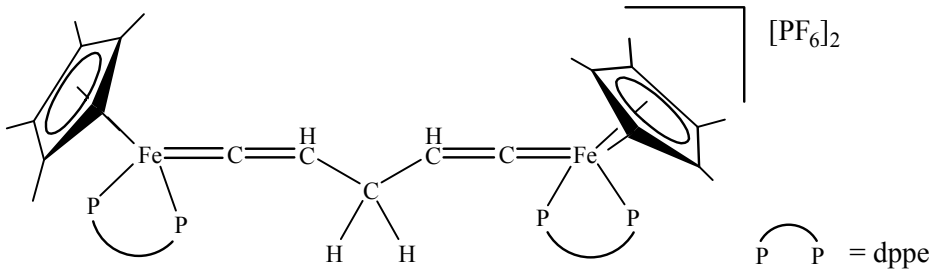

SCHEME 2–3. MOLECULAR FORMULA OF [{Cp*Fe(dppe)}$_2$(μ-C=CHCH$_2$ CH=C)][PF$_6$]$_2$ (**5**).

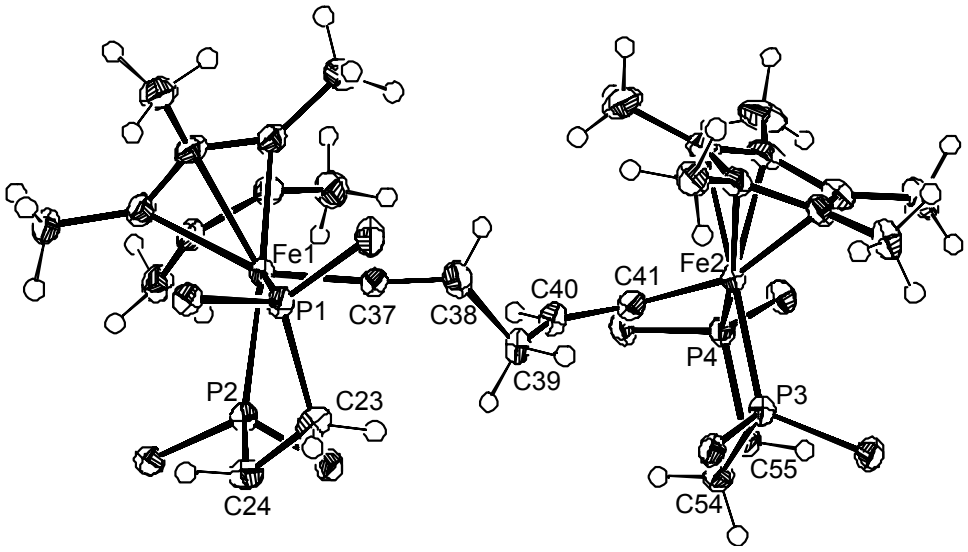

FIGURE 2–1. STRUCTURE OF THE CATION OF [{Cp*Fe(dppe)}$_2$(μ-C=CH CH$_2$CH=C)][PF$_6$]$_2$ (**5**) WITH 50% THERMAL ELLIPSOIDS. THE PHENYL GROUPS OF THE dppe LIGANDS HAVE BEEN OMITTED FOR CLARITY.

2.2.3 X-ray structure determination of [{Cp*Fe(dppe)}$_2$(μ-C=CHCH$_2$CH=C)][PF$_6$]$_2$ (5)

Crystals of **5** were grown by slow diffusion of hexane into CH_2Cl_2 solution. The unit cell contained one dimer and two PF_6^- counterions, as well as 1.5 dichloromethane molecules, which are disordered. The structure of the cation is shown in Figure 2-1, in which the phenyl groups of dppe ligands are omitted for clarity. The selected bond distances and bond angles are summarized in Table 2-1 and the X-ray data conditions are collected in Table 2-2.

The molecule contains two Cp*Fe(dppe) fragments connected by a C_5 chain. As usually observed for most of piano-stool complexes, the metal centers clearly adopt a pseudooctahedral geometry. Three coordination positions are occupied by Cp* ring, whereas the carbene carbon atom and the two phosphorus atom are positioned at the three remaining sites. The distances of iron atoms to the centers of the Cp* ligands are 1.781 Å (for Fe(1)) and 1.762 Å (for Fe(2)). The other bond lengths and bond angles of the two Cp*Fe(dppe) units in the cation compare well with the data determined for the parent compound[31] and other mononuclear complexes in the Cp*Fe(dppe) series.[38-40]

The bond distances of Fe(1)–C(37) (1.747(3) Å) and Fe(2)–C(41) (1.748(3) Å) reveal the strength of the metal–carbon bond. The Fe(1)–C(37)–C(38) and Fe(2)–C(41)–C(40) bond angles are nearly linear [Fe(1)–C(37)–C(38) 172.0(3)º, Fe(2)–C(41)–C(40), 175.4(3)º]. All data are in agreement with similar iron carbene complexes.[5,41] Moreover, the C(37)–C(38)–C(39) and C(39)–C(40)–C(41) bond angles are 128.3(3)º and 125.7(3)º respectively, which confirm the sp^2

hybridization of C(38) and C(40) atoms.[5] Two iron vinylidene fragments are connected by CH_2 group and the bond angles of C(38)–C(39)–C(40) is 112.4(3)º.

TABLE 2–1. SELECTED BOND LENGTHS [Å] AND ANGLES [DEG] FOR [{Cp*Fe(dppe)}$_2$(μ-C=CHCH$_2$CH=C)][PF$_6$]$_2$ (**5**).

Fe(1) – C(37)	1.747(3)	Fe(1) – P(1)	2.2195(10)
Fe(2) – C(41)	1.748(3)	Fe(1) – P(2)	2.2370(9)
C(37) – C(38)	1.298(5)	Fe(2) – P(3)	2.2281(9)
C(38) – C(39)	1.518(5)	Fe(2) – P(4)	2.2437(10)
C(39) – C(40)	1.506(5)	Fe(1) – Fe(2)	7.934
C(94) – C(95)	1.305(5)		
P(1) – Fe(1) – P(2)	86.13(3)	C(39) – C(40) – C(41)	125.7(3)
P(1) – Fe(1) – C(37)	82.56(11)	C(40) – C(41) – Fe(2)	175.4(3)
P(2) – Fe(1) – C(37)	92.03(10)	P(3) – Fe(2) – P(4)	86.25(3)
Fe(1) – C(37) – C(38)	172.0(3)	P(3) – Fe(2) – C(41)	84.14(11)
C(37) – C(38) – C(39)	128.3(3)	P(4) – Fe(2) – C(41)	91.19(11)
C(38) – C(39) – C(40)	112.4(3)	Fe(2) – P(3) – C(54)	105.69(11)
Fe(1) – P(1) – C(23)	106.17(11)	P(3) – C(54) – C(55)	108.0(2)
P(1) – C(23) – C(24)	106.1(2)	C(54) – C(55) – P(4)	108.1(2)
C(23) – C(24) – P(2)	107.7(2)	Fe(2) – P(4) – C(55)	108.02(11)
Fe(1) – P(2) – C(24)	108.21(11)		

TABLE 2–2. CRYSTAL DATA AND STRUCTURE REFINEMENT FOR

[{Cp*Fe(dppe)}$_2$(μ-C=CHCH$_2$CH=C)][PF$_6$]$_2$ (**5**).

Empirical formula	$C_{78.5}H_{85}Cl_3F_{12}Fe_2P_6$
Formula weight	1660.33
Temperature	100(2) K
Wavelength	0.71073 Å
Crystal system, space group	Monoclinic, P2(1)/c
Unit cell dimensions	a = 20.2861(8) Å, α = 90 deg. b = 13.1769 (5) Å, β = 103.124(2) deg. c = 30.6650(12) Å, γ = 90 deg.
Volume	7982.9(5) Å^3
Z, Calculated density	4, 1.381 g/cm^3
Absorption coefficient	0.645 mm^{-1}
F(000)	3428
Crystal size	0.1 x 0.1 x 0.4 mm
θ range for data collection	1.90 to 28.28 deg.
Limiting indices	$-27 \le h \le 26$, $0 \le k \le 17$, $0 \le l \le 40$
Reflections collected /unique	19735 /19735 [R(int) = 0.0000]
Observed reflections [I>2σ(I)]	13781
Completeness to θ = 28.28	99.6 %
Absorption correction	Semi-empirical from equivalents
Refinement method	Full-matrix least-squares on F^2
Data / restraints / parameters	19735 / 0 / 844
Goodness-of-fit on F^2 [a]	1.049
Final R indices [I>2σ(I)]	R1 [b] = 0.0661, wR2 [c] = 0.1609
R indices (all data)	R1 [b] = 0.0920, wR2 [c] = 0.1743
Largest diff. peak and hole	0.920 and -0.451 e. Å^{-3}

[a] Goof = $\Sigma[[w(F_o^2 - F_c^2)2]/(n-p)]^{1/2}$.
[b] R1 = $\Sigma||F_o| - |F_c||/\Sigma|F_o|$.
[c] wR2 = $\{\Sigma\omega|[(F_o^2 - F_c^2)^2]/\Sigma\omega F_o^4\}^{1/2}$; $\omega = [(F_o^2, \theta) + 2F_c^2]/3$.

2.2.4 Reaction of $Mo_2(O_2C\text{-}C{\equiv}C\text{-}H)_4(THF)_2$ (2) with *cis*-$RuCl_2(dppm)_2$ (6)

Similar to the reaction of Cp*Fe(dppe)Cl with alkynes,[2,4] the reactions of terminal alkynes at the ruthenium (II) center in complex **6** leads to the formation of reactive ruthenium (II) vinylidene species.[42,43] Deprotonations of the vinylidene complexes with bases such as NEt_3 and DBU (1,8-diazabicyclo[5.4.0]undec-7-ene) produce σ-acetylide complexes.[9,11,44-46] So the reaction of *cis*-$RuCl_2(dppm)_2$ with complex **2** as proposed Mo-Ru cluster in Scheme 2-1 is reasonable.

Stirring a solution of complex **6** and **2** in dichloromethane overnight in the presence of $NaPF_6$ resulted in a color change from yellow to red and then brown. Addition of DBU followed by the chromatography on the alumina column gave a yellow green solid. Recrystallization from CH_2Cl_2/hexane afforded complex **7** as green solid, which was characterized by ^1H, ^{13}C and ^{31}P NMR.

The ^1H NMR spectrum of **7** shows a multiplet at 5.24 ppm due to $=CH_2$. The C atom of this group is shown at 91.3 ppm in the ^{13}C NMR spectrum. Similar to complex **5**, no signal at the region of 160 to 200 ppm is observed in the ^{13}C NMR spectrum of **7**. These results prove that there is no molybdenum carboxylate center in complex **7** and suggest that the compound may be a ruthenium vinylidene. The dppm ligands display a signal at 2.37 ppm in ^1H NMR, a triplet at 46.8 ppm in ^{13}C NMR and a singlet at -14.76 ppm in ^{31}P NMR, which indicates that the two dppm ligands are *trans* to each other. The ^{31}P NMR spectrum of **7** also shows a septet at -143.2 ppm from the P atom of PF_6^-. These spectroscopic results are similar to those of trans-$[(dppm)_2ClRu{=}C{=}CH_2]PF_6$ reported by Touchard *et al.*[9] The X-ray

structure of compound **7** shown in Figure 2-2 is also the same as reported previously.[9]

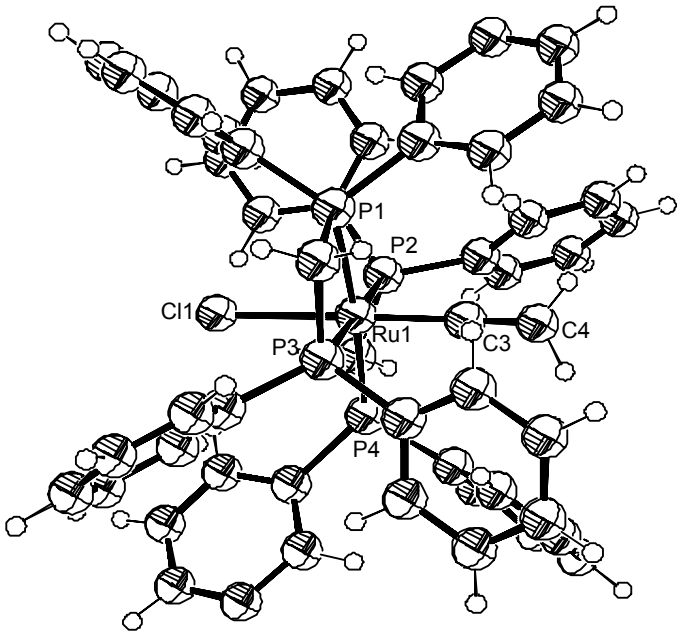

FIGURE 2–2. STRUCTURE OF THE CATION OF [*trans*-Ru(dppm)$_2$Cl (=C=CH$_2$)]PF$_6$ (**7**) WITH 50% THERMAL ELLIPSOIDS.[9]

2.2.5 Reaction of $Mo_2(O_2C\text{-}C{\equiv}C\text{-}Si(CH_3)_3)_4$ (3) with $Co_2(CO)_6$(dppm) (8)

$Co_2(CO)_6$(dppm) (**8**) reacts with alkynes to form complexes with alkyne-Co_2 units. The chemistry of these kinds of complexes is well known. So reaction of compound **3** with $Co_2(CO)_6$(dppm) (**8**) should lead to the proposed Mo-Co cluster in Scheme 2-1.

Reaction of complex **3** with compound **8** in the mixture of toluene and THF for 2 days at 110 ºC resulted in a dark brown solid. Chromatography on a silica gel column gave two bands. Elution with CH_2Cl_2/hexane (1:1) provided a green-brown solid (**9**), which was characterized by IR, ^{1}H, ^{13}C and ^{31}P NMR. The IR spectrum

shows three CO bands at 2005, 1969, 1759 cm^{-1}, which indicate that the complex has terminal and bridging CO ligands.[35] The ^{1}H NMR spectrum of **9** shows a broad peak at 3.60 ppm and the ^{31}P NMR spectrum gives a singlet at 24.5 ppm, which proves the presence of dppm ligands. The C atoms of the carbonyl ligands are not observed in the ^{13}C NMR. Furthermore, the carbon atoms of the alkyne and molybdenum carboxylate are not observed. The spectroscopic information plus the X-ray diffraction analysis (*vide infra*) of **9** demonstrate that the compound is not the one with alkyne-Co_2 unit, but a cluster of cobalt. The formula of **9** is $Co_4(\mu\text{-}CO)_3(CO)_5(dppm)_2$ and the structure is shown in Figure 2-3 and Figure 2-4.

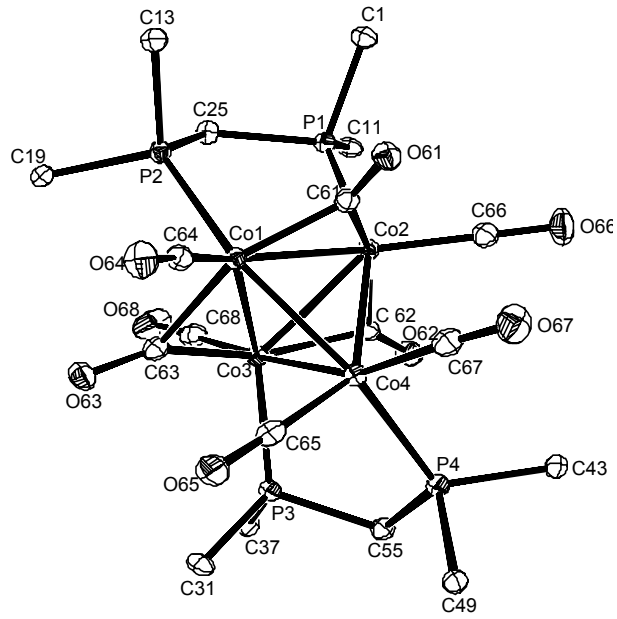

FIGURE 2–3. THE CORE OF THE MOLECULAR STRUCTURE OF $Co_4(\mu\text{-}CO)_3(CO)_5(dppm)_2$ (**9**). THE PHENYL GROUPS AND H ATOMS HAVE BEEN OMITTED FOR CLARITY.

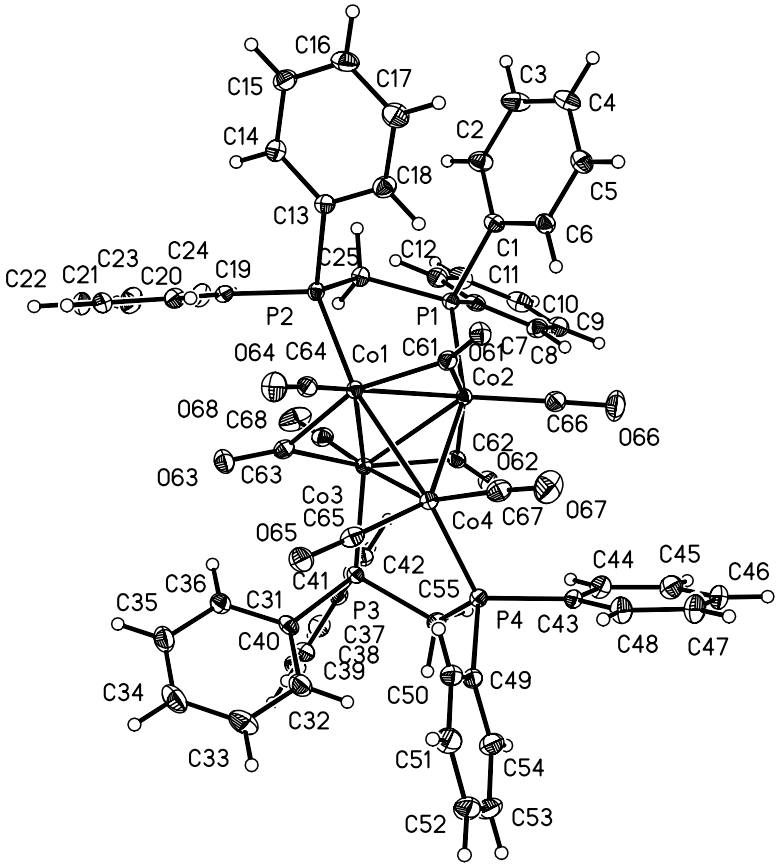

FIGURE 2–4. MOLECULAR STRUCTURE OF $Co_4(\mu\text{-}CO)_3(CO)_5(dppm)_2$ (**9**) WITH 50% THERMAL ELLIPSOIDS.

The second red compound was eluted with CH_2Cl_2. The IR spectrum of the compound not only shows the absorptions of the terminal CO ligands at 2023, 1996, 1975 and 1957 cm^{-1}, but also shows the bands of the carboxylic acid ($\nu_{O\text{-}H}$ 3050.9 cm^{-1}, $\nu_{C=O}$ 1638.2 cm^{-1} and ν_{C-O} 1243.9 cm^{-1}).[30] However, the frequencies of carboxylate group bridging the two molybdenum atoms (1514 and 1443 cm^{-1}) are not seen. Thus, there may be no molybdenum center in this new species (**10**). The ^1H NMR spectrum of **10** shows a multiple signal from the H atoms of the

dppm ligand at 3.02 ppm and a singlet at 0.30 ppm due to the trimethylsilyl group. The carboxylic acid group displays a singlet at 182.2 ppm in ^{13}C NMR spectrum, in which the two signals of the C atoms of alkyne at 89.1 and 86.4 ppm and the peaks from CO at 208.7 and 202.4 ppm are observed. Based on the IR and NMR spectroscopic information, it is difficult to formulate the structure of **10**. X-ray diffraction analysis provides the solution with the structure of **10** shown in Figure 2-5, and its formula is $Co_2(CO)_4$(dppm)(μ-Me_3Si−C≡C−COOH).

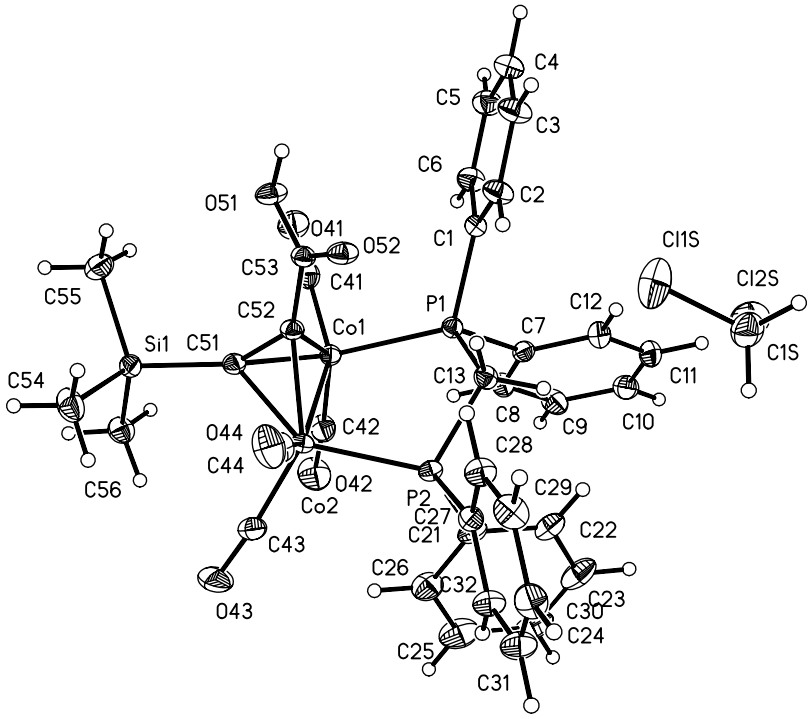

FIGURE 2–5. MOLECULAR STRUCTURE OF $Co_2(CO)_4$(dppm)(μ-Me_3Si−C≡C−COOH) (**10**) WITH 50% THERMAL ELLIPSOIDS (SOLVENT (CH_2Cl_2) IS INCLUDED).

Yields of **9** and **10** are strongly dependent on the conditions employed for the reaction and the procedure described gives the best yields for compound **10**. By

decreasing the temperature to 80 ºC and reducing the reaction time to 24 hours, the yield of **9** increases and the yield of **10** decreases.

2.2.6 X-ray structure determination of $Co_4(\mu\text{-}CO)_3(CO)_5(dppm)_2$ (9)

The molecular structure of **9**, established by an X-ray diffraction study, is shown in Figure 2-4. The asymmetric unit contains one metal cluster and two dichloromethane solvent molecules, one of which is two-fold disordered, with 70%/30% occupancies for the chlorine atoms. The crystal data and structure refinement information are given in Table 2-3. The important bond lengths and angles are listed in Table 2-4.

The molecule contains a central tetrahedron of cobalt atoms bridged on three edges by CO group. These bridges are approximately symmetrical, which is similar to the configuration found in its Rh analogue.[47] The diphosphine ligands (dppm) span the edges Co(1)–Co(2) and Co(3)–Co(4) and the molecule has no element of symmetry. The factor which is mainly responsible for negating any possible symmetry is the diphosphine bridge across Co(3) and Co(4).

The basal–basal cobalt–cobalt bonding distances have little scatter, varying from 2.4309(3) to 2.4952(3)Å [Co(1)–Co(2) 2.4309(3) Å, Co(2)–Co(3) 2.4776(3) Å, Co(1)–Co(3) 2.4952(3) Å]. While, the apical–basal cobalt–cobalt bonds have a narrower range from 2.5045(3) to 2.5415(3) Å [Co(1)–Co(4) 2.5130(3) Å, Co(2)–Co(4) 2.5045(3) Å, Co(3)–Co(4) 2.5415(3) Å]. The average cobalt–cobalt bond distance (2.493 Å) is in close agreement with that determined in the parent $Co_4(CO)_{12}$ species (2.492 Å).[47-51]

TABLE 2–3. CRYSTAL DATA AND STRUCTURE REFINEMENT FOR $Co_4(\mu\text{-}CO)_3(CO)_5(dppm)_2$ (**9**).

Empirical formula	$C_{60}H_{48}Cl_4Co_4O_8P_4$
Formula weight	1398.38
Temperature	100(2) K
Wavelength	0.71073 Å
Crystal system, space group	Orthorhombic, Pbca
Unit cell dimensions	a = 23.8784(10) Å, α = 90 deg. b = 20.1025 (8) Å, β = 90 deg. c = 24.0660(10) Å, γ = 90 deg.
Volume	11552.1(8) $Å^3$
Z, Calculated density	8, 1.608 g/cm^3
Absorption coefficient	1.480 mm^{-1}
F(000)	5664
Crystal size	0.08 x 0.1 x 0.4 mm
θ range for data collection	1.90 to 28.31 deg.
Limiting indices	$-31 \le h \le 31$, $-26 \le k \le 26$, $-32 \le l \le 32$
Reflections collected / unique	123367 / 14358 [R(int) = 0.0557]
Completeness to θ = 28.32	99.9 %
Absorption correction	Empirical
Max. and min. transmission	1.0000 and 0.8396
Refinement method	Full-matrix least-squares on F^2
Data / restraints / parameters	14358 / 0 / 741
Goodness-of-fit on F^2 [a]	1.030
Final R indices [I>2σ(I)]	R1 [b] = 0.0292, wR2 [c] = 0.0657
R indices (all data)	R1 [b] = 0.0389, wR2 [c] = 0.0703
Largest diff. peak and hole	0.470 and -0.358 e. $Å^{-3}$

[a] $\text{Goof} = \Sigma[[w(F_o^2 - F_c^2)2]/(n\text{-}p)]^{1/2}$.
[b] $R1 = \Sigma||F_o| - |F_c||/\Sigma|F_o|$.
[c] $wR2 = \{\Sigma\omega|[(F_o^2 - F_c^2)^2]/\Sigma\omega F_o^4\}^{1/2}$; $\omega = [(F_o^2, \theta) + 2F_c^2]/3$.

TABLE 2–4. SELECTED BOND LENGTHS [Å] AND ANGLES [DEG] FOR $Co_4(\mu\text{-}CO)_3(CO)_5(dppm)_2$ (**9**).

Co(1) – Co(2)	2.4309(3)	Co(2) – C(61)	1.9382(18)
Co(1) – Co(3)	2.4952(3)	Co(2) – C(62)	1.8950(18)
Co(1) – Co(4)	2.5130(3)	Co(3) – C(62)	1.9496(18)
Co(2) – Co(3)	2.4776(3)	Co(3) – C(63)	1.9121(18)
Co(2) – Co(4)	2.5045(3)	Co(1) – P(2)	2.1998(5)
Co(3) – Co(4)	2.5415(3)	Co(2) – P(1)	2.2009(5)
Co(1) – C(61)	1.8857(18)	Co(3) – P(3)	2.2033(5)
Co(1) – C(63)	1.9288(18)	Co(4) – P(4)	2.2181(5)
Co(3) – Co(1) – Co(2)	60.375(10)	Co(1) – C(63) – Co(3)	79.67(7)
Co(1) – Co(2) – Co(3)	61.097(9)	Co(2) – C(62) – Co(3)	80.23(7)
Co(1) – Co(3) – Co(2)	58.528(9)	P(2) – Co(1) – Co(2)	97.973(16)
Co(3) – Co(4) – Co(1)	59.159(9)	P(1) – Co(2) – Co(1)	97.094(15)
Co(3) – Co(1) – Co(2)	58.808(9)	P(3) – Co(3) – Co(4)	87.598(15)
Co(1) – Co(1) – Co(2)	57.956(9)	P(4) – Co(4) – Co(3)	98.614(15)
Co(1) – C(61) – Co(2)	78.93(7)		

2.2.7 X-ray structure determination of $Co_2(CO)_4(dppm)(\mu\text{-}Me_3Si{-}C{\equiv}C{-}COOH)$ (10)

The detailed structure of **10** was examined by X-ray crystal structure analysis. A view of the molecule is shown in Figure 2-5. The crystallographic data are listed in Table 2-5 and the selected bond lengths and angles are summarized in Table 2-6.

TABLE 2–5. CRYSTAL DATA AND STRUCTURE REFINEMENT FOR $Co_2(CO)_4(dppm)(\mu\text{-}Me_3Si{-}C{\equiv}C{-}COOH)$ (**10**).

Empirical formula	$C_{36}H_{34}Cl_2Co_2O_6P_2Si$
Formula weight	841.42
Temperature	100(2) K
Wavelength	0.71073 Å
Crystal system, space group	Monoclinic, P2(1)/n
Unit cell dimensions	a = 17.7893(6) Å, α = 90 deg. b = 12.6322 (5) Å, β = 117.2560 deg. c = 19.0332(7) Å, γ = 90 deg.
Volume	3802.2(2) $Å^3$
Z, Calculated density	4, 1.470 g/cm^3
Absorption coefficient	1.172 mm^{-1}
F(000)	1720
Crystal size	0.1 x 0.2 x 0.4 mm
θ range for data collection	2.01 to 30.52 deg.
Limiting indices	$-25 \le h \le 25$, $-18 \le k \le 18$, $-27 \le l \le 27$
Reflections collected / unique	47953 / 11606 [R(int) = 0.0268]
Completeness to θ = 30.52	99.8 %
Absorption correction	Empirical
Max. and min. transmission	1.0000 and 0.9063
Refinement method	Full-matrix least-squares on F^2
Data / restraints / parameters	11606 / 0 / 446
Goodness-of-fit on F^2 [a]	1.043
Final R indices [I>2σ(I)]	R1 [b] = 0.0292, wR2 [c] = 0.0751
R indices (all data)	R1 [b] = 0.0342, wR2 [c] = 0.0780
Largest diff. peak and hole	0.581 and -0.327 e. $Å^{-3}$

[a] $\text{Goof} = \Sigma[[w(F_o^2 - F_c^2)2]/(n\text{-}p)]^{1/2}$.
[b] $R1 = \Sigma||F_o| - |F_c||/\Sigma|F_o|$.
[c] $wR2 = \{\Sigma\omega|[(F_o^2 - F_c^2)^2]/\Sigma\omega F_o^4\}^{1/2}$; $\omega = [(F_o^2, \theta) + 2F_c^2]/3$.

TABLE 2–6. SELECTED BOND LENGTHS [Å] AND ANGLES [DEG] FOR $Co_2(CO)_4(dppm)(\mu\text{-}Me_3Si{-}C{\equiv}C{-}COOH)$ (**10**).

Co(1) – Co(2)	2.5012(2)	C(52) – C (53)	1.4560(16)
Co(1) – C (51)	1.9765(12)	C(53) – O(52)	1.2340(15)
Co(1) – C(52)	1.9417(12)	C(53) – O(51)	1.3194(15)
Co(2) – C(51)	1.9886(13)	C(51) – Si(1)	1.8455(13)
Co(2) – C(52)	1.9353(12)	Co(1) – P(1)	2.2324(4)
C(51) – C (52)	1.3575(17)	Co(2) – P(2)	2.2059(4)
C(52) – C(51) – Si(1)	146.74(10)	C(52) – Co(1) – P(1)	94.80(4)
C(51) – C(52) – C(53)	137.60(12)	P(1) – Co(1) – Co(2)	98.547(11)
C(52) – C (53) – O(51)	113.28(11)	P(2) – Co(2) – Co(1)	89.685(11)
P(1) – C(13) – P(2)	108.246(2)	C(51) – Co(2) – P(2)	138.61(4)
C(51) – Co(1) – P(1)	134.71(4)	C(52) – Co(2) – P(2)	107.63(4)

The molecule consists of a distorted tetrahedral (μ-alkyne)dicobalt core, which is evidenced by the nonequivalence of the Co–C bond lengths [Co(1)–C(51) 1.9765(12) Å, Co(1)–C(52) 1.9417(12) Å, Co(2)–C(51)1.9886(13) Å, Co(2)–C(52) 1.9353(12) Å]. The alkyne C(51)–C(52) bond length is 1.3575(17) Å, in reasonable agreement with those found in other C_2Co_2 system.[26,52] The C_2Co_2 unit is linked to the carboxylic group (C(52)–C(53) bond distance is 1.4560(16) Å.) and the Me_3Si group (C(51)–Si(1) bond length is 1.8455(13) Å.) directly. The alkyne unit adopts the normal *cis*-bent configuration, as expected for perpendicular acetylenes. The alkyne bend-back angle to the Me_3Si substitute, Si(1)–C(51)–C(52), is 146.74(10)º,

and to the carboxylic group, C(51)–C(52)–C(53), is 137.60(12)º. The C–O bond distances are 1.2340(15) Å (C(53)–O(52)) and 1.3194(15) Å (C(53)–O(51)) respectively, which are all reasonable for the C=O and C–O.[30,53]

Each cobalt atom has one "axial" and one "pseudo-equatorial" CO ligand and a P donor atom from the dppm ligand in the alternative equatorial site. The dppm ligand adopts μ-η^2 coordination bridging the Co–Co bond. The Co(1)–Co(2) bond distance is 2.5012(2) Å, which is longer than that in most (μ-alkyne)dicobalt complexes with (μ-η^2)-bound dppm ligand. [54-56] In such compounds Co–Co bond distances are generally in the range 2.46-2.47 Å. The extension of the Co–Co bond may be due to the steric effect of the trimethylsilyl group.

2.3 Discussion

Although the reactions of compounds **4**, **6** and **8** with terminal alkynes or trimethylsilyl substituted terminal alkynes are well known, and the proposed synthetic strategy for the clusters are quite reasonable, the syntheses of the clusters proposed in Scheme 2-1 all failed to produce the desired square of metal complexes. The reactions of complexes **4**, **6** and **8** with the molybdenum propiolate are much more complicated than the reactions of the same metal complexes with simple alkynes.

It has been reported that access to $(Cp^*Fe(dppe))_n$-alkyne compounds is feasible from the protected trimethylsilyl alkyne precursor using *in situ* deprotection in the presence of methanol, KF and KPF_6. This route was proven to

be both more direct and safer.[6] The first step of the reaction is the fluoride-induced cleavage of the terminal trimethylsilyl group to form a terminal alkyne and a base (CH_3OK). The PF_6^- anion acts as a halide abstractor[37] to form [Cp*Fe(dppe)][PF_6]. In the experimental conditions employed, it was shown that 16-electron species [Cp*Fe(dppe)][PF_6], in equilibrium with the chloro complex Cp*Fe(dppe)Cl, is easily reduced by a base into the 17-electron iron (I) radical [Cp*Fe(dppe)]$^{\cdot}$.[40]

It is known that radicals can cause degradation of carboxylate compounds.[57,58] So possibly the iron (I) radical may promote decomposition of the Mo_2 center ($Mo_2(O_2C{-}C{\equiv}CSi(CH_3)_3)_4(THF)_2$) and the resultant alkyne reacts with CH_2 radical coming from solvent (CH_2Cl_2) thereby forming the observed product (**5**). The suggested mechanism is shown in Scheme 2-4.

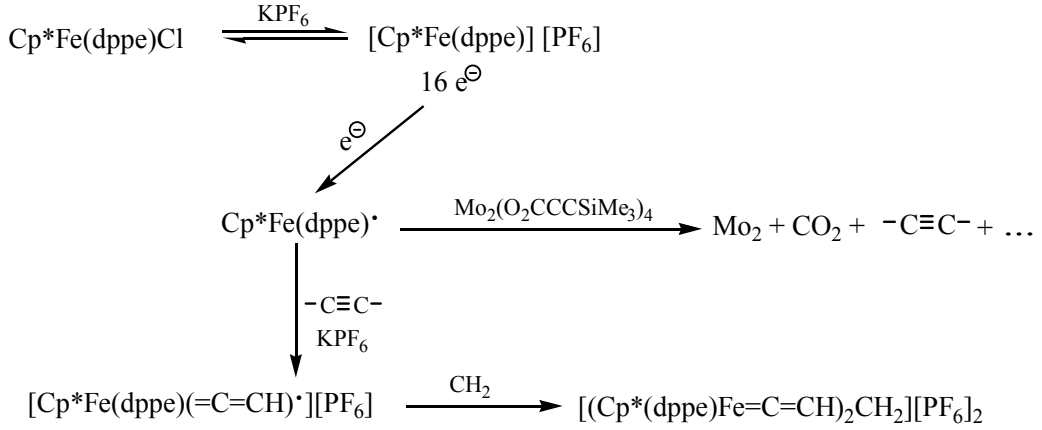

SCHEME 2–4. MECHANISM FOR THE FORMATION OF [{Cp*Fe(dppe)}$_2$(μ-C=CH−CH_2−CH=C)][PF_6]$_2$ (**5**).

Similar to Cp*Fe(dppe)Cl (**4**), reaction of *cis*-Ru(dppm)$_2$Cl$_2$ (**6**) with molybdenum propiolate affords the ruthenium vinylidene compound (**7**). The

mechanism for the formation of ruthenium vinylidene and ruthenium acetylide proposed by Touchard and his coworker[9] is shown is Scheme 2-5. It is likely that a polar solvent favors the dissociation of the Ru–Cl bonds to form a 16-electron fragment $[Ru(dppm)_2Cl]^+$ and then a 17-electron radical. The radical will decompose the molybdenum propiolate and the resulting terminal alkyne may then react with the remaining $[Ru(dppm)_2Cl][PF_6]$ to form complex **7**.

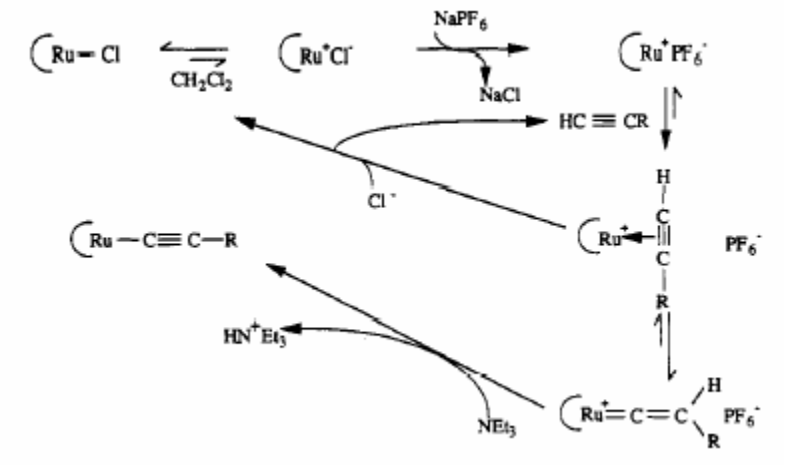

SCHEME 2–5. MECHANISM FOR THE FORMATION OF [*trans*-$Ru(dppm)_2$ $Cl(=C=CH_2)]PF_6$ (**7**) REPRODUCED FROM *Organometallics* **1993**, *12*, 3132-3139.[9]

Although the molecular structure of **7** is the same as reported, the color is totally different. The color of the reported compound is orange, while, the color of compound **7** is green. The green color may come from an impurity of the decomposed molybdenum carboxylate linker.

It is known that the first step in coordination of $Co_2(CO)_8$ or $Co_2(CO)_6(dppm)$ across −C≡C− is the loss of two CO ligands to produce an unsaturated Co_2 species

(30 e) or radical.[59,60] The self-reaction of this fragment forms the cobalt cluster **9**. As described above, the radicals can induce decomposition of the molybdenum compound as shown in Scheme 2-4. One of the possible fragments is $(CH_3)_3Si{-}C{\equiv}C{-}COO^-$ which can then react with the Co_2 species to form complex **10**.

Molybdenum propiolate has the perfect square geometry and active functional groups as the core linker of a molecular square. However, decomposition induced by radicals makes the molybdenum carboxylate center unsuitable for coupling to the "dot" synthons explored under the reaction conditions employed. Therefore a different linker was sought.

Cyclobutadiene is planar and square. If metal fragments with specific properties can be connected with the four carbons of cyclobutadiene directly or through a polyene, four dot square compounds could be synthesized. Due to the π system of the cyclobutadiene, the metals connected by this linker should have a pronounced electronic interaction.

The work in the following chapter is focused on the compounds using cyclobutadiene as the core linker.

2.4 Summary

Linker compounds **2** ($Mo_2(O_2C{-}C{\equiv}CH)_4(THF)_2$) or **3** ($Mo_2(O_2C{-}C{\equiv}CSi(CH_3)_3)_4(THF)_2$) react with the complexes Cp*Fe(dppe)Cl (**4**), *cis*-$Ru(dppm)_2Cl_2$ (**6**) and $Co_2(CO)_6$(dppm) (**8**) respectively. However, in all cases the molybdenum

propiolate linker is decomposed, possibly due to the generation of radicals, and the preparation of the molecular square shown in Scheme 2-1 was not achieved.

The complexes **5**, **7**, **9** and **10** are obtained through the reactions of alkynes arising from the decomposition of molybdenum propiolate with the metal fragments (for **5**, **7**, **10**) or simply from the interaction of the metal fragments (for **9**). Furthermore, new compounds **5**, **9** and **10** are fully characterized.

2.5 Experimental section

General

All reactions were carried out under dry, high-purity nitrogen using standard Schlenk techniques.[61] All solvents except methanol were distilled immediately before use under N_2 from the following drying agents: sodium benzophenone ketyl for hexane, pentane, THF and diethyl ether, molten sodium metal for toluene and calcium hydride for CH_2Cl_2. CH_3OH was spectroscopic grade and dried over activated 3Å molecular sieves before use. The compounds $FeCl_2(dppe)_2$[32] and $RuCl_2(dmso)_4$[34] were prepared by standard literature methods. All other reagents were used as purchased from Aldrich or Strem.

Infrared (IR) spectra were recorded on a Perkin-Elmer Paragon 1000 FT-IR spectrometer, and samples were prepared as KBr pellets. Mass Spectra (FAB^+) were recorded on a JEPL JMS-AX505HA mass spectrometer from a matrix of *p*-nitrobenzyl alcohol.

NMR spectra were taken on 300 MHz Varian UnityPlus FT-NMR instrument (^{1}H at 300 MHz, ^{13}C at 75 MHz, ^{31}P at 121 MHz). All 13C and 31P NMR are proton decoupled. Chemical shifts are given in parts per million (ppm) and coupling constants are given in hertz (Hz). For references, residual protons were used for ^{1}H (C_6D_6: 7.16 ppm; $CDCl_3$: 7.27 ppm; acetone-d_6: 2.05 ppm) and ^{13}C (C_6D_6: 128.39 ppm; $CDCl_3$: 77.23 ppm; acetone-d_6: 29.92 ppm).

Preparation of $Mo_2(O_2CCH_3)_4$ (1)

Following the literature method,[29] a mixture of $Mo(CO)_6$ (1.392 g, 5.01 mmol), 8 mL of acetic anhydride and 50 mL of glacial acetic acid was refluxed with stirring for 8 hours. The reaction solution was cooled down to the room temperature and the resultant yellow microcrystals were filtered off, washed with ether and dried under vacuum (0.5732 g, 54%). IR (cm^{-1}): 2930.5 (m), 2362.3 (m), 1514.1 (s), 1495.8 (s), 1443.7 (s), 1410.8 (s), 1352.3(s), 1046.3 (w), 1031.8 (w), 936.2 (w), 675.3 (w), 628.4 (s).

Preparation of $Mo_2(O_2C{-}C{\equiv}CH)_4(THF)_2$ (2)

The complexes was prepared followed a modified procedure reported by literature.[27] To a yellow slurry of **1** (0.468 g, 1.09 mmol) in THF (60 mL) was added propiolic acid (0.5 mL, 8.13 mmol) drop by drop with stirring. After 4 hours, the reaction solution was filtered through a 2 cm layer celite bed and the filtrate was evaporated to dryness to give the yellow analysis pure compound. The yield is 0.569 g (87.5%). IR (cm^{-1}): 2117.4 (m, C≡C). ^{1}H NMR (Acetone-d_6): δ 3.91 (s, 4H, C≡CH); 3.61 (m, 8H, CH_2); δ 1.78 (m, 8H, CH_2).

Preparation of $Mo_2(O_2C{-}C{\equiv}CSi(CH_3)_3)_4(THF)_2$ (3)

The method of preparation of compound **3** is similar to that of preparation of compound **2**.[27] To stirred suspension of **1** (97.9 mg, 0.229 mmol) in THF (20mL) were added 0.2 mL of $(CH_3)_3SiC{\equiv}C{-}COOH$ (1.125 mmol), which resulted the solution change to clear immediately. After it was stirred at room temperature for 16 hours, the resultant orange reaction solution was dried under vacuum to give the yellow solid. Recrystallization from THF/hexane at 0 °C gave big yellow-orange crystals (173 mg, 84%). IR (cm^{-1}): 2175.5 (m, C≡C). ^1H NMR (Acetone-d_6): δ 3.62(m, 8H, CH_2), 1.78(m, 8H, CH_2), 0.313 (s, 36H, CH_3). ^{13}C NMR (Acetone-d_6): δ 161.4 (O_2C), 96.8 ($C{\equiv}C$), 91.2 ($C{\equiv}C$), δ 68.1 (CH_2O), 25.8 (CH_2CH_2O), -0.606 ($Si{-}CH_3$). FABMS m/z: 756 ($M^+ - 2THF$).

Preparation of Cp*Fe(dppe)Cl (4)

The compound was prepared by modified synthetic methods.[31] The solution of Cp*-H (0.45 mL, 2.87 mmol) in THF (150 mL) was cooled down to -78°C. To this solution was added n-BuLi (1.6 M in hexane, 2.5 mL, 4.0 mmol) with stirring. The reaction mixture was warm up to the room temperature slowly and the resulted white slurry (Cp*-Li) was not isolated and used in-situ in the next reaction. 1.44g (2.75 mmol) of $Fe(dppe)Cl_2$ in THF (150 ml) was added to the Cp*-Li slurry. The reaction mixture was stirred overnight at room temperature and the solution turned to dark green. The solvent was evaporated under vacuum, the dark residue was extracted with ether and filtered through 2 cm layer celite bed. Removal of the solvent followed by recrystallization from CH_2Cl_2/pentane provided 1.41 g (82%)

of **4** as dark green crystals. ^{1}H NMR (Benzene-d6): δ 8.02-7.05 (m, 20H, Ph), 2.41 (m, 2H, CH_2), 1.83 (m, 2H, CH_2), 1.37 (s, 15H, CH_3).

Reaction of $Mo_2(O_2CCCSi(CH_3)_3)_4(THF)_2$ (3) with Cp*Fe(dppe)Cl (4)

To a solution of **4** (200 mg, 0.32 mmol) in THF (10 mL) was added a solution of **3** (45 mg, 0.06 mmol), KF (19 mg, 0.32 mmol) and KPF_6 (59 mg, 0.32 mmol) in CH_3OH. The reaction mixture was refluxed for 36 hours. The resulting brown solution was evaporated to dryness and the crude residue was extracted with CH_2Cl_2. After removal of the solvent, the orange-brown solid was washed with THF and pentane respectively. Recrystallization from CH_2Cl_2/hexane gave orange crystals **(5)** suitable for X-ray diffraction. IR (cm^{-1}): 1613 (m, C=C), 837 (s, PF_6). ^{1}H NMR (Acetone-d_6): δ 7.8-7.2 (m, 40H, Ph), 4.08 (t, 2H, C=CH), 2.72 (m. 4H, CH_2), 2.95 (m, 4H, CH_2), 1.54 (s, 30H, CH_3). ^{13}C NMR (Acetone-d_6): δ 134.0−129.9 (m, Ph); 121.2 (Fe=C=*C*); 100.5 (Cp ring at Cp*); 10.43 (*C*H_3 at Cp*). ^{31}P NMR (Acetone-d_6): δ 87.5 (s, CH_2*P*); -143.1 (sept, PF_6).

Preparation of *Cis*-$RuCl_2(dppm)_2$ (6)

The literature preparation[33] of this compound was followed. $RuCl_2(dmso)_4$ (0.5 g, 1.03 mmol) was added to a solution of dppm (0.788g, 2.05 mmol) in toluene (40 mL). The suspension was stirred at 80°C for 15 hours during which time the color changed from golden yellow to lemon yellow. The analysis pure precipitate was filtered off, washed with toluene and ether respectively and dried under vacuum. The yield is 0.92 g (95%). ^{1}H NMR ($CDCl_3$): δ 8.4 – 6.5 (m, 40H, Ph), 4.9 (m, 2H, CH_2), 4.7 (m, 2H, CH_2). ^{31}P NMR ($CDCl_3$): δ 0.253 (t, CH_2*P*); -26.01 (t, CH_2*P*).

Reaction of $Mo_2(O_2C\text{-}C{\equiv}C\text{-}H)_4(THF)_2$ (2) with *Cis*-$RuCl_2(dppm)_2$ (6)

To a stirred solution of **6** (200 mg, 0.21 mmol) in CH_2Cl_2 (25 mL) was added to a solution of **2** (27 mg, 0.058 mmol) and $NaPF_6$ (42 mg, 0.25 mmol) in THF (2 mL). The reaction solution was stirred for overnight, then 32 μL of DBU (0.21 mmol) was added to the solution. After another 2 hours, the solvent was removed *in vacuo*. The resulting brown solid was dissolved in a minimum amount of CH_2Cl_2 and run through a neutral Al_2O_3 column. A yellow-green solution was eluted with CH_2Cl_2-THF (10:1). Evaporation of the solvent resulted in a yellow-green solid. Green crystals **(7)** suitable for X-ray analysis were obtained by crystallization from CH_2Cl_2/hexane. ^{1}H NMR ($CDCl_3$): δ 7.60~7.20 (m, 40H, Ph), 5.24 (m, J = 4.8 Hz, 4H, CH_2), 2.37 (quint, $^4J_{P\text{-}H}$ = 3 Hz, 2H, =CH_2). ^{13}C NMR ($CDCl_3$): δ 133.79~128.64 (m, Ph at dppm), 91.289 (s, =*C*H_2), 46.798 (t, *C*H_2). ^{31}P NMR ($CDCl_3$): δ -14.76 (s, CH_2*P*), -143.18 (sept, PF_6).

Preparation of $Co_2(CO)_6$(dppm) (8)

The compound was prepared with the modified synthesized procedures.[35,36] A mixture of $Co_2(CO)_8$ (0.5 g, 1.46 mmol) and dppm (0.563 g, 1.46 mmol) in toluene (25 ml) was stirred at room temperature. After about 2 hours, the evolution of carbon monoxide stopped and the resulting red solution was evaporated to dryness. The crude residue was dissolved in a minimum amount of CH_2Cl_2 and chromatographed on a neutral Al_2O_3 column. The major orange-red band was eluted with CH_2Cl_2/hexane (1:1). After removal of the solvent, the orange-red solid was recrystallized from CH_2Cl_2/hexane to give the red crystals (505mg, 54.5%). IR

(cm^{-1}): 2043.9, 1997.1, 1982.3, 1972.0, 1809.6, 1796.9 (s, CO). ^{1}H NMR ($CDCl_3$): δ 7.5 – 7.2 (m, 20H, Ph), 2.94 (t, $^{2}J_{P-H}$ = 10 Hz, 2H, CH_2). ^{31}P NMR ($CDCl_3$): δ 61.4 (s, *P*CH_2*P*).

Reaction of $Mo_2(O_2C\text{-}C{\equiv}C\text{-}Si(CH_3)_3)_4$ (3) with $Co_2(CO)_6$(dppm) (8)

To a solution of **8** (203 mg, 0.320 mmol) in toluene (40 mL) was added a solution of **3** (60 mg, 0.08 mmol) in THF (10 mL) with stirring. The reaction mixture was refluxed for 2 days and the solvent was removed *in vacuo*. The residue was dissolved in a minimum amount of toluene and chromatographed on a silica gel column. The first green brown band was eluted with CH_2Cl_2/hexane (1:1). After removal of the solvent, the resultant solid was recrystallization from CH_2Cl_2/hexane to give green-brown need crystals **(9).** IR (cm^{-1}): 2005.6, 1969.1, 1759.9 (s, CO). ^{1}H NMR (C_6D_6): δ 7.5 ~ 6.9 (m, 80H, ph), 3.60 (b, 8H, CH_2). ^{31}P NMR (C_6D_6): δ 24.5 (s, *P*CH_2*P*). ^{13}C NMR (C_6D_6): δ 137.6 ~ 127.8 (m, Ph), 45.2 (t, P*C*H_2P).

The followed major red band was eluted with CH_2Cl_2. The solvent was removed *in vacuo* and the resulting red solid was recrystallized from CH_2Cl_2/hexane to provide red crystals **(10)**. IR (cm^{-1}): 3050.9 (m, O−H), 2023.6 (s, CO), 1996.2 (s, CO), 1975.5 (s, CO), 1957.5 (s, CO), 1638.2 (m, C=O), 1243.9 (m, C−O). ^{1}H NMR (C_6D_6): δ 7.49 ~ 6.71 (m, 20H, Ph), 3.02 (m, 2H, CH_2), 0.30 (s, 9H, CH_3). ^{31}P NMR (C_6D_6): δ 37.9 (s, *P*CH_2*P*). ^{13}C NMR (C_6D_6): δ 208.7, 202.4 (2×br, *C*O), 182.2 (s, O_2C), 131.6 ~ 128.5 (m, Ph), 89.1, 86.4 (2×s, *C*≡*C*), 38.4 (t, P*C*H_2P), δ 1.75(s, *C*H_3).

Structure Determinations

Single crystals of **5**, **7**, **9** and **10** suitable for X-ray single-crystal diffraction were obtained by slow diffusion from CH_2Cl_2 to hexane. The crystals were placed in inert oil, mounted on a glass pin, and transferred to the cold gas stream of the diffractometer. Crystal data were collected and integrated using a Bruker Apex system, with graphite monochromated Mo-Kα (λ = 0.71073 Å) radiation at 100K. The structures were solved by heavy atom methods using SHELXS-97 and refined using SHELXL-97 (Sheldrick, G.M., University of Göttingen). Non-hydrogen atoms were found by successive full matrix least squares refinement on F^2 and refined with anisotropic thermal parameters.

For compound **5**, hydrogen atoms were generated at idealized positions, except for the four hydrogen atoms on the bridging C5 chain, which were located from the difference map and a riding model with fixed thermal parameters [$u_{ij} = 1.2U_{ij}$(eq) for the atom to which they are bonded], was used for subsequent refinements. The asymmetric unit contained one dimer and two PF_6^- counterions, as well as 1.5 dichloromethane molecules, which are disordered. Attempts to model the disordered molecules as discrete sites were less satisfactory than modeling with the SQUEEZE routine of PLATON (Spek, T., University of Utrecht, 2004.)

For compound **9**, hydrogen atom positions were located from difference Fourier maps and a riding model with fixed thermal parameters [$u_{ij} = 1.2U_{ij}$(eq) for the atom to which they are bonded], was used for subsequent refinements. The asymmetric unit contains one metal cluster and two dichloromethane solvent

molecules, one of which is two-fold disordered, with 70%/30% occupancies for the chlorine atoms.

For compound **10**, hydrogen atom positions were placed at idealized positions and a riding model with fixed thermal parameters [$u_{ij} = 1.2U_{ij}(eq)$ for the atom to which they are bonded], was used for subsequent refinements, except for the carboxylic acid proton H51, which was located from the difference Fourier map and refined isotropically.

2.6 References

(1) Paul, F.; Lapinte, C. *Coord. Chem. Rev.* **1998**, *180*, 431-509.

(2) Lenarvor, N.; Lapinte, C. *J. Chem. Soc., Chem. Commun.* **1993**, 357-359.

(3) Lenarvor, N.; Lapinte, C. *Organometallics* **1995**, *14*, 634-639.

(4) Lenarvor, N.; Toupet, L.; Lapinte, C. *J. Am. Chem. Soc.* **1995**, *117*, 7129-7138.

(5) Mahias, V.; Cron, S.; Toupet, L.; Lapinte, C. *Organometallics* **1996**, *15*, 5399-5408.

(6) Weyland, T.; Lapinte, C.; Frapper, G.; Calhorda, M. J.; Halet, J. F.; Toupet, L. *Organometallics* **1997**, *16*, 2024-2031.

(7) Le Stang, S.; Paul, F.; Lapinte, C. *Organometallics* **2000**, *19*, 1035-1043.

(8) Hurst, S. K.; Cifuentes, M. P.; McDonagh, A. M.; Humphrey, M. G.; Samoc, M.; Luther-Davies, B.; Asselberghs, I.; Persoons, A. *J. Organomet. Chem.* **2002**, *642*, 259-267.

(9) Touchard, D.; Haquette, P.; Pirio, N.; Toupet, L.; Dixneuf, P. H. *Organometallics* **1993**, *12*, 3132-3139.

(10) Haquette, P.; Pirio, N.; Touchard, D.; Toupet, L.; Dixneuf, P. H. *J. Chem. Soc., Chem. Commun.* **1993**, 163-165.

(11) Long, N. J.; Martin, A. J.; White, A. J. P.; Williams, D. J.; Fontani, M.; Laschi, F.; Zanello, P. *J. Chem. Soc., Dalton Trans.* **2000**, 3387-3392.

(12) Colbert, M. C. B.; Lewis, J.; Long, N. J.; Raithby, P. R.; Younus, M.; White, A. J. P.; Williams, D. J.; Payne, N. N.; Yellowlees, L.; Beljonne, D.; Chawdhury, N.; Friend, R. H. *Organometallics* **1998**, *17*, 3034-3043.

(13) Younus, M.; Long, N. J.; Raithby, P. R.; Lewis, J. *J. Organomet. Chem.* **1998**, *570*, 55-62.

(14) Li, Z. H.; Beatty, A. M.; Fehlner, T. P. *Inorg. Chem.* **2003**, *42*, 5707-5714.

(15) Li, Z. H.; Fehlner, T. P. *Inorg. Chem.* **2003**, *42*, 5715-5721.

(16) Rubin, Y.; Knobler, C. B.; Diederich, F. *J. Am. Chem. Soc.* **1990**, *112*, 4966-4968.

(17) Lewis, J.; Lin, B.; Khan, M. S.; Almandhary, M. R. A.; Raithby, P. R. *J. Organomet. Chem.* **1994**, *484*, 161-167.

(18) Worth, G. H.; Robinson, B. H.; Simpson, J. *Organometallics* **1992**, *11*, 3863-3874.

(19) Elder, S. M.; Robinson, B. H.; Simpson, J. *J. Organomet. Chem.* **1990**, *398*, 165-176.

(20) Arewgoda, M.; Rieger, P. H.; Robinson, B. H.; Simpson, J.; Visco, S. J. *J. Am. Chem. Soc.* **1982**, *104*, 5633-5640.

(21) Arewgoda, M.; Robinson, B. H.; Simpson, J. *J. Am. Chem. Soc.* **1983**, *105*, 1893-1903.

(22) Casagrande, L. V.; Chen, T.; Rieger, P. H.; Robinson, B. H.; Simpson, J.; Visco, S. J. *Inorg. Chem.* **1984**, *23*, 2019-2025.

(23) Aggarwal, R. P.; Connelly, N. G.; Crespo, M. C.; Dunne, B. J.; Hopkins, P. M.; Orpen, A. G. *J. Chem. Soc. Chem. Comm.* **1989**, 33-35.

(24) Aggarwal, R. P.; Connelly, N. G.; Crespo, M. C.; Dunne, B. J.; Hopkins, P. M.; Orpen, A. G. *J. Chem. Soc., Dalton Trans.* **1992**, 655-662.

(25) Osella, D.; Milone, L.; Nervi, C.; Ravera, M. *Eur. J. Inorg. Chem.* **1998**, 1473-1477.

(26) McAdam, C. J.; Duffy, N. W.; Robinson, B. H.; Simpson, J. *Organometallics* **1996**, *15*, 3935-3943.

(27) Calvo-Perez, V. C. Ph. D. Thesis, University of Notre Dame, 1996.

(28) Bailey, A.; Fehlner, T. P. *unpublished result*.

(29) Dori, Z.; Wilkinson, G. *Inorg. Synth.* **1972**, *13*, 87-89.

(30) Mehrotra, R. C.; Bohra, R. *Metal carboxylates*; Academic Press: London ; New York, 1983.

(31) Roger, C.; Hamon, P.; Toupet, L.; Rabaa, H.; Saillard, J. Y.; Hamon, J. R.; Lapinte, C. *Organometallics* **1991**, *10*, 1045-1054.

(32) Mays, M. J.; Sears, P. L. *J. Chem. Soc., Dalton Trans.* **1973**, 1873-1875.

(33) Chaudret, B.; Commenges, G.; Poilblanc, R. *J. Chem. Soc., Dalton Trans.* **1984**, 1635-1639.

(34) Evans, I. P.; Spencer, A.; Wilkinson, G. *J. Chem. Soc., Dalton Trans.* **1973**, 204-209.

(35) Chia, L. S.; Cullen, W. R. *Inorg. Chem.* **1975**, *14*, 482-485.

(36) Fukumoto, T.; Matsumura, Y.; Okawara, R. *J. Organomet. Chem.* **1974**, *69*, 437-444.

(37) Bruce, M. I. *Chem. Rev.* **1991**, *91*, 197-257.

(38) Hamon, P.; Toupet, L.; Hamon, J. R.; Lapinte, C. *Organometallics* **1992**, *11*, 1429-1431.

(39) Hamon, P.; Toupet, L.; Hamon, J. R.; Lapinte, C. *J. Chem. Soc., Chem. Commun.* **1994**, 931-932.

(40) Hamon, P.; Toupet, L.; Hamon, J. R.; Lapinte, C. *Organometallics* **1996**, *15*, 10-12.

(41) Iyer, R. S.; Selegue, J. P. *J. Am. Chem. Soc.* **1987**, *109*, 910-911.

(42) Pilette, D.; Ouzzine, K.; Lebozec, H.; Dixneuf, P. H.; Rickard, C. E. F.; Roper, W. R. *Organometallics* **1992**, *11*, 809-817.

(43) Lebozec, H.; Ouzzine, K.; Dixneuf, P. H. *Organometallics* **1991**, *10*, 2768-2772.

(44) Krocher, O.; Koppel, R. A.; Baiker, A. *J. Chem. Soc., Chem. Commun.* **1997**, 453-454.

(45) Zhu, Y. B.; Wolf, M. O.; Yap, G. P. A. *Inorg. Chem.* **1997**, *36*, 5483-5487.

(46) Winter, R. F.; Hornung, F. M. *Organometallics* **1999**, *18*, 4005-4014.

(47) Carre, F. H.; Cotton, F. A.; Frenz, B. A. *Inorg. Chem.* **1976**, *15*, 380-387.

(48) Wei, C. H. *Inorg. Chem.* **1967**, *8*, 2384-2397.

(49) Wei, C. H.; Wilkes, G. R.; Dahl, L. F. *J. Am. Chem. Soc.* **1967**, *89*, 4792-4793.

(50) Wei, C. H.; Dahl, L. F. *J. Am. Chem. Soc.* **1966**, *88*, 1821-1822.

(51) Farrugia, L. J.; Braga, D.; Grepioni, F. *J. Organomet. Chem.* **1999**, *573*, 60-66.

(52) Snaith, T. J.; Low, P. J.; Rousseau, R.; Puschmann, H.; Howard, J. A. K. *J. Chem. Soc., Dalton Trans.* **2001**, 292-299.

(53) Calvo-Perez, V.; Vega, A.; Cortes, P.; Spodine, E. *Inorg. Chim. Acta* **2002**, *333*, 15-24.

(54) Bird, P. H.; Fraser, A. R.; Hall, D. N. *Inorg. Chem.* **1977**, *16*, 1923-1931.

(55) Gelling, A.; Jeffery, J. C.; Povey, D. C.; Went, M. J. *J. Chem. Soc., Chem. Commun.* **1991**, 349-351.

(56) Nicolaou, K. C.; Maligres, P.; Suzuki, T.; Wendeborn, S. V.; Dai, W. M.; Chadha, R. K. *J. Am. Chem. Soc.* **1992**, *114*, 8890-8907.

(57) Steffen, L. K.; Glass, R. S.; Sabahi, M.; Wilson, G. S.; Schoneich, C.; Mahling, S.; Asmus, K. D. *J. Am. Chem. Soc.* **1991**, *113*, 2141-2145.

(58) Hiller, K. O.; Masloch, B.; Gobl, M.; Asmus, K. D. *J. Am. Chem. Soc.* **1981**, *103*, 2734-2743.

(59) Greenfield, H.; Sternberg, H. W.; Friedel, R. A.; Wotiz, J. H.; Markby, R.; Wender, I. *J. Am. Chem. Soc.* **1956**, *78*, 120-124.

(60) Hore, L. A.; McAdam, C. J.; Kerr, J. L.; Duffy, N. W.; Robinson, B. H.; Simpson, J. *Organometallics* **2000**, *19*, 5039-5048.

(61) Shriver, D. F.; Drezdzon, M. A. *The manipulation of air-sensitive compounds*; 2nd ed.; Wiley: New York, 1986.

CHAPTER 3

SYNTHESIS AND CHARACTERIZATION OF $\{(\eta^5\text{-}C_5H_5)Fe(\eta^5\text{-}C_5H_4)\}_4(\eta^4\text{-}C_4)Co(\eta^5\text{-}C_5H_5)$

3.1 Introduction

Chapter 2 describes the synthetic approaches to the molecular squares with molybdenum propiolate as the core. Due to the decomposition of molybdenum propiolate induced by the radicals in the reaction process, the syntheses of molecular squares failed. In this chapter, the work is focused on molecules using cyclobutadiene as the core linker.

Cyclobutadiene, the first member of the benzenoid series, has been studied relatively thoroughly.[1-4] Associated with its planarity, cyclobutadiene has a π-electronic system, which permits the electron transfer from one side to the other side. These properties make cyclobutadiene a potentially good core linker of the square of redox centers for QCA application.

Although various methods and procedures have been used to prepare the cyclobutadiene-metal complexes, dicarbonyl(η^5-cyclopentadienyl) cobalt (CpCo $(CO)_2$) is known to be a convenient and efficient reagent for the dimerization of alkynes to form cyclobutadiene.[5-7] Many CpCo-complexes of cyclobutadienes have

been prepared with $CpCo(CO)_2$.[8-11] The disadvantage of the metal supported dimerization of alkyne is that, for unsymmetrical substituted alkynes isomers are always produced.[12] This is no problem here since in order to gain a "4-dot" symmetrical molecular square, bis-metalsubstituted acetylenes are used to react with $CpCo(CO)_2$.

As described in chapter 2, metal fragments, Cp*Fe(dppe) and $Ru(dppm)_2Cl$, posses specific properties making then suitable as the "dot". However, because of the steric crowding caused by the ancillary ligands, it is impossible to form the bis-metal substituted acetylene for these two metal fragments.

Considerable attention has been given recently to the chemistry of ferrocene, which has played a major role in the rapidly expanding areas of "new material science" such as molecular ferromagnet,[13,14] self assembly[15,16] and molecular sensors.[17,18] Ferrocene has the simple redox behavior and the redox chemistry of biferrocene, which displays two reversible one-electron couples, has attracted attention for many years. In this compound, electronic communication between the two $Fc^{+/0}$ couples is well established.[19-22] So ferrocene is a suitable compound as the "dot" of square molecule for QCA application.

The reaction of biferrocenylacetylene and $CpCo(CO)_2$ has been reported.[23,24] Although the reported electrochemistry of one of the products, $\{CpFe(\eta^5\text{-}C_5H_4)\}_4(\eta^4\text{-}C_4)CoCp$ (**18**), was discouraging (a wave at 0.29 V with the "remaining 3 redox waves blended into a broad wave centered at … 0.4 V), visible and near-IR band positions were published for the 1+, 2+ and 3+ ions generated by bulk

electrolysis.[25] None of these ions were isolated. On the other hand, the latter promising spectroscopic data provided sufficient impetus to revisit the system.[26]

3.2 Results

3.2.1 Synthesis

Starting from ferrocene and ferrocenecarboxaldehyde, the synthetic routes to compounds **11**-**18** are summarized in Scheme 3-1.

(η^5-C_5H_5)Fe(η^5-$C_5H_4CH{=}CCl_2$) (11) and Ferrocenylacetylene (12)

As literature describes,[27] treating ferrocenecarboxaldehyde with 4 equiv. of triphenyl phosphine and 2 equiv. of carbon tetrachloride gives **11**. Treatment of **11** with n-BuLi followed by the hydrolysis results in the formation of **12** (94%). Carbon-carbon triple bond in **12** displays absorption at 2102.8 cm^{-1} in IR spectrum and δ_H 2.72 ppm in ^1H NMR spectrum.

(Tri-n-butylstannyl)ferrocene (13) and Iodoferrocene (14)

The reaction of ferrocene with t-BuLi and then $^nBu_3SnCl$ results in the formation of mono-substituted and bis-substituted compounds.[28] A good yield (63%) of mono-substituted compound **13** could be obtained with the following conditions: ferrocene/t-BuLi/$^nBu_3SnCl$ = 1/2/1.5, metalation at 0 ºC over 60 min in THF/hexane (1:1). ^1H NMR spectrum shows a singlet at 4.12 ppm, two triplets at 4.34 and 4.03 ppm due to the hydrogen atoms on Cp ring, which confirm monosubstitution.

The Fc-Sn bond is readily cleaved by iodine in CH_2Cl_2,[29] leading to pure iodo-ferrocene **14** (74%). Compared with **13**, all hydrogen atoms on ferrocenyl group

shift to lower field due to the iodine substitution in the ^{1}H NMR spectrum (a singlet at 4.21 ppm and two triplets at 4.43 and 4.17 ppm). In ^{13}C NMR spectrum, α-C resonance is not observed.

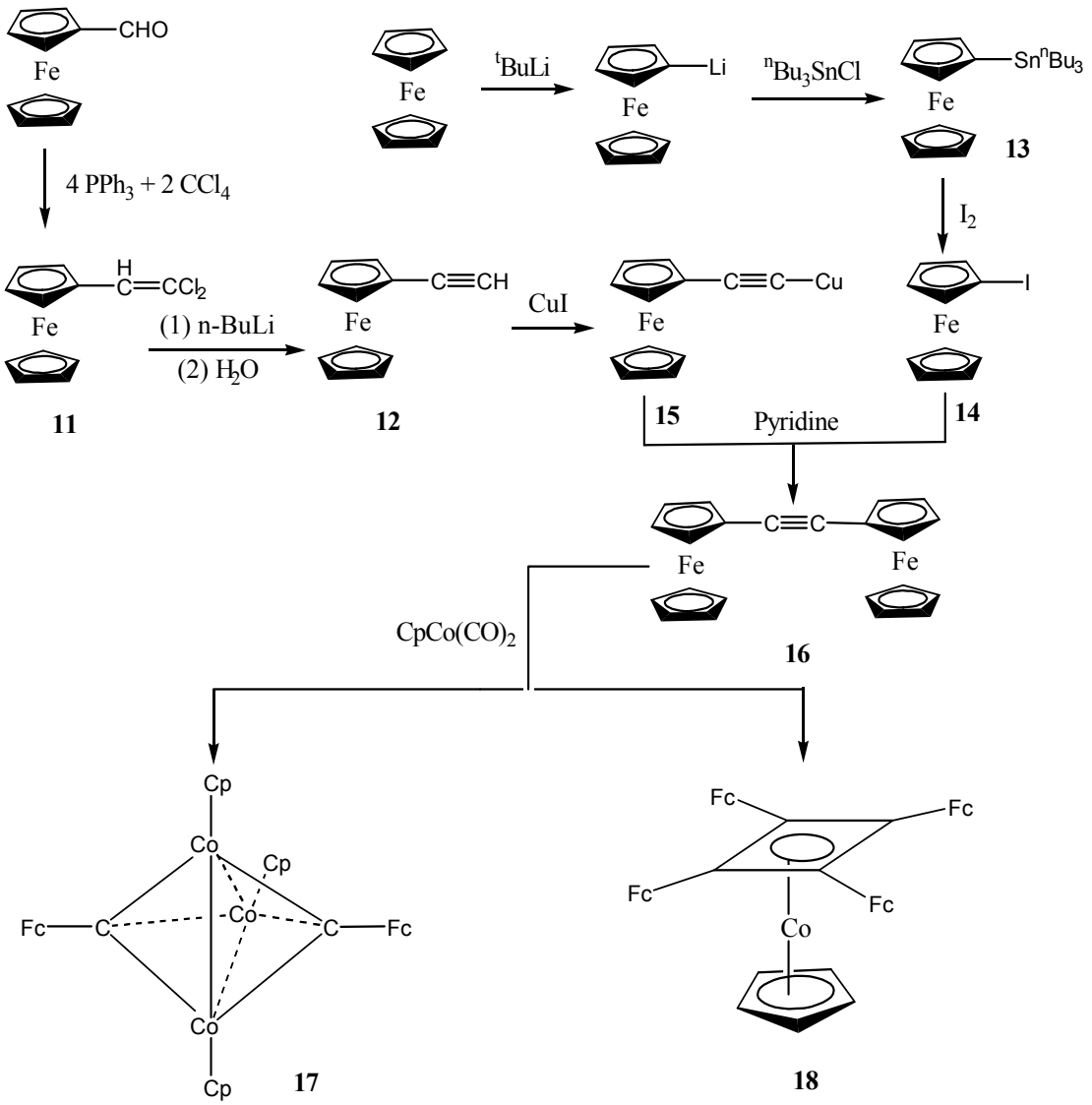

SCHEME 3–1. SYNTHETIC STRATEGY FOR CpFe(η^5-C_5H_4)−C(CpCo)$_3$C−(η^5-C_5H_4)FeCp (**17**) AND {CpFe(η^5-C_5H_4)}$_4$(η^4-C_4)CoCp (**18**).

Cuprous Ferrocenylacetylide (15) and Diferrocenylacetylene (16)

Ferrocenylacetylene (**12**) is easily converted to a stable cuprous salt on treatment with cuprous iodide in ethanolic ammonium solution[30] to obtain **15** as yellow solids, which are purified by washing with ethanol and ether. In order to get the best yield of **15**, the cuprous salt must be washed only briefly with ethanol and ether since continued washing in air leads to the formation of the coupling product.

Diferrocenylacetylene (**16**) is prepared by heating complex **15** in pyridine solution with idioferrocene (**14**). As the literature reported,[31] to purify compound **16**, the crude products are chromatographed on a basic alumina column and eluted with benzene. However, due to the poor solubility of **16**, chromatography results in the reduction of the yield of the product. Actually, washing the crude product with ether several times gives adequately purified compound **16** as confirmed by the spectroscopic data. IR spectrum of **16** shows a band at 2152 cm^{-1} ($\nu_{C\equiv C}$) and in the proton NMR the compound displays a singlet at 4.24 ppm and two triplets at 4.46 and 4.21 ppm. FAB-MS gives the formula weight as 394.

CpFe(η^5-C_5H_4)−C(CpCo)$_3$C−(η^5-C_5H_4)FeCp (17) and {CpFe (η^5-C_5H_4)}$_4$ (η^4-C_4)CoCp (18)

A xylene solution of **16** and $CpCo(CO)_2$ (1:1) is heated to 135 ºC for 24 hours to obtain a red-brown solid. Chromatography on a neutral alumina column gives two bands. The first red-brown band, eluted with hexane/toluene (1:3), is compound **17**. In addition to all the H atoms on the ferrocenyl group, the ^{1}H NMR spectrum also shows a singlet at 4.86 ppm due to the Cp ligands of the Co atoms.

The two μ_3-capping carbon atoms of the cluster display a resonance at 115.2 ppm in the ^{13}C NMR; however, the α-C atoms on the ferrocenyl group are not observed.

Elution with toluene affords compound **18** as brownish orange solid, which was characterized by ^{1}H, ^{13}C NMR and FABMS. The ^{1}H NMR spectrum shows two singlet peaks at 4.82 ppm (Cp ligand of Co) and 4.11 ppm (Cp on ferrocenyl group). The ratio is 1 to 4. The ^{13}C NMR spectrum of the compound presents a peak at 82.9 ppm assigned to cyclobutadiene, which is in agreement with the reported compounds with the similar cyclobutadiene ring.[9,32] According to the NMR spectra at room temperature, the compound is symmetric with a C_4 axis and FAB-MS gives that the formula weight is 912.

The ratio of the starting materials (**16** and $CpCo(CO)_2$) affects the yield of the final products. The synthetic procedure described gives 35% yield of **17** and 30% yield of **18**. If the ratio of **16** to $CpCo(CO)_2$ is changed from 1:1 to 2:1 as reported in literature,[23] only compound **18** is obtained. While, a large excess of $CpCo(CO)_2$ just affords **17**.[24]

3.2.2 X-ray structure determination of $CpFe(\eta^5\text{-}C_5H_4)-C(CpCo)_3C-(\eta^5\text{-}C_5H_4)FeCp$ (17)

The detailed structure of **17** was examined by X-ray crystal structure analysis. The asymmetric unit contains two pentametallic units. One is a *cis* isomer and the other one is a *trans* isomer, as shown in Figure 3-1. The crystallographic data are summarized in Table 3-1 and the selected bond lengths and angles are listed in Table 3-2.

The orientation of the two Fc moieties with respect to the cluster units determines whether the molecule is a *cis* isomer or *trans* isomer. In the *cis* isomer, two C–C bonds connecting the ferrocenyl groups (C(1)–C(2) and C(21)–C(22)) bend to the same side compared to the threefold axis of the cluster unit. While, these C–C bonds (C(51)–C(52) and C(71)–C(72)) bend to different sides in the *trans* isomer.

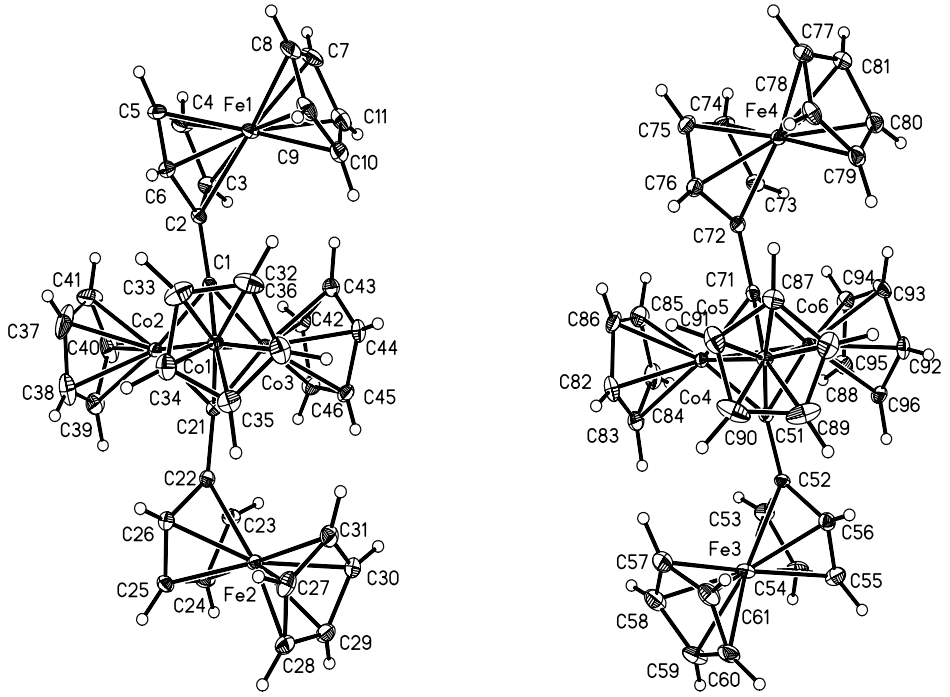

FIGURE 3–1. MOLECULAR STRUCTURE OF CpFe(η^5-C_5H_4)−C(CpCo)$_3$C−(η^5-C_5H_4)FeCp (**17**) WITH 50% THERMAL ELLIPSOIDS. (a): *CIS* ISOMER; (b): *TRANS* ISOMER.

TABLE 3–1. CRYSTAL DATA AND STRUCTURE REFINEMENT FOR

CpFe(η^5-C_5H_4)−C(CpCo)$_3$ C−(η^5-C_5H_4)FeCp (**17**).

Empirical formula	$C_{37}H_{33}Co_3Fe_2$
Formula weight	766.12
Temperature	100(2) K
Wavelength	0.71073 Å
Crystal system, space group	Orthorhombic, Pna2(1)
Unit cell dimensions	a = 41.0505(18) Å, α = 90 deg. b = 15.7638 (7) Å, β = 90 deg. c = 8.8457(4) Å, γ = 90 deg.
Volume	5724.2(4) Å^3
Z, Calculated density	8, 1.778 g/cm^3
Absorption coefficient	2.719 mm^{-1}
F(000)	3104
Crystal size	0.4 x 0.2 x 0.2 mm
θ range for data collection	1.97 to 18.32 deg.
Limiting indices	-54 ≤ h ≤ 54, -21 ≤ k ≤ 21, -11 ≤ l ≤ 11
Reflections collected / unique	60100 / 14163 [R(int) = 0.0218]
Completeness to θ = 18.32	99.6 %
Absorption correction	Empirical
Max. and min. transmission	1.0000 and 0.8030
Refinement method	Full-matrix least-squares on F^2
Data / restraints / parameters	14163 / 1 / 955
Goodness-of-fit on F^2 [a]	1.080
Final R indices [I>2σ(I)]	R1 [b] = 0.0201, wR2 [c] = 0.0493
R indices (all data)	R1 [b] = 0.0208, wR2 [c] = 0.0496
Absolute structure parameter	0.014(7)
Largest diff. peak and hole	0.440 and -0.291 e. Å^{-3}

[a] Goof = $\Sigma[[w(F_o^2 - F_c^2)2]/(n-p)]^{1/2}$.
[b] R1 = $\Sigma||F_o| - |F_c||/\Sigma|F_o|$.
[c] wR2 = $\{\Sigma\omega|[(F_o^2 - F_c^2)^2]/\Sigma\omega F_o^4\}^{1/2}$; $\omega = [(F_o^2, \theta) + 2F_c^2]/3$.

TABLE 3–2. SELECTED BOND LENGTHS [Å] AND ANGLES [DEG] FOR CpFe(η^5-C_5H_4)−C(Cp Co)$_3$C−(η^5-C_5H_4)FeCp (**17**).

C(1) – C(2)	1.454(2)	C(1) – Co(1)	1.874(2)
C(1) – Co(2)	1.8717(17)	C(1) – Co(3)	1.8742(17)
C(21) – Co(1)	1.8808(19)	C(21) – Co(2)	1.8666(19)
C(21) – Co(3)	1.8656(19)	C(21) – C(22)	1.464(3)
Co(1) – Co(2)	2.3697(4)	Co(2) – Co(1) –Co(3)	60.582(11)
Co(1) – Co(3)	2.3733(4)	Co(1) – Co(2) – Co(3)	59.784(11)
Co(2) – Co(3)	2.3923(4)	Co(1) – Co(3) – Co(2)	59.634(11)
C(51) – C(52)	1.458(2)	C(51) – Co(4)	1.8665(17)
C(51) – Co(5)	1.873(2)	C(51) – Co(6)	1.8772(17)
C(71) – C(72)	1.464(3)	C(71) – Co(4)	1.8926(19)
C(71) – Co(5)	1.8832(19)	C(71) – Co(6)	1.8462(19)
Co(4) – Co(5)	2.3593(4)	Co(4) – Co(5) – Co(6)	60.694(11)
Co(4) – Co(6)	2.3945(4)	Co(4) – Co(6) – Co(5)	59.227(10)
Co(5) – Co(6)	2.3799(4)	Co(4) – Co(6) – Co(5)	60.0789(10)

It is known that the CpCo fragment is isolobal to the BH fragment.[33] Thus, the structure of compound **17** is very similar to that of *closo*-$B_3C_2H_5$.[34] The trigonalbipyramidal CCo_3C core in both isomers consists of a triangle of cobalt atoms capped on opposite sides by two μ_3-bonded carbyne ligands, derived from alkyne cleavage of biferrocenylacetylene (FcC≡CFc). Each cobalt atom achieves a filled valence-shell electronic configuration by bonding to two adjacent Co atoms through 2-electron single bonds, to each of the two μ_3-bonded carbyne ligands and

to a Cp ligand. The mean distances between the carbon atoms on the Cp rings and the cobalt atoms are 2.089, 2.079, 2.086, 2.084, 2.085 and 2.082 for Co(1), Co(2), Co(3), Co(4), Co(5) and Co(6) respectively, in a good agreement with the values previously observed in the cobalt cluster with Cp ligands.[35,36] In *cis* isomer, the orientation of these Cp rings with respect to the Co_3 plane is that the dihedral angles are 90.4º (C(32) --- C(36)), 88.1º (C(37) --- C(42)) and 91.2º (C(43) --- C(46)). In *trans* isomer, these dihedral angles are 87.9º (C(82) --- C(86)), 87.9º (C(87) --- C(91)), 86.1º (C(92) --- C(96)). Hence each cobalt bound Cp ring is bent slightly away from an orientation normal to the Co_3 triangle.

For the *cis* isomer, the Co_3 triangle is distorted slightly with the three different Co–Co bonds [Co(1)–Co(2) 2.3697(4) Å, Co(1)–Co(3) 2.3733(4) Å, Co(2)–Co(3) 2.3923(4) Å]. However, the distances of cobalt atoms and the capped carbon atoms show no significant variation. The averaged bond lengths of Co–C(1) and Co–C(21) are 1.873 Å and 1.871 Å respectively, which are in the range normally found in tricobalt biscarbyne complexes.[35-37] The distance between the capping carbyne atoms C(1) ··· C(21) is 2.545 Å. Similar to the *cis* isomer, in *trans* isomer, the three Co–Co bond distances are different [Co(4)–Co(5) 2.3593(4) Å, Co(4)–Co(6) 2.3945(4) Å, Co(5)–Co(6) 2.3799(4) Å]. However, the distances of cobalt atoms and the capped carbon atoms have a little bitter scattering compared with the *cis* isomer. The bond distances for Co–C(51) vary from 1.8665(17) Å to 1.8772(17) Å. For Co–C(71), the range is from 1.8462(19) Å to 1.8926(19) Å. The distance between the capping carbyne atoms C(51) ··· C(71) is 2.548 Å, similar to the *cis* isomer.

In common with many ferrocenyl compounds,[23,36] the Cp ligands in **17** adopt an eclipsed configuration with the twist angles of 4.8º [Fe(1)], 5.1º [Fe(2)], 9.7º [Fe(3)], 6.0º [Fe(4)]. The dihedral angles with each other are 2.7º, 4.0º, 2.2º, 4.3º for Fe(1), Fe(2), Fe(3) and Fe(4) respectively.

3.2.3 X-ray structure determination of {CpFe(η^5-C_5H_4)}$_4$(η^4-C_4)CoCp (18)

The crystals of **18** were grown by slow diffusion of hexane into CH_2Cl_2 solution. The structure of **18** is illustrated in Figure 3-2. The crystallographic data are summarized in Table 3-3 and the relevant bond lengths and angles are listed in Table 3-4.

The Cp ring bonded to cobalt is regular with an average carbon-carbon bond distance of 1.420(2) Å and an average bond angle of 107.99(15)º, which is in good agreement with the similar complexes.[23,38,39] The cyclobutadiene group is square and almost exactly planar. The distance of each atom from the mean plane is 0.0084 Å (2 above, two below the plane). The bond lengths in the cyclobutadiene ring average 1.466(2) Å and the bond angles are very close to 90º. The five and four member rings are almost parallel with a dihedral angle of 3.3º, which is similar to other cobalt-cyclobutadiene-Cp sandwich compounds.[8,10,23]

The cobalt-carbon distances are normal, ranging from 1.9758(16) to 2.0010(15) Å, with an average of 1.9883 Å, for the carbon atoms in the cyclobutadiene ring and from 2.0558(16) to 2.0787(18) Å with an average of 2.0699 Å for the Cp carbons. The distances of cobalt and the ring centers are 1.697 and 1.681 Å for the four and five member rings respectively. The iron-carbon distance in four

ferrocenyl molecules is quite regular.[40] The averaged iron-carbon bond lengths are 2.051, 2.045, 2.047, 2.046 Å for the ferrocenyl groups with Fe(1), Fe(2), Fe(3) and Fe(4) respectively.

The ferrocenyl groups are twisted to some extent about the C–C bonds to the cyclobutadiene ring with the magnitude of the twist given by the torsion angles in the Table 3-4. The positive angle indicates anti-clockwise rotation about the C–C bond when viewed from cobalt atom to the cyclobutadiene ring. The distances between the iron atoms and the cyclobutadiene plane are -0.1530, 2.0850, -0.2955 and 2.1156 Å for Fe(1), Fe(2), Fe(3) and Fe(4) respectively, which indicates that two ferrocenyl groups at the diagonal position are above the four member ring and point away from the cobalt atom and the other two are slightly below the ring as shown in Figure 3-2b. The averaged distance between the iron atoms is 5.862 Å.

The ferrocenyl C_5 rings are in a near eclipsed conformation with the twist angles from eclipsed of 10.1º [Fe(1)], 3.3º [Fe(2)], 7.4º [Fe(3)], 2.2º [Fe(4)]. The dihedral angles with each other are 5.5º, 2.3º, 4.2º, 1.1º for Fe(1), Fe(2), Fe(3) and Fe(4) respectively.

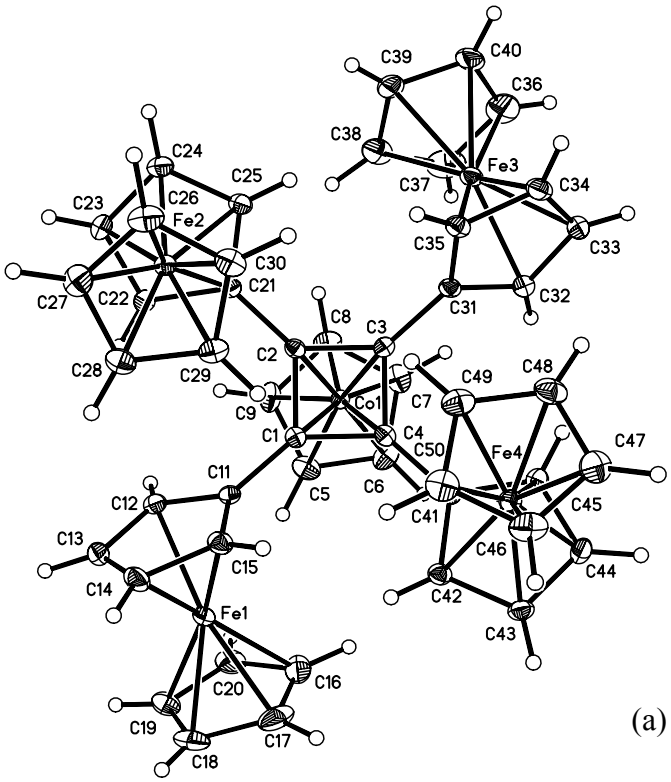

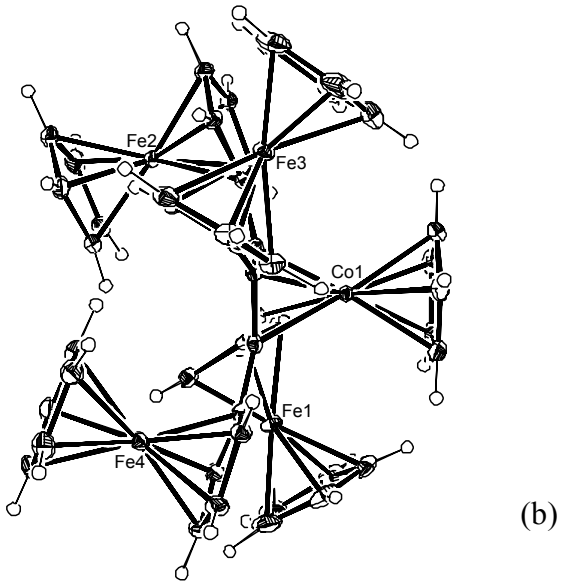

FIGURE 3–2. MOLECULAR STRUCTURE OF $\{CpFe(\eta^5\text{-}C_5H_4)\}_4(\eta^4\text{-}C_4)CoCp$ (**18**) WITH 50% THERMAL ELLIPSOIDS. (a): TOP VIEW; (b): SIDE VIEW.

TABLE 3–3. CRYSTAL DATA AND STRUCTURE REFINEMENT FOR $\{CpFe(\eta^5\text{-}C_5H_4)\}_4(\eta^4\text{-}C_4)$ CoCp (**18**).

Empirical formula	$C_{49}H_{41}CoFe_4$
Formula weight	912.15
Temperature	100(2) K
Wavelength	0.71073 Å
Crystal system, space group	Monoclinic, P2(1)
Unit cell dimensions	a = 11.7557(5) Å, α = 90 deg. b = 10.2852 (4) Å, β = 91.1200(10) deg. c = 15.3256(6) Å, γ = 90 deg.
Volume	1852.66(13) $Å^3$
Z, Calculated density	2, 1.635 g/cm^3
Absorption coefficient	2.004 mm^{-1}
F(000)	932
Crystal size	0.35 x 0.3 x 0.3 mm
θ range for data collection	2.20 to 28.30 deg.
Limiting indices	$-15 \le h \le 15$, $-13 \le k \le 13$, $-20 \le l \le 20$
Reflections collected / unique	19947 / 9143 [R(int) = 0.0159]
Completeness to θ = 28.30	99.7 %
Absorption correction	Empirical
Max. and min. transmission	1.0000 and 0.9036
Refinement method	Full-matrix least-squares on F^2
Data / restraints / parameters	9143 / 1 / 651
Goodness-of-fit on F^2 [a]	1.031
Final R indices [I>2σ(I)]	R1 [b] = 0.0184, wR2 [c] = 0.0434
R indices (all data)	R1 [b] = 0.0189, wR2 [c] = 0.0435
Absolute structure parameter	0.005(6)
Largest diff. peak and hole	0.333 and -0.373 e. $Å^{-3}$

[a] Goof = $\Sigma[[w(F_o^2 - F_c^2)2]/(n\text{-}p)]^{1/2}$.
[b] R1 = $\Sigma||F_o| - |F_c||/\Sigma|F_o|$.
[c] wR2 = $\{\Sigma\omega|[(F_o^2 - F_c^2)^2]/\Sigma\omega F_o^4\}^{1/2}$; $\omega = [(F_o^2, \theta) + 2F_c^2]/3$.

TABLE 3–4. BOND LENGTHS [Å] AND ANGLES [DEG] FOR {CpFe(η^5-C_5H_4)}$_4$(η^4-C_4)CoCp (**18**).

C(1) – C(2)	1.473 (2)	Co(1) – C(8)	2.0751(16)
C(2) – C(3)	1.459(2)	Co(1) – C(9)	2.0787(18)
C(3) – C(4)	1.470(2)	C(5) – C(6)	1.420 (2)
C(1) – C(4)	1.463(2)	C(5) – C(9)	1.422 (2)
Co(1) – C(1)	1.9758(16)	C(6) – C(7)	1.417 (3)
Co(1) – C(2)	1.9857(15)	C(7) – C(8)	1.420 (2)
Co(1) – C(3)	1.9907(14)	C(8) – C(9)	1.422 (2)
Co(1) – C(4)	2.0010(15)	Fe(1) --- Fe(2)	6.014
Co(1) – C(5)	2.0558(16)	Fe(2) --- Fe(3)	5.708
Co(1) – C(6)	2.0674(16)	Fe(3) --- Fe(4)	6.032
Co(1) – C(7)	2.0727(17)	Fe(1) --- Fe(4)	5.695
C(2) – C(1) – C(4)	89.38(11)	C(11) – C(1) – C(4)	137.12(14)
C(3) – C(2) – C(1)	90.47(11)	C(3) – C(2) – C(21)	135.25(13)
C(2) – C(3) – C(4)	89.69(11)	C(31) – C(3) – C(4)	129.95(13)
C(1) – C(4) – C(3)	90.43(12)	C(41) – C(4) – C(3)	132.65(13)
C(6) – C(5) – C(9)	108.24(15)	C(11) – C(1) – C(2)	130.59(13)
C(7) – C(6) – C(5)	107.84(15)	C(21) – C(2) – C(1)	132.90(13)
C(6) – C(7) – C(8)	108.21(15)	C(31) – C(3) – C(2)	137.86(13)
C(7) – C(8) – C(9)	108.04(14)	C(41) – C(4) – C(1)	135.45(14)
C(5) – C(9) – C(8)	107.66(15)		
Torsion Angles			
C(2) – C(1) – C(11) – C(12)		60.1	
C(3) – C(2) – C(21) – C(25)		-12.1	
C(4) – C(3) – C(31) – C(32)		60.3	
C(1) – C(4) – C(41) – C(42)		-10.6	

3.2.4 ^{1}H variable temperature (VT) NMR of {CpFe(η^5-C_5H_4)}$_4$(η^4-C_4)CoCp (18)

The ^{1}H VT NMR study of **18** was conducted in toluene-d_8 from room temperature to 193 K. The ^{1}H VT NMR spectra are shown in Figure 3-3 and the temperature-dependent chemical shift data are listed in Table 3-5. The compound exhibits fluxional behavior on the NMR time scale at experimental temperatures. At room temperature, the compound displays four signals: a triplet at 4.814 ppm (H_α), a singlet at 4.752 ppm (H of Cp ring ligand of Co), a triplet at 4.179 ppm (H_β) and a singlet at 4.076 ppm (H of Cp ring ligand of Fe), which indicates that the four ferrocenyl groups are equivalent at room temperature and the compound has a C_4 axis.

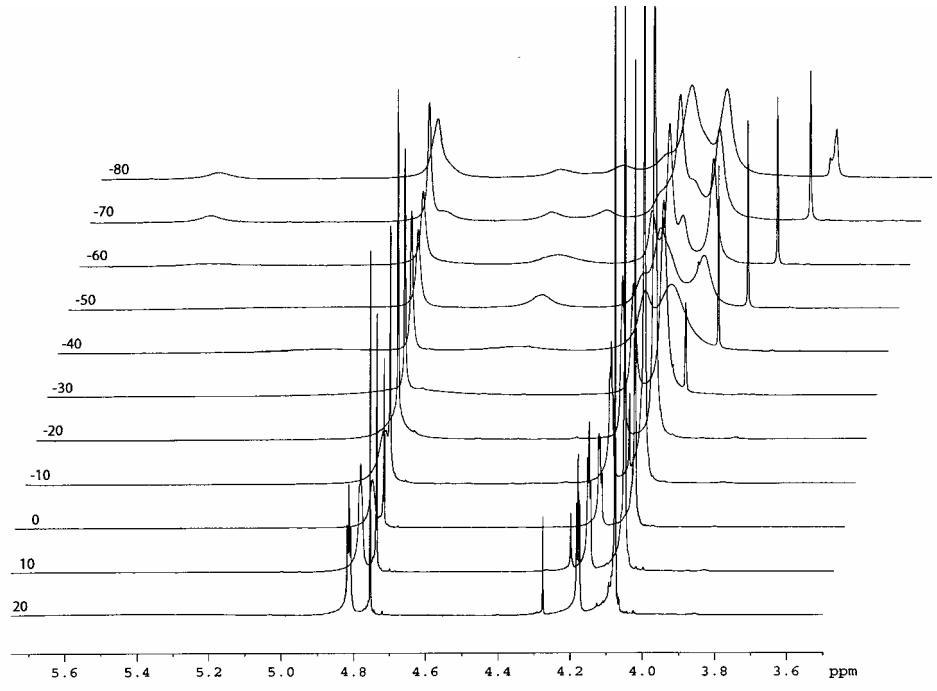

FIGURE 3–3. THE ^{1}H VT-NMR SPECTRA OF {CpFe(η^5-C_5H_4)}$_4$(η^4-C_4)CoCp (**18**) IN TOLUENE-D_8 AT 400 MHZ.

TABLE 3–5. CHEMICAL SHIFTS FROM ^{1}H NMR SPECTRA FOR {CpFe(η^5-C_5H_4)}$_4$(η^4-C_4) CoCp (**18**).

T (K)	H_α	H_β	Cp-Fe	Cp-Co
293	4.814 (t)	4.179 (t)	4.076 (s)	4.752 (s)
283	4.811 (t)	4.178 (t)	4.079 (s)	4.766 (s)
273	4.807 (s)	4.177 (t)	4.081 (s)	4.776 (s)
263	4.799 (br)	4.176 (t)	4.085 (s)	4.788 (s)
253	4.796 (br)	4.175 (s)	4.088 (s)	4.797 (s)
243	4.807 (br)	4.175 (br)	4.093 (br)	4.807 (s)
233	4.517 (br)	4.174 (br)	4.102 (br)	4.819 (s)
	5.068 (br)			
223	4.492 (br)	4.141 (br)	4.041 (br)	4.831 (s)
	5.203 (br)	4.207 (br)	4.160 (br)	
213	4.478 (br)	4.130 (s)	4.045 (s)	4.847 (s)
	5.431 (br)	4.214 (s)	4.170 (s)	
203	4.372 (br)	4.127 (br)	4.059 (s)	4.860 (s)
	4.526 (br)	4.221 (br)	4.168 (s)	
	4.865 (br)			
	5.469 (br)			
193	4.349 (br)	?	4.062 (s)	4.860 (s)
	4.523 (br)	4.231(br)	4.159 (s)	
	4.860 (br)			
	5.463 (br)			

With decreasing temperature, the $\delta_{H\alpha}$ signal at 4.814 ppm broadens. At 243 K, this signal is very broad and overlapped by the signal at 4.807 ppm (Cp-Co). At 233 K, the broad peak splits into two peaks at 4.517 and 5.068 ppm respectively.

The further temperature decreasing results in the separation of these two peaks and at 203 K, the two peaks split into four peaks as listed in Table 3-5. The signal at Cp ring of Cp-Co remains as a singlet at all temperatures. The coalescence temperature of the other two signals is 233 K and the peaks split into two peaks at 223 K. For δ_H of Cp-Fe, the static state is reached at 213 K. The two sharp peaks of $\delta_{H\beta}$ begin to broaden at 203 K, however, at the lowest experimental temperature, the splitting is not observed.

The low temperature solid structure of the compound illustrates that the four ferrocenyl groups are twisted (Scheme 3-2). Two of them are up and the other two are down with respect to the cyclobutadiene plane. Due to free rotation around the C−C bond joining the ferrocenyl group to the cyclobutadiene ring, the ferrocenyl groups are equivalent at room temperature. As the temperature decreases, the rotation rate also decreases and when it stops, the two ferrocenyl moieties at diagonal positions become equivalent, which means that the Fc1 and Fc3 (Fc2 and Fc4) are equivalent and the compound has a C_2 axis.

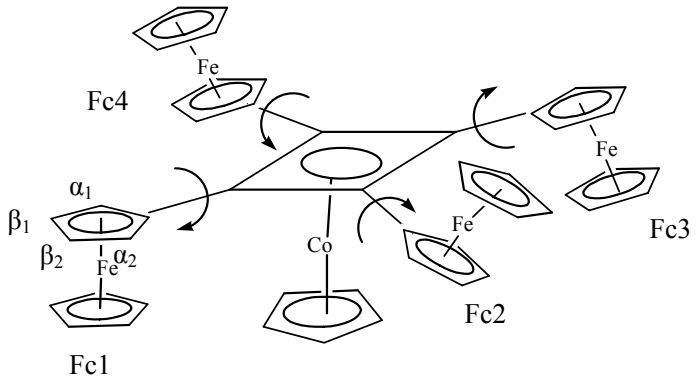

SCHEME 3–2. THE SCHEMED STRUCTURE OF $\{CpFe(\eta^5\text{-}C_5H_4)\}_4(\eta^4\text{-}C_4)CoCp$ (**18**).

However, at this temperature, the rocking rate of the ferrocenyl groups is fast enough to make the hydrogen atoms at the two α and two β positions are still equivalent on the NMR time scale. The rocking rate of the ferrocenyl groups decreases with decreasing temperature and results in the hydrogen atoms at the two α and two β positions to become to non-equivalent as revealed by further splitting of the peaks observed at the lowest temperature.

The free energy associated with the motion can be estimated from the NMR data. At the coalescence temperature, the lifetime τ is give by the equation 3-1, where δυ is the difference in resonance frequencies in the absence of rotation.[41]

$$\tau = \sqrt{2} / \pi(\delta\upsilon) \qquad \textbf{(3-1)}$$

From transition state theory we know that, equation 3-2,

$$k_{rxn} = \frac{kT}{h} e^{(-\Delta G^{\ddagger} / RT)} = \frac{1}{\tau} \qquad \textbf{(3-2)}$$

where k_{rxn} is the rate constant, k is Boltzmann constant, h is Planck constant. R is gas constant and $\Delta G^{\ddagger}$ is the free energy of the rotation. Combining equation 3-1 and 3-2, we find equation 3-3 at coalescence.

$$\Delta G^{\ddagger} = RT_c \ln(\frac{\sqrt{2}kT_c}{\pi(\delta\upsilon)h}) \qquad \textbf{(3-3)}$$

The value of $\Delta G^{\ddagger}$ is estimated as 20.7 kJ·mol^{-1} from equation 3-3 and the NMR data. Since the static state is not observed, the free energy of the rocking motion can not be estimated.

3.2.5 Electrochemistry

The cyclic voltammograms (CVs) of **18** in CH_2Cl_2 containing 0.1 M $[NBu_4][PF_6]$ ($TBAPF_6$) are shown in Figure 3-4. The CV and square wave voltammogram (SWV) of **18** in the mixed solvent (CH_2Cl_2/CH_3CN=1:1) with 0.1 M $[NBu_4][PF_6]$ are shown in the Figure 3-5. The electrochemical data for **18** are summarized in Table 3-6.

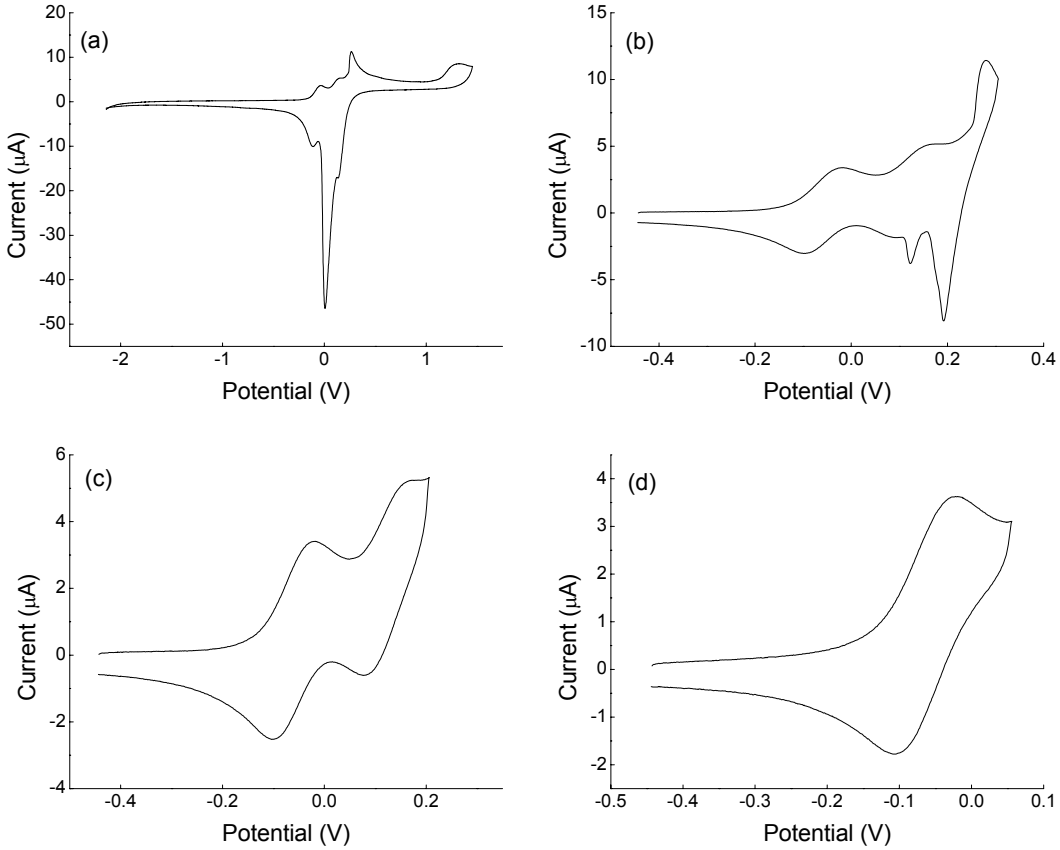

FIGURE 3–4. CYCLIC VOLTAMMETRY OF $\{CpFe(\eta^5\text{-}C_5H_4)\}_4(\eta^4\text{-}C_4)CoCp$ (**18**) IN CH_2Cl_2 (SCAN RATE 100 $mV{\cdot}s^{-1}$, REFERENCED TO FcH/FcH^+ (0.344V)): (a) SCAN FROM -2.1 TO 1.5 V; (b) SCAN FROM -0.45 TO 0.3 V; (c) SCAN FROM -0.45 TO 0.25 V; (d) SCAN FROM -0.45 TO 0.05 V.

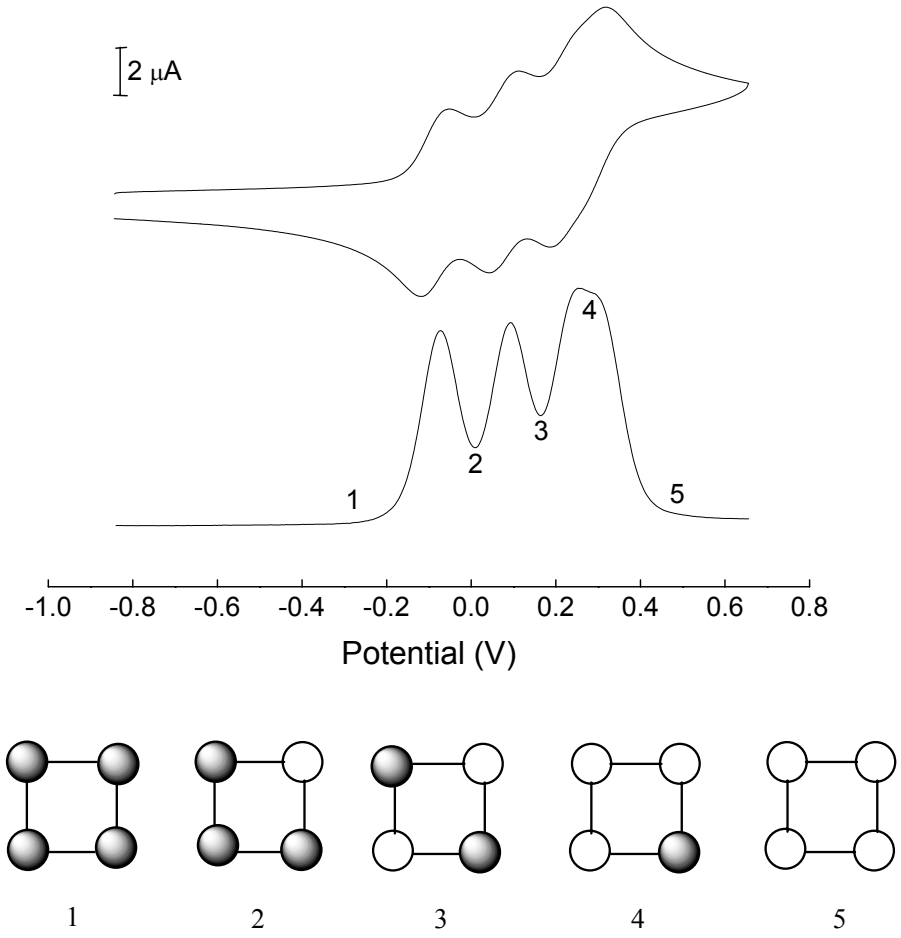

FIGURE 3–5. CYCLIC AND SQUARE WAVE VOLTAMMETRY OF {CpFe (η^5-C_5H_4)}$_4$(η^4-C_4)CoCp (**18**) AT 100 mV·s^{-1} IN CH_2Cl_2/CH_3CN MIXED SOLVENT ($E_{1/2}(FcH^+/FcH)$ = 0.344 V). THE FIVE OXIDATION STATES ARE SHOWN AT THE BOTTOM OF THE FIGURE. THE GRAY SOLID DOT AND THE OPEN CIRCLE IN THE DIAGRAMS REPRESENT Fe(II) AND Fe(III) RESPECTIVELY.

TABLE 3–6. CV DATA FOR $\{CpFe(\eta^5\text{-}C_5H_4)\}_4(\eta^4\text{-}C_4)CoCp$ (**18**).

Solvent	CH_2Cl_2	CH_2Cl_2:CH_3CN=1:1
Supporting Electrolyte	$TBAPF_6$	$TBAPF_6$
E_{pa} (1) (V)	-0.019	-0.041
E_{pc}(1) (V)	-0.106	-0.129
$E_{1/2}$(1) (V)	-0.062	-0.085
ΔE_p(1) (V)	0.087	0.088
E_{pa} (2)(V)	0.164	0.118
E_{pc} (2) (V)	0.077	0.031
$E_{1/2}$ (2) (V)	0.121	0.075
ΔE_p(2) (V)	0.087	0.087
$\Delta E_{1/2}$ (1) (V)	0.183	0.160
E_{pa} (3) (V)	0.287	0.267
E_{pc}(3) (V)	0.189	0.183
$E_{1/2}$(3) (V)	—	0.225
ΔE_p(3) (V)	—	0.084
$\Delta E_{1/2}$ (2) (V)	—	0.150
E_{pa} (4) (V)	—	0.327
E_{pc} (4) (V)	—	0.239
$E_{1/2}$ (4) (V)	—	0.283
ΔE_p(4) (V)	—	0.088
$\Delta E_{1/2}$ (3) (V)	—	0.058

$E_{1/2} = (E_{pa} + E_{pc})/2$;
$\Delta E_p = | E_{pa} - E_{pc} |$;
$\Delta E_{1/2}(1) = E_{1/2}(2) - E_{1/2}(1)$;
$\Delta E_{1/2}(2) = E_{1/2}(3) - E_{1/2}(2)$;
$\Delta E_{1/2}(3) = E_{1/2}(4) - E_{1/2}(3)$.

CVs of **18** were first measured in CH_2Cl_2 as shown in Figure 3-4. When scanning from -2.1 V to 1.5 V, the compound exhibits irreversible oxidation peaks and the cathodic peak is very sharp. Scanning from -0.45 V to 0.3 V gives a similar result. However, when scanning stopped at 0.25 V, the CV of **18** shows two reversible 1e oxidization waves at -0.062 V [$\Delta E_p(1)$ = 0.087 V] and 0.121 V [$\Delta E_p(2)$ = 0.087 V] (vs FcH/FcH^+). If scanning stopped at 0.05 V, only one reversible peaks at -0.062 V [$\Delta E_p(1)$ = 0.087 V] is observed in the CV of **18**.

However, if solvent was changed to the mixture of CH_2Cl_2 and CH_3CN (1:1), the compound exhibits four reversible one-electron oxidized processes at -0.085 V [$\Delta E_p(1)$ = 0.088 V], 0.075 V [$\Delta E_p(2)$ = 0.087 V], 0.225 V [$\Delta E_p(3)$ = 0.084 V] and 0.283 V [$\Delta E_p(4)$ = 0.087 V] respectively. SWV gives the same results as shown in Figure 3-5. Compared with the redox potentials of other ferrocenyl compounds,[21,42] the four reversible waves are assigned to redox reactions of the ferrocenyl groups. All of these observations indicate that compound **18** has five accessible reversible oxidation states (four reversible couples), which are within a range of about 700 mV and corresponding to charges of 0 to +4 on the square of four ferrocenyl groups. The oxidation of the Co(I) center is much more difficult and is not observed in the experimental range. As shown in Figure 3-5, the first and second oxidations are well separated ($\Delta E_{1/2}$ (1) = 0.160 V), presumably corresponding to oxidizing ferrocenyl groups in a diagonal position of the square. The potential difference between the second and the third oxidizations is 0.150 V, which suggests that it is possible to isolate a mixed-valence compound with two ferrocenyl groups

and two ferrocenium groups, i.e., it is thermodynamically stable with respect to charge disproportionation. The third and the forth oxidations are barely separated ($\Delta E_{1/2}$ (3) = 0.058 V) and not promising in terms of chemical oxidation and isolation. The equilibrium for every oxidation state and the comproportionation constants for equilibria will be discussed below (refer to section 3.3).

The different electrochemical behaviors of **18** in various solvents can be rationalized by considering the solubility of oxidized states of the compound in CH_2Cl_2 and CH_3CN. In CH_2Cl_2 with $TBAPF_6$, a change in solubility of **18** accompanied the change in oxidation state, so that the higher oxidation state of the compound appears to result in the precipitation onto the electrode surface, and on the reverse scan, the compound redissolves as it is reduced. However, all oxidation states of the compound are soluble in CH_3CN. Thus, when the mixture of CH_2Cl_2 and CH_3CN was used as solvent in CV experiment, the cathodic stripping peaks disappeared. Similar type behavior was reported by Cuadrado.[43]

3.2.6 ^{57}Fe Mössbauer Characteristics of {CpFe(η^5-C_5H_4)}$_4$(η^4-C_4)CoCp (18)

Variable-temperature ^{57}Fe Mössbauer spectra taken for **18** are shown in Figure 3-6. The absorption peaks were fitted to Lorentzian lines and the selected fitting parameters are summarized in Table 3-7.

The parameters elucidated by the Mössbauer effect technique are the isomer shift (δ) which reflects the s-electron density at the iron nucleus, the quadrupole splitting (ΔE_Q) which can be related to the symmetry and magnitude of the charge distribution around the metal center, and the area under the resonance curve, which

can be related to the mean-square amplitude of vibration of the metal atom around its equilibrium position.[44]

In general, ferrocenyl groups give spectra characterized by large quadrupole splitting (ΔE_Q) in the range 2.0–2.5 mm/s.[20] Compound **18** gives well separated doublets at all temperatures with ΔE_Q from 2.33 to 2.37 mm/s. This pattern of a single doublet is what is expected for a neutral ferrocene-derived compound.

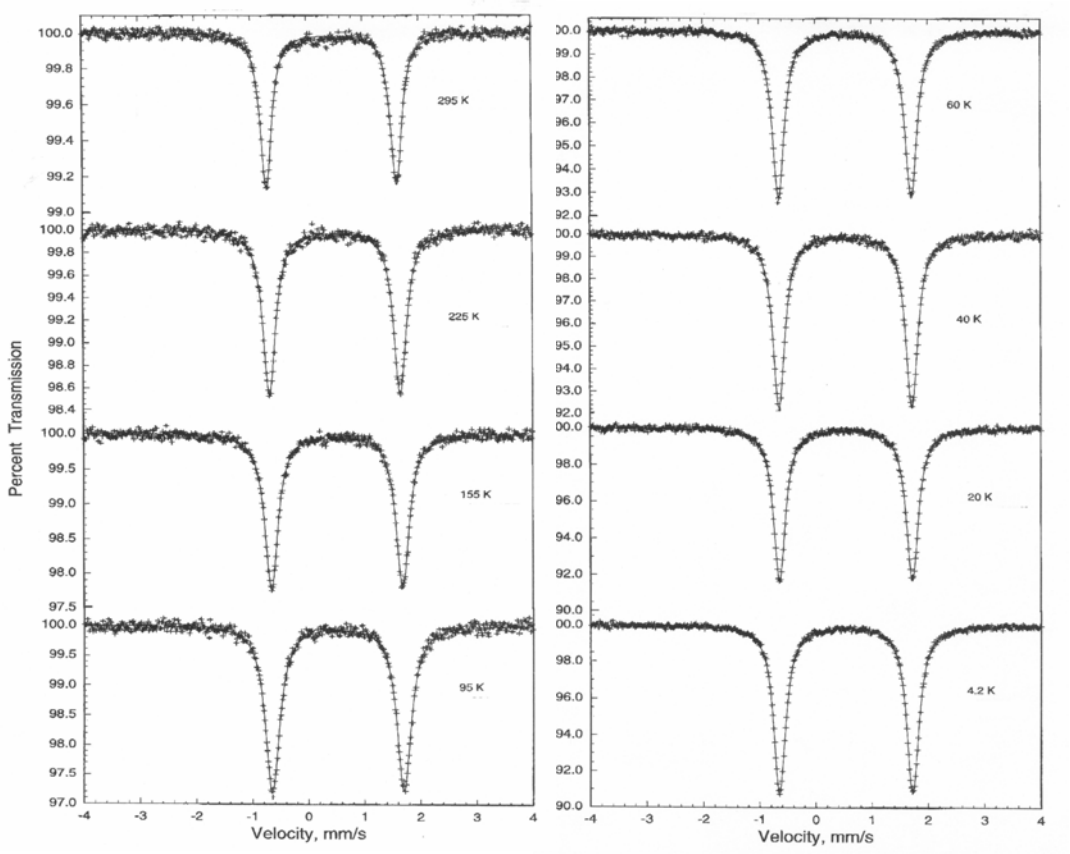

FIGURE 3–6. VARIABLE-TEMPERATURE ^{57}Fe MÖSSBAUER SPECTRA FOR {CpFe(η^5-C_5H_4)}$_4$(η^4-C_4)CoCp (**18**).

TABLE 3–7. SELECTED ^{57}Fe MÖSSBAUER SPECTRAL HYPERFINE PARAMETER FOR {CpFe(η^5-C_5H_4)}$_4$(η^4-C_4)CoCp (**18**).

T K	δ mm/s [a]	ΔE_Q mm/s	Γ [b] mm/s	Area %	Area [(%ε)(mm/s)]/mgFe/cm^2
295	0.438	2.33	0.25	100	0.45
225	0.482	2.35	0.27	100	0.84
155	0.510	2.34	0.28	100	1.31
95	0.526	2.35	0.31	100	1.80
4.2	0.536	2.37	0.27	100	2.70

[a] The isomer shifts are given relative to room temperature α-iron foil.

[b] Γ is the linewidth.

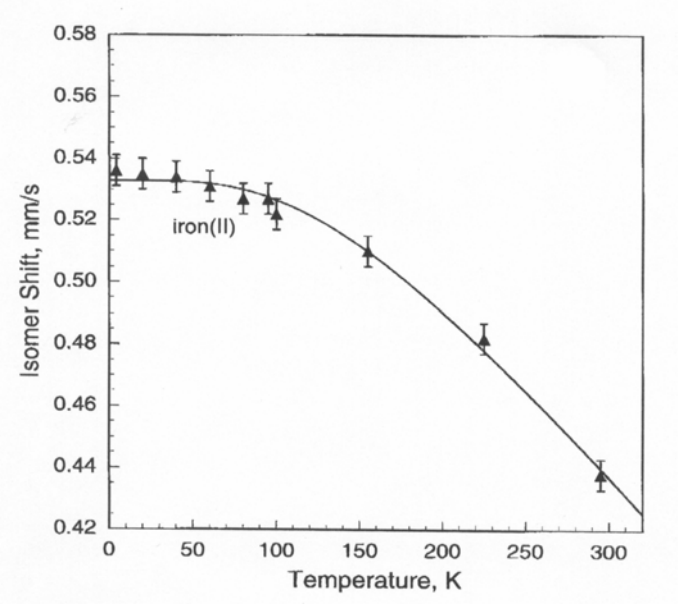

FIGURE 3–7. TEMPERATURE DEPENDENCE OF THE ISOMER SHIFT FOR {CpFe(η^5-C_5H_4)}$_4$(η^4-C_4)CoCp (**18**). THE ERROR BARS ARE THOSE OF THE INDIVIDUAL DATA POINTS. THE SOLID LINE REPRESENTS THE SECOND-ORDER POLYNOMIAL REGRESSION THROUGH THE DATA POINTS.

The temperature dependence of the isomer shift parameter is summarized in Figure 3-7. At high temperature, the isomer shift exhibits a linear increase as the temperature decreases. However, this increase is less pronounced at lower temperature. All data is in good agreement with the ferrocene[45] and the neutral biferrocene compounds.[46,47]

3.2.7 Electronic spectroscopy

Visible and near-IR spectra of **18** were measured in $CDCl_3$ as shown in Figure 3-8. In the near-IR region, there is no absorption. There is a broad peak at 440 nm due to the metal to ligand charge transfer (MLCT) of the ferrocenyl groups, which is in good agreement of with the visible spectrum of ferrocene.[48,49]

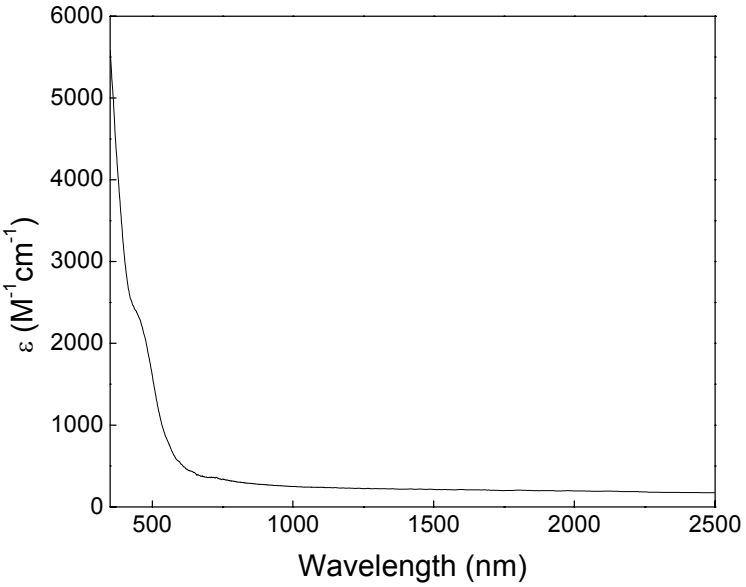

FIGURE 3–8. VIS-NEAR-IR SPECTRA OF $\{CpFe(\eta^5\text{-}C_5H_4)\}_4(\eta^4\text{-}C_4)CoCp$ (**18**).

3.3 Discussion

Compounds **17** and **18** are obtained by treating diferrocenylacetylene with $CpCo(CO)_2$ in boiling xylenes. Scheme 3-3 illustrates the possible reaction pathway.

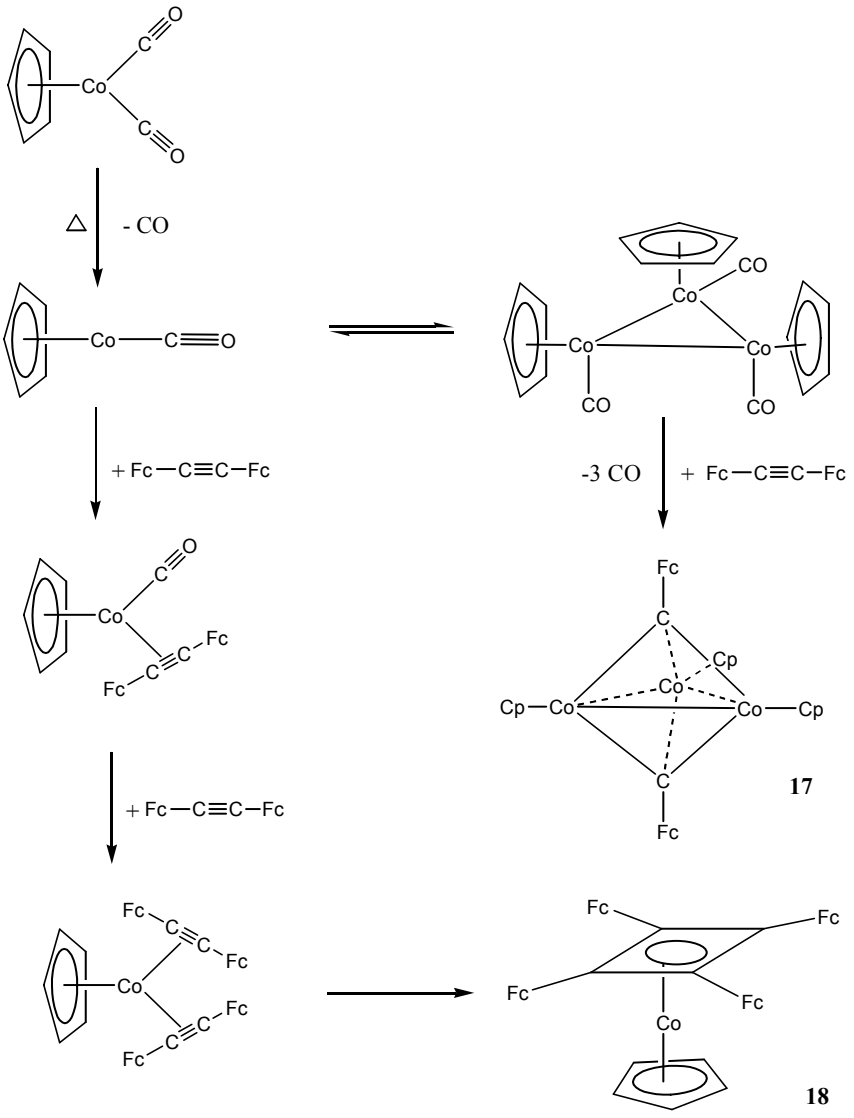

SCHEME 3–3. REACTION PATHWAYS IN THE REACTION OF $CpCo(CO)_2$ WITH DIFERROCENYL-ACETYLENE.

A stepwise mechanism for the reaction of $CpCo(CO)_2$ with diphenylacetylene was suggested by Lee and Brintzinger,[50] who were able to support it by means of IR spectroscopy. A similar reaction mechanism probably takes place in the reaction of $CpCo(CO)_2$ with diferrocenylacetylene. Thus, on heating a reaction mixture, $CpCo(CO)_2$ loses a CO ligand first and then coordinates to an alkyne or reacts with another such intermediate to form a cobalt dimer and then trimer cluster. The resultant intermediate compounds react with alkyne again to form the final compounds (**17** and **18**) at the high temperature.

Although complexes **17** and **18** have been synthesized previously,[23,24] nobody reported the X-ray crystal structures of these two compounds before. The structure of **17** is typical of bis(carbyne) clusters of cobalt, in which the ferrocenyl groups are tilted from the ideal positions of the C_3 axis to form *cis*- and *trans*- isomers. This feature, also found in the structures of $FcCCo_3Cp_3CH$ [24] and $FcCCo_3(CO)_9$ [36], is attributed to the non-degeneracy of the carbyne pπ orbitals arising from an interaction between the ferrocenyl groups and the Co_3C_2 unit.[36] As expected, the structure of **18** shows that the four ferrocenyl groups are twisted with two up and two down relative to the cyclobutadiene center in order to reduce the steric hindrance.

The electrochemical behavior of the tetraferrocenyl compound, **18**, observed by Kotz *et. al.* shows "one-electron, reversible wave at 0.29 V in CH_2Cl_2, but the waves representing the next three electrons blend into one broad wave centered at about 0.4 V" in air.[25] However, our experiments give different results (refer to section 3.2.5). The cyclic voltammogram of **18** in CH_2Cl_2 shows the stripping

behavior with higher oxidation potential such as 1.0 V (vs. FcH/FcH^+) due to the lower solubility of the higher oxidation states of the compound. In fact, the ions of 2+ or higher charge are considerably less stable in the solvent (next chapter), which may be the reason that Kotz and coworkers did not observe the separated peaks in the cyclic voltammogram of **18**.

The CV and SWV in a 1:1 mixture of CH_2Cl_2 and CH_3CN show four reversible couples, which indicates that five oxidation states are reversibly available in compound **18** (equation 3-4).

$$\begin{array}{ccccc} Fe^{II}{}_4 & \overset{E_1}{\rightleftharpoons} & [Fe^{II}{}_3Fe^{III}]^+ & \overset{E_2}{\rightleftharpoons} & [Fe^{II}{}_2Fe^{III}{}_2]^{2+} \\ & & & & \Vert \; E_3 \\ & & [Fe^{III}{}_4]^{4+} & \overset{E_4}{\rightleftharpoons} & [Fe^{II}Fe^{III}{}_3]^{3+} \end{array} \qquad \textbf{(3-4)}$$

The potential differences between the redox waves in the cyclic voltammogram of **18** are 160 mV, 150 mV and 58 mV respectively. The separations between the oxidation waves could be used to evaluate the comproportionation constants (K_c) associated with the following equilibria:

$$Fe^{II}{}_4 + [Fe^{II}{}_2Fe^{III}{}_2]^{2+} \overset{K_{c1}}{\rightleftharpoons} 2\,[Fe^{II}{}_3Fe^{III}]^+ \qquad \textbf{(3-5)}$$

$$[Fe^{II}{}_3Fe^{III}]^+ + [Fe^{II}Fe^{III}{}_3]^{3+} \overset{K_{c2}}{\rightleftharpoons} 2\,[Fe^{II}{}_2Fe^{III}{}_2]^{2+} \qquad \textbf{(3-6)}$$

$$[Fe^{II}{}_2Fe^{III}{}_2]^{2+} + [Fe^{III}{}_4]^{4+} \overset{K_{c3}}{\rightleftharpoons} 2\,[Fe^{II}Fe^{III}{}_3]^{3+} \qquad \textbf{(3-7)}$$

The relationship of the comproportionation constants and the separations between the oxidation waves are described by Nernst equation (equation 3-8),

$$\Delta E = \frac{RT}{nF} \ln K_c \qquad (\mathbf{3\text{-}8})$$
$$K_c = e^{(n\Delta EF/RT)}$$

where F is Faraday constant and R is gas constant.[51] The calculated comproportionation constants for mono-, di- and trications are: K_{c1} = 510, K_{c2} = 346 and K_{c3} = 10.

TABLE 3–8. ELECTROCHEMICAL PARAMETER FOR SOME COMPOUNDS CONTAINING TWO FERROCENYL GROUPS.[a]

Compound	$E_{1/2}$ (V) [b]	$\Delta E_{1/2}$ (mV) [c]	K_c [d]
Fc−Fc [21]	0.44 0.79	350	8.4 x 10^5
Fc−C≡C−Fc [21]	0.46 0.60	140	234
Fc−$(C\equiv C)_2$−Fc [42]	0.62 0.98	360	1.2 x 10^6
Fc−C≡C−C≡C−Fc [42]	0.58 0.68	100	49
cis-[CpCo($Fc_2Ph_2C_4$)] [25]	0.33 0.52	190	1.6 x 10^3
trans-[CpCo($Fc_2Ph_2C_4$)] [25]	0.33 0.50	170	753

[a] All data obtained in CH_2Cl_2 containing $TBAPF_6$ (0.1 M).
[b] Values are calculated by averaging the anodic (E_{pa}) and cathodic (E_{pc}) peak potentials in volts vs. SCE.
[c] $\Delta E_{1/2} = E_{pa} - E_{pc}$ in millivolts.
[d] K_c is the comproportionation constant for the disproportion reaction:
$2[2,3]^+ \rightleftharpoons [2,2] + [3,3]^{2+}$.

Compared with the comproportionation constants of some diferrocenyl compounds which are listed in Table 3-8, K_{c1} and K_{c2} of **18** are large enough for our purposes. Thus, it should be possible to isolate the mono-oxidized and di-oxidized mixed-valence salts without extensive disproportionation into the adjoining charge states. The chemical oxidations of complex **18** are described in the next chapter.

3.4 Summary

Starting from ferrocene and ferrocenecarboxaldehyde, compounds CpFe(η^5-C_5H_4)−C(CpCo)$_3$C−(η^5-C_5H_4)FeCp (**17**) and {CpFe(η^5-C_5H_4)}$_4$(η^4-C_4)CoCp (**18**) are obtained through the multiple step reactions. The solid structure of **18** at low temperature shows that two of the ferrocenyl groups are up and the other two are down relative to the cyclobutadiene plane. However, ^{1}H NMR spectrum at room temperature shows four equivalent ferrocenyl groups. The ^{1}H VT-NMR spectra of complex **18** confirms the fluxional behavior and permits the free energy of rotation of the ferrocenyl groups around the C−C bond joining them to the cyclobutadiene moiety to be estimated as 20.7 kJ·mol^{-1}.

Compound **18** displays four reversible waves in cyclic voltammetry and square wave voltammetry. Based on the separations of the oxidation waves, the comproportationation constants are calculated. The results indicate that the mixed-valence mono- and di- oxidized salts are thermodynamically stable with

respect to charge disproportionation and it should be possible to isolate them with chemical methods.

3.5 Experimental section

General

All reactions were carried out under dry, high-purity nitrogen using standard Schlenk techniques.[52] Solvents were distilled immediately before use under N_2 from the following dry agents: sodium benzophenone ketyl for hexane, pentane, THF and diethyl ether, molten sodium metal for toluene and calcium hydride for CH_2Cl_2. Other solvents were spectroscopic grade and dried over activated 3Å molecular sieves before use. All reagents were used as purchased from Aldrich, Acros or Strem.

Infrared (IR) spectra were recorded on a Perkin-Elmer Paragon 1000 FT-IR spectrometer, and samples were prepared as KBr pellets. Visible spectra were recorded on a Beckman DU-7500 spectrophotometer. Near-IR spectra were recorded on a Thermo Nicolet Nexus 670 FT-IR spectrometer. Mass Spectra (FAB^+) were recorded on a JEPL JMS-AX505HA mass spectrometer from a matrix of *p*-nitrobenzyl alcohol. Elemental analysis was conducted in the M-H-W Laboratories.

NMR spectra were taken on 300 MHz Varian Unity Plus FT-NMR instrument (^1H at 300 MHz, ^{13}C at 75 MHz). Chemical shifts are given in parts per million (ppm) and coupling constants are given in hertz (Hz). For references, residual

protons were used for ^{1}H ($CDCl_3$: 7.27 ppm) and ^{13}C ($CDCl_3$: 77.23). Variable Temperature NMR (VT-NMR) spectra were measured on Bruker DPX Avance NMR (^{1}H at 400 MHz) using toluene-d_8 as solvent. The reference was calibrated at 2.09 ppm. The temperature was adjusted manually with a temperature editing program.

Cyclic Voltammetric (CV) and Square Wave Voltammetric (SWV) measurements were performed on a BAS Epsilon-EC using a Pt working electrode, Pt-flag counter electrode and Pt-wire pseudo-reference electrode. Tetrabutyl ammonium hexafluorophosphate ($TBAPF_6$) was used as the supporting electrolyte. All measurements were taken in dry box under N_2 and referenced to ferrocene ($E_{1/2}(FcH/FcH^+) = 0.344V$).

The ^{57}Fe Mössbauer spectra were obtained between 4.2 and 295 K on a constant-acceleration spectrometer which utilized the room-temperature rhodium matrix cobalt-57 source and were calibrated at room temperature with α-iron foil. The measurements were performed by Professor Gary J. Long in Department of Chemistry, University of Missouri-Rolla and Professor Fernande Grandjean in Department of Physics, University of Liège, Belgium.

Preparations of (η^5-C_5H_5)Fe(η^5-$C_5H_4CH{=}CCl_2$) (11)

Compound **11** was prepared by following a similar experimental procedure from literature.[27] CCl_4 (1.54 g, 10 mmol) was introduced into a solution of ferrocenecarboxaldehyde (1.07 g, 5 mmol) and PPh_3 (5.24 g, 20 mmol) in 10 mL of anhydrous acetonitrile at 0 °C under N_2 flowing. The reaction mixture was warmed up to room temperature and stirred another 30 min to complete the reaction. Then

10 mL of distilled water was added into the solution. The mixture was extracted with ether until the organic phase is colorless. The collected organic solution was washed with brine and dried over $MgSO_4$ overnight. The solvent was removed under vacuum. The residue was dissolved in a minimum amount of CH_2Cl_2 and chromatographed on a column with neutral alumina. The compound was eluted with pentane to give 1.1 g orange solids (78%). ^{1}H NMR ($CDCl_3$): δ 6.54 (s, 1H, =C*H*-), 4.59 (t, *J* = 2Hz, 2H, α-*H*), 4.29 (t, *J* = 2Hz, 2H, β-*H*), δ 4.19 (s, 5H, Cp).

Preparation of Ferrocenylacetylene (12)

Following the literature methods,[27] the solution of **11** (0.84 g, 3 mmol) in THF (10 mL) was cooled down to -78°C. To this solution, 3.8 mL (6 mmol) of n-BuLi (1.6 M in hexane) was added. The mixture was warmed up to room temperature and stirred for additional 15 min. Then 10 mL of distilled water was added into it. The solution was extracted with ether and dried over $MgSO_4$ overnight. The solution was concentrated to 5 mL and chromatographed on silica gel column. After elution with pentane and removal the solvent, 0.53 g (94%) of compound **12** was obtained. IR (cm^{-1}): 2102.8 (C≡C). ^{1}H NMR ($CDCl_3$): δ 4.47 (t, *J* = 1.8Hz, 2H, α-*H*), 4.23 (s, 5H, Cp), 4.21 (t, *J* = 1.8Hz, 2H, β-*H*), 2.72(s, 1H, ≡C*H*).

Preparation of (Tri-n-butylstannyl)ferrocene (13)

The compound was prepared by modified known methods.[28,29] Ferrocene (5g, 26.9 mmol) solution in THF (15 mL) and hexane (15 mL) was stirred for 30 min under N_2 at room temperature to form an orange suspension and then cooled down to 0 °C. To this suspension was added 32 mL (54.4 mmol) of t-BuLi (1.7 M in

pentane) drop by drop. The mixture was stirred for about 2 hours before 11mL of $^{n}Bu_3SnCl$ was added. After another 90 min, the hydrolysis was performed with aqueous NaOH (2M, 30 mL). The product was extracted with diethyl ether, and the organic layer was washed with brine and water and dried over $MgSO_4$ overnight. After removal of the solvent, the crude product as red oil was taken up in hexane and chromatographed on a neutral alumina column. Using pentane as eluent, the first orange band is the bi-substituted product and the second orange band is the mono-substituted product with unreactive ferrocene. After the removal of the solvent and sublimation of the remaining ferrocene, compound **13** (8 g, 63%) was obtained as red oil. ^{1}H NMR ($CDCl_3$): δ 4.34 (t, *J* = 1.8Hz, 2H, α-*H*), 4.12 (s, 5H, Cp), 4.03 (t, *J* = 1.8Hz, 2H, β-*H*), 1.7~ 0.9 (m, Bu).

Preparation of Iodoferrocene (14)

The synthesis is a modification of the known procedures.[28,29] Iodine (1.4 g, 5.5 mmol) was added to a solution of **13** (2.38 g, 5 mmol) in CH_2Cl_2 (20 mL) at room temperature. The mixture was stirred overnight, and then washed with aqueous sodium thiosulfate. The organic layer was separated and filtered through neutral alumina. The solution was evaporated to dryness. The resulting crude product was taken up in methanol, and 1g of KF was added to precipitate the stannylated byproducts, which was removed by filtration through neutral alumina. The solvent was removed *in vacuo*, the product was extracted with ether, washed with water and dried over $MgSO_4$ for 4 hours. After the evaporation of the solvent, recrystallization from pentane afforded 1.15g of brownish orange crystals. The yield is 74%. ^{1}H NMR ($CDCl_3$): δ 4.43 (t, *J* = 1.8Hz, 2H, α-*H*), 4.21 (s, 5H, Cp),

4.17 (t, J = 1.8Hz, 2H, β-*H*). ^{13}C NMR ($CDCl_3$): δ 74.6 (2C, β-*C*), 71.2(5C, Cp), 69.0 (2*C*, γ-C). FABMS: m/z 312 (M^+).

Preparation of Cuprous Ferrocenylacetylide (15) and Diferrocenyl acetylene (16)

Compounds **15** and **16** were prepared by following similar experimental procedure from literature.[31] A solution of cuprous iodide (700 mg, 3.64 mmol) in 10 mL of 30% aqueous ammonia was added to 500 mg (2.38 mmol) of ferrocenylacetylene in 20 mL of absolute ethanol. After the stirring for 15 min at room temperature, the golden yellow precipitate was filtered off and washed with water, then absolute ethanol and finally diethyl ether. The salt was dried under vacuum to give 540 mg of **15**. The yield is 84%.

413 mg (1.5 mmol) of **15** and 624 mg (2.0 mmol) of **14** were mixed into degassed pyridine (16 mL) to generate orange solution. The reaction mixture was refluxed for 30 min and then poured into 50 mL of ice. The resultant orange precipitated was collected by filtration and washed repeatedly with toluene until the washings were colorless. The combined toluene extract was washed with water to neutrality and dried over $MgSO_4$ overnight. The solution was evaporated to the dryness. The resulting orange solid was washed with ether several times and dried under vacuum to afford 468 mg (79%) of the analytically pure compound **16**. IR (cm^{-1}): 2152.8 (C≡C). ^{1}H NMR ($CDCl_3$): δ 4.46 (t, J = 1.8Hz, 2H, α-*H*), 4.24 (s, 5H, Cp), 4.21 (t, J = 1.8Hz, 2H, β-*H*). FABMS: m/z 394 (M^+).

Preparation of CpFe(η^5-C_5H_4)−C(CpCo)$_3$C−(η^5-C_5H_4)FeCp (17) and {CpFe (η^5-C_5H_4)}$_4$(η^4-C_4)CoCp (18)

The procedure for the syntheses was a modification from that used by Rausch.[23] To 100 mg (0.254 mmol) of **16** was added degassed xylenes (20 mL) to generate orange solution. Then $CpCo(CO)_2$ (45 mg, 0.254 mmol) was introduced into this solution. The reaction mixture was refluxed with stirring under a nitrogen atmosphere for 24 hours and was allowed to cool under nitrogen. After removal of the solvent, the resulting red-brown solid was extracted with toluene. The toluene extract was filtered through a 2 cm layer-bed celite, and the solution was concentrated to about 5 mL. The concentrated solution was chromatographed on a column with neutral alumina. The first red-purple band was eluted with hexane/toluene (1:3), which provided 68 mg (35%) of red-purple solid as compound **17**. Recrystallization from CH_2Cl_2/hexane gave black needle crystals suitable for X-ray diffraction analysis. ^{1}H NMR ($CDCl_3$): δ 4.86 (t, *J* = 2Hz, 4H, α-*H*), 4.61 (t, *J* = 2Hz, 4H, β-*H*), 4.55 (s, 15H, Cp-Co), 4.36 (s, 10H, Cp-Fe). ^{13}C NMR ($CDCl_3$): δ 115.2 (2C, *C*-Co), 84.6 (15C, Cp-Co), 70.0 (4C, β-*C*), 69.9 (10C, Cp-Fe), 68.4 (4*C*, γ-C). FABMS: m/z 766 (M^+).

The second brownish orange band was eluted with toluene. Evaporation of the solution to dryness afforded 35 mg (30%) of orange solid as compound **18**. Brownish orange block crystals were obtained from the recrystallization from CH_2Cl_2/hexane. Anal. Calcd. for $C_{49}H_{41}Fe_4Co$: C, 64.52%, H, 4.53%. Found: C, 64.64%, H, 4.65%. ^{1}H NMR ($CDCl_3$): δ 4.82 (t, *J* = 2Hz, 8H, α-*H*), 4.79 (s, 5H,

Cp-Co), 4.32 (t, *J* = 2Hz, 8H, β-*H*), 4.11 (s, 20H, Cp-Fe). ^{13}C NMR ($CDCl_3$): 82.9 (4C, Cyclobutadiene), δ 81.3 (5C, Cp-Co), 70.2 (8C, β-C), 69.9 (4C, α-*C*), 69.6 (20C, Cp-Fe), 67.8 (8*C*, γ-C). FABMS: m/z 912 (M^+).

In a typical synthesis of compound **18**, the reaction ratio of **16** to $CpCo(CO)_2$ is 2:1. In this process, the compound **17** can not be obtained. To a solution of **16** (418 mg, 1.06 mmol) in xylenes (25 mL) was added 95.5 mg (0.53 mmol) of $CpCo(CO)_2$. The solution was refluxed with stirring under a nitrogen atmosphere for 24 hours and then allowed to cool down to room temperature under nitrogen. The solvent was removed *in vacuo* and the resulting orange-brown solid was extracted with toluene. The toluene extract was filtered through a 2 cm layer-bed celite, concentrated to about 10 mL and run through a neutral alumina column. Elution with toluene afforded 300 mg (62%) of brownish orange solid (**18**).

Structure Determinations

Single crystals of **17** and **18** suitable for X-ray single-crystal diffraction were obtained by slow diffusion from CH_2Cl_2 to hexane. Crystalline samples were placed in inert oil, mounted on a glass pin, and transferred to the cold gas stream of the diffractometer. Crystal data were collected and integrated using a Bruker Apex system, with graphite monochromated Mo-Kα (λ = 0.71073 Å) radiation at 100K. The structures were solved by heavy atom methods using SHELXS-97 and refined using SHELXL-97 (Sheldrick, G.M., University of Göttingen). Non-hydrogen atoms were found by successive full matrix least squares refinement on F^2 and refined with anisotropic thermal parameters. All hydrogen atoms were located

from difference Fourier maps and allowed to refine isotropically with fixed thermal parameters [$u_{ij} = 1.2U_{ij}(eq)$ for the atom to which they are bonded].

3.6 References

(1) Masamune, S.; Soutobachiller, F. A.; Machiguchi, T.; Bertie, J. E. *J. Am. Chem. Soc.* **1978**, *100*, 4889-4891.

(2) Masamune, S.; Machiguchi, T.; Aratani, M. *J. Am. Chem. Soc.* **1977**, *99*, 3524-3526.

(3) Whitman, D. W.; Carpenter, B. K. *J. Am. Chem. Soc.* **1980**, *102*, 4272-4274.

(4) Fritch, J. R.; Vollhardt, P. C. *Organometallics* **1982**, *1*, 590-602.

(5) Abel, E. W.; Stone, F. G. A.; Wilkinson, G. *Comprehensive organometallic chemistry II : a review of the literature 1982-1994*; 1st ed.; Pergamon: Oxford ; New York, 1995.

(6) Gleiter, R. *Angew. Chem. Int. Ed.* **1992**, *31*, 27-44.

(7) Efraty, A. *Chem. Rev.* **1977**, *77*, 691-744.

(8) Laskoski, M.; Roidl, G.; Smith, M. D.; Bunz, U. H. F. *Angew. Chem. Int. Ed.* **2001**, *40*, 1460-1463.

(9) Roidl, G.; Enkelmann, V.; Adams, R. D.; Bunz, U. H. F. *J. Organomet. Chem.* **1999**, *578*, 144-149.

(10) Bunz, U. H. F.; Roidl, G.; Altmann, M.; Enkelmann, V.; Shimizu, K. D. *J. Am. Chem. Soc.* **1999**, *121*, 10719-10726.

(11) Benisch, C.; Werz, D. B.; Gleiter, R.; Rominger, F.; Oeser, T. *Eur. J. Inorg. Chem.* **2003**, 1099-1112.

(12) Benisch, C.; Gleiter, R.; Staeb, T. H.; Nuber, B.; Oeser, T.; Pritzkow, H.; Rominger, F. *J. Organomet. Chem.* **2002**, *641*, 102-112.

(13) Chi, K. M.; Calabrese, J. C.; Reiff, W. M.; Miller, J. S. *Organometallics* **1991**, *10*, 688-693.

(14) Kollmar, C.; Couty, M.; Kahn, O. *J. Am. Chem. Soc.* **1991**, *113*, 7994-8005.

(15) Medina, J. C.; Li, C.; Bott, S. G.; Atwood, J. L.; Gokel, G. W. *J. Am. Chem. Soc.* **1991**, *113*, 366-367.

(16) Grossel, M. C.; Goldspink, M. R.; Hriljac, J. A.; Weston, S. C. *Organometallics* **1991**, *10*, 851-860.

(17) Wagner, R. W.; Brown, P. A.; Johnson, T. E.; Lindsey, J. S. *J. Chem. Soc., Chem. Commun.* **1991**, 1463-1466.

(18) Constable, E. C. *Angew. Chem. Int. Ed.* **1991**, *30*, 407-408.

(19) Cowan, D. O.; Vanda, C. L.; Park, J.; Kaufman, F. J. *Acc. Chem. Res.* **1973**, *6*, 1-7.

(20) Morrison, W. H.; Hendrickson, D. N. *Inorg. Chem.* **1975**, *14*, 2331-2346.

(21) Powers, M. J.; Meyer, T. J. *J. Am. Chem. Soc.* **1978**, *100*, 4393-4398.

(22) Kramer, J. A.; Hendrickson, D. N. *Inorg. Chem.* **1980**, *19*, 3330-3337.

(23) Rausch, M. D.; Higbie, F. A.; Westover, G. F.; Clearfield, A.; Gopal, R.; Troup, J. M.; Bernal, I. *J. Organomet. Chem.* **1978**, *149*, 245-264.

(24) Colbran, S. B.; Robinson, B. H.; Simpson, J. *Organometallics* **1984**, *3*, 1344-1353.

(25) Kotz, J.; Neyhart, G.; Vining, W. J.; Rausch, M. D. *Organometallics* **1983**, *2*, 79-82.

(26) Jiao, J. Y.; Long, G. J.; Grandjean, F.; Beatty, A. M.; Fehlner, T. P. *J. Am. Chem. Soc.* **2003**, *125*, 7522-7523.

(27) Luo, S. J.; Liu, Y. H.; Liu, C. M.; Liang, Y. M.; Ma, Y. X. *Synthetic Commun.* **2000**, *30*, 1569-1572.

(28) Guillaneux, D.; Kagan, H. B. *J. Org. Chem.* **1995**, *60*, 2502-2505.

(29) Butler, I. R.; Wilkes, S. B.; Mcdonald, S. J.; Hobson, L. J.; Taralp, A.; Wilde, C. P. *Polyhedron* **1993**, *12*, 129-131.

(30) Stephens, R. D.; Castro, C. E. *J. Org. Chem.* **1963**, *28*, 3313-3315.

(31) Rosenblum, M.; Brawn, N.; Papenmeier, J.; Applebaum, M. *J. Organomet. Chem.* **1966**, *6*, 173-180.

(32) Johannessen, S. C.; Brisbois, R. G.; Fischer, J. P.; Grieco, P. A.; Counterman, A. E.; Clemmer, D. E. *J. Am. Chem. Soc.* **2001**, *123*, 3818-3819.

(33) Fehlner, T. P. *Inorganometallic chemistry*; Plenum: New York, 1992.

(34) Antipin, M.; Boese, R.; Blaser, D.; Maulitz, A. *J. Am. Chem. Soc.* **1997**, *119*, 326-333.

(35) Fritch, J. R.; Vollhardt, K. P. C.; Thompson, M. R.; Day, V. W. *J. Am. Chem. Soc.* **1979**, *101*, 2768-2770.

(36) Colbran, S. B.; Hanton, L. R.; Robinson, B. H.; Robinson, W. T.; Simpson, J. *J. Organomet. Chem.* **1987**, *330*, 415-428.

(37) Pardy, R. B. A.; Smith, G. W.; Vickers, M. E. *J. Organomet. Chem.* **1983**, *252*, 341-346.

(38) Riley, P. E.; Davis, R. E. *J. Organomet. Chem.* **1976**, *113*, 157-166.

(39) Clearfield, A.; Gopal, R.; Rausch, M. D.; Tokas, E. F.; Higbie, F. A.; Bernal, I. *J. Organomet. Chem.* **1977**, *135*, 229-248.

(40) Seiler, P.; Dunitz, J. D. *Acta Cryst. B* **1979**, *35*, 1068-1074.

(41) Iggo, J. A. *NMR spectroscopy in inorganic chemistry*; Oxford University Press: Oxford ; New York, 1999.

(42) Levanda, C.; Bechgaard, K.; Cowan, D. O. *J. Org. Chem.* **1976**, *41*, 2700-2704.

(43) Cuadrado, I.; Casado, C. M.; Alonso, B.; Moran, M.; Losada, J.; Belsky, V. *J. Am. Chem. Soc.* **1997**, *119*, 7613-7614.

(44) Herber, R. H. *Inorg. Chim. Acta* **1999**, *291*, 74-81.

(45) Herber, R. H.; Nowik, I. *Solid State Sciences* **2002**, *4*, 691-694.

(46) Herber, R. H.; Nowik, I.; Iyoda, M. *J. Organomet. Chem.* **2002**, *658*, 210-213.

(47) Dong, T. Y.; Schei, C. C.; Hwang, M. Y.; Lee, T. Y.; Yeh, S. K.; Wen, Y. S. *Organometallics* **1992**, *11*, 573-582.

(48) Sarhan, A. E. W.; Nouchi, Y.; Izumi, T. *Tetrahedron* **2003**, *59*, 6353-6362.

(49) Armstrong, A. T.; Carroll, D. G.; McGlynn, S. P. *J. Chem. Phys.* **1976**, *47*, 1104-1111.

(50) Lee, W. S.; Brintzinger, H. H. *J. Organomet. Chem.* **1977**, *127*, 93-103.

(51) Brett, C. M. A.; Brett, A. M. O. *Electroanalysis*; Oxford University Press: Oxford ; New York, 1998.

(52) Shriver, D. F.; Drezdzon, M. A. *The manipulation of air-sensitive compounds*; 2nd ed.; Wiley: New York, 1986.

CHAPTER 4

SYNTHESIS AND CHARACTERIZATION OF MIXED-VALENCE COMPOUNDS

4.1 Introduction

Generally, a building block for constructing QCA circuits is a square of four electronically coupled dots containing two mobile electrons.[1] The basic requirements for a molecular QCA cell are "dots" consisting of metal complexes with two stable redox states, a planar array of four such complexes with 4-fold symmetry, sufficient through-bond or through-space interaction so that the 2-electron, 2-hole mixed-valence state is stable with respect to lower and higher oxidization states, Class II or Class III mixed-valence behavior[2,3] appropriate for switching and the capability of isolation as a pure compound in useable yields.[4]

Complex $\{CpFe(\eta^5\text{-}C_5H_4)\}_4(\eta^4\text{-}C)CoCp$ (**18**), in which four ferrocenyl groups are connected by cyclobutadiene, shows four reversible waves in cyclic voltammetry and square wave voltammetry as described in chapter 3. Although molecular squares with similar redox behavior were reported before,[5-8] there is no

example of an isolated four-metal, mixed-valence compound containing two mobile electrons in a square geometry.

Cyclic and square wave voltammetry of {CpFe(η^5-C_5H_4)}$_4$(η^4-C)CoCp (**18**) reveals four waves sufficiently separated to suggest isolation of the 1+ and 2+ cations is feasible (chapter 3). Thus, the work of this chapter is focused on the oxidation of {CpFe(η^5-C_5H_4)}$_4$(η^4-C)CoCp (**18**) and full characterization of the resulted mixed-valence compounds. The types of the mixed-valence compounds are also analyzed via the intervalence charge transfer (IVCT) band to evaluate the possibility of a mixed-valence compound with two ferrocenes and two ferroceniums as a building block for a molecular QCA cell.

4.2 Results

4.2.1 Synthesis

In order to oxidize compound **18** to the mixed-valence compounds, a proper oxidant should be selected. In addition, the reduction byproduct could be removed easily from the product. With the guidance of Connely and Geiger's review,[9] several oxidants are used to obtain the higher oxidization state compounds. The formal potentials of these oxidants are listed in Table 4-1.

TABLE 4–1. FORMAL POTENTIALS (*VS.* FcH/FcH^+) OF OXIDIZING AGENTS.[9]

Oxidant	Solvent	$E^{o\prime}$ (V)
Ag^+	CH_2Cl_2	0.65
$[Fe(\eta^5\text{-}C_5H_4COMe)_2]^+$	CH_2Cl_2	0.49
Ag^+	THF	0.41
$[Fe(\eta^5\text{-}C_5H_4COMe)Cp]^+$	CH_2Cl_2	0.27
Ag^+	acetone	0.18
Cl_2	MeCN	0.18
DDQ	MeCN	0.13
Ag^+	MeCN	0.04
$[FeCp_2]^+$		0.0

The neutral compound $\{CpFe(\eta^5\text{-}C_5H_4)\}_4(\eta^4\text{-}C)CoCp$ (**18**) exhibits four reversible one-electron oxidation processes at -0.085, 0.075, 0.225 and 0.283 V respectively (refer to Table 3-6). Thus, ferrocenium ion is a suitable oxidant to convert the neutral compound to monocation. As expected, treatment of **18** with ferrocenium ion results in the formation of the mono-oxidized compound and the byproduct (ferrocene) is readily removed by washing with diethyl ether (Scheme 4-1). The yield is 76%. Since one of the ferrocenyl groups is oxidized to the ferrocenium moiety, the IR spectrum of $[\{CpFe(\eta^5\text{-}C_5H_4)\}_4(\eta^4\text{-}C)CoCp][BF_4]$ shows two $\delta_{C\text{-}H}$ bending frequencies at 850 and 821 cm^{-1} (*vide infra*). The purity of the compound is confirmed by elemental analysis.

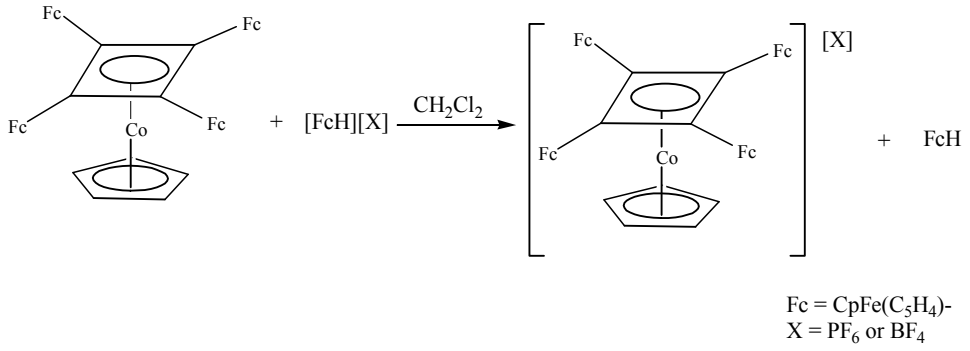

SCHEME 4–1. PREPARATION OF THE MONO-OXIDIZED SALTS OF $\{CpFe(\eta^5\text{-}C_5H_4)\}_4(\eta^4\text{-}C)CoCp$ (**18**).

In order to oxidize the neutral compound (**18**) to dicationic compound, dichlorodicyano-benzoquinone (DDQ), chlorine and 2 equivalents of silver ions were used. However, DDQ and chlorine destroyed the compound (**18**). Although the formal potential of silver ion in CH_2Cl_2 is strong enough to oxidize the neutral compound to the tetracationic complexes, only monocationic compound is obtained when **18** reacts with 2 equivalents of silver ion (the near-IR spectra and the unit cell of the crystals are the same as those of the monocationic compound). Excess silver ion results in the formation of precipitate. Finally, acetyl-substituted ferrocenium ion proved to be a satisfactory oxidant.

The stoichiometrical reaction of **18** with acetylferrocenium ions (1:2) results in the formation of the di-oxidized salts (Scheme 4-2). Since the powders slowly decompose in the process of the recrystallization, no X-ray suitable crystals are obtained. However, both elemental analysis and FT-IR spectrum (two peaks at 825

and 852 cm^{-1} with 1:1 of area ratio) prove the formation and the purity of the di-oxidized salt.

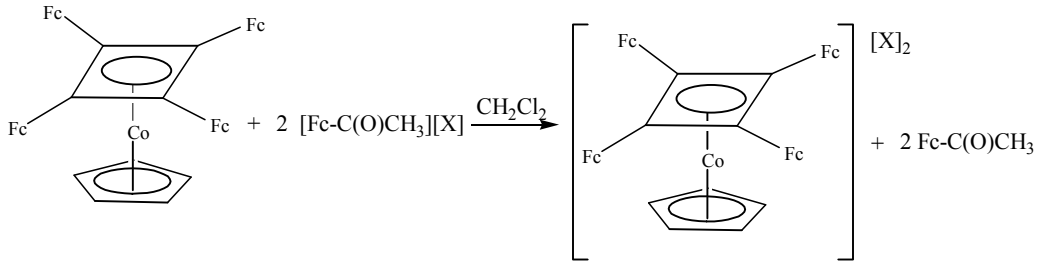

SCHEME 4–2. PREPARATION OF THE DI-OXIDIZED SALTS OF {CpFe(η^5-C_5H_4)}$_4$(η^4-C)CoCp (**18**).

Treating excess of acetylferrocenium ion with the neutral compound gives the salt of tri-oxidized **18**. Although the full characterization of the compound is limited because of the poor stability, the IR spectrum of [{CpFe(η^5-C_5H_4)}$_4$(η^4-C)CoCp][BF_4]$_3$ (**22**) shows $\delta_{C\text{-}H}$ bending bands at 853 cm^{-1} with a shoulder at 821 cm^{-1}. The ratio of the peak areas is estimated as ~3:1, which indicates the formation of tri-oxidized compound.

The reaction of 1, 1'-diacetylferrocenium ion with compound **18** affords the tetra-oxidized compound (**24**). Since the solubility of the product is similar to that of the oxidant, the separation of the tetra-oxidized compound from the oxidant is unsuccessful.

4.2.2 X-ray structure determination of [{CpFe(η^5-C_5H_4)}$_4$(η^4-C_4)CoCp][PF_6] (19).

The crystals of **19** were grown by slow diffusion of hexane into CH_2Cl_2 solution. The molecular structure of **19**, established by an X-ray diffraction study, is shown in Figure 4-1. The crystal data and structure refinement information are given in Table 4-2 and the selected bond length and angles are listed in Table 4-3.

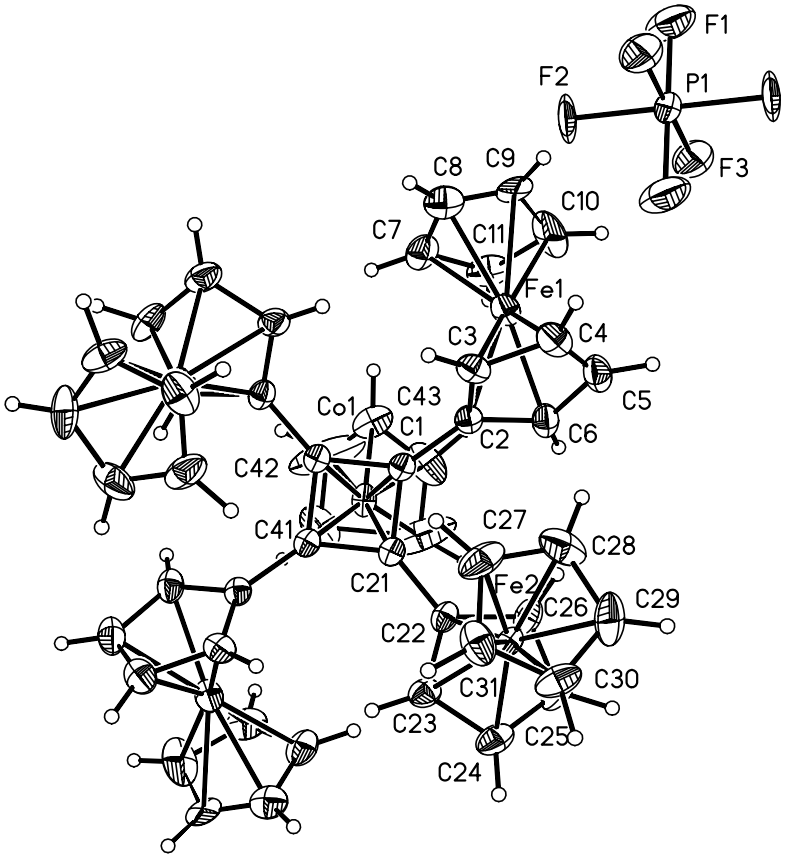

FIGURE 4–1. X-RAY STRUCTURE OF [{CpFe(η^5-C_5H_4)}$_4$(η^4-C)CoCp][PF_6] (**19**) WITH 50% THERMAL ELLIPSOIDS. ONLY MAJOR COMPONENTS OF DISORDER ARE SHOWN.

TABLE 4–2. CRYSTAL DATA AND STRUCTURE REFINEMENT FOR

[{CpFe(η^5-C_5H_4)}$_4$(η^4-C)CoCp][PF_6] (**19**).

Empirical formula	$C_{49}H_{41}CoFe_4PF_6$
Formula weight	1057.12
Temperature	100(2) K
Wavelength	0.71073 Å
Crystal system, space group	Orthorhombic, Pbcn
Unit cell dimensions	a = 12.7388(8) Å, α = 90 deg. b = 14.1918 (8) Å, β = 90 deg. c = 22.0301(13) Å, γ = 90 deg.
Volume	3982.8(4) $Å^3$
Z, Calculated density	4, 1.763 g/cm^3
Absorption coefficient	1.936 mm^{-1}
F(000)	2140
Crystal size	0.4 x 0.4 x 0.15 mm
θ range for data collection	2.15 to 28.32 deg.
Limiting indices	$-16 \le h \le 16$, $-18 \le k \le 18$, $-29 \le l \le 29$
Reflections collected / unique	40328 / 4946 [R(int) = 0.0159]
Completeness to θ = 28.32	99.9 %
Absorption correction	Empirical
Max. and min. transmission	1.0000 and 0.8673
Refinement method	Full-matrix least-squares on F^2
Data / restraints / parameters	4946 / 0 / 345
Goodness-of-fit on F^2 [a]	1.209
Final R indices [I>2σ(I)]	R1 [b] = 0.0448, wR2 [c] = 0.0932
R indices (all data)	R1 [b] = 0.0560, wR2 [c] = 0.0976
Absolute structure parameter	0.005(6)
Largest diff. peak and hole	0.609 and -0.442 e. $Å^{-3}$

[a] Goof = $\Sigma[[w(F_o^2 - F_c^2)2]/(n-p)]^{1/2}$.
[b] R1 = $\Sigma||F_o| - |F_c||/\Sigma|F_o|$.
[c] wR2 = $\{\Sigma\omega|[(F_o^2 - F_c^2)^2]/\Sigma\omega F_o^4\}^{1/2}$; $\omega = [(F_o^2, \theta) + 2F_c^2]/3$.

TABLE 4–3. SELECTED BOND LENGTH [Å] AND ANGLES [DEG] FOR [{CpFe(η^5-C_5H_4)}$_4$(η^4-C)CoCp][PF_6] (**19**).

C(1) – C(21)	1.479(4)	Co(1) – C(42)	2.037(4)
C(1) – C(21)#1	1.466(4)	Co(1) – C(43)	2.111(8)
C(21) – C(1)#1	1.466(4)	C(41) – C(42)	1.345(7)
Co(1) – C(1)#1	1.988(3)	C(42) – C(43)	1.056(10)
Co(1) – C(1)	1.988(3)	Fe(1) --- Fe(2)	5.980
Co(1) – C(21)#1	1.999(3)	Fe(1)#1 --- Fe(2)	5.907
Co(1) – C(21)	1.999(3)	Fe(1) --- Fe(2)#1	5.907
Co(1) – C(41)	2.052(4)	Fe(1)#1 --- Fe(2)#1	5.980
C(21) – C(1) – C(21)#1	88.9(2)	C(43) – C(42) – C(41)	131.9(9)
C(1) – C(21) – C(1)#1	91.0(2)	C(43)#1 – C(42) – C(41)	122.4(6)
C(2) – C(1) – C(21)#1	137.2(3)	C(42) – C(43) – C(41)#1	105.1(8)
C(2) – C(1) – C(21)	131.1(3)	C(42) – C(41) – C(42)#1	89.2(4)
C(22) – C(21) – C(1)#1	135.1(3)	C(41) – C(42) – C(41)#1	90.8(4)
C(22) – C(21) – C(1)	133.2(3)		

Symmetry transformations used to generate equivalent atoms: #1 –x+1, y, -z+1/2.

The asymmetric unit contains one half of a tetraferrocenyl cation and one half of the PF_6 anion. Both the PF_6 anion and one of the Fe-bound Cp ligands exhibited a two-fold disorder, with relative occupancies of 55% and 45% for the entire Cp ligand and for two unique fluorine atoms. The Cp unit attached to Co was located on a mirror plane and found to be severely disordered, and therefore was allowed to

refine as two whole carbon atoms and one half carbon atom, bond distances and angle for this ligand are therefore distorted.

The structure of the cation in compound **19** is similar to that of neutral compound **18** (refer to section 3.2.3), the four ferrocenyl groups are twisted to an extent about the C–C bonds to the cyclobutadiene ring. Two ferrocenyl groups at the diagonal position are above the four member ring and point away from the cobalt atom. Another two are slightly below the ring. The C_5 rings of Cp ligands bound to iron atoms are in the eclipsed conformation with the dihedral angles as 3.3º and 6.6º for Fe(1) and Fe(2) respectively. The averaged distance between the iron atoms is 5.944 Å.

The cyclobutadiene group is square and approximately planar. The distance of each atom from the mean plane is 0.0125 Å. The bond lengths in the cyclobutadiene ring average 1.473(2) Å and the bond angles are very close to 90º. The averaged cobalt-carbon distances are 1.994(3) Å and 2.067(4) Å for the atoms in the cyclobutadiene ring and the Cp carbons respectively, which is similar to other Cp-cobalt-cyclobutadiene sandwich compounds.[10-12]

4.2.3 FT-IR spectroscopy

IR spectroscopy has proven to be useful to tell whether a given mixed-valence compound is electron delocalized or not on the time scale of molecular vibrations (ca. 10^{-12} s).[13-15] When an Fe^{II} metallocene is oxidized to an Fe^{III} metallocene, there is a dramatic change in the IR spectrum. The perpendicular C−H bending band, which is observed at 815 cm^{-1} for ferrocene, appears to be the best diagnostic

parameter of the oxidation state of a ferrocene. This band is found at 851 cm^{-1} for ferrocenium salts and it does not change much in intensity in the process of oxidation.[13] Due to the peak of PF_6 at 840 cm^{-1}, which overlaps with the C–H bending band, the BF_4 salts were used to run the IR spectra. The FT-IR spectra of **18**, [**18**]BF_4, [**18**][BF_4]$_2$ and [**18**][BF_4]$_3$ are presented in Figure 4-2.

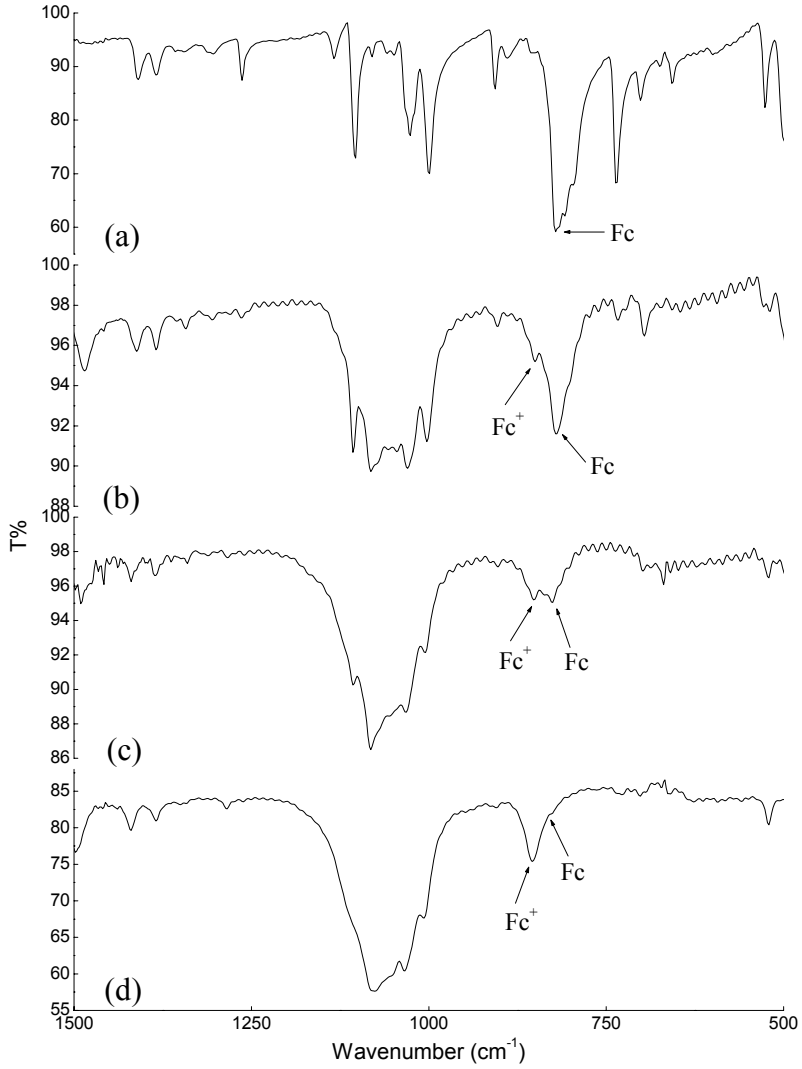

FIGURE 4–2. KBr-PALLET FT-IR SPECTRA OF (a){CpFe(η^5-C_5H_4)}$_4$(η^4-C)CoCp (**18**); (b) [{CpFe(η^5-C_5H_4)}$_4$(η^4-C)CoCp][BF_4], (c) [{CpFe(η^5-C_5H_4)}$_4$(η^4-C)CoCp] [BF_4]$_2$ AND (d) [{CpFe(η^5-C_5H_4)}$_4$(η^4-C)CoCp] [BF_4]$_3$ AT ROOM TEMPERATURE.

The upper tracing for the unoxidized molecule shows a strong structured band at 825 cm^{-1}. The IR spectrum of mono-oxidized mixed-valence compound ([**18**]BF_4) shows two C–H bending bands at 825 and 852 cm^{-1} respectively. The area ratio of these two peaks is 3:1. Similar to [**18**]BF_4, the di-oxidized mixed-valence complex ([**18**][BF_4]$_2$) displays two absorptions at 825 and 852 cm^{-1} with the area ratio of 1:1 in the IR spectrum. For tri-cationic compound (([**18**][BF_4]$_3$), a main peak at 852 cm^{-1} with a shoulder at 821 cm^{-1} is observed. The area ratio is estimated as 3:1.

For the bi-ferrocene mixed-valence compounds such as 1', 6'-dibromobiferrocenium triiodide, in which electron is localized on FT-IR time scale (~ 10^{-12} s), there are two bands at 822 and 849 cm^{-1} respectively in the IR spectrum.[16] It is very clear that mono-, di- and tri- oxidized mixed-valence cations have localized Fe^{II} and Fe^{III} moieties on the FT-IR time scale. Thus, the electron transfer rates in these three mixed-valence complexes are less than ~10^{12} s^{-1} at room temperature in the solid state.[15]

4.2.4 Electron paramagnetic resonance (EPR)

With the IR data of mono- and di- oxidized mixed-valence compounds in hand, EPR spectra of the mixed-valence compounds ([{CpFe(η^5-C_5H_4)}$_4$(η^4-C)CoCp][PF_6] (**19**) and [{CpFe(η^5-C_5H_4)}$_4$(η^4-C)CoCp][PF_6]$_2$ (**21**)) were measured to determine whether the electron transfer rate in **19** and **21** are greater than the electron paramagnetic resonance (EPR) time scale (10^{-9} s) or not. In addition, g values of these two compounds can be estimated based on the EPR data and spin-

spin interaction in **21** can be evaluated. The X-band EPR spectra for powder samples of **19** and **21** were run at 4K as shown in Figure 4-3. EPR spectra of these two compounds as a function of temperature are shown in Figure 4-4 and the g values extracted from all of these spectra are collected in Table 4-4.

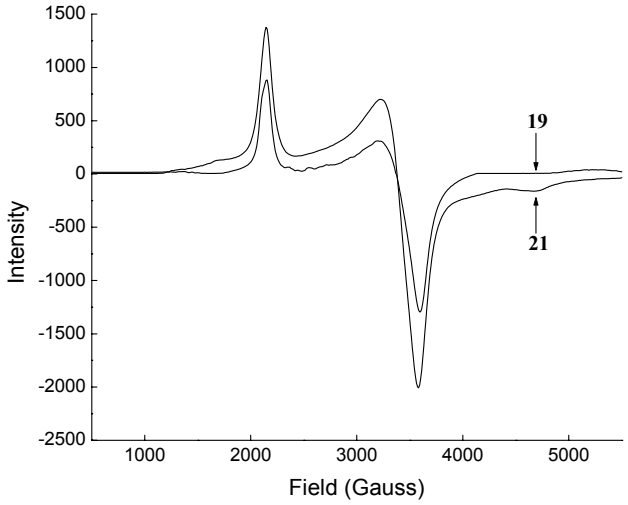

FIGURE 4–3. X-BAND EPR SPECTRA FOR POWDERED SAMPLES OF [{CpFe(η^5-C_5H_4)}$_4$(η^4-C)CoCp][PF_6] (**19**) AND [{CpFe(η^5-C_5H_4)}$_4$(η^4-C)CoCp][PF_6]$_2$ (**21**) AT 4 K.

At 4 K, complex [{CpFe(η^5-C_5H_4)}$_4$(η^4-C)CoCp][PF_6] (**19**) displays an EPR spectrum with g values of 3.129 ($g_{//}$) and 1.868 ($g_{\perp}$) and a g-tensor anisotropy, $\Delta g = g_{//} - g_{\perp}$, equal to 1.261. The EPR spectrum of [{CpFe(η^5-C_5H_4)}$_4$(η^4-C)CoCp][PF_6]$_2$ (**21**) at 4 K yields 3.133 ($g_{//}$), 1.874 ($g_{\perp}$) and 1.259 (Δg) respectively. Although the peak positions in the EPR spectra of **21** were almost the same as those of **19**, the intensity is twice as high. (Figure 4-3) Thus it is concluded that the two unpaired electrons in **21** are almost independent and the energy of spin-spin interaction in **21** is very small.

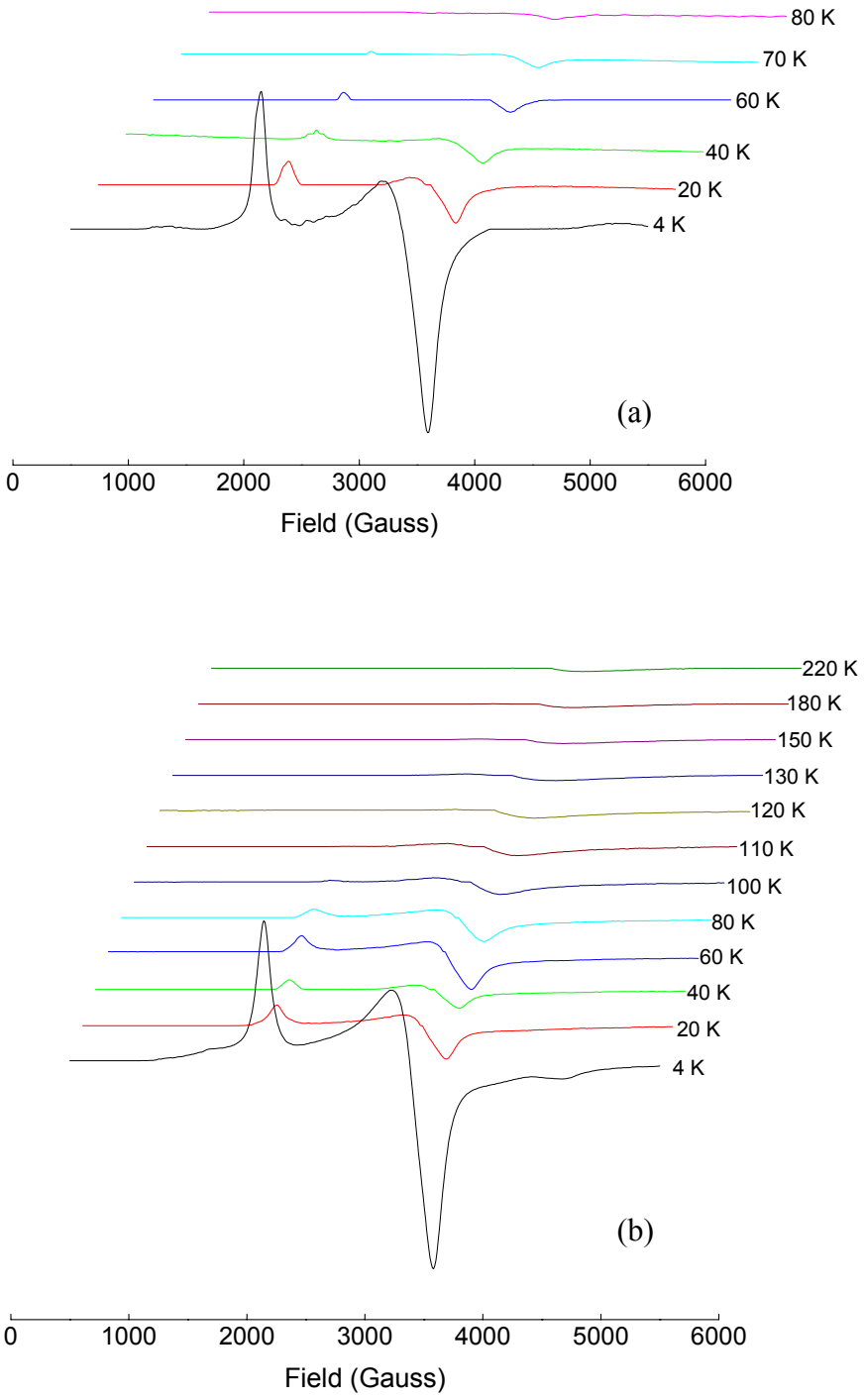

FIGURE 4–4. VARIABLE TEMPERATURE X-BAND EPR SPECTRA OF POWDERED SAMPLES OF (a) [{CpFe(η^5-C_5H_4)}$_4$(η^4-C)CoCp][PF_6] (**19**) AND (b) [{CpFe(η^5-C_5H_4)}$_4$(η^4-C)CoCp] [PF_6]$_2$ (**21**).

TABLE 4–4. EPR DATA FOR [{CpFe(η^5-C_5H_4)}$_4$(η^4-C)CoCp][PF_6] (**19**) AND [{CpFe(η^5-C_5H_4)}$_4$(η^4-C)CoCp] [PF_6]$_2$ (**21**).

19				**21**			
T (K)	$g_{//}$	$g_{\perp}$	Δg	T (K)	$g_{//}$	$g_{\perp}$	Δg
4	3.129	1.868	1.261	4	3.133	1.874	1.259
20	3.123	1.864	1.259	20	3.134	1.872	1.262
40	3.129	1.868	1.261	40	3.140	1.872	1.268
60	3.136	1.866	1.270	60	3.146	1.874	1.272
70	3.136	1.864	1.272	80	3.158	1.876	1.282
80	3.190	1.923	1.267	100	3.098	1.861	1.237
150	----	----	----	110	3.075	1.842	1.233
180	----	----	----	120	----	1.822	----
220	----	----	----	130	----	1.786	----
298	----	----	----	150	----	1.806	----
				180	----	1.820	----
				220	----	1.842	----
				298	----	----	----

Figure 4-4 illustrates the temperature dependence of the EPR spectra for the samples of **19** and **21**, where it can be seen that the peaks for these two compounds become broader and less intense with an increase in temperature. However, the values of Δg remain nearly invariable. The peaks disappear by 150 K for **19** and by 220 K for **21**.

It is known that the g-tensor anisotropy, Δg, is 3.09 for a ferrocenium salt.[17] However, in case of the binuclear mixed-valence biferrocenium ions, a reduction of

Δg was seen.[15,16,18-20] It has been suggested that Δg can be used to determine whether the rate of electron transfer is greater than the EPR time scale. If $\Delta g < 0.8$, the rate of intramolecular electron transfer in biferrocenium system is greater than the EPR time scale.[16] This rule is suitable for the tetraferrocenium mixed-valence complexes. From Table 4-3, the Δg values for **19** and **21** indicate that the cations in the complexes are localized on the EPR time scale.

The g factor can be calculated from the EPR data at 4 K with the equation 4-1.

$$g = \left(\frac{1}{3} g_{//}{}^2 + \frac{2}{3} g_{\perp}{}^2 \right)^{1/2} \qquad \textbf{(4-1)}$$

The value of g is 2.362 for **19** and 2.369 for **21** respectively.

4.2.5 ^{57}Fe Mössbauer spectroscopy

Mössbauer spectroscopy is a very useful technique to explore the electronic states of iron ions in mixed-valence complexes. The Mössbauer spectra of ferrocenyl groups are characterized by large quadrupole splitting (ΔE_Q) in the range of 2.0 to 2.5 mm/s, while the ferrocenium cations give spectra with small or disappearing quadrupole splitting.[21]

Variable-temperature ^{57}Fe Mössbauer spectra were run for [{CpFe(η^5-C_5H_4)}$_4$ (η^4-C)CoCp][PF_6] (**19**) and [{CpFe(η^5-C_5H_4)}$_4$(η^4-C)CoCp][PF_6]$_2$ (**21**) from 4.2 K to 295 K, as illustrated in Figures 4-5 and 4-6, respectively. All of the spectra were least-squares fitted with Lorentzian lineshapes and the selected fitting parameters are collected in Tables 4-5 and 4-6.

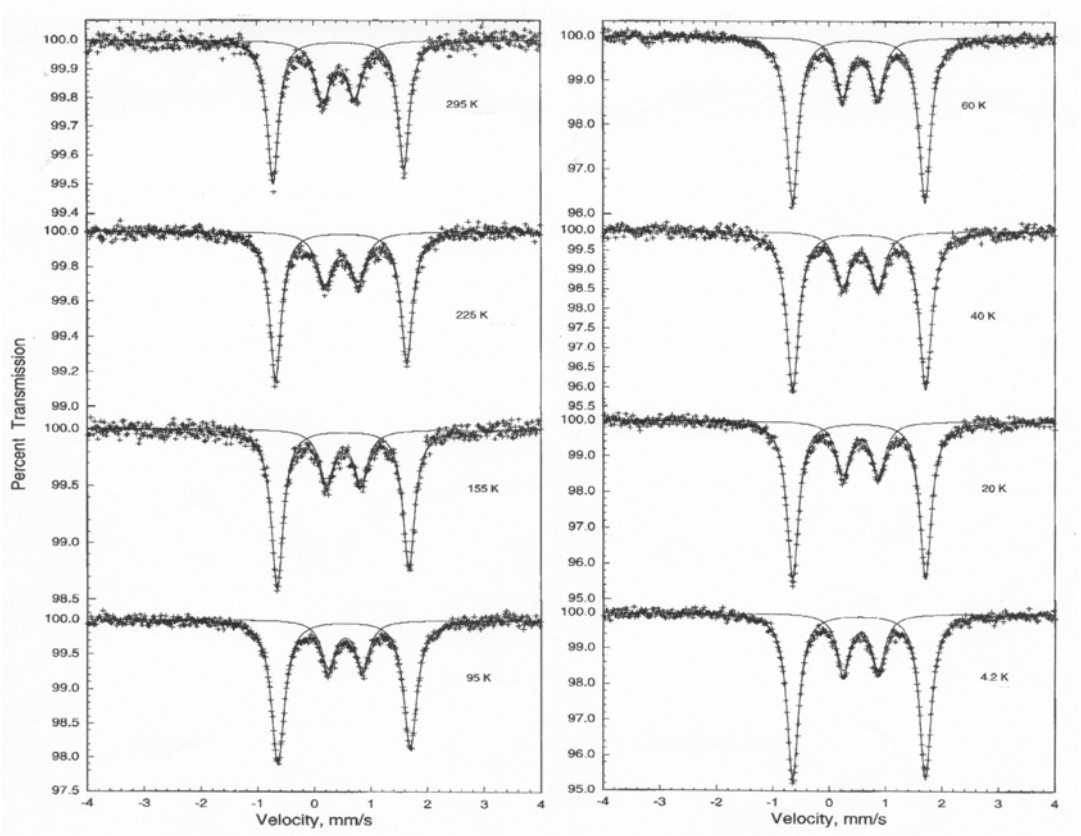

FIGURE 4–5. VARIABLE-TEMPERATURE ^{57}Fe MÖSSBAUER SPECTRA OF [{CpFe(η^5-C_5H_4)}$_4$(η^4-C)CoCp][PF_6] (**19**).

At all experimental temperatures, the Mössbauer spectra of **19** consist of two quadrupole-split doublets, one with the quadrupole splitting (ΔE_Q) from 2.32 to 2.36 mm/s, which is close to the quadrupole splitting seen for ferrocene and the other with from 0.56 to 0.62 mm/s characteristic of an Fe(III) metallocene. The area ratio of two doublets is about 3:1 (Fe(II):Fe(III)) at 4.2 K and decreases with the increase of temperature. The Mössbauer spectra of **21** at all temperatures employed also show two doublets with ΔE_Q from 2.31 to 2.37 mm/s for ferrocenyl units and from 0.38 to 0.44 mm/s for ferrocenium moiety, respectively. Both doublets have

almost the same spectral area at 4.2 K. However, when the temperature increases, the area ratio of Fe(II) site to Fe(III) site decreases. The changes of the area ratio may come from a difference in sensitivities for ferrocenyl unit and ferrocenium moiety.

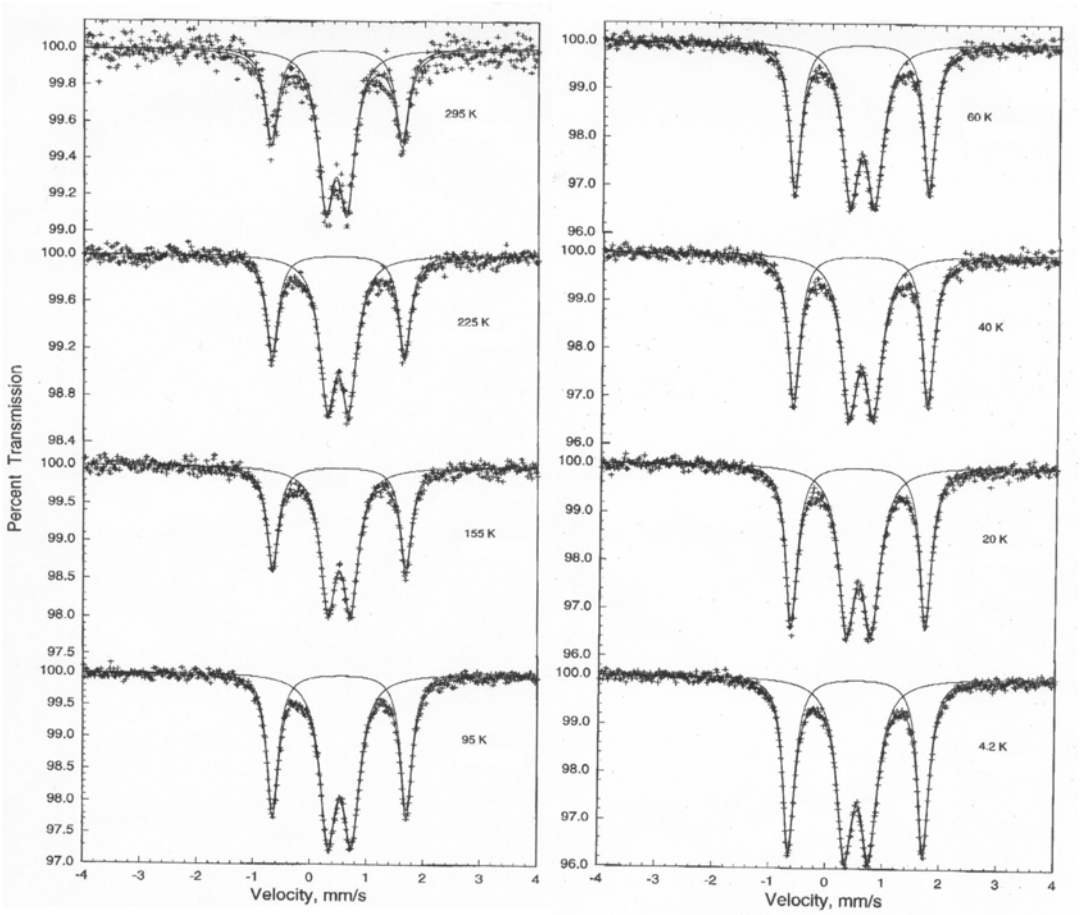

FIGURE 4–6. VARIABLE-TEMPERATURE ^{57}Fe MÖSSBAUER SPECTRA OF [{CpFe(η^5-C_5H_4)}$_4$(η^4-C)CoCp][PF_6]$_2$ (**21**).

It has been reported that a doublet with ΔE_Q of 1.0 ~ 1.2 is observed for mixed-valence biferrocene with an intra-molecular electron-transfer rate greater than ~ 10^7 s^{-1}.[13,15,22] Both complexes **19** and **21** show two doublets with the ΔE_Q, which is appropriate for ferrocene and ferrocenium, at all experimental temperatures. This pattern of two doublets is expected for a mixed-valence compound which is valence trapped on the time scale of the ^{57}Fe Mössbauer experiment (10^{-7} s).

TABLE 4–5. ^{57}Fe MÖSSBAUER PARAMETERS FOR [{CpFe(η^5-C_5H_4)}$_4$(η^4-C)CoCp][PF_6] (**19**).

T K	δ, mm/s [a]	ΔE_Q, mm/s	Γ, [b] mm/s	Area, %	Assignment
4.2	0.538	2.36	0.25	71.3	Iron(II)
	0.563	0.62	0.30	28.7	Iron(III)
95	0.525	2.34	0.28	72.2	Iron(II)
	0.546	0.60	0.31	27.8	Iron(III)
155	0.509	2.33	0.25	70.1	Iron(II)
	0.522	0.61	0.30	29.9	Iron(III)
225	0.479	2.32	0.25	67.4	Iron(II)
	0.485	0.59	0.34	32.6	Iron(III)
295	0.440	2.32	0.24	63.9	Iron(II)
	0.447	0.56	0.32	36.1	Iron(III)

[a] The isomer shifts are given relative to room temperature α-iron foil.

[b] Γ is the linewidth.

TABLE 4–6. ^{57}Fe MÖSSBAUER PARAMETERS FOR [{CpFe(η^5-C_5H_4)}$_4$(η^4-C)CoCp][PF_6]$_2$ (**21**).

T K	δ, mm/s [a]	ΔE_Q, mm/s	Γ, [b] mm/s	Area, %	Assignment
4.2	0.534	2.37	0.25	43.1	Iron(II)
	0.549	0.44	0.35	56.9	Iron(III)
95	0.525	2.36	0.26	40.2	Iron(II)
	0.535	0.42	0.35	59.8	Iron(III)
295	0.448	2.31	0.29	36.0	Iron(II)
	0.439	0.38	0.34	64.0	Iron(III)

[a] The isomer shifts are given relative to room temperature α-iron foil.

[b] Γ is the linewidth.

4.2.6 Magnetic susceptibility

Magnetic susceptibility data were measured for [{CpFe(η^5-C_5H_4)}$_4$(η^4-C) CoCp][PF_6] (**19**) and [{CpFe(η^5-C_5H_4)}$_4$(η^4-C)CoCp][PF_6]$_2$ (**21**) in the range 5–250 K. The temperature dependences of molar magnetic susceptibility are present in Figure 4-7 and the data are given in Table 4-7.

The magnetic susceptibilities of both compounds show Curie-Weiss behavior. The Curie-Weiss susceptibility is given by

$$\chi = C/(T - \Theta) + \chi_0 \qquad \textbf{(4-2)}$$

where C is a constant, Θ is the Curie-Weiss temperature and χ_0 is a temperature-independent contribution to the para-magnetism.[23] Fitting the collected data (Table

4-7) with equation 4-2 give values of constant C of 0.649 emu·K·mol^{-1} for complex **19** and 1.42 emu·K·mol^{-1} for compound **21**.

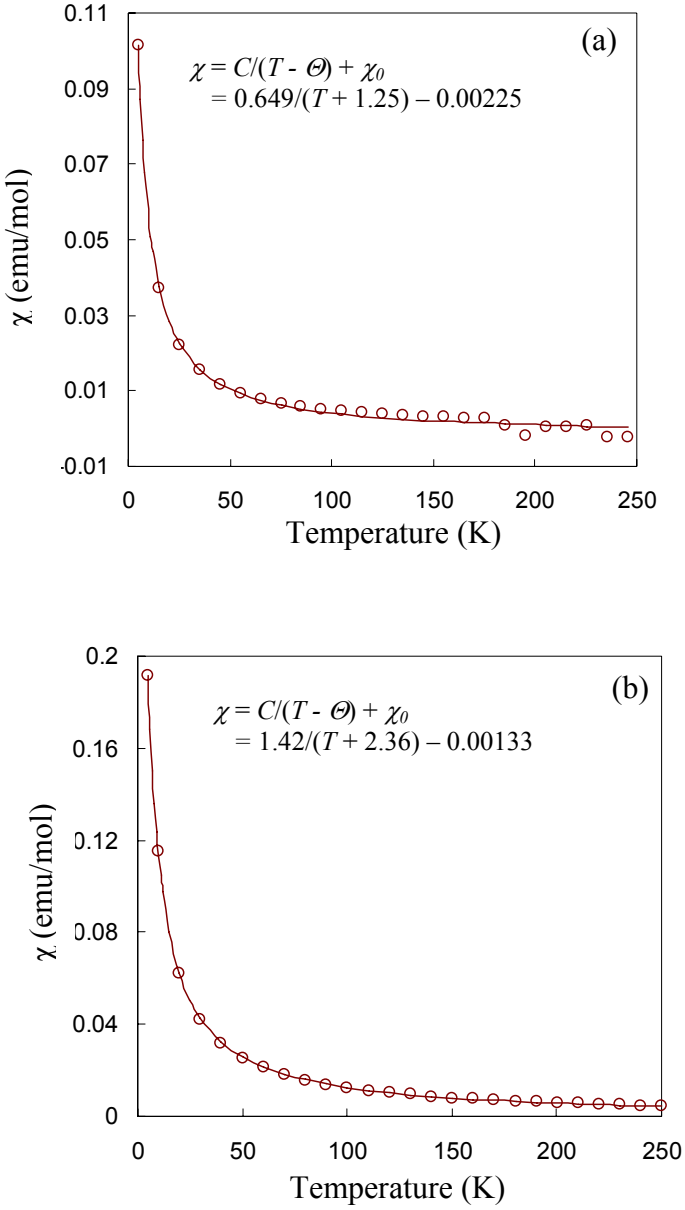

FIGURE 4–7. EXPERIMENTAL MOLAR PARAMAGNETIC SUSCEPTIBILITY VS. TEMPERATURE FOR (a) [{CpFe(η^5-C_5H_4)}$_4$(η^4-C)CoCp][PF_6] (**19**) AND (b) [{CpFe(η^5-C_5H_4)}$_4$(η^4-C)CoCp] [PF_6]$_2$ (**21**). THE SOLID LINES REPRESENT THE LEAST-SQUARES FIT TO THE CURIE–WEISS LAW $\chi = C/(T - \Theta) + \chi_0$.

TABLE 4–7. THE PARAMAGNETIC SUSCEPTIBILITY DATA FOR [{CpFe(η^5-C_5H_4)}$_4$(η^4-C) CoCp][PF_6] (**19**) AND [{CpFe(η^5-C_5H_4)}$_4$(η^4-C)CoCp][PF_6]$_2$ (**21**).

19		**21**	
Temperature(K)	χ (emu·mol^{-1})	Temperature(K)	χ (emu·mol^{-1})
5	0.101626	5	0.191613
15	0.037062	10.01	0.115349
24.97	0.022118	19.99	0.061932
35	0.015493	30	0.041937
45	0.011836	40	0.031645
55.04	0.009392	50.01	0.02535
65.07	0.007681	60.05	0.021202
75.1	0.006726	70.08	0.018098
85.1	0.005839	80.1	0.01571
95.15	0.005155	90.1	0.013877
105.17	0.004605	100.16	0.01243
115.2	0.004158	110.19	0.011237
125.22	0.003788	120.21	0.010248
135.18	0.003473	130.24	0.009415
145.26	0.003212	140.25	0.008697
155.3	0.002988	150.28	0.008073
165.3	0.002797	160.2	0.007528
175.31	0.00263	170.31	0.007051
185.33	0.000942	180.32	0.006616
195.35	-0.00179	190.34	0.006234
205.34	0.000623	200.36	0.005843
215.35	0.000482	210.35	0.005594
225.35	0.000852	220.36	0.005319
235.46	-0.00232	230.38	0.005067
245.38	-0.00229	240.12	0.004841
		250.14	0.004627

To get the effective magnetic moment (μ_{eff}), we use the complete formula

$$\mu_{eff} = \left(\frac{3k}{N\beta^2}\right)^{1/2} (\chi T)^{1/2} \approx \left(\frac{3kC}{N\beta^2}\right)^{1/2} = 2.828(C)^{1/2}\,\mu_B \qquad \textbf{(4-3)}$$

where N is Avogadro's number (6.022 x 10^{23}), β is Bohr magneton (9.274 x 10^{24} $J{\cdot}T^{-1}$) and k is Boltzmann's constant (1.38 x 10^{-23} $J{\cdot}K^{-1}$).[24] Based on the fitting constant C and equation 4-3, the value of μ_{eff} for complex **19** is 2.27 μ_B, which corresponds to one unpaired electron.[13,25] The effective magnetic moment is 3.36 μ_B for compound **21** correspondent to two unpaired electrons.

As to a compound with two unpaired electrons, if there is spin-spin interaction between the electrons, the compound shows either ferromagnetic or anti-ferromagnetic behavior if the coupling constant is finite.[26] However, the di-cationic mixed-valence compound (**21**) exhibits Curie-Weiss behavior down to the lowest temperature measured which indicates that the compound is paramagnetic and the spin-spin interaction in di-oxidized ionic compound is negligible. This is consistent with the EPR measurements.

The Curie-Weiss law can be generalized for the systems with multiple unpaired electrons as:

$$\chi = \frac{Ng^2\beta^2}{3kT} S(S+1) \qquad \textbf{(4-4)}$$

where S is the quantum number for the electron angular momentum and g is g-factor.[24] Thus, the g-factor can be estimated by transfer the equation 4-4 as:

$$g = \left(\frac{3k\chi T}{N\beta^2 S(S+1)} \right)^{1/2} \approx \left(\frac{3kC}{N\beta^2 S(S+1)} \right)^{1/2} = 2.828 \left(\frac{C}{S(S+1)} \right)^{1/2} \qquad \textbf{(4-5)}$$

For the complex **19** which has one unpaired electron, S equals ½ and value of g is 2.631. The compound **21** has two unpaired electrons and S = 1. Hence the evaluated value of g is 2.383. These two values are consistent with those obtained from EPR data (2.362 for **19** and 2.369 for **21**).

4.2.7 Near infrared (near-IR) spectroscopy

Figure 4-8 illustrates the near-IR spectra of [{CpFe(η^5-C_5H_4)}$_4$(η^4-C)CoCp][PF_6] (**19**) and [{CpFe(η^5-C_5H_4)}$_4$(η^4-C)CoCp][PF_6]$_2$ (**21**) measured in $CDCl_3$, CD_3CN and acetone-d_6 respectively. Deuterated solvents are used due to the interferences in the near-IR region from C–H overtone vibrational modes.[27] The spectra in deuterated dimethyl sulfoxide were attempted. However, since the solvent or an impurity in the solvent reacts with the mixed-valence ions rapidly, it is impossible to obtain good spectra. The properties of the IVCT band for [{CpFe(η^5-C_5H_4)}$_4$(η^4-C)CoCp][PF_6] (**19**) and [{CpFe(η^5-C_5H_4)}$_4$(η^4-C)CoCp][PF_6]$_2$ (**21**) are summarized in Table 4-8.

Complex **19** shows an absorption at 1062 nm in $CDCl_3$, 1519 nm in acetone-d_6 and 1517 nm in CD_3CN. Similar peaks at the region of 1300 to 2000 nm are observed for the biferrocenium mixed-valence systems.[27,28] Consistent with the literature, the absorption in the near IR region is assigned to IVCT involving

electron transfer between a ferrocenyl unit and ferrocenium moiety, which is solvent dependent.

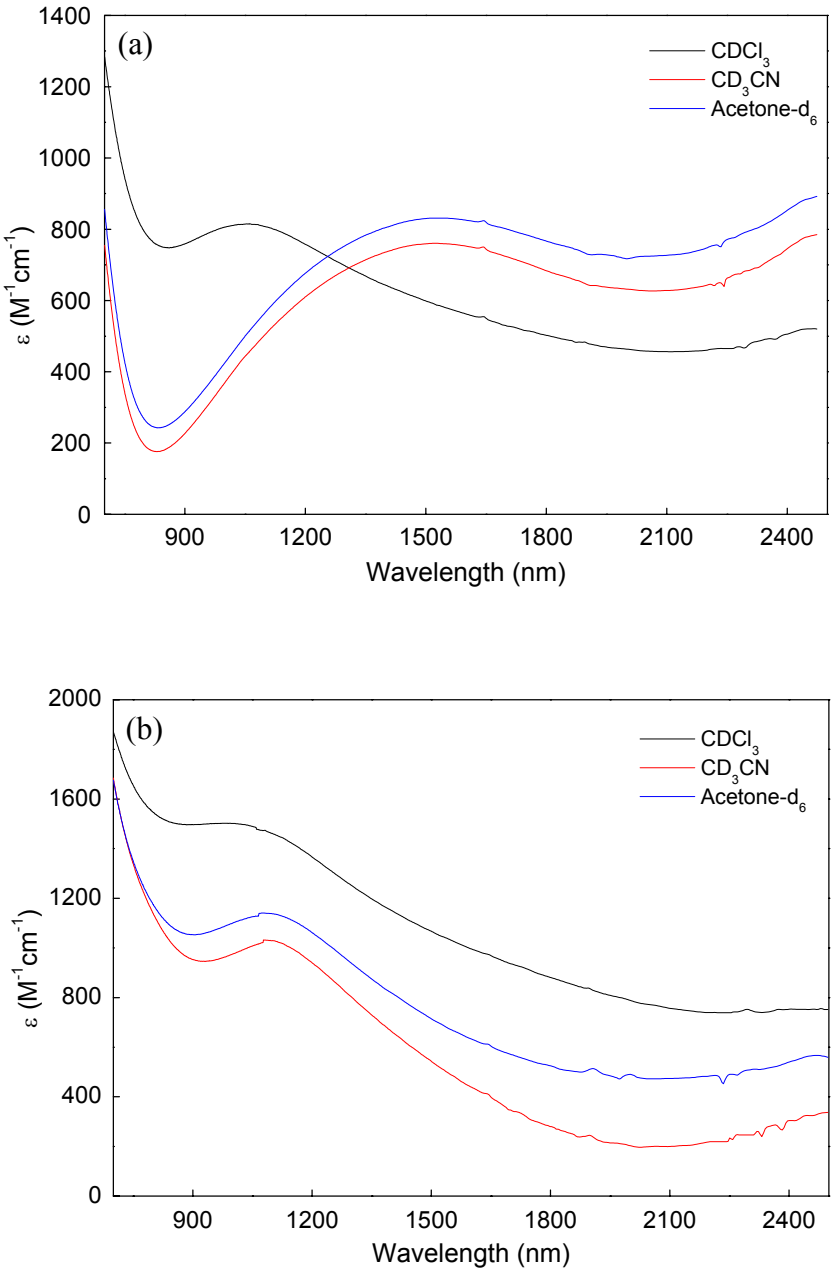

FIGURE 4–8. NEAR-IR SPECTRA FOR (a) [{CpFe(η^5-C_5H_4)}$_4$(η^4-C)CoCp][PF_6] (**19**) AND (b) [{CpFe(η^5-C_5H_4)}$_4$(η^4-C)CoCp][PF_6]$_2$ (**21**) IN DIFFERENT SOLVENTS.

TABLE 4–8. PROPERTIES OF THE INTERVALENCE TRANSFER BAND FOR [{CpFe(η^5-C_5H_4)}$_4$(η^4-C)CoCp][PF_6] (**19**) AND [{CpFe(η^5-C_5H_4)}$_4$(η^4-C)CoCp] [PF_6]$_2$ (**21**).

	Solvent	$CDCl_3$	Acetone-d_6	CD_3CN
	$1/n^2$-1/D [a]	0.2710	0.4963	0.5280
19	λ_{max} (nm) [b]	1062	1519	1517
	ν_{max} (cm^{-1}) [c]	9416	6583	6591
	$(\Delta\nu_{1/2})_{obs}$ (cm^{-1}) [d]	5000	5000	5000
	$(\Delta\nu_{1/2})_{calc}$ (cm^{-1}) [e]	4370	3465	3490
	$(\Delta\nu_{1/2})_{obs}/(\Delta\nu_{1/2})_{calc}$	1.14	1.44	1.43
	ε_{max} ($M^{-1}cm^{-1}$) [f]	815	832	761
	α^2 (1) [g]	5.1×10^{-3}	7.4×10^{-3}	6.7×10^{-3}
	α^2 (2) [h]	4.4×10^{-3}	5.1×10^{-3}	4.7×10^{-3}
21	λ_{max} (nm) [b]	1029	1071	1080
	ν_{max} (cm^{-1}) [c]	9997	9303	9280
	$(\Delta\nu_{1/2})_{obs}$ (cm^{-1}) [d]	5257	4743	4687
	$(\Delta\nu_{1/2})_{calc}$ (cm^{-1}) [e]	4496	4315	4309
	$(\Delta\nu_{1/2})_{obs}/(\Delta\nu_{1/2})_{calc}$	1.17	1.10	1.09
	ε_{max} ($M^{-1}cm^{-1}$) [f]	1502	1140	1032
	α^2 (1) [g]	9.3×10^{-3}	6.8×10^{-3}	6.1×10^{-3}
	α^2 (2) [h]	7.9×10^{-3}	6.2×10^{-3}	5.6×10^{-3}

[a] n^2, the square of the refractive index, is the optical dielectric constant of the solvent and D is the static dielectric constant.
[b] λ_{max} is the wavelength of maximum absorbance for the IVCT band.
[c] $\nu_{max} = E_{op}$ is the energy of the band at λ_{max}.
[d] $(\Delta\nu_{1/2})_{obs}$ is the observed bandwidth at half-height.
[e] $(\Delta\nu_{1/2})_{calc}$ is calculated using equation 4-6.
[f] ε_{max} is the molar extinction coefficient at λ_{max}.
[g] α^2 is calculated using equation 4-8 with $\Delta\nu_{1/2}$ (obs).
[h] α^2 is calculated using equation 4-8 with $\Delta\nu_{1/2}$ (calc).

Compared with the mono-oxidized complex (**19**), compound **21** displays an absorption in the different solvents at the almost same position (1029 nm in $CDCl_3$, 1071 nm in acetone-d_6 and 1080 nm in CD_3CN). The IVCT band is nearly solvent independent and solvent reorganization associated with the electronic transition for compound **21** is small.

It is suggested that the stabilization of a mixed-valence complex by solvation is strongly dependent on the extent of electron delocalization in the system.[2] The influence of solvent on the IVCT band becomes smaller as the interaction of metals in the mixed-valence complex becomes larger. Thus, compound **19** is a member of Class-II mixed-valence compounds (the solvent and exchanging electron are localized). However, the compound **21** is placed in the Class II-III (the solvent is averaged and the exchanging electron is localized) or Class III (the solvent is averaged and the exchanging electron is delocalized).[2]

To seek more information concerning which type the compound **21** is, Hush theory [29] is used to analyze the spectroscopic data. The interaction parameters generated gives an approximate measure of the extent of ground-state delocalization in a mixed-valence complex. Hush has derived an expression for the bandwidth at the half-maximum ($\Delta\nu_{1/2}$) of the IVCT band of a mixed-valence compound as shown in equation 4-6:

$$\nu_{max} - \nu_0 = (\Delta\nu_{1/2})^2 / 2310 \qquad \textbf{(4-6)}$$

where ν_{max} is the energy of maximum absorbance for the IVCT band and ν_0 is the internal energy difference between the two oxidation states isomers which can be

estimated by the difference in the redox potentials (ΔE) of the metal centers in the molecule (refer to section 3.2.5) through equation 4-7:

$$n\Delta EF = Nh\nu_0 \qquad \textbf{(4-7)}$$

where n is number of electrons, F is Faraday's constant, N is Avogadro's constant and h is Planck's constant.[30] Therefore, the difference potential is 0.16 V for **19** (Table 3-6), which corresponds to a value of ν_0 of 1290 cm^{-1}. For compound **21**, ν_0 equals to 1209 cm^{-1}. The ratio of $(\Delta\nu_{1/2})_{obs}/(\Delta\nu_{1/2})_{calc}$ in the various solvents has an average value of 1.34 for **19** and 1.12 for **21**. These values are similar to results obtained for the Class II mixed-valence compounds where the ratios average from 1.1 to 1.4.[27,31-33]

Hush further proposed an expression for the delocalization parameter α^2 (equation 4-8) which is also used to classify mixed-valence system. In this equation, ν_{max} is the energy of maximum absorbance for the IVCT band, ε_{max} is the molar extinction coefficient at ν_{max} and d is the distance between the metal centers.

$$\alpha^2 = \frac{(4.2\times10^{-4})\varepsilon_{max}\Delta\nu_{1/2}}{\nu_{max}d^2} \qquad \textbf{(4-8)}$$

The average distance between the adjacent iron centers in complex **19** is 5.943 Å. Because of the absence of the crystal data, this distance in **21** is taken to be 5.86 Å which is the distance in the neutral compound. Using the observed ε_{max}, $\Delta\nu_{1/2}$ and ν_{max}, the calculated average α^2 are 6.3 x 10^{-3} for **19** and 7.4 x 10^{-3} for **21,** respectively. These are also comparable to some reported Class II systems.[27,30,34]

The relationship of the ν_{max} of the IVCT band with the polarity of the solvent is also helpful in classifying the mixed-valence compounds. The polarity of the

solvents are estimated by the solvent polarity function $1/n^2$-1/D, where n is the solvent's refractive index and D is the dielectric constant.[29,35,36] The values of ν_{max} are plotted against $1/n^2$-1/D as shown in Figure 4-9. For compound **19**, the plot gives a straight line with intercept of 1.2 x 10^4 cm^{-1}. The value of intercept is 1.0 x 10^4 cm^{-1} for compound **21**. The intercept is interpreted as the Franck-Condon inner sphere optical activation energy. The values of this energy for **19** and **21** are larger than delocalized mixed-valence compounds (Class-III) [37,38] but in good agreement with Class-II mixed valence compounds.[27] In addition, a linear relationship is expected for typical Class-II IVCT bands. [39] However, the IVCT band maximum in complex **21** varies much less with solvent polarity than that of **19**. This implies that the solvent reorganization for the electronic transition is smaller.[38,40] Thus, the compound **19** is classified as Class II and compound **21** as Class II-III as defined by Meyer.[2]

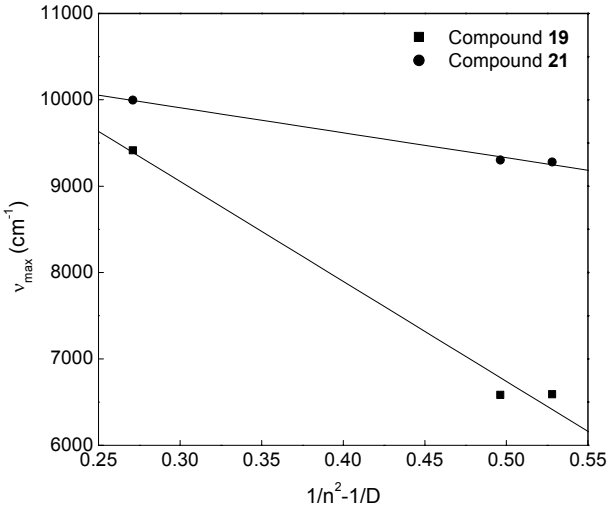

FIGURE 4–9. VARIATION IN THE IVCT PEAK MAXIMA WITH SOLVENT POLARITY FOR [{CpFe (η^5-C_5H_4)}$_4$(η^4-C)CoCp][PF_6] (**19**) AND [{CpFe(η^5-C_5H_4)}$_4$(η^4-C)CoCp] [PF_6]$_2$ (**21**).

Near-IR spectra of the tetrafluoroborate salt of the mono-oxidized ion, the tetrafluoroborate and triflate salts of the di-oxidized mixed-valence compounds were also measured in acetone-d_6. The IVCT band positions of these compounds are almost the same as those for the PF_6^- salts. Thus, at room temperature in solution, the counterion properties do not strongly affect the electron transfer rate in the mixed- valence compound.

The near-IR spectrum of the tri-oxidized compound [{CpFe(η^5-C_5H_4)}$_4$(η^4-C) CoCp][BF_4]$_3$ (**22**) in acetone-d_6 shows one broad peak at 922 nm. If the solution of the compound is stored for a while, the near-IR spectrum shifts to lower frequency, which indicates that the tricationic compound is unstable and may decompose in solution. The mixture of the tetra-oxidized compound [{CpFe(η^5-C_5H_4)}$_4$(η^4-C)CoCp][BF_4]$_4$ (**24**) and [Fe(η^5-$C_5H_4C(O)CH_3)_2$][BF_4] (**23**) shows no absorption in the near-IR region, consistent with the lack of any intervalence charge transfer behavior for tetra-cationic compound as expected.

4.2.8 ^{1}H VT-NMR spectroscopy

Based on near-IR spectra of dicationic compound (**21**), it is known that the dicationic mixed-valence compound displays electron transfer in solution at room temperature. To be used as a building block for molecular QCA, it is essential to evaluate whether the electron transfer rate is affected by temperature. Variable-temperature (VT) NMR can give the answers. As described in chapter 3, in neutral compound **18**, the rotation rate of ferrocene around the C–C bond to the

cyclobutadiene center decreases with decreasing temperature and peak splits are observed in ^{1}H NMR at low temperature. For mono- and di-cationic paramagnetic compounds, the decrease of the rotation rate still exists with a decrease in temperature. Meanwhile, if electron transfer rate is decreased with a temperature decreasing, the resonances of ferrocenium can be separated from those of ferrocene in ^{1}H NMR at low temperature (ferrocenium has unusual chemical shift[26]). Furthermore, ^{1}H VT-NMR of the dicationic compound can tell if the dicationic mixed-valence compound is *cis*-isomer.

Figure 4-10 shows the ^{1}H NMR spectra of [{CpFe(η^5-C_5H_4)}$_4$(η^4-C)CoCp] [PF_6] (**19**) in acetone-d_6 solution at variable temperatures. Although the paramagnetism of the molecule has not obliterated the spectra, it causes abnormal chemical shifts and broadened lines. At 293 K, two signals were observed at 3.14 ppm and 8.04 ppm, which are assigned to the Cp ligand coordinated to cobalt atom and all the ferrocene/ferrocenium moieties respectively. This indicates that the electron transfer rate in solution at room temperature is rapid on the ^{1}H NMR time scale (ca. 10^{-3} s).

At 248 K, ^{1}H NMR spectrum of **19** shows 6 peaks: 3 peaks at 24.4 ppm (β-H), 11.4 ppm (Cp ligand coordinated to Fe) and -5.91 ppm (α-H) are assigned to ferrocenium, one peak at 6.57 ppm is assigned to the two ferrocenyl moieties adjacent to the ferrocenium and the resonance from the other ferrocenyl group at the diagonal position appears at -0.11 ppm. A sharp peak at 3.29 ppm is assigned to the Cp ligand coordinated to cobalt atom. Obviously, ferrocenyl groups and ferrocenium moiety can be separated in ^{1}H NMR of **19** at 248 K. Hence, the

electron transfer rate at 248 K is slower than 10^3 s^{-1}. In the neutral compound **18**, the rotation rate of four ferrocenyl groups decreases with decreasing temperature and splitting is observed at 243 K (refer to 3.2.4). With compound **19**, one ferrocenyl group is oxidized to ferrocenium and the conformations of ferrocenium (above or below the cyclobutadiene plane) cause the splitting of the resonance of the Cp ligand coordinated to Co. Thus, at 238 K, the two peaks at 3.40 ppm and 3.13 ppm are assigned to the Cp-Co ligand.

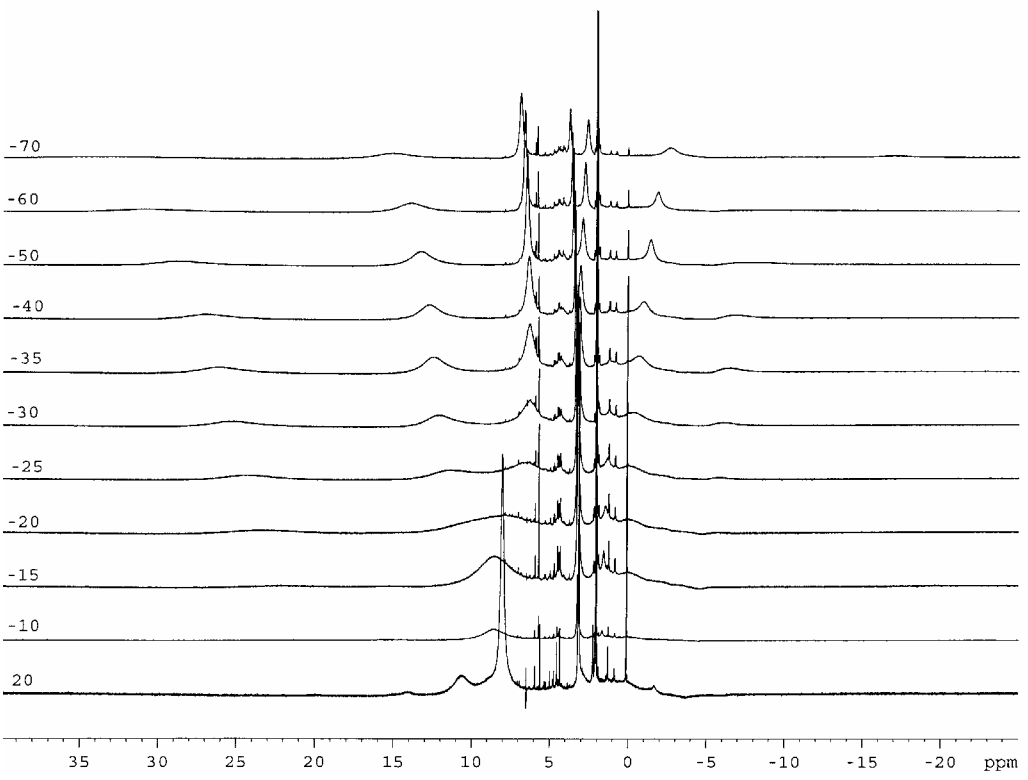

FIGURE 4–10. THE ^{1}H VT-NMR SPECTRA OF [{CpFe(η^5-C_5H_4)}$_4$(η^4-C)CoCp][PF_6] (**19**) IN ACETONE-D_6.

With temperature decrease, all peaks become sharper and then broader due to the decrease of the rocking rate of ferrocene/ferrocenium group. This rate decreasing can result in the further split for α-H and β-H (refer to 3.2.4). For **19**, the coalescence temperature for α-H on ferrocenium is 213 K and this peak splits into two peaks at -2.6 ppm and -17.1 ppm at 203 K, which is consistent with the structure of the neutral complex **18**. However, other splits due to the different conformations in the static structure are not observed.

In addition, peak positions are expected to depend on temperature. Table 4-9 lists the chemical shifts of every peak as a function of temperatures. As shown in Figure 4-11, plots of chemicals shifts *vs.* 1/*T* give straight lines. Thus, the monocationic compound **19** exhibits Curie law behavior,[26] consistent with the magnetic susceptibility measurements (refer to 4.2.6).

TABLE 4–9. CHEMICAL SHIFTS FROM ^{1}H NMR SPECTRA FOR [{CpFe(η^5-C_5H_4)}$_4$(η^4-C) CoCp][PF_6] (**19**) IN ACETONE-D_6.

T (K)	1/T (K^{-1})	Chemical shifts (ppm)			
248	0.00403	24.365	11.392	-0.107	-5.914
243	0.00412	25.426	12.052	-0.405	-5.934
238	0.00420	26.126	12.462	-0.635	-6.418
233	0.00429	26.898	12.893	-0.957	-6.898
223	0.00448	28.854	13.309	-1.374	-7.957
213	0.00469	30.835	13.866	-1.857	-----
203	0.00493	33.724	15.091	-2.622	-----

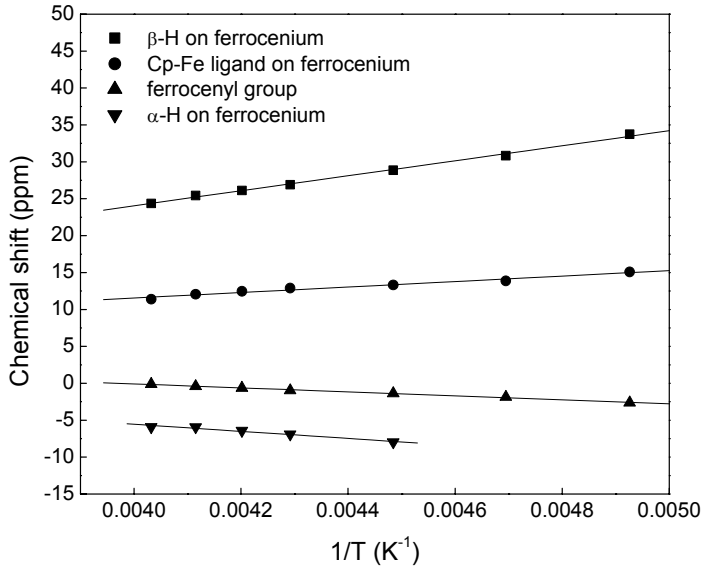

FIGURE 4–11. TEMPERATURE DEPENDENCE OF ^{1}H NMR CHEMICAL SHIFTS FOR [{CpFe(η^5-C_5H_4)}$_4$(η^4-C) CoCp][PF_6] (**19**) IN ACETONE-D_6.

Variable-temperature ^{1}H NMR spectra of [{CpFe(η^5-C_5H_4)}$_4$(η^4-C)CoCp] [CF_3SO_3]$_2$ in acetone-d_6 are shown in Figure 4-12. Similar to the monocationic compound, the paramagnetism of compound causes abnormal chemical shifts and broadened peaks. At 293 K, NMR spectrum of the compound shows 3 peaks at 15.2 ppm (Cp-Fe and α-H or β-H), 10.7 ppm (α-H or β-H) and 9.17 ppm (Cp-Co) respectively. It is impossible to distinguish the ferrocenyl groups from ferrocenium. Thus, at this temperature, the electron transfer rate of compound is faster than 10^3 s^{-1} in solution.

When the temperature decreases, the signal from the Cp-Co ligand at 9.17 ppm shifts to low field and becomes broader. Finally, it is overlapped by the peak at 11.9 ppm at 248 K. The other two peaks also become broader and the intensities of these two peaks decrease with decreasing temperature. Meanwhile, a peak at 3.4

ppm appears which is assigned to ferrocenyl groups. Hence, it is possible to differentiate ferrocenyl groups from ferrocenium at low temperature. The electron transfer rate in dicationic compound also decreases with the decrease of temperature.

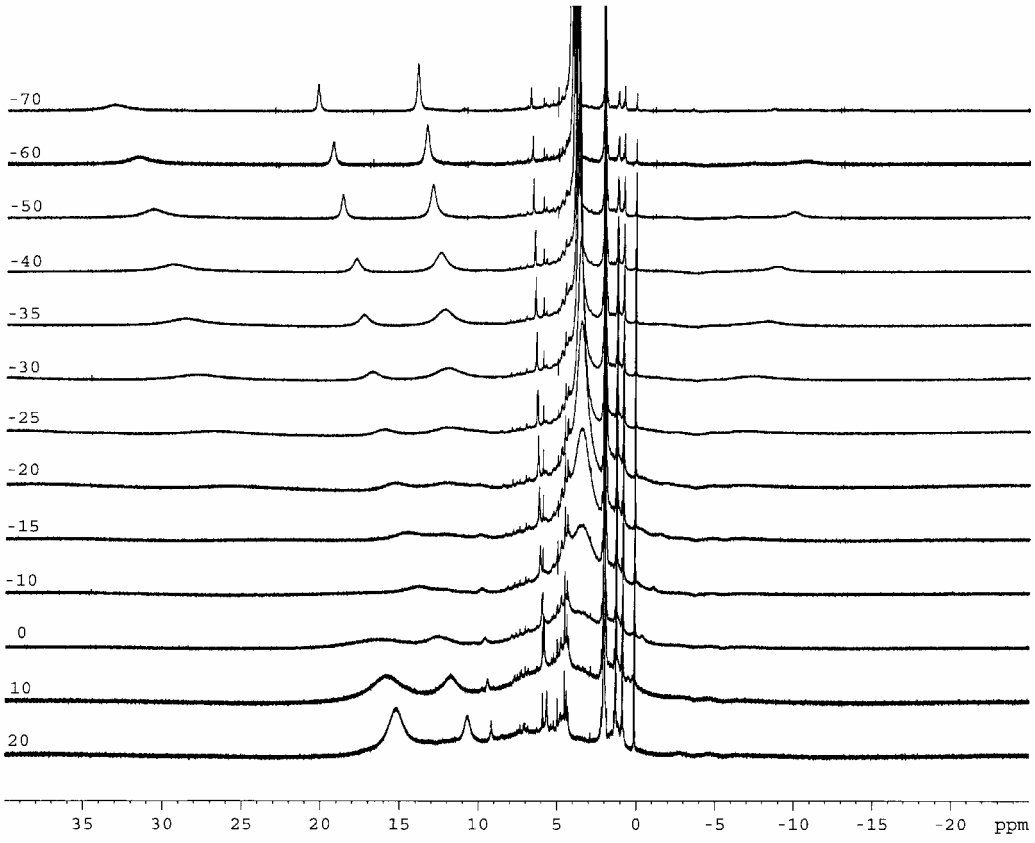

FIGURE 4–12. THE ^{1}H VT-NMR SPECTRA OF [{CpFe(η^5-C_5H_4)}$_4$(η^4-C)CoCp] [CF_3SO_3]$_2$ IN ACETONE-D_6 AT 400 MHZ.

When the temperature decreases, the rotation rate of ferrocene/ferrocenium is decreased. Thus, there are two conformations, one where two ferrocenyl groups are on the same side as the Cp-Co fragment and one where they are located on the

opposite side. In the NMR spectra, the separation of the peaks is observed. At 248 K, ^{1}H NMR spectrum of compound shows five signals. The one at 3.56 ppm is due to the ferrocenyl groups and the other four are assigned to the ferrocenium moieties. That is, the peaks at 11.9 ppm (Cp-Fe) and 21.7 ppm (α-H and β-H) are assigned to one of the two conformations and the signals at 16.1 ppm and -6.58 ppm belong to the ferrocenium in another conformation. Based on ^{1}H NMR spectra of the dicationic mixed-valence compound, it is concluded that the compound is *trans*-isomer and no *cis*-isomer is present in the product.

Similar to the monocationic compound, all peak positions in NMR spectra are temperature dependent. Chemical shifts as a function of temperature are summarized in Table 4-10 and Figure 4-13 illustrates the linear relationship between the chemical shifts and 1/*T*. Hence, the dicationic compound shows Curie law behavior as revealed by magnetic susceptibility measurements.

TABLE 4–10. CHEMICAL SHIFTS FROM ^{1}H NMR SPECTRA FOR [{CpFe(η^5-C_5H_4)}$_4$(η^4-C)CoCp] $[CF_3SO_3]_2$ IN ACETONE-D_6.

T (°C)	1/T (K^{-1})	Chemical shifts (ppm)			
248	0.00403	26.679	16.061	11.919	-6.578
143	0.00412	27.816	16.808	11.977	-7.662
238	0.00420	28.787	17.368	12.143	-8.375
233	0.00429	29.300	17.812	12.463	-8.911
223	0.00448	30.711	18.713	12.971	-9.989
213	0.00469	31.856	19.520	13.466	-11.065
203	0.00493	33.213	20.274	13.965	-----

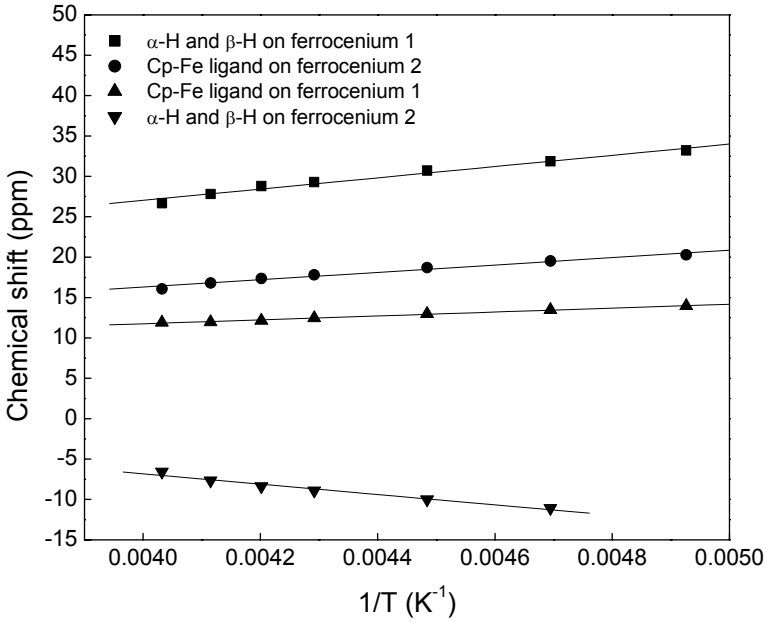

FIGURE 4–13. TEMPERATURE DEPENDENCE OF ^{1}H NMR CHEMICAL SHIFTS FOR [{CpFe(η^5-C_5H_4)}$_4$(η^4-C)CoCp][CF_3SO_3]$_2$ IN ACETONE-D_6.

4.3 Discussion

Molecular square, {CpFe(η^5-C_5H_4)}$_4$(η^4-C)CoCp (**18**), can be oxidized to higher-oxidization states by proper choice of oxidants. Based on the structure of the mono-cationic compound (**19**), it can be assumed that the structures of the cations for the more highly oxidized compounds are similar to the neutral compound (**18**). In terms of FT-IR, EPR and Mössbauer spectroscopy, the di-cationic mixed-valence compound has two ferrocene (2 electrons) and two ferrocenium (2 holes) moieties, suitable for the diagram of QCA cell. So far, it is the first reported square mixed-valence compound with 2-holes and 2-electrons.[4]

For the dicationic compound, there may be two isomers. One is the *cis*-isomer, in which two ferrocenium moieties are placed on adjacent positions. The other is

the *trans*-isomers, in which two ferrocenium moieties lie on diagonal positions of the cyclobutadiene center. Low-temperature ^{1}H NMR spectra of the compound suggest that the mixed-valence compound is *trans*-isomer. Computational analysis also suggests that "the positive charges occupied antipodal, not geminal, sites, indicating that the complex behaves in a way desirable for QCA, which requires charge to localize at opposite corners of a square."[41]

Although Kotz and coworkers [42] reported the electronic spectral data for mono-, di- and tri-oxidized ions of neutral complex (**18**), they never isolated the mixed-valence compounds and all spectra were recorded with the supporting electrolyte (0.1 M $TBAPF_6$). The band position in near-IR region in their report is in good agreement with our results for mono- and di- cationic compounds. They hypothesized that the near-IR bands arise from a Co(I)–Fe(III) interaction. However, in our measurement, the tetra-oxidized compound does not show any peak in the near-IR region, which indicates that no electron transfer between Fe(III) and Co(I) and the IVCT band of the mixed-valence compound is due to the electron transfer between Fe(II) and Fe(III).

Although FT-IR, EPR and Mössbauer spectra of the dicationic mixed-valence compound show that the electron transfer rate in the solid state is less than 10^7 s^{-1}, the IVCT band in the near-IR region affords information from which to estimate the electron transfer rate of the mixed-valence compounds in the solvent. The electron transfer rate k_{et} can be estimated by equation 4-9:

$$k_{et} = \kappa \nu_n \exp(-\frac{\nu_{\max}}{4kT}) \qquad \textbf{(4-9)}$$

where κ is the electronic factor (equal to 1 for adiabatic reaction), ν_n is a nuclear vibration frequency taken to be 6 x 10^{12} s^{-1}, ν_{max} is the energy the of maximum absorbance for the IVCT band (9.3 x 10^3 cm^{-1} for **21** in acetone) and *k* is Boltzmann constant.[39,43,44] Thus, the electron transfer rate of compound **21** in acetone is about 3.5 x 10^7 s^{-1} ($10^{7.5}$ s^{-1}) at room temperature in the absence of a field. This is appropriately fast for the QCA application.

4.4 Summary

Stoichiometric reaction of neutral compound, {CpFe(η^5-C_5H_4)}$_4$(η^4-C)CoCp (**18**), with ferrocenium ion or acetyl-ferrocenium ion affords the pure mixed-valence complexes **19** or **21** respectively, which are characterized by FT-IR, EPR, Mössbauer spectroscopy, magnetic susceptibility, near-IR and VT-NMR . The electron transfer rate of dicationic mixed-valence compound in solution is about $10^{7.5}$ s^{-1}, but slower at low temperature. There is a thermal barrier for the electron transfer between the iron centers. The EPR and magnetic susceptibility measurement imply that the spin-spin interaction is small and does not distort the energies of the pair of degenerate states for the necessary signal transmission. Thus, the mixed-valence complex **21** is a suitable compound as the building block for molecular QCA application.

4.5 Experimental section

General

All reactions were carried out under dry, high-purity nitrogen using standard Schlenk techniques.[45] Solvents were distilled immediately before use under N_2 from the following dry agents: sodium benzophenone ketyl for hexane, pentane, THF and diethyl ether, molten sodium metal for toluene and calcium hydride for CH_2Cl_2. The others were spectroscopic grade and dried over activated 3Å molecular sieves before use. All reagents were purchased from Aldrich and were used as received.

Infrared (IR) spectra were recorded on a Perkin-Elmer Paragon 1000 FT-IR spectrometer, and samples were prepared as KBr pellets. Near-IR spectra were recorded on Thermo Nicolet Nexus 670 FT-IR spectrometer. Mass Spectra (FAB^+) were recorded on a JEPL JMS-AX505HA mass spectrometer from a matrix of *p*-nitrobenzyl alcohol. Elemental analysis was conducted in the M-H-W Laboratories.

^1H Variable Temperature NMR (VT-NMR) spectra were measured on Bruker DPX Avance NMR using acetone-d_6 as solvent for low temperature. The reference was calibrated at 2.05 ppm. The temperature was adjusted manually with a temperature editing program.

Electron paramagnetic resonance (EPR) spectra were collected on a Bruker EMX X-band EPR spectrometer from room temperature to 4K using powder samples. The measurements were made using a cavity with attached Oxford Continuous flow Cryostat (ESR 900). The cavity position and instrument set-up

were checked prior use by running an anisotropic g = 2.0 standard sample provided by Professor R. G. Hayes. Spectra were collected and analyzed using Bruker's EPR Acquisition and WinEPR programs.

The ^{57}Fe Mössbauer spectra were obtained between 4.2 and 295 K on a constant-acceleration spectrometer which utilized the room-temperature rhodium matrix cobalt-57 source and were calibrated at room temperature with α-iron foil. The measurements were performed by Professor Gary J. Long in Department of Chemistry, University of Missouri-Rolla and Professor Fernande Grandjean in Department of Physics, University of Liège, Belgium.

Variable-temperature magnetic susceptibility data of 10.7 mg of [{CpFe(η^5-C_5H_4)}$_4$(η^4-C)CoCp][PF_6] (**19**) and 10 mg of [{CpFe(η^5-C_5H_4)}$_4$(η^4-C)CoCp][PF_6]$_2$ (**21**) were collected from 5K to 250K on a Quantum Design SQUID (Superconducting Quantum Interference Device) magnetometer at the field of 3T. When plotted versus the temperature, the molar magnetic susceptibility of both samples indicated Curie-Weiss behavior. Fitted the curve with $\chi = C/(T-\Theta) + \chi_0$, where Θ is called the Curie-Weiss temperature and χ_0 is a temperature-independent contribution to the Para magnetism. The accuracies of two fits are higher than 99.9%. The parameters for [{CpFe(η^5-C_5H_4)}$_4$(η^4-C)CoCp][PF_6] (**19**) are: C = 0.649 emu·K/mol, Θ = -1.25K and χ_0 = -2.25 x 10^{-3} emu/mol. The parameters for [{CpFe(η^5-C_5H_4)}$_4$(η^4-C)CoCp][PF_6]$_2$ (**21**) are C = 1.42 emu·K/mol, Θ = -2.36 K and χ_0 = -1.33 x 10^{-3} emu/mol.

Preparation of [{CpFe(η^5-C_5H_4)}$_4$(η^4-C)CoCp][PF_6] (19)

To a solution of 45.6 mg (0.05 mmol) of {CpFe(η^5-C_5H_4)}$_4$(η^4-C)CoCp (**18**) in 15 mL of freshly distilled CH_2Cl_2 was added [FcH]PF_6 (16.6 mg, 0.05 mmol). The color changed to deep brown in 5 minutes. The reaction mixture was stirred about 3 hours and the solvent was removed under vacuum. The resulted brown solid was washed with ether three times and dried under vacuum to give 40 mg of dark brown solid. The yield is 76%. Anal. Calcd. for $C_{49}H_{41}CoF_6Fe_4P$: C, 55.76, H, 3.91%. Found: C, 55.72, H, 3.83%. FT-IR (KBr): 850 cm^{-1} (δ_{C-H} for Fc^+), 833 cm^{-1} (ν_{PF_6}), 821 (δ_{C-H} for Fc). FABMS: 911.9 (M-PF_6).

The tetrafluoroborate salt was synthesized by the similar procedure as hexafluorophosphate salt.

Preparation of [CpFe(η^5-C_5H_4)-C(O)CH_3]PF_6 (20)

The compound was prepared by following modified experimental procedure from literature.[9] 154 mg (0.675 mmol) of CpFe(η^5-C_5H_4)-C(O)CH_3 was placed into a 100 mL of Schlenk tube and 50 mL of freshly distilled ethyl ether was added to generate orange solution. Then $AgPF_6$ (170 mg 0.67 mmol) was added to the solution, which resulted in the immediate color change to blue and the formation of blue precipitate. The reaction mixture was continued to stir about 30 min and dried under vacuum. The resultant green-blue residue was extracted with CH_2Cl_2 and filtered through a 2 cm layer celite. The filtrate was concentrated to 5 ml and 50 mL of ether was added slowly with stirring to generate blue precipitate. Isolated the solid, washed it with ether three times and dried under vacuum to give 120 mg of product. The yield is 48%.

Preparation of [{CpFe(η^5-C_5H_4)}$_4$(η^4-C)CoCp][PF_6]$_2$ (21)

To a stirred solution of {CpFe(η^5-C_5H_4)}$_4$(η^4-C)CoCp (**18**) (45.6 mg, 0.05 mmol) in CH_2Cl_2 (15 mL) was added 37.3 mg (0.1 mmol) [CpFe(η^5-C_5H_4)-C(O)CH_3]PF_6 (**20**), which resulted in an immediate color change from orange to deep red brown. After 2 hours, the solution was evaporated to dryness. The resulted red-brown residue was washed with diethyl ether three times and dried under vacuum to give 57 mg (95%) red-brown powder. Anal. Calcd. for $C_{49}H_{41}CoF_{12}Fe_4P_2$: C, 48.96, H, 3.44%. Found: C, 48.76, H, 3.60%.

The tetrafluoroborate and triflate salts were synthesized by the similar procedure as hexafluorophosphate salt.

Preparation of [{CpFe(η^5-C_5H_4)}$_4$(η^4-C)CoCp][BF_4]$_3$ (22)

30 mg (0.09 mmol) of [CpFe(η^5-C_5H_4)-C(O)CH_3]BF_4 was added to the solution of {CpFe(η^5-C_5H_4)}$_4$(η^4-C)CoCp (**18**) (14 mg, 0.015 mmol) in 10 mL of CH_2Cl_2. A red brown solid was precipitated immediately. The reaction mixture was stirred about 2 hours. The red-brown solid was filtered off, washed with CH_2Cl_2 and ether twice respectively and dried under vacuum. FT-IR (KBr): 853 cm^{-1} ($\delta_{C\text{-}H}$ for Fc^+), 821 ($\delta_{C\text{-}H}$ for Fc). Due to the poor stability, the further purification and characterization is impossible.

Preparation of [Fe(η^5-$C_5H_4C(O)CH_3)_2$][BF_4] (23)

Following a modified known method, [9,46] HBF_4•OEt_2 (54% in diethyl ether, 1 mL, 7.2 mmol) was added to a stirred solution of *p*-benzoquinone (200 mg, 1.85 mmol). On adding a solution of 1, 1'-diacetylferrocene (964.2 mg, 3.57 mmol) in 20 mL of CH_2Cl_2 and 20 mL of diethyl ether, a blue precipitate was formed

immediately. The reaction mixture was stirred about 10 minutes and the resultant precipitated was filtered off, washed with ether 3 times and dried under vacuum to give 1.05 g (2.94 mmol) of the product. The yield is 82%.

Oxidization of {CpFe(η^5-C_5H_4)}$_4$(η^4-C)CoCp (18) with excess of [Fe(η^5-$C_5H_4C(O)CH_3)_2$][BF_4] (23)

Adding [Fe(η^5-$C_5H_4C(O)CH_3)_2$][BF_4] (**23**) (33 mg, 0.09 mmol) to a stirring solution of {CpFe(η^5-C_5H_4)}$_4$(η^4-C)CoCp (**18**) (14 mg, 0.015 mmol) in 10 mL of CH_2Cl_2 results in the formation of the red brown precipitate immediately. The reaction mixture was stirred about 2.5 hours and the red brown solid was isolated. The solid was washed with CH_2Cl_2 and ether twice respectively and dried under vacuum. Since the oxidant [Fe(η^5-$C_5H_4C(O)CH_3)_2$][BF_4] is also un-dissolved in CH_2Cl_2, the product is the mixture of tetra-oxidized compound, [{CpFe(η^5-C_5H_4)}$_4$(η^4-C)CoCp][BF_4]$_4$ (**24**) and the complex [Fe(η^5-$C_5H_4C(O)CH_3)_2$][BF_4] (**23**).

Structure Determination

Single crystals of **19** suitable for X-ray diffraction analysis were obtained by slow diffusion from CH_2Cl_2 to hexane. A crystalline sample of **19** was placed in inert oil, mounted on a glass pin, and transferred to the cold gas stream of the diffractometer. Crystal data were collected and integrated using a Bruker Apex system, with graphite monochromated Mo-Kα (λ = 0.71073 Å) radiation at 100K. The structure was solved by direct methods using SHELXS-97 and refined using SHELXL-97 (Sheldrick, G.M., University of Göttingen). Non-hydrogen atoms were found by successive full matrix least squares refinement on F^2 and refined

with anisotropic thermal parameters. All hydrogen atoms were placed at idealized positions and a riding model was applied, with fixed thermal parameters [u_{ij} = $1.2U_{ij}$(eq) for the atom to which they are bonded].

4.6 References

(1) Lent, C. S.; Isaksen, B.; Lieberman, M. *J. Am. Chem. Soc.* **2003**, *125*, 1056-1063.

(2) Demadis, K. D.; Hartshorn, C. M.; Meyer, T. J. *Chem. Rev.* **2001**, *101*, 2655-2685.

(3) Robin, M. B.; Day, P. *Adv. Inorg. Chem. Radiochem.* **1967**, *10*, 247-422.

(4) Jiao, J. Y.; Long, G. J.; Grandjean, F.; Beatty, A. M.; Fehlner, T. P. *J. Am. Chem. Soc.* **2003**, *125*, 7522-7523.

(5) Cotton, F. A.; Lin, C.; Murillo, C. A. *Acc. Chem. Res.* **2001**, *34*, 759-771.

(6) Cotton, F. A.; Lin, C.; Murillo, C. A. *J. Am. Chem. Soc.* **2001**, *123*, 2670-2671.

(7) Lau, V. C.; Berben, L. A.; Long, J. R. *J. Am. Chem. Soc.* **2002**, *124*, 9042-9043.

(8) Yao, H.; Sabat, M.; Grimes, R. N.; de Biani, F. F.; Zanello, P. *Angew. Chem. Int. Ed.* **2003**, *42*, 1002-1005.

(9) Connelly, N. G.; Geiger, W. E. *Chem. Rev.* **1996**, *96*, 877-910.

(10) Laskoski, M.; Roidl, G.; Smith, M. D.; Bunz, U. H. F. *Angew. Chem. Int. Ed.* **2001**, *40*, 1460-1463.

(11) Bunz, U. H. F.; Roidl, G.; Altmann, M.; Enkelmann, V.; Shimizu, K. D. *J. Am. Chem. Soc.* **1999**, *121*, 10719-10726.

(12) Rausch, M. D.; Higbie, F. A.; Westover, G. F.; Clearfield, A.; Gopal, R.; Troup, J. M.; Bernal, I. *J. Organomet. Chem.* **1978**, *149*, 245-264.

(13) Kramer, J. A.; Hendrickson, D. N. *Inorg. Chem.* **1980**, *19*, 3330-3337.

(14) Dong, T. Y.; Cohn, M. J.; Hendrickson, D. N.; Pierpont, C. G. *J. Am. Chem. Soc.* **1985**, *107*, 4777-4778.

(15) Dong, T. Y.; Schei, C. C.; Hwang, M. Y.; Lee, T. Y.; Yeh, S. K.; Wen, Y. S. *Organometallics* **1992**, *11*, 573-582.

(16) Dong, T. Y.; Hendrickson, D. N.; Pierpont, C. G.; Moore, M. F. *J. Am. Chem. Soc.* **1986**, *108*, 963-971.

(17) Duggan, D. M.; Hendrickson, D. N. *Inorg. Chem.* **1975**, *14*, 955-970.

(18) Dong, T. Y.; Lee, T. Y.; Wen, Y. S.; Lee, S. H.; Hsieh, C. F.; Lee, G. H.; Peng, S. M. *J. Organomet. Chem.* **1993**, *456*, 239-242.

(19) Dong, T. Y.; Huang, C. H.; Chang, C. K.; Wen, Y. S.; Lee, S. L.; Chen, J. A.; Yeh, W. Y.; Yeh, A. *J. Am. Chem. Soc.* **1993**, *115*, 6357-6368.

(20) Dong, T. Y.; Lee, T. Y.; Lee, S. H.; Lee, G. H.; Peng, S. M. *Organometallics* **1994**, *13*, 2337-2348.

(21) Morrison, W. H.; Hendrickson, D. N. *Inorg. Chem.* **1975**, *14*, 2331-2346.

(22) Dong, T. Y.; Kambara, T.; Hendrickson, D. N. *J. Am. Chem. Soc.* **1986**, *108*, 4423-4432.

(23) Gascoin, F.; Sevov, S. C. *Inorg. Chem.* **2002**, *41*, 5920-5924.

(24) Cullity, B. D. *Introduction to magnetic materials*; Addison-Wesley Pub. Co.: Reading, Mass., 1972.

(25) Morrison, W. H.; Krogsrud, S.; Hendrickson, D. N. *Inorg. Chem.* **1973**, *12*, 1998-2004.

(26) Drago, R. S. *Physical methods for chemists*; 2nd ed.; Saunders College Pub.: Ft. Worth, 1992.

(27) Powers, M. J.; Meyer, T. J. *J. Am. Chem. Soc.* **1978**, *100*, 4393-4398.

(28) Cowan, D. O.; Vanda, C. L.; Park, J.; Kaufman, F. J. *Acc. Chem. Res.* **1973**, *6*, 1-7.

(29) Hush, N. S. *Prog. Inorg. Chem.* **1967**, *8*, 391-444.

(30) Dowling, N.; Henry, P. M.; Lewis, N. A.; Taube, H. *Inorg. Chem.* **1981**, *20*, 2345-2348.

(31) Powers, M. J.; Meyer, T. J. *Inorg. Chem.* **1978**, *17*, 2955-2958.

(32) Colbran, S. B.; Robinson, B. H.; Simpson, J. *Organometallics* **1983**, *2*, 943-951.

(33) Colbran, S. B.; Robinson, B. H.; Simpson, J. *Organometallics* **1983**, *2*, 952-957.

(34) Li, Z. H.; Beatty, A. M.; Fehlner, T. P. *Inorg. Chem.* **2003**, *42*, 5707-5714.

(35) Barlow, S. *Inorg. Chem.* **2001**, *40*, 7047-7053.

(36) Chang, J. P.; Fung, E. Y.; Curtis, J. C. *Inorg. Chem.* **1986**, *25*, 4233-4241.

(37) Chellamma, S.; Lieberman, M. *Inorg. Chem.* **2001**, *40*, 3177-3180.

(38) Creutz, C. *Inorg. Chem.* **1978**, *17*, 3723-3725.

(39) Creutz, C. *Prog. Inorg. Chem.* **1983**, *30*, 1-73.

(40) Ernst, S.; Kasack, V.; Kaim, W. *Inorg. Chem.* **1988**, *27*, 1146-1148.

(41) Braun-Sand, S. B. Ph. D. Thesis, University of Notre Dame, 2003.

(42) Kotz, J.; Neyhart, G.; Vining, W. J.; Rausch, M. D. *Organometallics* **1983**, *2*, 79-82.

(43) Parise, A. R.; Baraldo, L. M.; Olabe, J. A. *Inorg. Chem.* **1996**, *35*, 5080-5086.

(44) Dong, T. Y.; Lee, S. H.; Lee, T. Y. *Organometallics* **1996**, *15*, 2354-2359.

(45) Shriver, D. F.; Drezdzon, M. A. *The manipulation of air-sensitive compounds*; 2nd ed.; Wiley: New York, 1986.

(46) Guillon, C.; Vierling, P. *J. Organomet. Chem.* **1994**, *464*, C42-C44.

CHAPTER 5

APPROACH TO SURFACE ATTACHMENT OF MIXED-VALENCE COMPLEXES

5.1 Introduction

As described in chapter 4, the mixed-valence compound $[\{CpFe(\eta^5\text{-}C_5H_4)\}_4(\eta^4\text{-}C)CoCp]^{2+}$ is a suitable building block for molecular QCA. To realize a molecular QCA device, the next step is to attach the molecules onto a substrate surface. As attachment may cause significant perturbations, it is necessary to investigate the properties of molecules on the surface such as chemical stability, electron transfer rate and so on. Assembling the squares into device structures is a much more challenging task and not treated here.

Although many methods, such as Langmuir-Blodgett deposition,[1] vacuum sublimation,[2] vapor deposition[3] and spin-coating,[4] have been used to attach molecules on surface, the technique of self-assembly has attractive advantages since it can afford reproducible and stable monolayer films due to chemical bond formation between films and substrates.[5-7] The formation and characterization of organic self-assembled monolayers (SAMs) have been widely reported.[7,8]

Attachment of inorganic molecules on a substrate surface can be achieved by binding inorganic molecules on organic SAMs with special anchoring group through covalent bonds.[9-11] However, other molecular interactions, such as acid-base interactions,[12] hydrogen bonding[13-15] and electrostatic interactions,[15-17] can also be used to bind the inorganic molecules on the SAMs/substrates. For example, Lieberman and coworkers reported the formation of inorganic molecular films on the top of organic SAMs with hydrophilic terminating groups through hydrogen bonding.[14] In addition, the heteropolyanion, $PMo_{12}O_{40}^{3-}$, can be linked with the 4-aminothiophenol SAM on Au substrate through electrostatic interaction.[17]

The strategy adopted here incorporates aspects of several of these approaches. A SAM with sufficient oxidizing power to oxidize **18** will serve to activate and bind the square via electrostatic interaction between the cation $[\mathbf{18}]^{n+}$ and the surface tethered anions. As long as reduction to neutral **18** is avoided, surface attachment should be strong and stable. Nobody has previously reported that a redox active mixed-valence compound could be attached to a surface via oxidation reactions. The possibility of this strategy is not known. However, if the strategy works, the anions corresponding to the mixed-valence cations are fixed on the surface and do not affect the electron transfer between the metal centers. This feature is what the QCA application requires.

SAMs of organosilicon derivatives can be generated from alkylchlorosilanes, alkylalkoxysilanes and alkylaminosilane with hydroxylated substrates such as silicon oxide.[18,19] The driving force for this self-assembly is the *in situ* formation of the polysiloxane, which is connected to surface hydroxyl groups (–SiOH) via

formation of covalent siloxane bonds (Si–O–Si).[8] Since the Si–C (~76 kcal·mol^{-1}) and Si–O (~108 kcal·mol^{-1}) bonds[20] between Si surface and organic adsorbates are much stronger than bonds such as Au–S (~45 kcal·mol^{-1}),[21] the organosiloxane films are very stable compared to other SAMs such as organothiolate on a gold surface.[7] In addition, the technologies for handling and patterning semiconductor materials, such as silicon wafer are well established.[15,22-24] Therefore, the SAM of organosilicon on Si/SiO_2 is used as substrate to link the inorganic mixed-valence complexes in this chapter. Scheme 5-1 illustrates the strategy for attaching acetylferrocenium and the mixed-valence compounds $[\{CpFe(\eta^5\text{-}C_5H_4)\}_4(\eta^4\text{-}C)CoCp]^{n+}$ ([**18**]$^{n+}$, n=1, 2) on a SAM/Si/SiO_2 through electrostatic interaction.

It is known that silver ion can be attached on the top of organosilane SAMs through electrostatic interaction if the organic SAM have a thiol or disulfide group.[25,26]

$$R\text{—}SH + Ag^+ \rightleftharpoons R\text{—}SAg + H^+ \qquad \textbf{(5-1)}$$

The mixed-valence mono-cationic and di-cationic compounds, $[\{CpFe(\eta^5\text{-}C_5H_4)\}_4(\eta^4\text{-}C)CoCp]^{n+}$ (n=1, 2), can be obtained by oxidization of compound **18** with silver ion and acetylferrocenium respectively (refer to chapter 4). Acetylferrocenium can be obtained by oxidizing acetylferrocene with silver ion.[27] Thus, the oxidization reaction of acetylferrocene or compound **18** with silver ion on silicon surface should result in the attachment of acetylferrocenium or [**18**]$^+$ on surface as shown in Scheme 5-1.

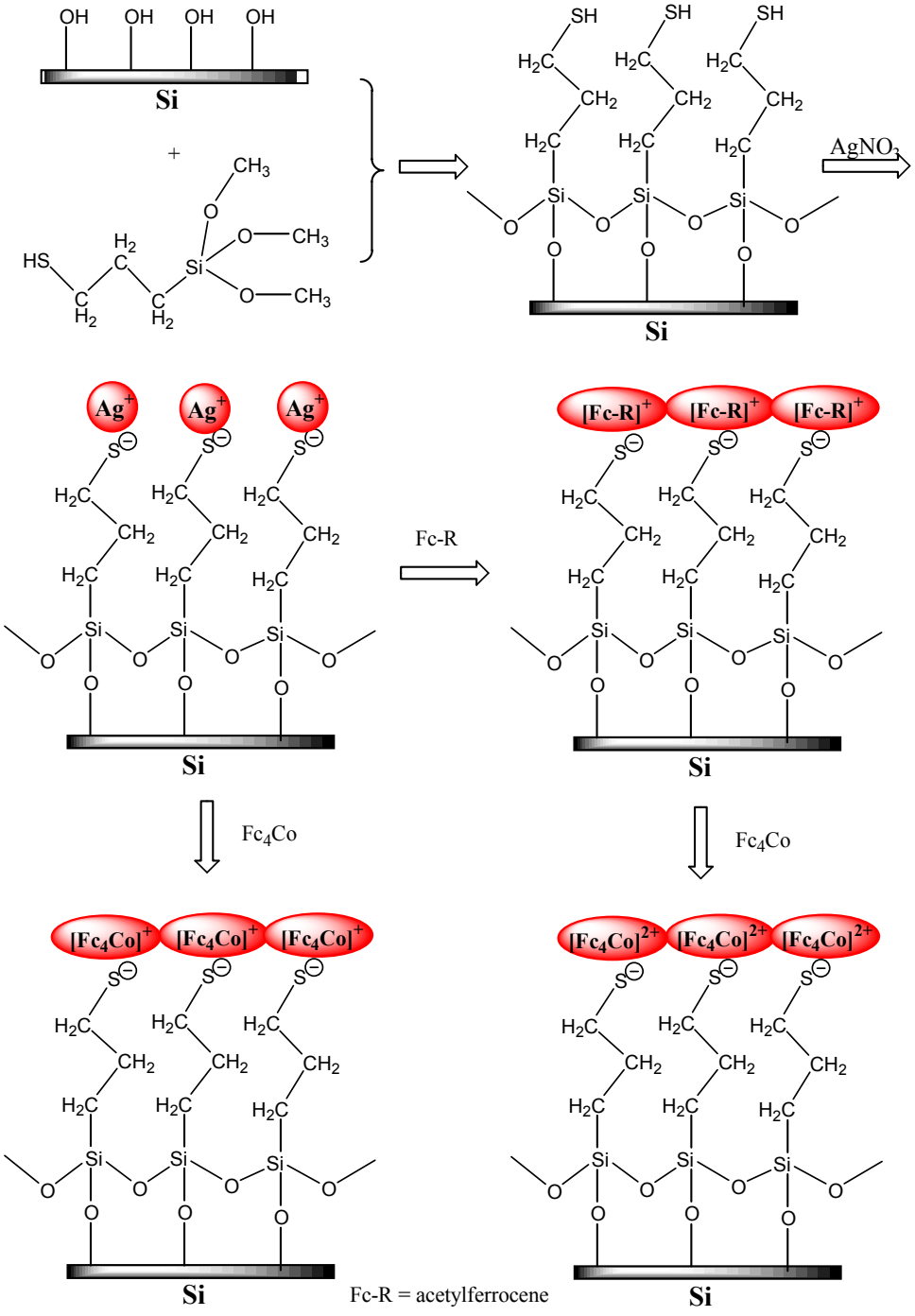

SCHEME 5–1. STRATEGY FOR THE SURFACE ATTACHMENTS OF ACETYLFERROCENIUM AND {CpFe (η^5-C_5H_4)}$_4$(η^4-C)CoCp (**18**).

Unfortunately, the reaction gives the reduction product from silver ion, Ag, which may be deposited on surface. However, whether the existence of Ag will affect the properties of mixed-valence compounds on surface or not is not clear in advance. In addition, the acetylferrocenium on the surface can react with neutral **18** or monocation $[\mathbf{18}]^{+}$ to get $[\mathbf{18}]^{2+}$ on the surface. This chapter describes the investigation of the possibility of attachment of the tetra-nuclear mixed-valence compound on a surface through electrostatic interactions. Technologies used include ellipsometry, X-ray photoelectron spectroscopy (XPS) and electrochemistry.

5.2 Results

5.2.1 Surface preparations

To obtain an organosilane monolayer, the silicon wafers were cleaned with piranha solution (a 3:1 solution of concentrated sulfuric acid : 30% hydrogen peroxide) to form a high density of Si–OH functional groups on the surface and to remove any organic and inorganic contaminants. Then, the silicon wafer was immersed in a solution of (3-mercaptopropyl)trimethoxysilane (3-MPTMS) in octane overnight. The alkoxy groups are hydrolyzed by trace water on the surface to form the monolayer of 3-MPTMS (sample **1**). The thickness of the top layer by ellipsometry is about 5.4 ± 0.5 Å, consistent with molecular dimensions (5.5 Å). The dimensions of 3-MPTMS are shown in Figure 5-1a.

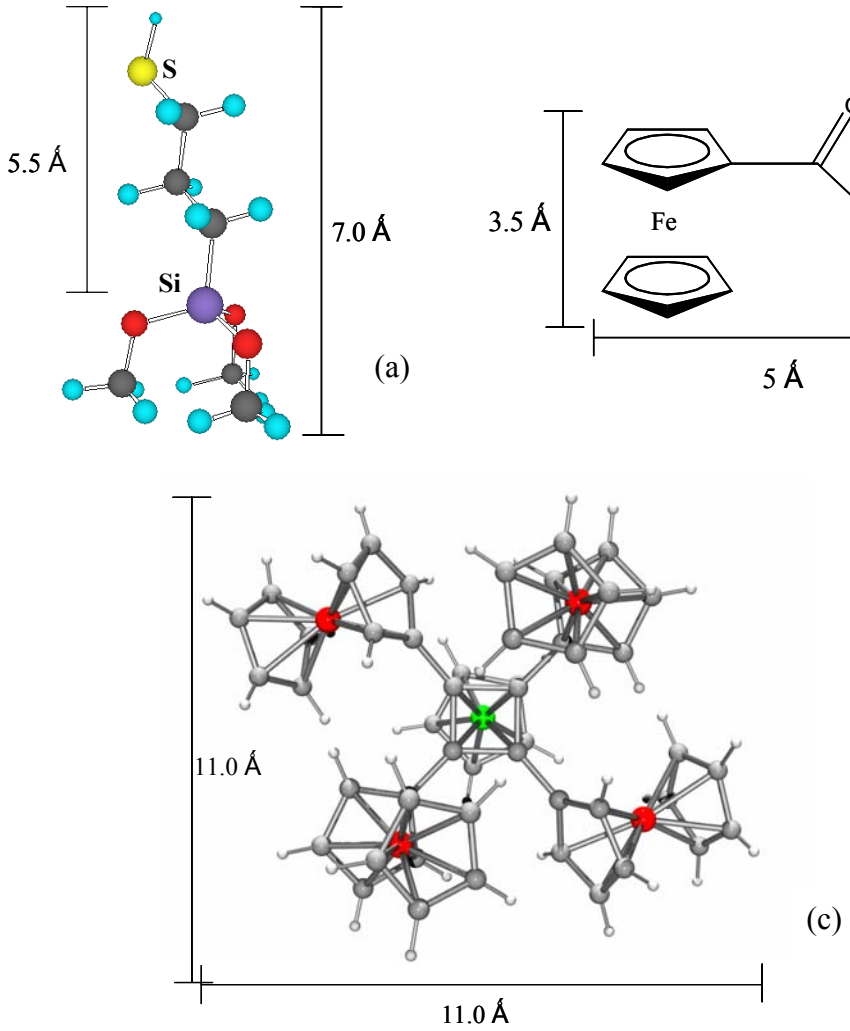

FIGURE 5–1. MOLECULAR DIMENSIONS FOR (a) (3-MERCAPTOPROPYL) TRIMETHOXYSILANE, (b) ACETYLFERROCENE AND (c) $\{CpFe(\eta^5\text{-}C_5H_4)\}_4(\eta^4\text{-}C)CoCp$ (**18**).

The surface with the organosilane layer was then soaked into an aqueous solution of $AgNO_3$ and the silver ion reacted with thiol on the top of the surface to form a S–Ag bond (sample **2**).[26] In this way, the silver ion is bound to the surface, which is confirmed by X-ray photoelectron spectra (*vide infra*). The thickness of the top layer is about 12.6 ± 0.8 Å, which, unfortunately, is much larger than

expected based on the size of the silver ion (the radius of silver ion is 0.67 Å). In determining the thickness of the layer, a two-layer model (adsorbate/SiO_2/Si) was used and the refractive index of adsorbate is assumed as 1.46. Since the silver is bound on an organic SAM and the refractive index is very hard to determine, this model may not give an accurate thickness. This is one of the reasons that the measured thickness is much larger than the theoretical one. Another possible reason is that the silver nitrate may aggregate on the surface.

Acetylferrocene can be oxidized to acetylferrocenium with silver ion.[27] Dipping the surface bound with silver ion into the solution of acetylferrocene in CH_2Cl_2 may result in the oxidization of acetylferrocene and the resultant acetylferrocenium is attached to the surface (sample **3**). After this reaction, the thickness of the top layer is measured as 9.1 ± 0.6 Å, which again is larger than the expected thickness (~ 5 Å) as shown in Figure 5-1b. The difference between the measured and calculated thickness may be due to the errors in ellipsometry measurements.

In the same manner as acetylferrocene, {CpFe(η^5-C_5H_4)}$_4$(η^4-C)CoCp (**18**) is oxidized by silver ion to form the monocationic compound (refer to chapter 4). Thus, [**18**]$^+$ could be attached to the surface by dipping the surface with silver ion into the solution of {CpFe(η^5-C_5H_4)}$_4$(η^4-C)CoCp (**18**) (sample **4**). The thickness of the modified surface is 14.0 ± 0.5 Å, which is now in good agreement with the dimension of the molecule (11 Å x 11 Å x 10 Å) as shown in Figure 5-1c. Since the molecule is attached on the surface through electrostatic interaction, there is no a priori preferred orientation. Unfortunately, the orientation of the molecule on the

surface can not be determined by the thickness the molecular layer because in solid state, it occupies a ~cubic volume. If the ferrocenyl groups were oriented optimally (four ferrocenes are on the same side relative to the cyclobutadiene center), the dimensions of the molecule would be 11 Å x 11 Å x 5 Å. But the errors in ellipsometry measurements preclude a definitive conclusion.

5.2.2 X-ray photoelectron spectroscopy (XPS) of the cleaned silicon wafer

X-ray photoelectron spectra of every sample were measured. The cleaned silicon wafer has a thin SiO_2 layer on the top. XPS shows two Si 2p peaks assigned to Si (99.3 eV) and SiO_2 (102.9 eV) as shown in Figure 5-2. In addition, the XPS also shows the O 1s peak at 532.2 eV and the C 1s peak at 285.2 eV.

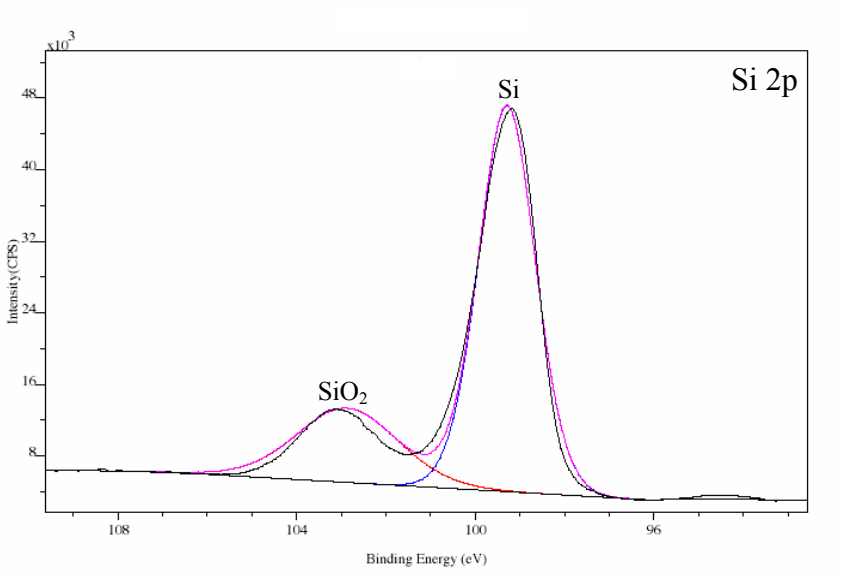

FIGURE 5–2. HIGH RESOLUTION X-RAY PHOTOELECTRON SPECTRUM OF THE CLEANED SILICON WAFER IN THE Si 2p REGION.

5.2.3 XPS of silicon wafer with 3-MPTMS layer (sample 1)

When the silicon wafer was immersed into the solution of 3-MPTMS, an organosilane layer with thiol group was formed on the Si/SiO_2 substrate. Elements Si, O, C, and S are found in XPS of sample **1**. Figure 5-3 illustrates the high resolution S 2p X-ray photoelectron spectrum, which shows two broad peaks: one is at 168.4 eV and the other one is at 164.0 eV.

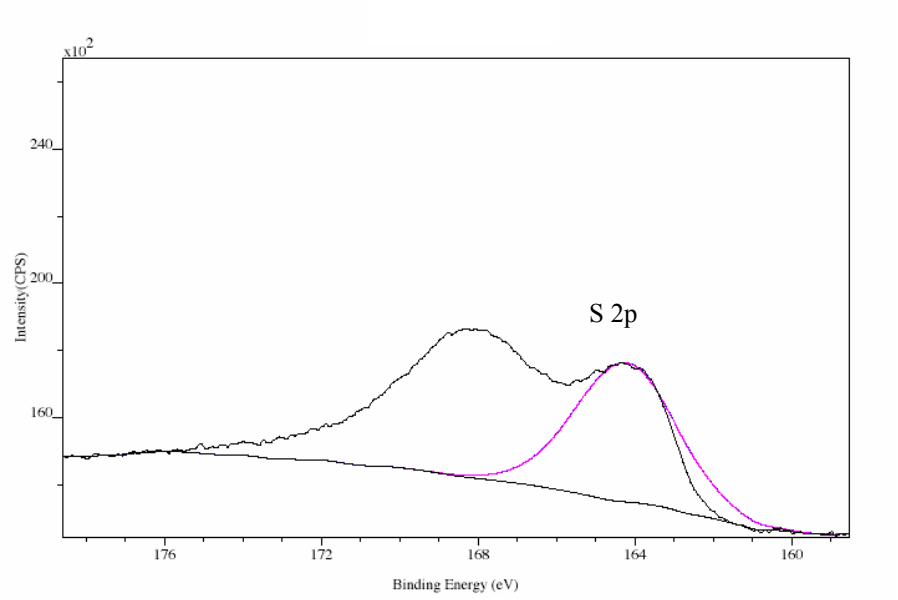

FIGURE 5–3. HIGH RESOLUTION X-RAY PHOTOELECTRON SPECTRUM OF THE SAMPLE 1 IN THE S 2p REGION.

It is known that the typical S $2p_{3/2}$ binding energies for unbound alkanethiols are between 163 and 164 eV.[28] Since the molecular monolayer was grown on a native thin SiO_2 substrate (about 10 Å), the peak at 168.4 eV due to the energy loss band of the Si 2s peak is observed. This comes from the interaction between the photoelectron and the other electrons in the surface region.[29] Similar results are

observed by other chemists.[26] If the molecular layer is grown on a thick SiO_2 substrate such as 500 nm, this peak will shift to higher binding energy.[26] The XPS results indicate that the monolayer with thiol group has been formed.

5.2.4 XPS of surface with silver ion (sample 2)

The X-ray photoelectron survey scan of sample **2** shows the elements C, O, N, Ag, S and Si. The detailed results are listed in the Table 5-1.

C 1s peak appears at 284.7 eV, which is typical of aliphatic carbons.[14] Due to the limited resolution of the S 2p peaks, it is difficult to verify the formation of the S–Ag bond from the XPS. However, there is some evidence for it. The high resolution scans of the Ag 3d region present two peaks at 374.4 eV and 368.4 eV with a ratio of about 2:3, which corresponds to Ag $3d_{3/2}$ and Ag $3d_{5/2}$ respectively. In addition, high resolution scans in the region between 390 eV to 410 eV give a peak at 401.6 eV assigned to N 1s.

The area ratio of Ag to N is 1.83, which indicates that there are some silver nitrate molecules on the surface. The amount is not as large as the ellipsometry measurements might suggest, i.e., a ratio of Ag to N of about 1: 10. Washing the surface with deionized water more extensively causes the area ratio of Ag/N to increase, consistent with this hypothesis. However, even after a long-term washing, N 1s peak can be observed in XPS spectra. Moreover, the N 1s peak of the film is broad and the total peak area may not belong to a single species ($AgNO_3$). Hence, there are silver nitrate molecules on the surface, but the amount appears small.

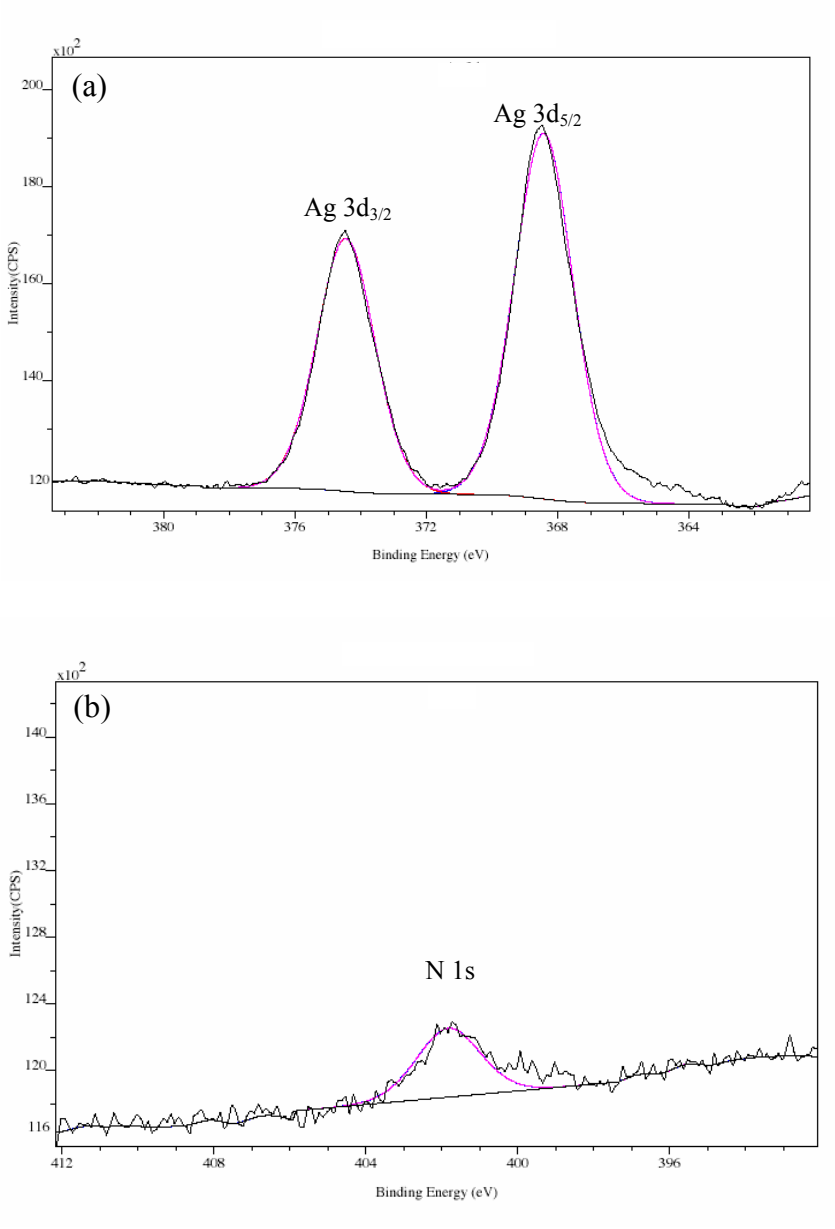

FIGURE 5–4. HIGH RESOLUTION X-RAY PHOTOELECTRON SPECTRA OF SAMPLE **2** FOR (a) Ag 3d AND (b) N 1s.

TABLE 5–1. XPS DATA FOR SAMPLE **2**.

Peak	Position BE (eV)	FWHM [a] (eV)	Raw Area (CPS)	RSF [b]	Intensity [c] (CPS)
C 1s	284.722	1.801	66337.1	0.318	208607.2
Si 2p	99.300	1.488	36383.5	0.371	98068.7
Si 2p (SiO_2)	102.768	2.236	13526.5	0.371	36459.6
O 1s	532.088	2.013	120685.4	0.736	163974.7
S $2p_{(1/2+3/2)}$	163.726	2.601	5172.9	0.723	7154.8
N 1s	401.612	2.420	1016.0	0.505	2011.9
Ag $3d_{3/2}$	374.351	1.682	7122.9	6.345	2835.5
Ag $3d_{5/2}$	368.351	1.756	10868.6		

[a] FWHM is the full width of the half maximum.
[b] RSF is the relative sensitivity factor.[30]
[c] Intensity is the integrated area of the peak corrected by RSF. Intensity = Raw area/RSF.

5.2.5 Powder XPS of acetylferrocene

The XPS spectra of powder acetylferrocene show all expected elements Fe, C and O. The data are listed in Table 5-2. Fe 2p is revealed by the peaks at 707.2 eV and 719.8 eV, corresponding to Fe^{II} $2p_{3/2}$ and Fe^{II} $2p_{1/2}$, respectively, as shown in Figure 5-5a. The peak positions and shapes are consistent with ferrocene and its derivatives.[31] High resolution scans for C 1s shows three peaks at 284.6, 286.3, 288.6 eV respectively (Figure 5-5b). The peaks at 284.6 and 286.3 eV are assigned to the C atoms of ferrocenyl group and carbon tape, while the peak at 288.6 eV is due to the carbon atom of the C=O group.[19] Since the powder of acetylferrocene

was dusted directly on the carbon tape, the ratio of C to Fe is much larger than the actual one.

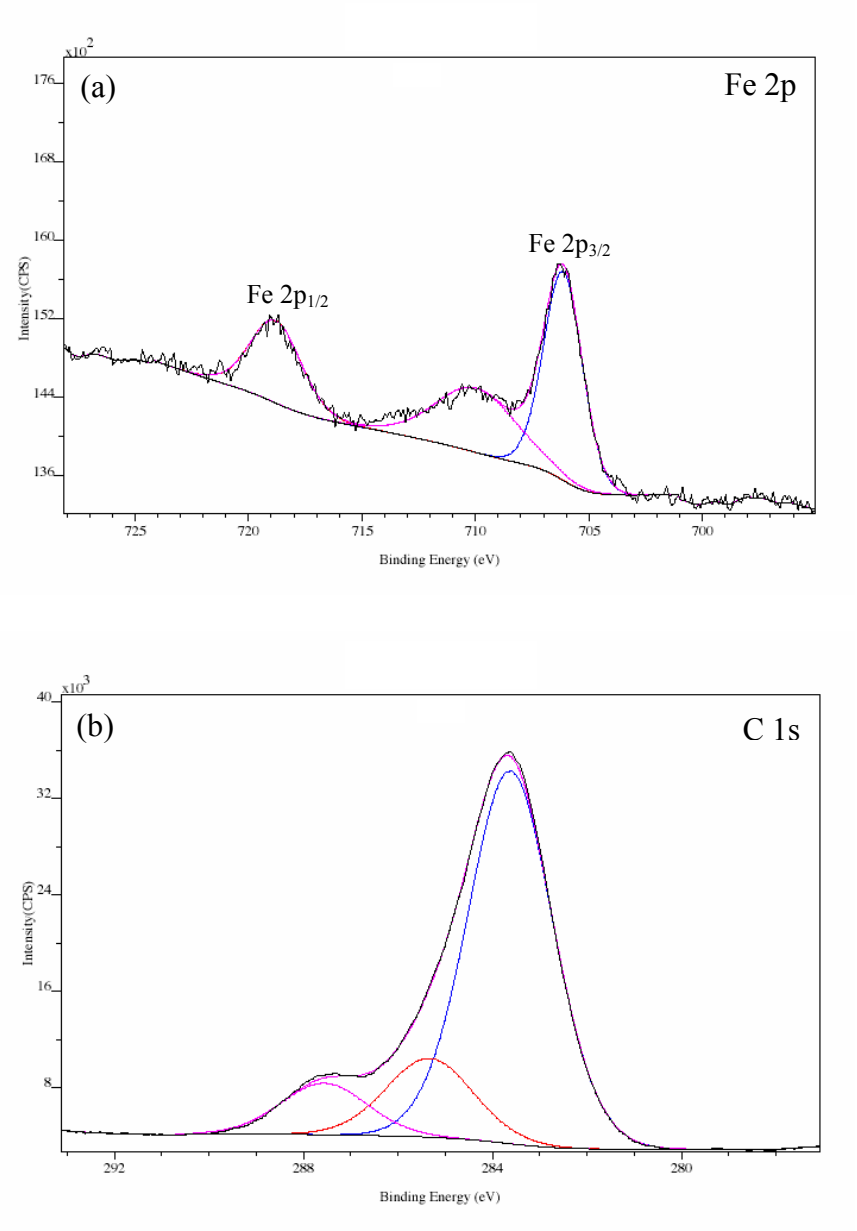

FIGURE 5–5. HIGH RESOLUTION X-RAY PHOTOELECTRON SPECTRA OF A POWDER SAMPLE OF ACETYLFERROCENE FOR (a) Fe 2p AND (b) C 1s.

TABLE 5–2. POWDER XPS DATA FOR ACETYLFERROCENE.

Peak	Position BE (eV)	FWHM [a] (eV)	Raw Area (CPS)	RSF [b]	Intensity [c] (CPS)
C 1s	284.636	2.088	30938.0	0.318	97289.3
	286.316	2.123	6540.0	0.318	20566.0
	288.550	2.108	4276.7	0.318	13448.7
O 1s	531.000	2.996	23193.0	0.736	31512.2
Fe $2p_{1/2}$	719.826	2.616	2974.5	2.947	1009.8
Fe $2p_{3/2}$	707.167	1.977			

[a] FWHM is the full width of the half maximum.
[b] RSF is the relative sensitivity factor.[30]
[c] Intensity is the integrated area of the peak corrected by RSF.
Intensity = Raw area/RSF.

5.2.6 XPS of surface sample 3

X-ray photoelectron survey scans of the surface show the elements Si, O, C, Ag, S, N and Fe. The detailed XPS data are summarized in Table 5-3. High resolution scans for every element were performed to determine the binding energies of every element. Figure 5-6 illustrates the high resolution XPS spectra of sample **3** for C 1s, Fe 2p and Ag 3d.

Similar to the powder sample, high resolution scans for C 1s present 3 peaks, in which, the peak at 289.1 eV is assigned to C=O group. In addition, scans on the region from 700 eV to 730 eV give a Fe 2p doublet at 720.4 eV and 707.7 eV. All indicate that the inorganic compound is attached on the surface. Ag 3d peaks also appear at 373.9 eV and 367.9 eV. It is impossible to differentiate ionic silver from

neutral silver metal based on the XPS since both have almost same Ag 3d binding energy.[32] Thus, it is difficult to tell if the Ag peaks in XPS spectra are due to unreacted silver ions or the reduced silver metal. However, the ratio of Ag/Fe is 1.49, which implies that the Ag peaks come from a mixture of silver ion and silver or just from silver ion (as $AgNO_3$ and –SAg). Furthermore, a broad N 1s peak at 401 eV indicates only a small amount of silver nitrate on the surface.

TABLE 5–3. XPS DATA FOR SAMPLE **3**.

Peak	Position BE (eV)	FWHM [a] (eV)	Raw Area (CPS)	RSF [b]	Intensity [c] (CPS)
C 1s	284.906	1.910	28641.8	0.318	90068.6
	286.886	2.416	8799.0	0.318	27669.8
	289.135	2.698	2499.6	0.318	7860.4
Si 2p	99.300	1.512	50229.7	0.371	135390.0
Si 2p (SiO_2)	102.904	2.083	15044.2	0.371	40550.4
O 1s	532.118	2.077	156886.1	0.736	213160.5
N 1s	401.065	4.008	285.1	0.505	564.6
S $2p_{(1/2+3/2)}$	164.340	3.456	6771.5	0.723	9365.8
Ag $3d_{3/2}$	373.945	1.896	2906.06	6.345	1115.5
Ag $3d_{5/2}$	367.878	1.954	4171.6		
Fe $2p_{1/2}$	720.368	2.587	776.6	2.947	746.7
Fe $2p_{3/2}$	707.668	1.923	1423.8		

[a] FWHM is the full width of the half maximum.
[b] RSF is the relative sensitivity factor.[30]
[c] Intensity is the integrated area of the peak corrected by RSF. Intensity = Raw area/RSF.

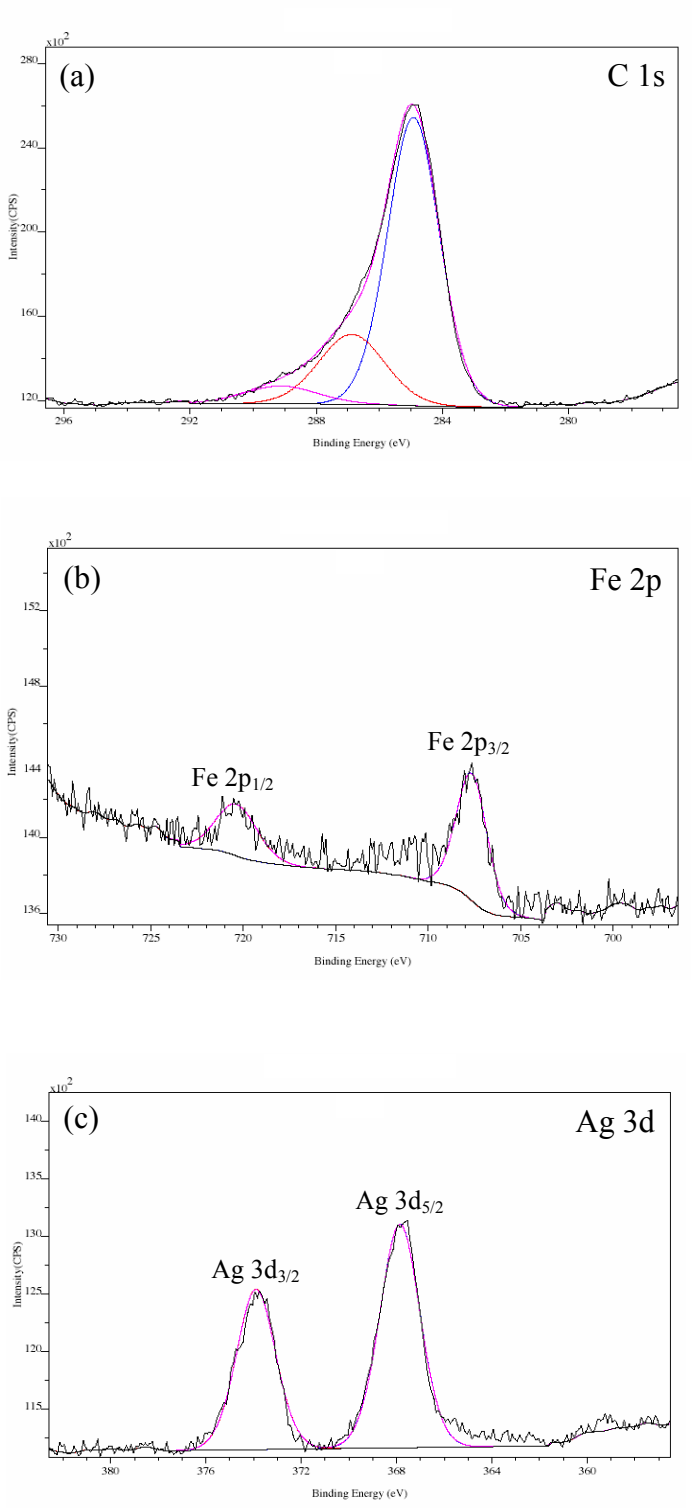

FIGURE 5–6. HIGH RESOLUTION X-RAY PHOTOELECTRON SPECTRA OF SAMPLE **3** FOR (a) C 1s, (b) Fe 2p AND (c) Ag 3d.

In organosilicon SAMs on silicon oxide, the mean area per molecule is about 20 $Å^2$.[33] For the surface attachment sample of inorganic complexes on the organosilicon SAM with thiol groups, surface coverage may be estimated by the ratio of the area of Fe peaks to that of S peak according to equation 5-2,[14] where n=1 since acetylferrocene has one iron atom.

$$\textit{Area per molecule} = 20\ Å^2 \times \textit{ratio (S: Fe)} \times n \qquad \textbf{(5-2)}$$

According to the data in Table 5-3, the ratio of peak intensity of S to that of Fe is about 13 ± 0.5, corresponding to a value of 260 ± 10 $Å^2$ per molecule of acetylferrocenium. Based on the dimensions of acetylferrocene, the area of a molecule is between 10 $Å^2$ and 18 $Å^2$ depending on whether the molecule is vertical or flat on the surface. Thus the surface coverage is 4~7%.

5.2.7 XPS of surface sample 4

XPS data of sample **4** indicate elements Fe, Ag, S, Si, C and O. Since the Co 2p is overlapped by the Auger peak of O, it can not be observed. The detailed data are summarized in Table 5-4. High resolution XPS spectra of Ag 3d and Fe 2p are shown in Figure 5-7.

As expected, C 1s spectrum shows two peaks at 285.0 eV and 286.9 eV, contributed from the alkyl chains of the monolayer and the carbon atoms of attached molecules. Similar to sample **3**, the iron 2p region has one doublet at 720.3

eV and 707.7 eV, which confirms the attachment of compound **18** on the surface. Ag 3d peaks appear at 374.1eV and 368.1 eV and the Ag/Fe ratio is 2.15.

XPS results indicate that molecules of **18** have been attached on the surface. The surface coverage can be estimated by equation 5-2, where n are 4 for **18**. Based on the ratio of peak intensity of S to that of Fe (9.4 ± 0.5), the mean area per molecule is 756 ± 10 $Å^2$. The structure determination gives the area of molecule **18** (or cation of molecule **19**) of 120 $Å^2$. Hence, the surface coverage is 16~17%.

TABLE 5–4. XPS DATA FOR SAMPLE **4**.

Peak	Position BE (eV)	FWHM [a] (eV)	Raw Area (CPS)	RSF [b]	Intensity [c] (CPS)
C 1s	284.995	1.848	22817.4	0.318	71752.8
	286.886	3.751	13102.4	0.318	41202.5
Si 2p	99.300	1.515	47138.8	0.371	127058.8
Si 2p (SiO_2)	102.997	2.247	15079.3	0.371	40645.0
O 1s	532.317	2.104	155688.8	0.736	211533.7
N 1s	400.723	4.060	365.0	0.505	722.8
S $2p_{(1/2+3/2)}$	164.068	2.691	5238.4	0.723	7245.3
Ag $3d_{3/2}$	374.145	2.483	4133.1	6.345	1644.9
Ag $3d_{5/2}$	368.145	2.506	6304.0		
Fe $2p_{1/2}$	720.267	2.608	834.2	2.947	766.8
Fe $2p_{3/2}$	707.730	1.821	1425.4		

[a] FWHM is the full width of the half maximum.
[b] RSF is the relative sensitivity factor.[30]
[c] Intensity is the integrated area of the peak corrected by RSF. Intensity = Raw area/RSF.

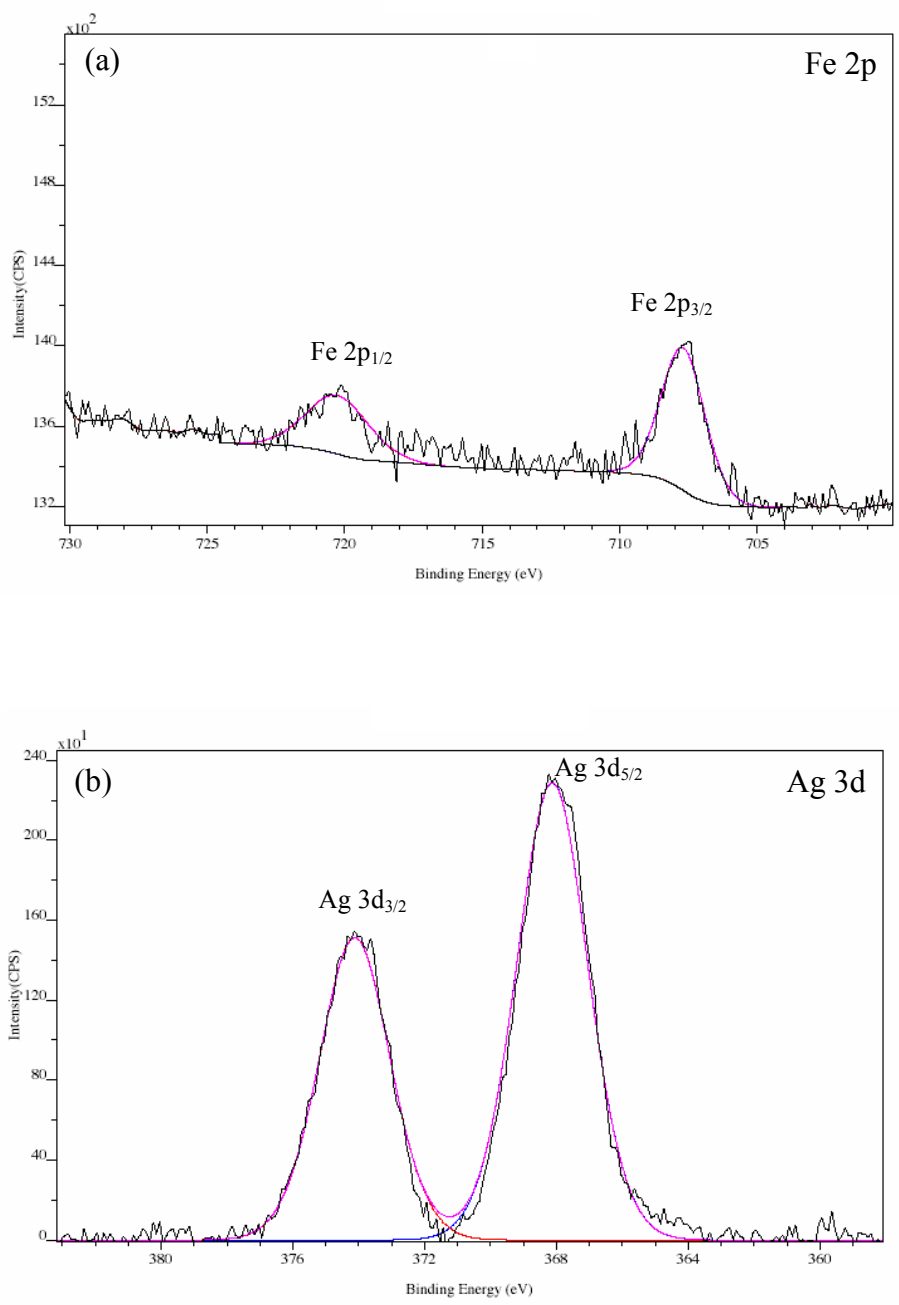

FIGURE 5–7. HIGH RESOLUTION X-RAY PHOTOELECTRON SPECTRA OF SAMPLE **4** FOR (a) Fe 2p AND (b) Ag 3d.

5.2.8 Electrochemical characterization

It is known that a compound on the surface exhibits electrochemical behavior related to that in solution if it is bound to the surface covalently.[10] However, in our case, molecules are thought to be bound to a surface by electrostatic interactions through redox reaction as shown in Scheme 5-1. Then what will be observed in a cyclic voltammogram (CV) of the surface with an electrochemically active compound bound through electrostatic interactions? Using acetylferrocene (acetylferrocene shows a reversible redox couple in CV[27]) as an example, the molecules exist on a surface in an oxidized state (acetylferrocenium). Hence, an oxidizing scan in CV should not yield any peak. If the scan begins at reducing potential, the molecules are lost. However, a reduction scan beginning at an oxidizing potential should give a reduction peak. Once the compound is reduced to a neutral state, the surface loses the molecules. Thus the corresponding return oxidization wave is not observed. Since the loss of the compound from surface, the subsequent scan should give nothing. Scheme 5-2 is a cartoon illustrating possible CVs in this process.

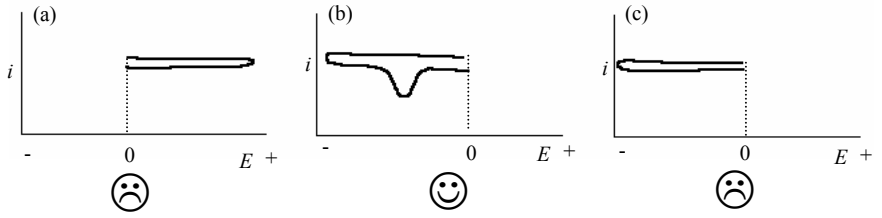

SCHEME 5–2. A CARTOON FOR CYCLIC VOLTAMMETRY OF A SURFACE BOUND WITH ACETYLFERROCENIUM THROUGH ELECTROSTATIC INTERACTION. (a) AN OXIDIZING SCAN, (b) THE FIRST REDUCTION SCAN, (c) THE SECOND REDUCTION SCAN.

Prior to the measurements of electrochemical behavior of the inorganic compound (acetylferrocene or **18**) on the surface, CVs of a bare substrate (Si/SiO_2) and a film with silver ion on the $SAM/Si/SiO_2$ are measured respectively as control experiments as shown in Figure 5-8 and Figure 5-9 (Note that all potentials given in this chapter are relative to a Pt pseudo-reference wire rather than ferrocene/ferrocenium pair with a redox couple 0.344 V more positive than Pt). CVs of the bare silicon wafer at variable scan rates (Figure 5-8) show an irreversible wave at about -0.15 V, which is assigned to the oxidization of the silicon substrate.[34,35]

The CVs of a surface sample in which silver ions are bound to the SAM/Si substrate are shown in Figure 5-9. An irreversible peak at about -0.18 V is observed. Comparison with the CV of the bare Si/SiO_2 substrate in Figure 5-8 shows that the observed wave can be assigned to the oxidization of the silicon substrate.

It was reported that for inorganic silver thiolate compounds, no observable reduction wave was found upon reductive scan to ca. -2.0 V *vs.* SCE and a irreversible oxidization wave was observed at ca. +1.5 V *vs.* SCE, which was assigned as $Ag^+ \rightarrow Ag^{2+}$ oxidization.[36] However, due to the limited redox window of the boron doped silicon substrates, the scan range is selected between -0.8 V and 0.6 V (*vs.* Pt wire). Thus, the redox waves of silver thiolate on the surface are not expected to be observed under the experimental conditions. Although XPS spectra of the surface (sample **2**) suggest the existence of a little amount of silver nitrate molecules, no redox wave of Ag/Ag^+ (0.65 V vs. FcH/FcH^+ in CH_2Cl_2) is found in

CV of the film in CH_2Cl_2. The reason may be that the amount of $AgNO_3$ is too little to be observed.

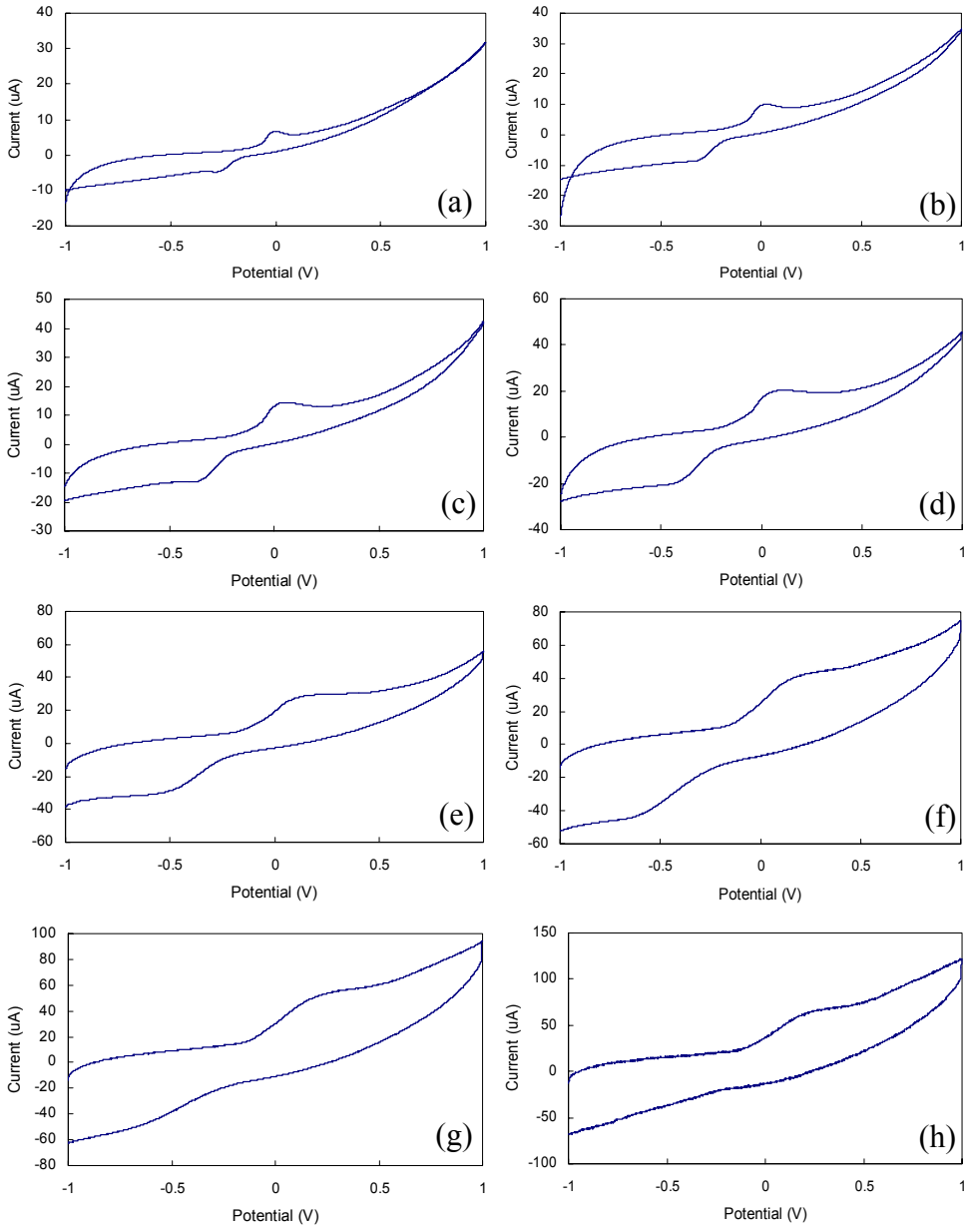

FIGURE 5–8. CV FOR A SILICON WAFER (Si/SiO_2) IN CH_2CL_2 (0.1 M $TBAPF_6$ IN CH_2CL_2 AS ELECTROLYTE), SCANNING FROM -1.0 V TO 1.0 V. SCAN RATE ($mV \cdot s^{-1}$) IS (a) 10, (b) 25, (c) 50, (d) 100, (e) 200, (f) 400, (g) 600, (h) 800.

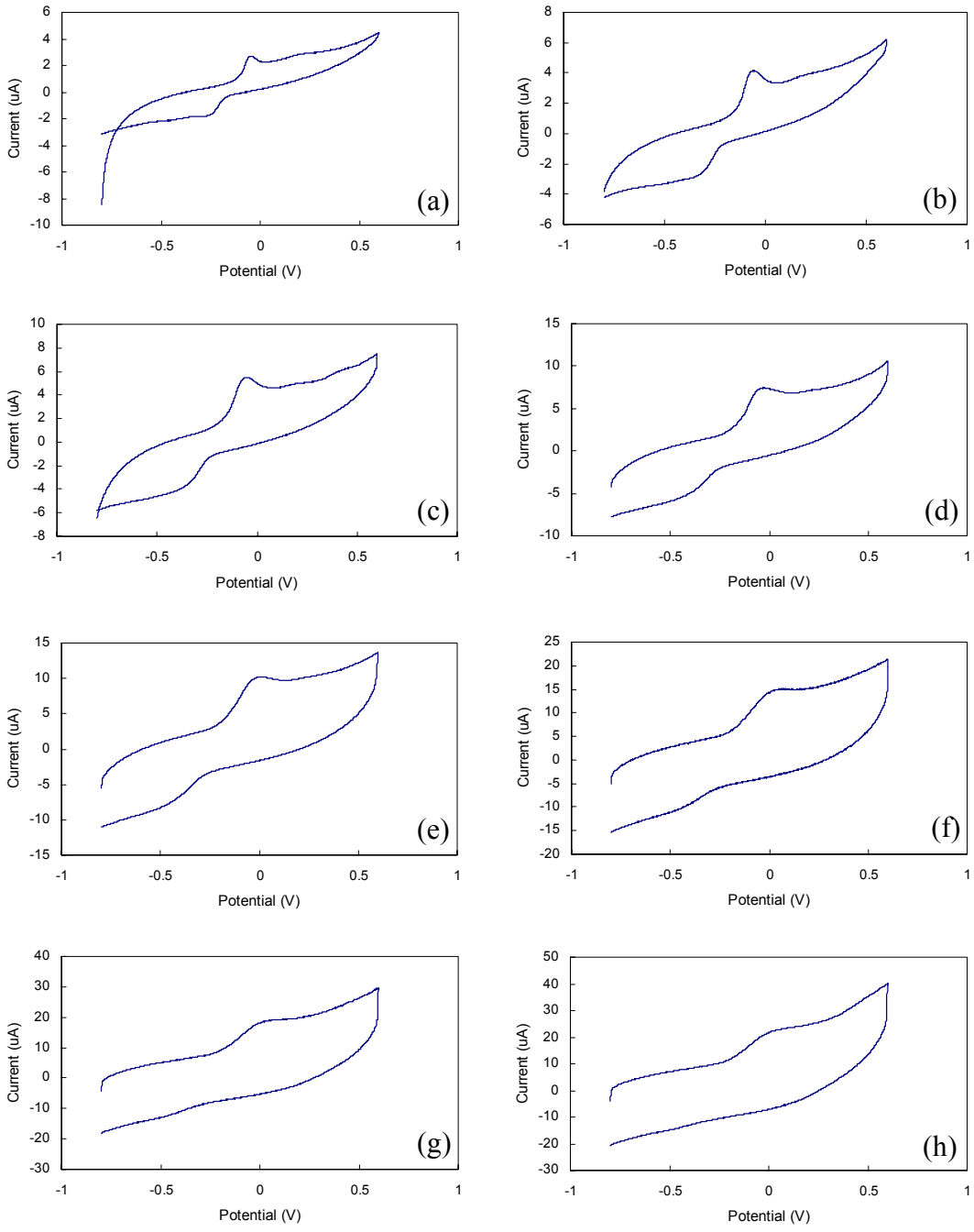

FIGURE 5–9. CV FOR A FILM IN WHICH SILVER ION HAS BEEN DEPOSITED ON A SILICON WAFER IN CH_2CL_2 (0.1 M $TBAPF_6$ IN CH_2Cl_2 AS ELECTROLYTE), SCANNING FROM -0.8 V TO 0.6 V. SCAN RATE ($mV \cdot s^{-1}$) IS (a) 10, (b) 25, (c) 50, (d) 100, (e) 200, (f) 400, (g) 600, (h) 800.

It is known that the CV of acetylferrocene in solution exhibits one reversible oxidization couple as shown in Figure 5-10.[27] The oxidization potential is 0.548 V (*vs.* Pt wire).

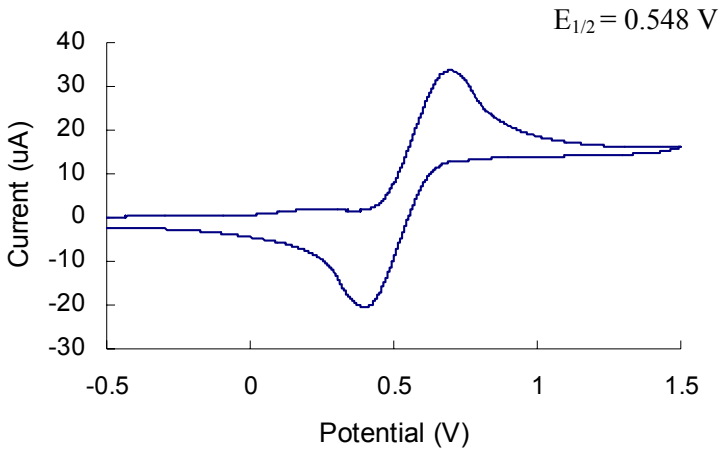

FIGURE 5–10. CYCLIC VOLTAMMETRY OF ACETYLFERROCENE AT 100 mV/s IN CH_2Cl_2.

Figure 5-11 illustrates the CV behaviors of acetylferrocene bound to a SiO_2/Si substrate at variable scan rates when scanning from -0.8 V to 0.6 V. Reversed scanning (from 0.6 V to -0.8 V) gives similar results. Compared with the CVs in Figure 5-8 and Figure 5-9, the first peak at -0.12 V is assigned to the oxidization of silicon substrate.[34,35] Except for this redox wave, an oxidation wave at about 0.3 V was observed, which may be assigned to the oxidization of acetylferrocene. The detailed data are summarized in Table 5-5.

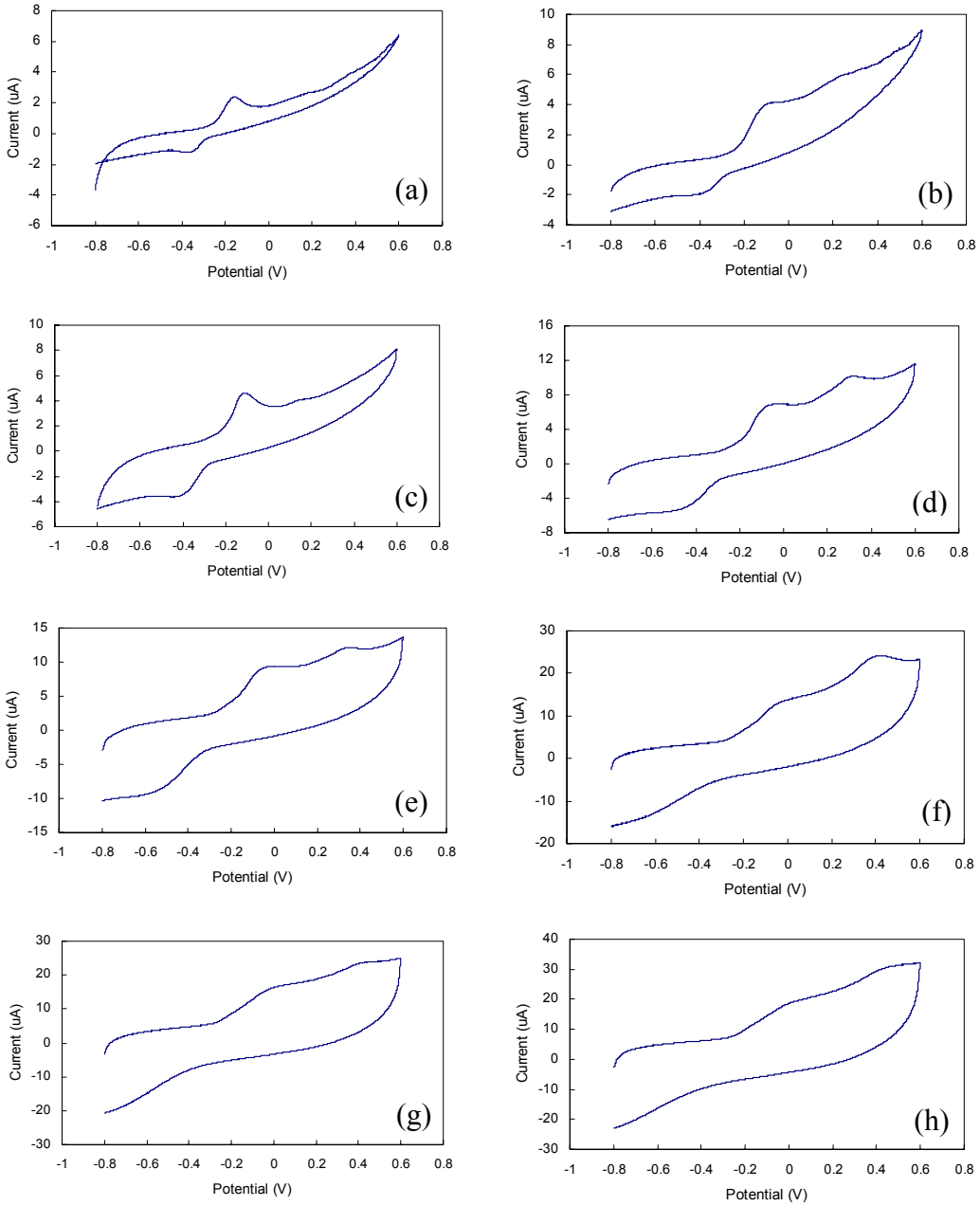

FIGURE 5–11. CV FOR A FILM IN WHICH ACETYLFERROCENE HAS BEEN DEPOSITED ON A SILICON WAFER FROM 5 mM SOLUTION IN CH_2Cl_2 (0.1 M $TBAPF_6$ IN CH_2Cl_2 AS ELECTROLYTE), SCANNING FROM -0.8 V TO 0.6 V. SCAN RATE ($mV \cdot s^{-1}$) IS (a) 10, (b) 25, (c) 50, (d) 100, (e) 200, (f) 400, (g) 600, (h) 800.

TABLE 5–5. CV DATA FOR A FILM IN WHICH ACETYLFERROCENE HAS BEEN DEPOSITED ON A SILICON WAFER.

Scan Rate (mV/s)	E_{pa} (V)	i_{pa} (μA)
10	0.195	2.698
25	0.226	4.015
50	0.265	6.293
100	0.334	10.14
200	0.366	12.10
400	0.412	16.21
600	0.441	23.80
800	0.458	30.91

These observations are very different from the expected CV behavior as shown in Scheme 5-2. The first scan (Figure 5-11 d, scan rate is 100 $mV \cdot s^{-1}$) as well as the following scans at different scan rates shows the oxidation wave at ~0.3 V. This means that our expected scheme is not right and the molecules on the surface are present as neutral species (acetylferrocene). An alternative possibility is that this wave is due to some impurities and compound acetylferrocene/acetylferrocenium is not attached on the surface. We can see if the number of oxidation event corresponds to the number of acetylferrocene molecules on the surface (by XPS) in the following way.

When the redox active molecules are bound on the surface, the peak current of the redox wave is expressed by:

$$i_p = \frac{n^2 F^2 N}{4RT}\upsilon \qquad \textbf{(5-3)}$$

where n is the number of electron transferred, F is Faraday constant, N is the number of redox active sites on the surface, R is gas constant and υ is scan rate.[37,38] Figure 5-12 illustrates the linear dependence of peak current on scan rate. The slope of the plot (33.0 μA·s·V^{-1}) and the electrode surface area (0.8 cm^2) give the area density of redox sites as 2.6 x 10^{13} cm^{-2}, corresponding to 380 $Å^2$ per molecule. The surface coverage is 3~5%. Considering the errors for the peak area in XPS and current maximum in CV, the surface coverage obtained from CV data is reasonably comparable with that gotten from XPS data. This implies that the oxidization wave at 0.3 V can be assigned to acetylferrocene on the surface.

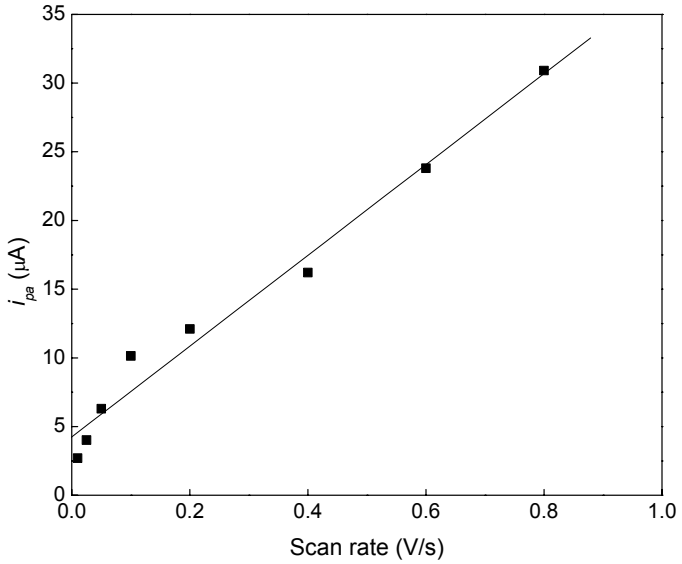

FIGURE 5–12. PLOT OF MAXIMUM CURRENT FOR OXIDIZATION WAVE OF ACETYLFERROCENE VERSUS SCAN RATE FOR A FILM OF ACETYLFERROCENE ON A Si/SiO_2 SUBSTRATE (0.1 M $TBAPF_6$ IN CH_2Cl_2).

Since the compound on the surface displays an oxidation wave, acetylferrocene is deposited on the surface as the neutral state instead of in an oxidized state. Actually, to oxidize acetylferrocene, the silver ion must be dissociated from the R–S– linker. Since the dissociation constant for the equilibrium 5-4 is pretty low (10^{-20}),[25] the oxidizing power of silver thiolate on the surface with acetylferrocene in solution will be very slow. In addition, the amount of silver nitrate molecules on the surface is very small. Hence, a few of acetylferrocenium molecules can be formed on the surface even for a long time reaction (4 days). Clearly, it is neutral acetylferrocene that is bound on the surface by other forces such as Van de Waals forces. Perhaps these forces generated by entanglement with SAM are strong enough to keep the compound on the surface for several scans.

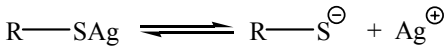

(5-4)

The CV wave assigned to the acetylferrocene bound on the Si/SiO_2 substrate shows irreversible behavior. As described above, acetylferrocene displays a reversible redox couple in solution. Several reasons may cause the absence of the reduction wave: (1) chemical decomposition of the compound, (2) due to the existence of the organic SAM between the electrode and molecule, the electron transfer rate may be so slow that the reduction wave is out of the experimental range,[39] or (3) there is a redox barrier to block the electron transfer from electrode to molecules. Since the oxidized state of acetylferrocene, acetylferrocenium, is stable in solid and in solution, the decomposition of acetylferrocenium is ruled out. Although an organic SAM can reduce the electron transfer rate between the

electrode and compounds, the separation of potential between the anodic wave and cathodic wave is not larger than 500 mV even if the scan rate is 4000 mV/s.[10] In addition, an oxidation wave assigned to the oxidization of acetylferrocene is observed. Thus, if there is a return reduction wave for the film of acetylferrocene, it should be in the experimental range. Excluding first two reasons, we are forced to consider that a redox potential barrier precludes the electron transfer from the electrode to acetylferrocenium molecules.

XPS spectra of the sample indicate the existence of ionic silver (Ag^+ from $AgNO_3$) on the surface though the amount is very small. However, a small amount of silver ion may introduce a redox barrier and precludes electron transfer from the electrode to the molecule. That is, electrons are shuttled between the acetyl-ferrocene molecules and the electrode via electron hopping between silver and silver ion on the surface. Silver ion has a higher oxidization potential (for Ag^+/Ag, 0.65 V in CH_2Cl_2 *vs.* FcH/FcH^+) than acetylferrocenium (0.27 V in CH_2Cl_2 referenced to FcH/FcH^+).[27] In the presence of the silver ion, the electron transfer from acetylferrocene to silver ion is thermodynamically downhill since silver ion is capable of oxidizing acetylferrocene. Thus the oxidization wave can be observed at the potential of Ag^+/Ag (Scheme 5-3 a). However, on the return sweep, silver ion on the film is first reduced to silver, which precludes electron transfer to acetylferrocenium because it involves a thermodynamically uphill electron transfer from silver to acetylferrocenium. Thus, the reduction wave is not observed (Scheme 5-3 b). Since the concentration of dissociated silver ion is very low, the wave assigned to the reduction of silver ion is negligible.

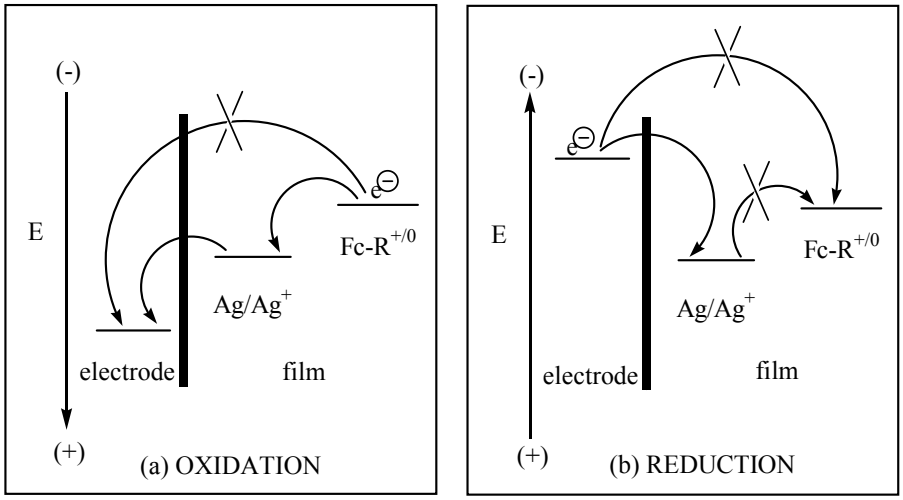

SCHEME 5–3. CARTOON OF ENERGETICS FOR THE MEDIATED ELECTRON TRANSFER.

This explanation is based on "electrochemical rectification" reported by Crook and coworkers.[40] In their work, CV of a gold electrode modified with ferrocenyl dendrimer/n-alkynethiol exhibits a redox wave at 0.5 V (*vs.* Ag/AgCl) and that of an aqueous 3 mM $Fe(CN)_6^{4-}$ electrolyte solution at a naked Au electrode shows a wave at 0.19 V (*vs.* Ag/AgCl). However, CV of a $Fe(CN)_6^{4-}$ solution at a Au electrode modified with ferrocenyl dendrimer/n-alkynethiol just exhibits an anodic current peak (oxidization of $Fe(CN)_6^{4-}$) at the ferrocene/ferrocenium potential (0.5 V) and the reversed cathodic peak is not observed.

Although the formal potential of Ag/Ag^+ on the surface is not observed in the CV of the film with silver only (sample **2**), the position of the oxidization wave of acetylferrocene on the film with silver ion (sample **3**) suggests an answer. The

formal potential of Ag/Ag^+ on the surface is about 0.3 V (*vs.* Pt wire) and shifts to more negative value compared to that in solution (ca 0.95 V vs. Pt wire). A similar result was reported previously.[10] The compound $[Ru(dppm)_2(C{\equiv}CFc)(N{\equiv}CCH_2CH_2NHC(O)(CH_2)_{10}SH)][PF_6]$ on a gold substrate displays an redox wave at 133 mV (*vs.* Pt wire) whereas the CV of this compound in solution shows a formal potential of the redox wave at 400 mV (*vs.* Pt wire).[10] Thus, a Ag/Ag^+ potential of 0.3 V observed here is reasonable.

The electrochemical behavior of **18** in solution is discussed in chapter 3 where it was shown that the compound displays four reversible oxidization couples under appropriate experiment conditions. The cyclic voltammograms of a surface with bound molecules scanning from -0.8 V to 0.6 V at various scan rates are shown in Figure 5-13 and the detailed data are listed in Table 5-6. Reversed direction scans (from 0.6 V to 0.8 V) give the similar cyclic voltammograms.

The surface sample displays two oxidization waves, which is similar to the electrochemical behavior of surface with acetylferrocene. Thus, the complex on surface may not be $[\mathbf{18}]^+$ but neutral **18**. The first wave at -0.10 V is assigned to the oxidation of the substrate. As described in chapter 4, silver ion can only oxidize neutral **18** to monocationic compound $[\mathbf{18}]^+$. The second wave at ca. 0.25 V may be the oxidization wave of **18** to $[\mathbf{18}]^+$.

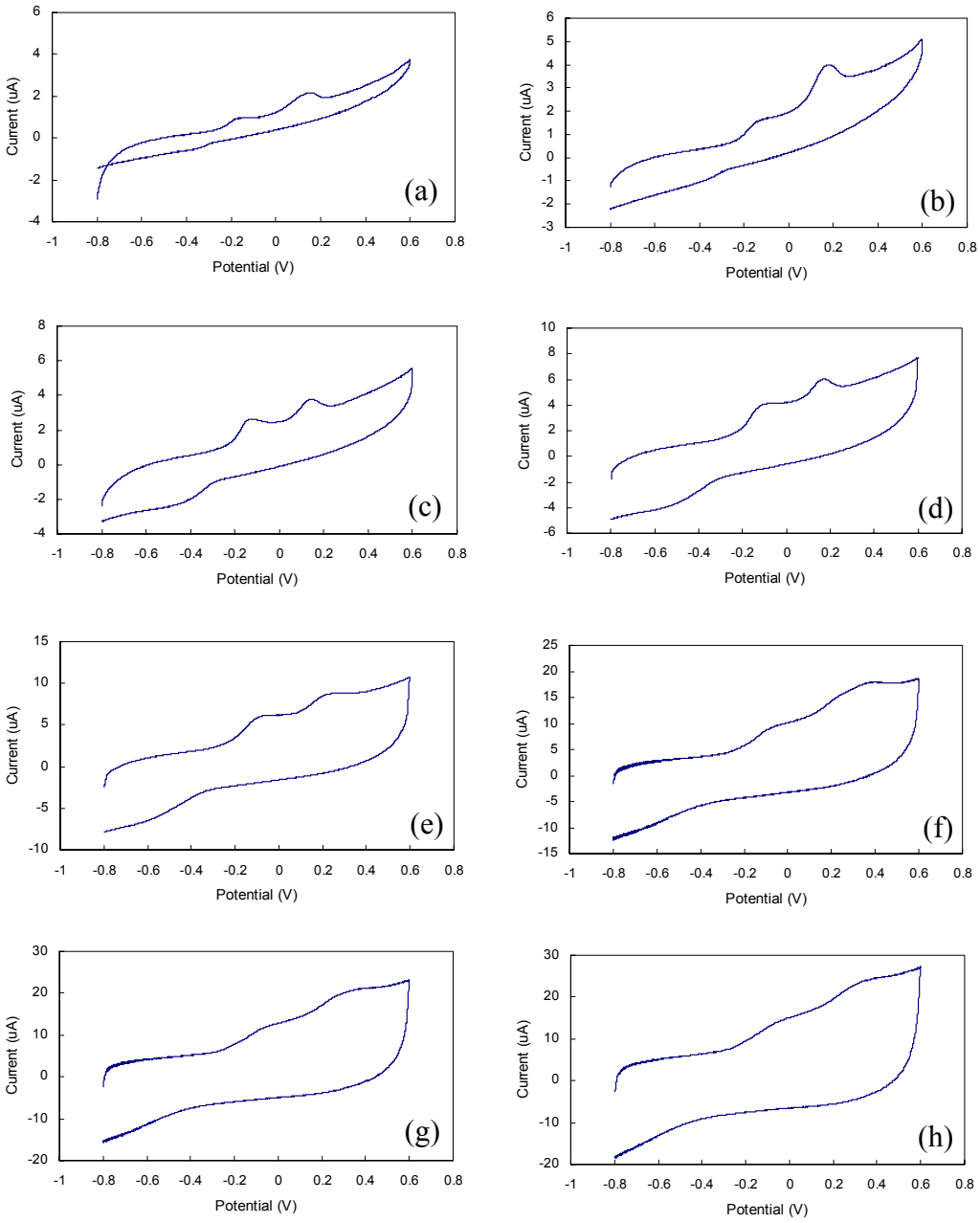

FIGURE 5–13. CV FOR A FILM IN WHICH {CpFe(η^5-C_5H_4)}$_4$(η^4-C)CoCp (**18**) HAS BEEN DEPOSITED ON A SILICON WAFER FROM 3 mM SOLUTION IN CH_2Cl_2 (0.1 M $TBAPF_6$ IN CH_2Cl_2 AS ELECTROLYTE), SCANNING FROM -0.8 V TO 0.6 V. SCAN RATE ($mV \cdot s^{-1}$) IS (a) 10, (b) 25, (c) 50, (d) 100, (e) 200, (f) 400, (g) 600, (h) 800.

TABLE 5–6. CV DATA FOR A FILM IN WHICH **18** HAS BEEN DEPOSITED ON A SILICON WAFER.

Scan Rate (mV/s)	E_{pa} (V)	i_{pa} (μA)
10	0.179	2.08
25	0.197	3.96
50	0.217	3.73
100	0.234	5.9
200	0.252	8.78
400	0.277	16.21
600	0.292	19.87
800	0.318	23.78

Figure 5-14 illustrates the linear dependence of current of peak at 0.25 V on various scan rates. The slope of the line is 27.7 $\mu A \cdot s \cdot V^{-1}$. According to the equation 5-3, the number of redox sites N = 2.9 x 10^{-11} mol for a geometric electrode surface area of 1.2 cm^2 yielding a density of redox sites as 1.4 x 10^{13} cm^{-2}, which corresponds to 714 $Å^2$ per molecule. Thus, surface coverage of molecule **18** is 17%, which is in agreement with the estimated value from XPS data. Hence, the oxidation wave at 0.25 V is assigned to the oxidization of **18** to $[\mathbf{18}]^+$.

In addition, the presence of a little amount of silver ion on the surface may suppress the reduction waves as postulated in the case of acetylferrocene. This is why the oxidized potential in CV of the film with acetylferrocene is almost the

same as that in the CV of the film with **18**. All oxidizations happen at the redox potential of Ag/Ag^{+}.

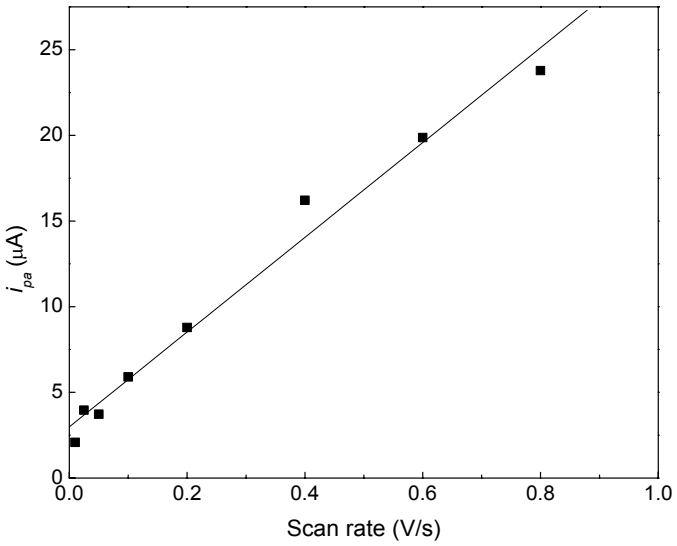

FIGURE 5–14. PLOT OF MAXIMUM CURRENT OF OXIDIZATION WAVE OF **18** VERSUS SCAN RATE FOR OXIDIZATION OF A FILM OF **18** ON A Si/SiO_2 SUBSTRATE (0.1 M $TBAPF_6$ IN CH_2Cl_2).

5.3 Discussion

High-quality organosilicon SAMs on silicon substrate are not simple to produce because of the need to carefully control the amount of water in solution,[8] and sometimes, organosilane molecules polymerize in the vertical direction to form multilayer.[26] However, under the experimental conditions employed, the monolayer of 3-MPTMS has been formed from the ellipsometry measurement.

The terminal thiol group (–SH) on the SAM can react with silver ion in solution, which result in the binding of silver ion on the surface. XPS spectra

confirm the existence of the silver ion bound to surface, but the structure of the layer remains unknown.

Attachments of acetylferrocene or compound **18** on the surface are confirmed by XPS spectra. It was reported that when the Fe^{II} was oxidized to Fe^{III}, the Fe 2p ionizations in XPS will shift to higher binding energy by 2 ~ 3 eV for powder sample[41,42] and sample on the gold surface.[43] However, Hua Qi in our group observed the compound with ferrocene on silicon wafer has the same Fe 2p binding energy as the compound with ferrocenium on surface.[11] XPS can not be used to determine the oxidization state of the iron in the compound on silicon surface. In our cases, the binding energies of Fe 2p in the acetylferrocene powder sample and surface sample are the same within experimental error, which implies that the oxidization state of acetylferrocene or **18** can not be defined merely based on the XPS data.

Electrochemical behavior of compounds on the surface may give the answer. CVs of surface samples with acetylferrocene and **18** give only oxidization waves, which indicated that molecules are bound to the surface in the neutral state. Thus, it is not electrostatic interactions that hold the molecules on the surface. Usually, surface coverage of inorganic compounds bound to the surface via covalent bonds is lager than 50%.[10,11] Other interactions such as hydrogen bond and electrostatic interaction also give good surface coverage for inorganic compounds.[14,15] However, based on XPS and CV data, surface coverage of acetylferrocene and **18** are much less than the general value. The interactions between the inorganic molecules and $SAM/SiO_2/Si$ may be caused by Van de Waals forces, which are very weak and

result in the low surface coverage. However, the forces keep the molecules on the surface even after several scans in CV experiment. Since it is neutral acetylferrocene on the surface, the dicationic mixed-valence compound $[\mathbf{18}]^{2+}$ can not be attached to the surface as designed and the proposed strategy does not work.

Since silver ion is hard to be dissociated from RAg–S and the amount of silver nitrate molecules on the surface is very small, oxidization reaction of silver ion and acetylferrocene or **18** does not occur. This results in the failure of attachment of acetylferrocenium or $[\mathbf{18}]^{+}$ on the surface. In addition, the electron transfer between the electrode and the compounds may be significantly influenced by the environmental ions such as silver ion even the amount is very small if the compound is not bound to the surface via covalent bonds. Ideal reversible CV waves may not be obtained.

5.4 Summary

A strategy, in which the inorganic compounds acetylferrocenium and $[\mathbf{18}]^{+}$ are bound to the organic SAM modified silicon wafers through the electrostatic interaction by using the oxidization reactions with silver ion was proposed. In addition to the signals from Ag 3d, XPS spectra of surface samples with inorganic compound show doublets at Fe 2p region, which indicate the attachment of the inorganic compounds. However, CVs of both surface samples only show oxidization waves. Hence, only molecules of neutral compound (acetylferrocene or **18**) are attached on the surface due to the low dissociation constant of RS–Ag. It

may be Van de Waals interactions that bind the molecules on the surface, consistent with the low surface coverage of the inorganic compounds. Furthermore, since the silver ion blocks the electron transfer from the electrode to the inorganic compound, the CVs of the samples just show the oxidized waves and returned reduced waves are not observed.

5.5 Experimental section

General

Toluene and CH_2Cl_2 were distilled immediately before use under N_2 from the following dry agents: molten sodium metal for toluene and calcium hydride for CH_2Cl_2. The others were spectroscopic grade and dried over activated 3Å molecular sieves before use. Si (111) wafers (p-type, highly B-doped, resistivity 0.001 Ω cm) were purchased from Virginia Semiconductor, Inc. All other reagents were used as purchased from Aldrich. All glasswares used to prepare monolayers were immersed into piranha solution (a 3:1 solution of concentrated sulfuric acid: 30% hydrogen peroxide). (*Warning: piranha solution is a strong oxidant, and it should be handled with extreme care and in the absence of organic solvent*). Then, the glassware was rinsed with large amount of deionized water and dried in the oven.

Monolayer preparation

Silicon wafers were cut into approximately 1cm x 1cm pieces and washed with high-purity water, CH_3OH, CH_2Cl_2 and acetone and dried in a stream of nitrogen.

The surfaces were then soaked into a freshly prepared piranha solution for about 30 minutes and rinsed with large amounts of deionized water and dried with a nitrogen stream. After that, the thickness of the native silicon oxide was measured by ellipsometry.

The cleaned silicon wafers were used immediately for the preparation of the films. The small pieces of wafers were first immersed into an octane solution of 5 mM (3-mercaptopropyl)trimethoxysilane (3-MPTMS)overnight, followed by ultrasonicating and rising with toluene three times and dried under nitrogen. The surfaces with 3-MPTMS layers were then soaked into a aqueous solution of 5 mM $AgNO_3$ for 2 hours, ultrasonicated in water for 3 minutes, washed with water three times to wash away any physically adsorbed material and dried with nitrogen stream. The final step is immersing the samples with silver ion into the solution of acetylferrocene in CH_2Cl_2 (5 mM) or $\{CpFe(\eta^5\text{-}C_5H_4)\}_4(\eta^4\text{-}C)CoCp$ (**18**) in CH_2Cl_2 (3 mM) for 4 days in a glove box (Innovative Technology) under nitrogen. The samples were then removed from the solutions and rinsed with large amounts of CH_2Cl_2 and dried under nitrogen.

Ellipsometric thickness measurement

Ellipsometric measurements were performed on a Rudolph AutoEL III ellipsometer equipped with 6328 Å (He-Ne laser) analyzing light operating at an incident angle of 70°. Each piece of clean silicon wafer was measured before monolayer growth to obtain the thickness of the native oxide layer. The thickness of the monolayer was determined by using a two-layer model (adsorbate/SiO_2/Si) with the previously measured thickness for the native oxide layer and an assumed

refractive index of 1.46 for the adsorbate. On each sample, at least five different sites were measured and the averaged results were record.

X-ray photoelectron spectroscopy (XPS)

X-ray photoelectron spectra were taken on a Kratos XSAM 800 spectrometer at a typical vacuum of 10^{-8} torr, with non-monochromatic MgK_{α} radiation at 1253.6 eV. The passing energy window of 40 eV was used for scans of all element regions. The take-off angle was fixed at 90°. The binding energies for each peak were calibrated to Si 2p at 99.3 eV.[30] The powder sample was dusted directly onto carbon tape on the measurement stub. The binding energies of peaks were referenced to O 1s peak at 531.0 eV. After the subtraction of a linear background, the spectra were fitted with 70% Gaussian/30% Lorentzian peaks, taking the minimum numbers of peaks consistent with the best fit. The peak area information is obtained using Kratos Vision II software.

Electrochemistry

The experimental condition for the measurement of cyclic voltammetry of acetylferrocene in CH_2Cl_2 is the same as described in chapter 3 for compound **18**. Cyclic voltammetric (CV) measurements of the surfaces with adsorbed compounds were performed on a BAS Epsilon-EC in a standard electrochemical cell with a Pt-flag counter electrode, a Pt-wire pseudo-reference and the silicon working electrode. The solvent is CH_2Cl_2 and tetrabutylammonium hexafluorophosphate ($TBAPF_6$) (0.1 M) was used as the supporting electrolyte. The electrode area, the geometric area exposed to the solution, was about 1 cm^2 but varied between 1.2 and

0.8 cm^2 for different samples. All measurements were done at room temperature in a nitrogen filled dry box.

5.6 Reference

(1) Bourgoin, J. P.; Doublet, F.; Palacin, S.; Vandevyver, M. *Langmuir* **1996**, *12*, 6473-6479.

(2) Yin, I.; Guo, Q.; Palmer, R. E.; Bampos, N.; Sanders, J. K. M. *J. Phys. Chem. B* **2003**, *107*, 209-216.

(3) Lu, X.; Hipps, K. W.; Wang, X. D.; Mazur, U. *J. Am. Chem. Soc.* **1996**, *118*, 7197-7202.

(4) Cook, M. J.; Mayer, D. A.; Poynter, R. H. *J. Mater. Chem.* **1995**, *5*, 2233-2238.

(5) Bain, C. D.; Troughton, E. B.; Tao, Y. T.; Evall, J.; Whitesides, G. M.; Nuzzo, R. G. *J. Am. Chem. Soc.* **1989**, *111*, 321-335.

(6) Whitesides, G. M.; Laibinis, P. E. *Langmuir* **1990**, *6*, 87-96.

(7) Ulman, A. *An introduction to ultrathin organic films : from Langmuir-Blodgett to self-assembly*; Academic Press: Boston, 1991.

(8) Ulman, A. *Chem. Rev.* **1996**, *96*, 1533-1554.

(9) Chidsey, C. E. D.; Bertozzi, C. R.; Putvinski, T. M.; Mujsce, A. M. *J. Am. Chem. Soc.* **1990**, *112*, 4301-4306.

(10) Li, Z. H.; Fehlner, T. P. *Inorg. Chem.* **2003**, *42*, 5715-5721.

(11) Qi, H.; Sharma, S.; Li, Z. H.; Snider, G. L.; Orlov, A. O.; Lent, C. S.; Fehlner, T. P. *J. Am. Chem. Soc.* **2003**, *125*, 15250-15259.

(12) Sun, L.; Crooks, R. M.; Ricco, A. J. *Langmuir* **1993**, *9*, 1775-1780.

(13) Credo, G. M.; Boal, A. K.; Das, K.; Galow, T. H.; Rotello, V. M.; Feldheim, D. L.; Gorman, C. B. *J. Am. Chem. Soc.* **2002**, *124*, 9036-9037.

(14) Varughese, B.; Chellamma, S.; Lieberman, M. *Langmuir* **2002**, *18*, 7964-7970.

(15) Hang, Q. L.; Wang, Y. L.; Lieberman, M.; Bernstein, G. H. *Appl. Phys. Lett.* **2002**, *80*, 4220-4222.

(16) Doblhofer, K.; Figura, J.; Fuhrhop, J. H. *Langmuir* **1992**, *8*, 1811-1816.

(17) Liu, S.; Tang, Z.; Bo, A.; Wang, E.; Dong, S. *J. Electroanal. Chem.* **1998**, *458*, 87-97.

(18) Legrange, J. D.; Markham, J. L.; Kurkjian, C. R. *Langmuir* **1993**, *9*, 1749-1753.

(19) Wasserman, S. R.; Tao, Y. T.; Whitesides, G. M. *Langmuir* **1989**, *5*, 1074-1087.

(20) Choi, C. H.; Liu, D. J.; Evans, J. W.; Gordon, M. S. *J. Am. Chem. Soc.* **2002**, *124*, 8730-8740.

(21) Dubois, L. H.; Nuzzo, R. G. *Annu. Rev. Phys. Chem.* **1992**, *43*, 437-463.

(22) Hang, Q. L.; Wang, Y. L.; Lieberman, M.; Bernstein, G. H. *J. Vac. Sci. Technol. B* **2003**, *21*, 227-232.

(23) Hang, Q. L.; Wang, Y. L.; Lieberman, M.; Bernstein, G. H. *J Nanosci Nanotechno* **2003**, *3*, 309-312.

(24) Roth, K. M.; Yasseri, A. A.; Liu, Z. M.; Dabke, R. B.; Malinovskii, V.; Schweikart, K. H.; Yu, L. H.; Tiznado, H.; Zaera, F.; Lindsey, J. S.; Kuhr, W. G.; Bocian, D. F. *J. Am. Chem. Soc.* **2003**, *125*, 505-517.

(25) Jocelyn, P. C. *Biochemistry of the SH group; the occurrence, chemical properties, metabolism and biological function of thiols and disulphides*; Academic Press: London, New York, 1972.

(26) Wang, X. Ph. D. Thesis, University of Notre Dame, 2003.

(27) Connelly, N. G.; Geiger, W. E. *Chem. Rev.* **1996**, *96*, 877-910.

(28) Castner, D. G.; Hinds, K.; Grainger, D. W. *Langmuir* **1996**, *12*, 5083-5086.

(29) Zhang, Y. F.; Liao, L. S.; Chan, W. H.; Lee, S. T.; Sammynaiken, R.; Sham, T. K. *Phys. Rev. B* **2000**, *61*, 8298-8305.

(30) Moulder, J. F.; Stickle, W. F.; Sobol, P. E.; Bomben, K. D. *Handbook of X-ray Photoelectron Spectroscopy*; Perkin-Elmer Corp.: Eden Prairie, MN, 1992.

(31) Fischer, A. B.; Wrighton, M. S.; Umana, M.; Murray, R. W. *J. Am. Chem. Soc.* **1979**, *101*, 3442-3446.

(32) Forouzan, F.; Bard, A. J. *J. Phys. Chem. B* **1997**, *101*, 10876-10879.

(33) Schreiber, F. *Prog. Surf. Sci.* **2000**, *65*, 151-256.

(34) Cleland, G.; Horrocks, B. R.; Houlton, A. *J. Chem. Soc., Faraday Trans.* **1995**, *91*, 4001-4003.

(35) Eagling, R. D.; Bateman, J. E.; Goodwin, N. J.; Henderson, W.; Horrocks, B. R.; Houlton, A. *J. Chem. Soc., Dalton Trans.* **1998**, 1273-1275.

(36) Yam, V. W. W.; Cheng, E. C. C.; Zhu, N. Y. *New J. Chem.* **2002**, *26*, 279-284.

(37) Bard, A. J.; Faulkner, L. R. *Electrochemical methods: fundamentals and applications*; 2nd ed.; John Wiley: New York, 2001.

(38) Brett, C. M. A.; Brett, A. M. O. *Electrochemistry: principles, methods, and applications*; Oxford University Press: Oxford; New York, 1993.

(39) Chidsey, C. E. D.; Loiacono, D. N. *Langmuir* **1990**, *6*, 682-691.

(40) Oh, S. K.; Baker, L. A.; Crooks, R. M. *Langmuir* **2002**, *18*, 6981-6987.

(41) Jones, N. D.; Wolf, M. O.; Giaquinta, D. M. *Organometallics* **1997**, *16*, 1352-1354.

(42) Li, Z. H.; Beatty, A. M.; Fehlner, T. P. *Inorg. Chem.* **2003**, *42*, 5707-5714.

(43) Umana, M.; Rolison, D. R.; Nowak, R.; Daum, P.; Murray, R. W. *Surf. Sci.* **1980**, *101*, 295-309.

CHAPTER 6

SUMMARY AND OUTLOOK

Molecular QCA cells can be mixed-valence compounds, in which the redox sites play the role of dots and the tunneling paths are provided by bridging ligands. A suitable building block for constructing QCA circuits is a square of four electronically coupled dots containing two mobile electrons. The work of the whole thesis is focused on the syntheses and characterizations of mixed-valence compounds with square shape and evaluating the possible uses for molecular QCA application.

A series of square compounds, in which molybdenum propiolate is the core linker and the metal fragments Cp*Fe(dppe), $Ru(dppm)_2Cl$ and $Co(CO)_4(dppm)$ are used as dots, were designed. However, the synthetic approaches to these square compounds failed though some other compounds with one or two metal centers were obtained and characterized. According to the structures of the products, a possible reaction pathway was proposed and radicals generated in the process in the reaction may be the reason of the synthetic failure.

Based on the general ideas of building the square compounds, a square with four ferrocenyl groups, $\{CpFe(\eta^5\text{-}C_5H_4)\}_4(\eta^4\text{-}C)CoCp$ (**18**), was synthesized from

ferrocene and $CpCo(CO)_2$ through a multiple-step reaction following known procedures.[1-3] The structure of the compound indicates that cyclobutadiene, as the core linker of the compound, is square and planar. Two of the ferrocenyl groups are up and the other two are down relative to the cyclobutadiene plane. At room temperature, these four ferrocenyl groups can rotate around the C–C bond joining them to the cyclobutadiene moiety freely. The free energy of the rotation was estimated as 20.7 $kJ \cdot mol^{-1}$ according to the variable temperature NMR data.

The square compound displays four reversible waves in cyclic voltammetry and square wave voltammetry corresponding to five oxidation states of the compounds. Compound **18** can be cleanly oxidized to the monocationic mixed-valence compound by ferrocenium ion. Stoichiometric reaction of neutral compound with acetylferrocenium afforded pure, stable dicationic mixed valence compound with two ferrocenium moieties and two ferrocenyl groups. FT-IR, EPR and Mössbauer spectra of the mixed-valence compounds imply that the electron transfer rates in both mixed-valence compounds are slower than 10^{-7} s^{-1} in solid state. Both mixed-valence compounds display inter-valence charge transfer bands in near-IR region. The band maximum of the monocationic compound is solvent dependent and that of the dicationic compound is solvent-independent. In addition to the comproportionation constants estimated from electrochemical data, it is concluded that the monocationic mix-valence compound belongs to Class-II and the dicationic mixed-valence compound is Class II-III. The electron hopping frequency of the dicationic compound in solution is estimated to be about $10^{7.5}$ s^{-1}, which is appropriately fast for QCA application. In addition, the EPR and magnetic

susceptibility measurement imply that the spin-spin interaction is small and does not distort the energies of the pair of degenerate states necessary for the signal transmission.

Although mixed-valence compounds with two metal centers have been thoroughly studied,[4-6] reports about mixed-valence compounds with four metal centers and square shape are rare.[7] Syntheses, structures and spectroscopic characterizations of mixed-valence mono- and di-cationic compounds enrich the mixed-valence field. Except for the square shape, Robin and Day's classification[6] and Hush's theory[8,9] for dinuclear mixed-valence compound are suitable to study the properties of square mixed-valence compounds.

A strategy, in which the mixed-valence compounds $[\mathbf{18}]^{+}$ and $[\mathbf{18}]^{2+}$ are bound to the organic SAM modified silicon wafers through the electrostatic interaction by using the oxidization reactions with silver ion was proposed. XPS spectra of surface samples indicate the attachment of the inorganic compounds (acetyl-ferrocene or **18**) though the oxidized states of compounds remain unknown. CVs of both surface samples only show oxidization waves, which implies that only molecules of neutral compound (acetylferrocene or **18**) are attached on the surface because of the low dissociation constant of RS–Ag, Hence, the original proposed strategy dose not work to attach the mixed-valence compounds on the surface. It may be Van de Waals interactions that bind the molecules on the surface, consistent with the low surface coverage of the inorganic compounds. Furthermore, since the silver ion blocks the electron transfer from the electrode to the inorganic

compound, reversible CV waves were not obtained and conclusive answers could not be drawn.

To get a satisfactory CV of the compound and to study the properties of the compound on the surface, the mixed-valence compound should be attached on the silicon surface directly or on SAM/surface via covalent bonds.[10,11] Recently, a number of methods have been explored to examine the attachment of organic molecules to Si surfaces, which include hydrosilylations of alkenes and alkynes on hydride-passivated Si,[12-14] the thermal reaction of alcohols and aldehydes with hydride-passivated Si,[14-17] the reaction of amines with chloride-terminated or neat Si surface[18-20] and the use of alkyl Grignard or alkyllithium reagent.[21,22] Similarly, an inorganic compound with these active anchoring groups can be linked on the silicon surface via covalent bonds.[11,23]

This creates a synthetic challenge. If the ferrocenyl groups or the Cp ligand coordinated to cobalt atom in compound **18** possess the anchoring group such as –OH, $–NH_2$, –C(O)H and alkyne or alkene, it is possible to covalently attach the compound to a Si surface and study its properties on the surface. Syntheses and characterizations of the ferrocene derivatives with functional groups have been studied extensively.[23-26] For examples, the reaction of ferrocene with 2-chlorobenzoyl chloride followed by *t*-butoxide gave the ferrocene carboxylic acid,[24] an important synthetic intermediate, which can generate ferrocene derivatives with anchoring groups such as amine through further reactions.[27] 4-(hydroxymethyl)phenyl ferrocene has been synthesized from ferrocene and 4-aminobenzoate and linked to the silicon surface.[23] Acylation of ferrocene has been

reported,[25] the resultant ferrocene derivative can be used as starting material to generate ferrocenyl alkyne.[28] In addition, Alley and Henderson synthesized ferrocenyl phosphonic acid,[26] which was shown to be attached to a silicon surface via P–O–Si linkage.[29]

All reactions to synthesize ferrocene derivatives from ferrocene can be used in compound **18** to give the resulted compound with an anchoring group in addition to the electrochemical activity of compound **18**. Several proposed compounds with anchoring groups based on compound **18** are shown in Figure 6-1.

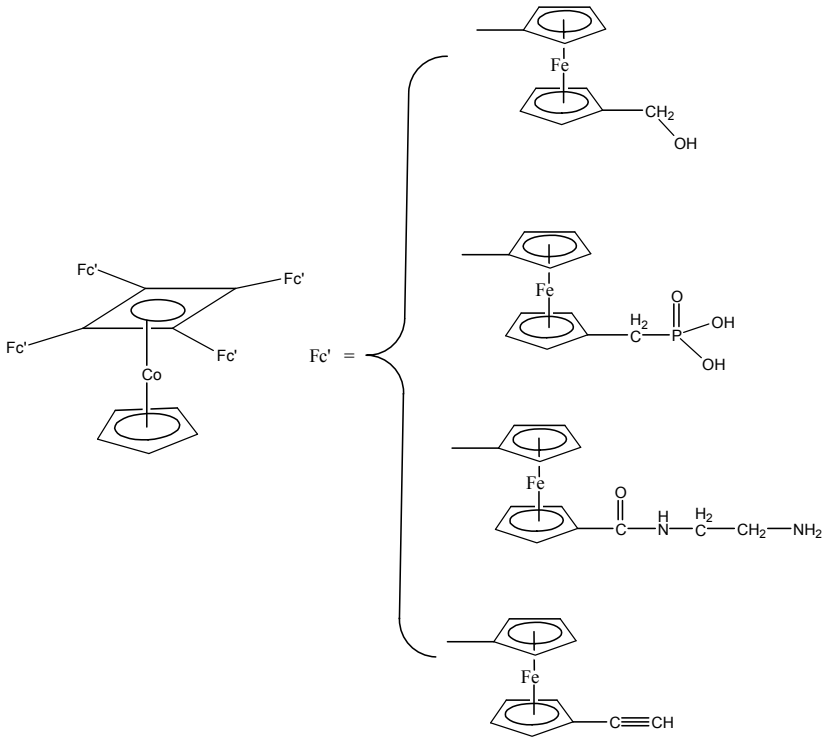

FIGURE 6–1. PROPOSED SQUARE MOLECULES BASED ON {CpFe(η^5-C_5H_4)}$_4$(η^4-C)CoCp (**18**) WITH ANCHORING GROUPS WHICH CAN LINK THE COMPOUNDS ON SILICON SUBSTRATES.

Z. Li in our group has synthesized the compounds in which the metal fragment [*trans*-Ru(dppm)$_2$(C≡C)Fc] was connected to a tail such as N≡CCH$_2$CH$_2$NH$_2$ and –C≡CPhOCH$_3$. It was reported that the CVs of the compounds with a tail are similar to the original compound [*trans*-ClRu(dppm)$_2$(C≡C)Fc] other than the shifts of the oxidization potentials.[10,30] Thus, the anchoring groups on the ferrocenyl moieties will not change the electrochemical properties of the original compound (**18**) except for the shifts of the formal redox potentials.

The mixed-valence dicationic compounds used as building blocks for molecular QCA application can be obtained by oxidization of these neutral compounds with a proper oxidant (based on the electrochemical behaviors of neutral compounds). Then, the mixed-valence compounds can be attached on the surface via covalent bonds formed between the anchoring groups and the substrates. Another method is to attach the neutral compounds to a silicon substrate first, and then oxidize the molecules on the surface with chemical methods by dipping the surface in the solution of a suitable oxidant[10,11] or electrochemical method by setting the oxidized potential at the proper value.

Once the dicationic mixed-valence compounds are bound to a surface, the molecular film can be studied by many technologies of surface analysis such as IR, X-ray photoelectron spectroscopy (XPS), electrochemistry and atomic force microscopy (AFM) to explore the properties of mixed-valence compounds on surface relevant to QCA application.

References

(1) Guillaneux, D.; Kagan, H. B. *J. Org. Chem.* **1995**, *60*, 2502-2505.

(2) Rosenblum, M.; Brawn, N.; Papenmeier, J.; Applebaum, M. *J. Organomet. Chem.* **1966**, *6*, 173-180.

(3) Rausch, M. D.; Higbie, F. A.; Westover, G. F.; Clearfield, A.; Gopal, R.; Troup, J. M.; Bernal, I. *J. Organomet. Chem.* **1978**, *149*, 245-264.

(4) Demadis, K. D.; Hartshorn, C. M.; Meyer, T. J. *Chem. Rev.* **2001**, *101*, 2655-2685.

(5) Ward, M. D. *Chem. Soc. Rev.* **1995**, *24*, 121-134.

(6) Robin, M. B.; Day, P. *Adv. Inorg. Chem. Radiochem.* **1967**, *10*, 247-422.

(7) Lau, V. C.; Berben, L. A.; Long, J. R. *J. Am. Chem. Soc.* **2002**, *124*, 9042-9043.

(8) Hush, N. S. *Prog. Inorg. Chem.* **1967**, *8*, 391-444.

(9) Creutz, C. *Prog. Inorg. Chem.* **1983**, *30*, 1-73.

(10) Li, Z. H.; Fehlner, T. P. *Inorg. Chem.* **2003**, *42*, 5715-5721.

(11) Qi, H.; Sharma, S.; Li, Z. H.; Snider, G. L.; Orlov, A. O.; Lent, C. S.; Fehlner, T. P. *J. Am. Chem. Soc.* **2003**, *125*, 15250-15259.

(12) Hovis, J. S.; Lee, S.; Liu, H. B.; Hamers, R. J. *J. Vac. Sci. Technol. B* **1997**, *15*, 1153-1158.

(13) Hovis, J. S.; Hamers, R. J. *J. Phys. Chem. B* **1998**, *102*, 687-692.

(14) Bateman, J. E.; Eagling, R. D.; Horrocks, B. R.; Houlton, A. *J. Phys. Chem. B* **2000**, *104*, 5557-5565.

(15) Boukherroub, R.; Morin, S.; Sharpe, P.; Wayner, D. D. M.; Allongue, P. *Langmuir* **2000**, *16*, 7429-7434.

(16) Zhu, X. Y.; Boiadjiev, V.; Mulder, J. A.; Hsung, R. P.; Major, R. C. *Langmuir* **2000**, *16*, 6766-6772.

(17) Kim, N. Y.; Laibinis, P. E. *J. Am. Chem. Soc.* **1997**, *119*, 2297-2298.

(18) Barrelet, C. J.; Robinson, D. B.; Cheng, J.; Hunt, T. P.; Quate, C. F.; Chidsey, C. E. D. *Langmuir* **2001**, *17*, 3460-3465.

(19) Zhu, X. Y.; Mulder, J. A.; Bergerson, W. F. *Langmuir* **1999**, *15*, 8147-8154.

(20) Bergerson, W. F.; Mulder, J. A.; Hsung, R. P.; Zhu, X. Y. *J. Am. Chem. Soc.* **1999**, *121*, 454-455.

(21) Bansal, A.; Li, X. L.; Lauermann, I.; Lewis, N. S.; Yi, S. I.; Weinberg, W. H. *J. Am. Chem. Soc.* **1996**, *118*, 7225-7226.

(22) Yu, H. Z.; Morin, S.; Wayner, D. D. M.; Allongue, P.; de Villeneuve, C. H. *J. Phys. Chem. B* **2000**, *104*, 11157-11161.

(23) Roth, K. M.; Yasseri, A. A.; Liu, Z. M.; Dabke, R. B.; Malinovskii, V.; Schweikart, K. H.; Yu, L. H.; Tiznado, H.; Zaera, F.; Lindsey, J. S.; Kuhr, W. G.; Bocian, D. F. *J. Am. Chem. Soc.* **2003**, *125*, 505-517.

(24) Biehl, E. R.; Reeves, P. C. *Synthesis* **1973**, *6*, 360-361.

(25) Schottenberger, H.; Lukassser, J.; Reichel, E.; Muller, A. G.; Steiner, G.; Kopacka, H.; Wurst, K.; Ongania, K. H.; Kirchner, K. *J. Organomet. Chem.* **2001**, *637*, 558-576.

(26) Alley, S. R.; Henderson, W. *J. Organomet. Chem.* **2001**, *637*, 216-229.

(27) Huang, R.; Wang, Q. *J. Organomet. Chem* **2001**, *637-639*, 94-98.

(28) Luo, S. J.; Liu, Y. H.; Liu, C. M.; Liang, Y. M.; Ma, Y. X. *Synthetic Commun.* **2000**, *30*, 1569-1572.

(29) Li, Q. L.; Surthi, S.; Mathur, G.; Gowda, S.; Misra, V.; Sorenson, T. A.; Tenent, R. C.; Kuhr, W. G.; Tamaru, S.; Lindsey, J. S.; Liu, Z. M.; Bocian, D. F. *Appl. Phys. Lett.* **2003**, *83*, 198-200.

(30) Li, Z. H.; Beatty, A. M.; Fehlner, T. P. *Inorg. Chem.* **2003**, *42*, 5707-5714.

REFERENCES

(1) Abel, E. W.; Stone, F. G. A.; Wilkinson, G. *Comprehensive organometallic chemistry II : a review of the literature 1982-1994*; 1st ed.; Pergamon: Oxford ; New York, 1995.

(2) Aggarwal, R. P.; Connelly, N. G.; Crespo, M. C.; Dunne, B. J.; Hopkins, P. M.; Orpen, A. G. *J. Chem. Soc. Chem. Commun.* **1989**, 33-35.

(3) Aggarwal, R. P.; Connelly, N. G.; Crespo, M. C.; Dunne, B. J.; Hopkins, P. M.; Orpen, A. G. *J. Chem. Soc., Dalton Trans.* **1992**, 655-662.

(4) Allen, G. C.; Hush, N. S. *Prog. Inorg. Chem.* **1967**, *8*, 357-389.

(5) Alley, S. R.; Henderson, W. *J. Organomet. Chem.* **2001**, *637*, 216-229.

(6) Amlani, I.; Orlov, A. O.; Toth, G.; Bernstein, G. H.; Lent, C. S.; Snider, G. L. *Science* **1999**, *284*, 289-291.

(7) Arewgoda, M.; Rieger, P. H.; Robinson, B. H.; Simpson, J.; Visco, S. J. *J. Am. Chem. Soc.* **1982**, *104*, 5633-5640.

(8) Arewgoda, M.; Robinson, B. H.; Simpson, J. *J. Am. Chem. Soc.* **1983**, *105*, 1893-1903.

(9) Armstrong, A. T.; Carroll, D. G.; McGlynn, S. P. *J. Chem. Phys.* **1976**, *47*, 1104-1111.

(10) Astruc, D. *Acc. Chem. Res.* **1997**, *30*, 383-391.

(11) Aviram, A.; Ratner, M. A. *Chem. Phys. Lett.* **1974**, *29*, 277-283.

(12) Avouris, P. *Acc. Chem. Res.* **2002**, *35*, 1026-1034.

(13) Bachtold, A.; Hadley, P.; Nakanishi, T.; Dekker, C. *Science* **2001**, *294*, 1317-1320.

(14) Bailey, A.; Fehlner, T. P. *unpublished result*.

(15) Bain, C. D.; Troughton, E. B.; Tao, Y. T.; Evall, J.; Whitesides, G. M.; Nuzzo, R. G. *J. Am. Chem. Soc.* **1989**, *111*, 321-335.

(16) Bansal, A.; Li, X. L.; Lauermann, I.; Lewis, N. S.; Yi, S. I.; Weinberg, W. H. *J. Am. Chem. Soc.* **1996**, *118*, 7225-7226.

(17) Bard, A. J.; Faulkner, L. R. *Electrochemical methods: fundamentals and applications*; 2nd ed.; John Wiley: New York, 2001.

(18) Barlow, S. *Inorg. Chem.* **2001**, *40*, 7047-7053.

(19) Barrelet, C. J.; Robinson, D. B.; Cheng, J.; Hunt, T. P.; Quate, C. F.; Chidsey, C. E. D. *Langmuir* **2001**, *17*, 3460-3465.

(20) Bateman, J. E.; Eagling, R. D.; Horrocks, B. R.; Houlton, A. *J. Phys. Chem. B* **2000**, *104*, 5557-5565.

(21) Beley, M.; Collin, J. P.; Louis, R.; Metz, B.; Sauvage, J. P. *J. Am. Chem. Soc.* **1991**, *113*, 8521-8522.

(22) Benisch, C.; Gleiter, R.; Staeb, T. H.; Nuber, B.; Oeser, T.; Pritzkow, H.; Rominger, F. *J. Organomet. Chem.* **2002**, *641*, 102-112.

(23) Benisch, C.; Werz, D. B.; Gleiter, R.; Rominger, F.; Oeser, T. *Eur. J. Inorg. Chem.* **2003**, 1099-1112.

(24) Bergerson, W. F.; Mulder, J. A.; Hsung, R. P.; Zhu, X. Y. *J. Am. Chem. Soc.* **1999**, *121*, 454-455.

(25) Biehl, E. R.; Reeves, P. C. *Synthesis* **1973**, *6*, 360-361.

(26) Bird, P. H.; Fraser, A. R.; Hall, D. N. *Inorg. Chem.* **1977**, *16*, 1923-1931.

(27) Boukherroub, R.; Morin, S.; Sharpe, P.; Wayner, D. D. M.; Allongue, P. *Langmuir* **2000**, *16*, 7429-7434.

(28) Bourgoin, J. P.; Doublet, F.; Palacin, S.; Vandevyver, M. *Langmuir* **1996**, *12*, 6473-6479.

(29) Braun-Sand, S. B. Ph. D. Thesis, University of Notre Dame, 2003.

(30) Brett, C. M. A.; Brett, A. M. O. *Electrochemistry: principles, methods, and applications*; Oxford University Press: Oxford; New York, 1993.

(31) Brett, C. M. A.; Brett, A. M. O. *Electroanalysis*; Oxford Universisty Press: Oxford ; New York, 1998.

(32) Bruce, M. I. *Chem. Rev.* **1991**, *91*, 197-257.

(33) Bunz, U. H. F.; Roidl, G.; Altmann, M.; Enkelmann, V.; Shimizu, K. D. *J. Am. Chem. Soc.* **1999**, *121*, 10719-10726.

(34) Buschel, M.; Helldobler, M.; Daub, J. *Chem. Commun.* **2002**, 1338-1339.

(35) Butler, I. R.; Wilkes, S. B.; Mcdonald, S. J.; Hobson, L. J.; Taralp, A.; Wilde, C. P. *Polyhedron* **1993**, *12*, 129-131.

(36) Calvo-Perez, V.; Vega, A.; Cortes, P.; Spodine, E. *Inorg. Chim. Acta* **2002**, *333*, 15-24.

(37) Calvo-Perez, V. C. Ph. D. Thesis, University of Notre Dame, 1996.

(38) Carre, F. H.; Cotton, F. A.; Frenz, B. A. *Inorg. Chem.* **1976**, *15*, 380-387.

(39) Casagrande, L. V.; Chen, T.; Rieger, P. H.; Robinson, B. H.; Simpson, J.; Visco, S. J. *Inorg. Chem.* **1984**, *23*, 2019-2025.

(40) Castner, D. G.; Hinds, K.; Grainger, D. W. *Langmuir* **1996**, *12*, 5083-5086.

(41) Chang, J. P.; Fung, E. Y.; Curtis, J. C. *Inorg. Chem.* **1986**, *25*, 4233-4241.

(42) Chaudret, B.; Commenges, G.; Poilblanc, R. *J. Chem. Soc., Dalton Trans.* **1984**, 1635-1639.

(43) Chellamma, S.; Lieberman, M. *Inorg. Chem.* **2001**, *40*, 3177-3180.

(44) Chen, J.; Reed, M. A.; Rawlett, A. M.; Tour, J. M. *Science* **1999**, *286*, 1550-1552.

(45) Chi, K. M.; Calabrese, J. C.; Reiff, W. M.; Miller, J. S. *Organometallics* **1991**, *10*, 688-693.

(46) Chia, L. S.; Cullen, W. R. *Inorg. Chem.* **1975**, *14*, 482-485.

(47) Chidsey, C. E. D.; Bertozzi, C. R.; Putvinski, T. M.; Mujsce, A. M. *J. Am. Chem. Soc.* **1990**, *112*, 4301-4306.

(48) Chidsey, C. E. D.; Loiacono, D. N. *Langmuir* **1990**, *6*, 682-691.

(49) Choi, C. H.; Liu, D. J.; Evans, J. W.; Gordon, M. S. *J. Am. Chem. Soc.* **2002**, *124*, 8730-8740.

(50) Clearfield, A.; Gopal, R.; Rausch, M. D.; Tokas, E. F.; Higbie, F. A.; Bernal, I. *J. Organomet. Chem.* **1977**, *135*, 229-248.

(51) Cleland, G.; Horrocks, B. R.; Houlton, A. *J. Chem. Soc., Faraday Trans.* **1995**, *91*, 4001-4003.

(52) Cobden, D. H. *Nature* **2001**, *409*, 32-33.

(53) Colbert, M. C. B.; Lewis, J.; Long, N. J.; Raithby, P. R.; Younus, M.; White, A. J. P.; Williams, D. J.; Payne, N. N.; Yellowlees, L.; Beljonne, D.; Chawdhury, N.; Friend, R. H. *Organometallics* **1998**, *17*, 3034-3043.

(54) Colbran, S. B.; Hanton, L. R.; Robinson, B. H.; Robinson, W. T.; Simpson, J. *J. Organomet. Chem.* **1987**, *330*, 415-428.

(55) Colbran, S. B.; Robinson, B. H.; Simpson, J. *Organometallics* **1983**, *2*, 943-951.

(56) Colbran, S. B.; Robinson, B. H.; Simpson, J. *Organometallics* **1983**, *2*, 952-957.

(57) Colbran, S. B.; Robinson, B. H.; Simpson, J. *Organometallics* **1984**, *3*, 1344-1353.

(58) Collier, C. P.; Jeppesen, J. O.; Luo, Y.; Perkins, J.; Wong, E. W.; Heath, J. R.; Stoddart, J. F. *J. Am. Chem. Soc.* **2001**, *123*, 12632-12641.

(59) Collier, C. P.; Wong, E. W.; Belohradsky, M.; Raymo, F. M.; Stoddart, J. F.; Kuekes, P. J.; Williams, R. S.; Heath, J. R. *Science* **1999**, *285*, 391-394.

(60) Collin, J. P.; Laine, P.; Launay, J. P.; Sauvage, J. P.; Sour, A. *J. Chem. Soc. Chem. Commun.* **1993**, 434-435.

(61) Connelly, N. G.; Geiger, W. E. *Chem. Rev.* **1996**, *96*, 877-910.

(62) Constable, E. C. *Angew. Chem. Int. Ed.* **1991**, *30*, 407-408.

(63) Cook, M. J.; Mayer, D. A.; Poynter, R. H. *J. Mater. Chem.* **1995**, *5*, 2233-2238.

(64) Cotton, F. A.; Daniels, L. M.; Lin, C.; Murillo, C. A. *J. Am. Chem. Soc.* **1999**, *121*, 4538-4539.

(65) Cotton, F. A.; Lin, C.; Murillo, C. A. *J. Am. Chem. Soc.* **2001**, *123*, 2670-2671.

(66) Cotton, F. A.; Lin, C.; Murillo, C. A. *Acc. Chem. Res.* **2001**, *34*, 759-771.

(67) Cowan, D. O.; Vanda, C. L.; Park, J.; Kaufman, F. J. *Acc. Chem. Res.* **1973**, *6*, 1-7.

(68) Credo, G. M.; Boal, A. K.; Das, K.; Galow, T. H.; Rotello, V. M.; Feldheim, D. L.; Gorman, C. B. *J. Am. Chem. Soc.* **2002**, *124*, 9036-9037.

(69) Creutz, C. *Inorg. Chem.* **1978**, *17*, 3723-3725.

(70) Creutz, C. *Prog. Inorg. Chem.* **1983**, *30*, 1-73.

(71) Creutz, C.; Taube, H. *J. Am. Chem. Soc.* **1969**, *91*, 3988-3989.

(72) Creutz, C.; Taube, H. *J. Am. Chem. Soc.* **1973**, *95*, 1086-1094.

(73) Cuadrado, I.; Casado, C. M.; Alonso, B.; Moran, M.; Losada, J.; Belsky, V. *J. Am. Chem. Soc.* **1997**, *119*, 7613-7614.

(74) Cullity, B. D. *Introduction to magnetic materials*; Addison-Wesley Pub. Co.: Reading, Mass., 1972.

(75) Das, A.; Maher, J. P.; Mccleverty, J. A.; Badiola, J. A. N.; Ward, M. D. *J. Chem. Soc., Dalton Trans.* **1993**, 681-686.

(76) Demadis, K. D.; Hartshorn, C. M.; Meyer, T. J. *Chem. Rev.* **2001**, *101*, 2655-2685.

(77) Doblhofer, K.; Figura, J.; Fuhrhop, J. H. *Langmuir* **1992**, *8*, 1811-1816.

(78) Dong, T. Y.; Cohn, M. J.; Hendrickson, D. N.; Pierpont, C. G. *J. Am. Chem. Soc.* **1985**, *107*, 4777-4778.

(79) Dong, T. Y.; Hendrickson, D. N.; Pierpont, C. G.; Moore, M. F. *J. Am. Chem. Soc.* **1986**, *108*, 963-971.

(80) Dong, T. Y.; Huang, C. H.; Chang, C. K.; Wen, Y. S.; Lee, S. L.; Chen, J. A.; Yeh, W. Y.; Yeh, A. *J. Am. Chem. Soc.* **1993**, *115*, 6357-6368.

(81) Dong, T. Y.; Kambara, T.; Hendrickson, D. N. *J. Am. Chem. Soc.* **1986**, *108*, 4423-4432.

(82) Dong, T. Y.; Lee, S. H.; Lee, T. Y. *Organometallics* **1996**, *15*, 2354-2359.

(83) Dong, T. Y.; Lee, T. Y.; Lee, S. H.; Lee, G. H.; Peng, S. M. *Organometallics* **1994**, *13*, 2337-2348.

(84) Dong, T. Y.; Lee, T. Y.; Wen, Y. S.; Lee, S. H.; Hsieh, C. F.; Lee, G. H.; Peng, S. M. *J. Organomet. Chem.* **1993**, *456*, 239-242.

(85) Dong, T. Y.; Schei, C. C.; Hwang, M. Y.; Lee, T. Y.; Yeh, S. K.; Wen, Y. S. *Organometallics* **1992**, *11*, 573-582.

(86) Dori, Z.; Wilkinson, G. *Inorg. Synth.* **1972**, *13*, 87-89.

(87) Dowling, N.; Henry, P. M.; Lewis, N. A.; Taube, H. *Inorg. Chem.* **1981**, *20*, 2345-2348.

(88) Drago, R. S. *Physical methods for chemists*; 2nd ed.; Saunders College Pub.: Ft. Worth, 1992.

(89) Drain, C. M.; Lehn, J. M. *J. Chem. Soc. Chem. Commun.* **1994**, 2313-2315.

(90) Dubois, L. H.; Nuzzo, R. G. *Annu. Rev. Phys. Chem.* **1992**, *43*, 437-463.

(91) Duggan, D. M.; Hendrickson, D. N. *Inorg. Chem.* **1975**, *14*, 955-970.

(92) Eagling, R. D.; Bateman, J. E.; Goodwin, N. J.; Henderson, W.; Horrocks, B. R.; Houlton, A. *J. Chem. Soc., Dalton Trans.* **1998**, 1273-1275.

(93) Efraty, A. *Chem. Rev.* **1977**, *77*, 691-744.

(94) Elder, S. M.; Robinson, B. H.; Simpson, J. *J. Organomet. Chem.* **1990**, *398*, 165-176.

(95) Ellenbogen, J. C.; Love, J. C. *Proc. IEEE* **2000**, *88*, 386-426.

(96) Ernst, S.; Kasack, V.; Kaim, W. *Inorg. Chem.* **1988**, *27*, 1146-1148.

(97) Evans, I. P.; Spencer, A.; Wilkinson, G. *J. Chem. Soc., Dalton Trans.* **1973**, 204-209.

(98) Farrugia, L. J.; Braga, D.; Grepioni, F. *J. Organomet. Chem.* **1999**, *573*, 60-66.

(99) Fischer, A. B.; Wrighton, M. S.; Umana, M.; Murray, R. W. *J. Am. Chem. Soc.* **1979**, *101*, 3442-3446.

(100) Forouzan, F.; Bard, A. J. *J. Phys. Chem. B* **1997**, *101*, 10876-10879.

(101) Fritch, J. R.; Vollhardt, K. P. C.; Thompson, M. R.; Day, V. W. *J. Am. Chem. Soc.* **1979**, *101*, 2768-2770.

(102) Fritch, J. R.; Vollhardt, P. C. *Organometallics* **1982**, *1*, 590-602.

(103) Fujita, M.; Yazaki, J.; Ogura, K. *J. Am. Chem. Soc.* **1990**, *112*, 5645-5647.

(104) Fukumoto, T.; Matsumura, Y.; Okawara, R. *J. Organomet. Chem.* **1974**, *69*, 437-444.

(105) Gascoin, F.; Sevov, S. C. *Inorg. Chem.* **2002**, *41*, 5920-5924.

(106) Gelling, A.; Jeffery, J. C.; Povey, D. C.; Went, M. J. *J. Chem. Soc., Chem. Commun.* **1991**, 349-351.

(107) Gleiter, R. *Angew. Chem. Int. Ed.* **1992**, *31*, 27-44.

(108) GoldhaberGordon, D.; Montemerlo, M. S.; Love, J. C.; Opiteck, G. J.; Ellenbogen, J. C. *Proc. IEEE* **1997**, *85*, 521-540.

(109) Greenfield, H.; Sternberg, H. W.; Friedel, R. A.; Wotiz, J. H.; Markby, R.; Wender, I. *J. Am. Chem. Soc.* **1956**, *78*, 120-124.

(110) Grossel, M. C.; Goldspink, M. R.; Hriljac, J. A.; Weston, S. C. *Organometallics* **1991**, *10*, 851-860.

(111) Guillaneux, D.; Kagan, H. B. *J. Org. Chem.* **1995**, *60*, 2502-2505.

(112) Guillon, C.; Vierling, P. *J. Organomet. Chem.* **1994**, *464*, C42-C44.

(113) Hamon, P.; Toupet, L.; Hamon, J. R.; Lapinte, C. *Organometallics* **1992**, *11*, 1429-1431.

(114) Hamon, P.; Toupet, L.; Hamon, J. R.; Lapinte, C. *J. Chem. Soc., Chem. Commun.* **1994**, 931-932.

(115) Hamon, P.; Toupet, L.; Hamon, J. R.; Lapinte, C. *Organometallics* **1996**, *15*, 10-12.

(116) Hang, Q. L.; Wang, Y. L.; Lieberman, M.; Bernstein, G. H. *Appl. Phys. Lett.* **2002**, *80*, 4220-4222.

(117) Hang, Q. L.; Wang, Y. L.; Lieberman, M.; Bernstein, G. H. *J. Vac. Sci.Technol. B* **2003**, *21*, 227-232.

(118) Hang, Q. L.; Wang, Y. L.; Lieberman, M.; Bernstein, G. H. *J. Nanosci. Nanotechno.* **2003**, *3*, 309-312.

(119) Haquette, P.; Pirio, N.; Touchard, D.; Toupet, L.; Dixneuf, P. H. *J. Chem. Soc., Chem. Commun.* **1993**, 163-165.

(120) Herber, R. H. *Inorg. Chim. Acta* **1999**, *291*, 74-81.

(121) Herber, R. H.; Nowik, I. *Solid State Sciences* **2002**, *4*, 691-694.

(122) Herber, R. H.; Nowik, I.; Iyoda, M. *J. Organomet. Chem.* **2002**, *658*, 210-213.

(123) Hiller, K. O.; Masloch, B.; Gobl, M.; Asmus, K. D. *J. Am. Chem. Soc.* **1981**, *103*, 2734-2743.

(124) Holliday, B. J.; Mirkin, C. A. *Angew. Chem. Int. Ed.* **2001**, *40*, 2022-2043.

(125) Hore, L. A.; McAdam, C. J.; Kerr, J. L.; Duffy, N. W.; Robinson, B. H.; Simpson, J. *Organometallics* **2000**, *19*, 5039-5048.

(126) Hovis, J. S.; Hamers, R. J. *J. Phys. Chem. B* **1998**, *102*, 687-692.

(127) Hovis, J. S.; Lee, S.; Liu, H. B.; Hamers, R. J. *J. Vac. Sci.Technol. B* **1997**, *15*, 1153-1158.

(128) Huang, R.; Wang, Q. *J. Organomet. Chem.* **2001**, *637-639*, 94-98.

(129) Huang, Y.; Duan, X. F.; Cui, Y.; Lauhon, L. J.; Kim, K. H.; Lieber, C. M. *Science* **2001**, *294*, 1313-1317.

(130) Hurst, S. K.; Cifuentes, M. P.; McDonagh, A. M.; Humphrey, M. G.; Samoc, M.; Luther-Davies, B.; Asselberghs, I.; Persoons, A. *J. Organomet. Chem.* **2002**, *642*, 259-267.

(131) Hush, N. S. *Prog. Inorg. Chem.* **1967**, *8*, 391-444.

(132) Iggo, J. A. *NMR spectroscopy in inorganic chemistry*; Oxford University Press: Oxford ; New York, 1999.

(133) Iyer, R. S.; Selegue, J. P. *J. Am. Chem. Soc.* **1987**, *109*, 910-911.

(134) Jiao, J. Y.; Long, G. J.; Grandjean, F.; Beatty, A. M.; Fehlner, T. P. *J. Am. Chem. Soc.* **2003**, *125*, 7522-7523.

(135) Jocelyn, P. C. *Biochemistry of the SH group; the occurrence, chemical properties, metabolism and biological function of thiols and disulphides*; Academic Press: London, New York, 1972.

(136) Johannessen, S. C.; Brisbois, R. G.; Fischer, J. P.; Grieco, P. A.; Counterman, A. E.; Clemmer, D. E. *J. Am. Chem. Soc.* **2001**, *123*, 3818-3819.

(137) Jones, N. D.; Wolf, M. O.; Giaquinta, D. M. *Organometallics* **1997**, *16*, 1352-1354.

(138) Jortner, J.; Ratner, M. A.; International Union of Pure and Applied Chemistry. *Molecular electronics*; Blackwell Science: Osney Mead, Oxford [England] ; Malden, MA, USA, 1997.

(139) Kaim, W.; Klein, A.; Glockle, M. *Acc. Chem. Res.* **2000**, *33*, 755-763.

(140) Kim, N. Y.; Laibinis, P. E. *J. Am. Chem. Soc.* **1997**, *119*, 2297-2298.

(141) Kim, Y.; Lieber, C. M. *Inorg. Chem.* **1989**, *28*, 3990-3992.

(142) Kollmar, C.; Couty, M.; Kahn, O. *J. Am. Chem. Soc.* **1991**, *113*, 7994-8005.

(143) Kotz, J.; Neyhart, G.; Vining, W. J.; Rausch, M. D. *Organometallics* **1983**, *2*, 79-82.

(144) Kramer, J. A.; Hendrickson, D. N. *Inorg. Chem.* **1980**, *19*, 3330-3337.

(145) Krocher, O.; Koppel, R. A.; Baiker, A. *J. Chem. Soc., Chem. Commun.* **1997**, 453-454.

(146) Lang, H. *Angew. Chem. Int. Ed.* **1994**, *33*, 547-550.

(147) Laskoski, M.; Roidl, G.; Smith, M. D.; Bunz, U. H. F. *Angew. Chem. Int. Ed.* **2001**, *40*, 1460-1463.

(148) Lau, V. C.; Berben, L. A.; Long, J. R. *J. Am. Chem. Soc.* **2002**, *124*, 9042-9043.

(149) Le Stang, S.; Paul, F.; Lapinte, C. *Organometallics* **2000**, *19*, 1035-1043.

(150) Lebozec, H.; Ouzzine, K.; Dixneuf, P. H. *Organometallics* **1991**, *10*, 2768-2772.

(151) Lee, W. S.; Brintzinger, H. H. *J. Organomet. Chem.* **1977**, *127*, 93-103.

(152) Legrange, J. D.; Markham, J. L.; Kurkjian, C. R. *Langmuir* **1993**, *9*, 1749-1753.

(153) Lehaire, M.-L.; Scopelliti, R.; Herdeis, L.; Polborn, K.; Mayer, P.; Severin, K. *Inorg. Chem.* **2004**, *43*, 1609-1617.

(154) Lei, X. J.; Wolf, E. E.; Fehlner, T. P. *Eur. J. Inorg. Chem.* **1998**, 1835-1846.

(155) Leininger, S.; Olenyuk, B.; Stang, P. J. *Chem. Rev.* **2000**, *100*, 853-907.

(156) Lenarvor, N.; Lapinte, C. *J. Chem. Soc., Chem. Commun.* **1993**, 357-359.

(157) Lenarvor, N.; Lapinte, C. *Organometallics* **1995**, *14*, 634-639.

(158) Lenarvor, N.; Toupet, L.; Lapinte, C. *J. Am. Chem. Soc.* **1995**, *117*, 7129-7138.

(159) Lent, C. S. *Science* **2000**, *288*, 1597-1599.

(160) Lent, C. S.; Isaksen, B.; Lieberman, M. *J. Am. Chem. Soc.* **2003**, *125*, 1056-1063.

(161) Lent, C. S.; Tougaw, P. D. *J. Appl. Phys.* **1993**, *74*, 6227-6233.

(162) Lent, C. S.; Tougaw, P. D. *Proc. IEEE* **1997**, *85*, 541-557.

(163) Lent, C. S.; Tougaw, P. D.; Porod, W.; Bernstein, G. H. *Nanotechnology* **1993**, *4*, 49-57.

(164) Levanda, C.; Bechgaard, K.; Cowan, D. O. *J. Org. Chem.* **1976**, *41*, 2700-2704.

(165) Lewis, J.; Lin, B.; Khan, M. S.; Almandhary, M. R. A.; Raithby, P. R. *J. Organomet. Chem.* **1994**, *484*, 161-167.

(166) Li, Q. L.; Surthi, S.; Mathur, G.; Gowda, S.; Misra, V.; Sorenson, T. A.; Tenent, R. C.; Kuhr, W. G.; Tamaru, S.; Lindsey, J. S.; Liu, Z. M.; Bocian, D. F. *Appl. Phys. Lett.* **2003**, *83*, 198-200.

(167) Li, Z. H.; Beatty, A. M.; Fehlner, T. P. *Inorg. Chem.* **2003**, *42*, 5707-5714.

(168) Li, Z. H.; Fehlner, T. P. *Inorg. Chem.* **2003**, *42*, 5715-5721.

(169) Lieberman, M.; Chellamma, S.; Varughese, B.; Wang, Y. L.; Lent, C.; Bernstein, G. H.; Snider, G.; Peiris, F. C. *Ann. NY. Acad. Sci.* **2002**, *960*, 225-239.

(170) Liu, S.; Tang, Z.; Bo, A.; Wang, E.; Dong, S. *J. Electroanal. Chem.* **1998**, *458*, 87-97.

(171) Long, N. J.; Martin, A. J.; White, A. J. P.; Williams, D. J.; Fontani, M.; Laschi, F.; Zanello, P. *J. Chem. Soc., Dalton Trans.* **2000**, 3387-3392.

(172) Lu, X.; Hipps, K. W.; Wang, X. D.; Mazur, U. *J. Am. Chem. Soc.* **1996**, *118*, 7197-7202.

(173) Luo, S. J.; Liu, Y. H.; Liu, C. M.; Liang, Y. M.; Ma, Y. X. *Synthetic Commun.* **2000**, *30*, 1569-1572.

(174) Mahias, V.; Cron, S.; Toupet, L.; Lapinte, C. *Organometallics* **1996**, *15*, 5399-5408.

(175) Masamune, S.; Machiguchi, T.; Aratani, M. *J. Am. Chem. Soc.* **1977**, *99*, 3524-3526.

(176) Masamune, S.; Soutobachiller, F. A.; Machiguchi, T.; Bertie, J. E. *J. Am. Chem. Soc.* **1978**, *100*, 4889-4891.

(177) Mays, M. J.; Sears, P. L. *J. Chem. Soc., Dalton Trans.* **1973**, 1873-1875.

(178) McAdam, C. J.; Duffy, N. W.; Robinson, B. H.; Simpson, J. *Organometallics* **1996**, *15*, 3935-3943.

(179) McCleverty, J. A.; Ward, M. D. *Acc. Chem. Res.* **1998**, *31*, 842-851.

(180) Medina, J. C.; Li, C.; Bott, S. G.; Atwood, J. L.; Gokel, G. W. *J. Am. Chem. Soc.* **1991**, *113*, 366-367.

(181) Mehrotra, R. C.; Bohra, R. *Metal carboxylates*; Academic Press: London ; New York, 1983.

(182) Meyer, W. E.; Amoroso, A. J.; Horn, C. R.; Jaeger, M.; Gladysz, J. A. *Organometallics* **2001**, *20*, 1115-1127.

(183) Moreira, I. D.; Franco, D. W. *Inorg. Chem.* **1994**, *33*, 1607-1613.

(184) Morrison, W. H.; Hendrickson, D. N. *Inorg. Chem.* **1975**, *14*, 2331-2346.

(185) Morrison, W. H.; Krogsrud, S.; Hendrickson, D. N. *Inorg. Chem.* **1973**, *12*, 1998-2004.

(186) Moulder, J. F.; Stickle, W. F.; Sobol, P. E.; Bomben, K. D. *Handbook of X-ray Photoelectron Spectroscopy*; Perkin-Elmer Corp.: Eden Prairie, MN, 1992.

(187) Nicolaou, K. C.; Maligres, P.; Suzuki, T.; Wendeborn, S. V.; Dai, W. M.; Chadha, R. K. *J. Am. Chem. Soc.* **1992**, *114*, 8890-8907.

(188) Niemier, M. T.; Kogge, P. M. *Int. J. Circ. Theor. App.* **2001**, *29*, 49-62.

(189) Oh, S. K.; Baker, L. A.; Crooks, R. M. *Langmuir* **2002**, *18*, 6981-6987.

(190) Orlov, A. O.; Amlani, I.; Bernstein, G. H.; Lent, C. S.; Snider, G. L. *Science* **1997**, *277*, 928-930.

(191) Osella, D.; Milone, L.; Nervi, C.; Ravera, M. *Eur. J. Inorg. Chem.* **1998**, 1473-1477.

(192) Pardy, R. B. A.; Smith, G. W.; Vickers, M. E. *J. Organomet. Chem.* **1983**, *252*, 341-346.

(193) Parise, A. R.; Baraldo, L. M.; Olabe, J. A. *Inorg. Chem.* **1996**, *35*, 5080-5086.

(194) Paul, F.; Lapinte, C. *Coord. Chem. Rev.* **1998**, *180*, 431-509.

(195) Phadke, R. S. *Appl. Biochem. Biotech.* **2001**, *96*, 269-276.

(196) Pilette, D.; Ouzzine, K.; Lebozec, H.; Dixneuf, P. H.; Rickard, C. E. F.; Roper, W. R. *Organometallics* **1992**, *11*, 809-817.

(197) Powers, M. J.; Meyer, T. J. *J. Am. Chem. Soc.* **1978**, *100*, 4393-4398.

(198) Powers, M. J.; Meyer, T. J. *Inorg. Chem.* **1978**, *17*, 2955-2958.

(199) Qi, H.; Sharma, S.; Li, Z. H.; Snider, G. L.; Orlov, A. O.; Lent, C. S.; Fehlner, T. P. *J. Am. Chem. Soc.* **2003**, *125*, 15250-15259.

(200) Rausch, M. D.; Higbie, F. A.; Westover, G. F.; Clearfield, A.; Gopal, R.; Troup, J. M.; Bernal, I. *J. Organomet. Chem.* **1978**, *149*, 245-264.

(201) Ribou, A. C.; Launay, J. P.; Takahashi, K.; Nihira, T.; Tarutani, S.; Spangler, C. W. *Inorg. Chem.* **1994**, *33*, 1325-1329.

(202) Riley, P. E.; Davis, R. E. *J. Organomet. Chem.* **1976**, *113*, 157-166.

(203) Robin, M. B.; Day, P. *Adv. Inorg. Chem. Radiochem.* **1967**, *10*, 247-422.

(204) Roger, C.; Hamon, P.; Toupet, L.; Rabaa, H.; Saillard, J. Y.; Hamon, J. R.; Lapinte, C. *Organometallics* **1991**, *10*, 1045-1054.

(205) Roidl, G.; Enkelmann, V.; Adams, R. D.; Bunz, U. H. F. *J. Organomet. Chem.* **1999**, *578*, 144-149.

(206) Rosenblum, M.; Brawn, N.; Papenmeier, J.; Applebaum, M. *J. Organomet. Chem.* **1966**, *6*, 173-180.

(207) Roth, K. M.; Dontha, N.; Dabke, R. B.; Gryko, D. T.; Clausen, C.; Lindsey, J. S.; Bocian, D. F.; Kuhr, W. G. *J. Vac. Sci. Technol. B* **2000**, *18*, 2359-2364.

(208) Roth, K. M.; Yasseri, A. A.; Liu, Z. M.; Dabke, R. B.; Malinovskii, V.; Schweikart, K. H.; Yu, L. H.; Tiznado, H.; Zaera, F.; Lindsey, J. S.; Kuhr, W. G.; Bocian, D. F. *J. Am. Chem. Soc.* **2003**, *125*, 505-517.

(209) Rubin, Y.; Knobler, C. B.; Diederich, F. *J. Am. Chem. Soc.* **1990**, *112*, 4966-4968.

(210) Rueckes, T.; Kim, K.; Joselevich, E.; Tseng, G. Y.; Cheung, C. L.; Lieber, C. M. *Science* **2000**, *289*, 94-97.

(211) Sarhan, A. E. W.; Nouchi, Y.; Izumi, T. *Tetrahedron* **2003**, *59*, 6353-6362.

(212) Schottenberger, H.; Lukassser, J.; Reichel, E.; Muller, A. G.; Steiner, G.; Kopacka, H.; Wurst, K.; Ongania, K. H.; Kirchner, K. *J. Organomet. Chem.* **2001**, *637*, 558-576.

(213) Schreiber, F. *Prog. Surf. Sci.* **2000**, *65*, 151-256.

(214) Seiler, P.; Dunitz, J. D. *Acta. Cryst. B* **1979**, *35*, 1068-1074.

(215) Shriver, D. F.; Drezdzon, M. A. *The manipulation of air-sensitive compounds*; 2nd ed.; Wiley: New York, 1986.

(216) Slone, R. V.; Hupp, J. T.; Stern, C. L.; AlbrechtSchmitt, T. E. *Inorg. Chem.* **1996**, *35*, 4096-4097.

(217) Snaith, T. J.; Low, P. J.; Rousseau, R.; Puschmann, H.; Howard, J. A. K. *J. Chem. Soc., Dalton Trans.* **2001**, 292-299.

(218) Steffen, L. K.; Glass, R. S.; Sabahi, M.; Wilson, G. S.; Schoneich, C.; Mahling, S.; Asmus, K. D. *J. Am. Chem. Soc.* **1991**, *113*, 2141-2145.

(219) Stephens, R. D.; Castro, C. E. *J. Org. Chem.* **1963**, *28*, 3313-3315.

(220) Stricklen, P. M.; Volcko, E. J.; Verkade, J. G. *J. Am. Chem. Soc.* **1983**, *105*, 2494-2495.

(221) Sun, L.; Crooks, R. M.; Ricco, A. J. *Langmuir* **1993**, *9*, 1775-1780.

(222) Sutter, J. P.; Grove, D. M.; Beley, M.; Collin, J. P.; Veldman, N.; Spek, A. L.; Sauvage, J. P.; Vankoten, G. *Angew. Chem. Int. Ed.* **1994**, *33*, 1282-1285.

(223) Tans, S. J.; Verschueren, A. R. M.; Dekker, C. *Nature* **1998**, *393*, 49-52.

(224) Timler, J.; Lent, C. S. *J. Appl. Phys.* **2002**, *91*, 823-831.

(225) Touchard, D.; Haquette, P.; Pirio, N.; Toupet, L.; Dixneuf, P. H. *Organometallics* **1993**, *12*, 3132-3139.

(226) Tougaw, P. D.; Lent, C. S.; Porod, W. *J. Appl. Phys.* **1993**, *74*, 3558-3566.

(227) Tseng, G. Y.; Ellenbogen, J. C. *Science* **2001**, *294*, 1293-1294.

(228) Ulman, A. *An introduction to ultrathin organic films : from Langmuir-Blodgett to self-assembly*; Academic Press: Boston, 1991.

(229) Ulman, A. *Chem. Rev.* **1996**, *96*, 1533-1554.

(230) Umana, M.; Rolison, D. R.; Nowak, R.; Daum, P.; Murray, R. W. *Surf. Sci.* **1980**, *101*, 295-309.

(231) Varughese, B.; Chellamma, S.; Lieberman, M. *Langmuir* **2002**, *18*, 7964-7970.

(232) Wagner, R. W.; Brown, P. A.; Johnson, T. E.; Lindsey, J. S. *J. Chem. Soc., Chem. Commun.* **1991**, 1463-1466.

(233) Wang, X. Ph. D. Thesis, University of Notre Dame, 2003.

(234) Ward, M. D. *Chem. Soc. Rev.* **1995**, *24*, 121-134.

(235) Wasserman, S. R.; Tao, Y. T.; Whitesides, G. M. *Langmuir* **1989**, *5*, 1074-1087.

(236) Wei, C. H. *Inorg. Chem.* **1967**, *8*, 2384-2397.

(237) Wei, C. H.; Dahl, L. F. *J. Am. Chem. Soc.* **1966**, *88*, 1821-1822.

(238) Wei, C. H.; Wilkes, G. R.; Dahl, L. F. *J. Am. Chem. Soc.* **1967**, *89*, 4792-4793.

(239) Weyland, T.; Costuas, K.; Toupet, L.; Halet, J. F.; Lapinte, C. *Organometallics* **2000**, *19*, 4228-4239.

(240) Weyland, T.; Lapinte, C.; Frapper, G.; Calhorda, M. J.; Halet, J. F.; Toupet, L. *Organometallics* **1997**, *16*, 2024-2031.

(241) Whitesides, G. M.; Laibinis, P. E. *Langmuir* **1990**, *6*, 87-96.

(242) Whitman, D. W.; Carpenter, B. K. *J. Am. Chem. Soc.* **1980**, *102*, 4272-4274.

(243) Winter, R. F.; Hornung, F. M. *Organometallics* **1999**, *18*, 4005-4014.

(244) Woodward, J. *Philos. Trans. R. Soc. London* **1724**, *33*, 15.

(245) Worth, G. H.; Robinson, B. H.; Simpson, J. *Organometallics* **1992**, *11*, 3863-3874.

(246) Wurthner, F.; Sautter, A. *Chem. Commun.* **2000**, 445-446.

(247) Yam, V. W. W.; Cheng, E. C. C.; Zhu, N. Y. *New J. Chem.* **2002**, *26*, 279-284.

(248) Yao, H.; Sabat, M.; Grimes, R. N.; de Biani, F. F.; Zanello, P. *Angew. Chem. Int. Ed.* **2003**, *42*, 1002-1005.

(249) Yin, I.; Guo, Q.; Palmer, R. E.; Bampos, N.; Sanders, J. K. M. *J. Phys. Chem. B* **2003**, *107*, 209-216.

(250) Younus, M.; Long, N. J.; Raithby, P. R.; Lewis, J. *J. Organomet. Chem.* **1998**, *570*, 55-62.

(251) Yu, H. Z.; Morin, S.; Wayner, D. D. M.; Allongue, P.; de Villeneuve, C. H. *J. Phys. Chem. B* **2000**, *104*, 11157-11161.

(252) Zhang, Y. F.; Liao, L. S.; Chan, W. H.; Lee, S. T.; Sammynaiken, R.; Sham, T. K. *Phys. Rev. B* **2000**, *61*, 8298-8305.

(253) Zhou, Y. L.; Seyler, J. W.; Weng, W. Q.; Arif, A. M.; Gladysz, J. A. *J. Am. Chem. Soc.* **1993**, *115*, 8509-8510.

(254) Zhu, X. Y.; Boiadjiev, V.; Mulder, J. A.; Hsung, R. P.; Major, R. C. *Langmuir* **2000**, *16*, 6766-6772.

(255) Zhu, X. Y.; Mulder, J. A.; Bergerson, W. F. *Langmuir* **1999**, *15*, 8147-8154.

(256) Zhu, Y. B.; Wolf, M. O.; Yap, G. P. A. *Inorg. Chem.* **1997**, *36*, 5483-5487.